Novel Architectures and Multiplexing Strategies for Optical CDMA

Denis Zaccarin, B.Sc.A., M.Sc.
December 1994

A thesis
submitted to the School of Graduate Studies and Research
in partial fulfillment of the requirements for the
Degree of Doctor of Philosophy
in Electrical Engineering

Ottawa-Carleton Institute for Electrical Engineering
Department of Electrical Engineering
Faculty of Engineering
University of Ottawa
Ottawa, Ontario
Canada

ISBN 0-612-00599-2

Abstract

The work presented in this thesis explores avenues to efficiently use code-division as the multiple-access technique in optical communication systems. Coding in the time domain is first considered. Novel architectures that allow the use of bipolar codes with simple direct detection receivers are first presented, for the case of coherent optical sources. We show that a proper combination of electro-optic elements and all optical processing elements leads to encoder and decoder complexities much reduced compared to the all optical solutions, without sacrifying the chip rate. This is further enhanced when we propose the use of Kronecker sequences whose inner sequences are choosen to be perfect autocorrelation sequences. In that case, even programmability of the delay lines is not required. We then modify the proposed architectures so that they can be used with incoherent optical sources. Although the sources can only be modulated in power, we show that still bipolar codes can be used and maintain their properties.

A detailed performance analysis of the proposed architectures is made, including multiple-access interference, shot noise and thermal noise. Two types of modulation: amplitude-shift-keying (ASK) and orthogonal coding (OC) are considered. Results presented give the probability of bit error as a function of the number of simultaneous users, for many code lengths values. Performances obtained using different combinations of inner and outer sequences are compared, and requirements in terms of number of delay lines and bandwidth of electro-optic elements are identified. The effect of partial cross-correlation due to non optimized optical filtering is studied by means of an upper bound on the probability of bit error. A new analytical technique is derived to analyze optical CDMA systems using coherent optical sources with direct detection.

A new and highly efficient coding technique based on amplitude spectral encoding of incoherent optical sources such as light-emitting diodes is then proposed. This is one of the major contributions of this thesis. Architectures for the encoder and decoder are given, and suitable codes are identified. The proposed system is insensitive to near-far effects and has a spreading gain independent of the bit rate. This property makes this coding technique a suitable one for networks serving users with different bit rates requirements. Detailed evaluation of the probability of error is done, and practical considerations such as the spectral shape of the sources, finite extinction ratio of the amplitude mask as well as its programmability speed are quantified. We show that more than 100 simultaneous users can be accomodated with a probability of error of 10^{-9}, for a code length as small as 127. Finally, the use of this coding strategy as the routing technique for Asynchronous Transfer Mode (ATM) switches is discussed.

Acknowledgements

I wish first to express my sincere gratitude to my supervisor, Dr. Mohsen Kavehrad, for his scientific guidance, interest and constant support during the course of this program. I would like to thank the members of my supervisory committee, Drs. W. Steenaart, D. Falconer and P. Galko, for their helpful recommandations. I also wish to thank Dr. J. Chrostowski from the Institute for Information Technology at the National Research Council of Canada, for the useful discussions and advice provided.

I also wish to thank all my colleagues at the University of Ottawa for the good academic atmosphere, their encouragement and valuable discussions, in particular Chris Barnard, Farideh Khaleghi, Emil Savov, Ellie Simova, Nilofar Tayebi and Gang Yun.

Most importantly, thanks are given to my family for their encouragement and support and, above all, to my wife, Denise Lemieux, and daughter Annie, for their constant reassurance and patience.

CONTENTS

List of Figures

List of Tables

List of Symbols and Abbreviations

A_k	Amplitude of the interfering vector from user k
$a_k(t)$	Spreading waveform of user k
$C_k(n)$	Aperiodic crosscorrelation function
$\vec{E}(t)$	Optical field
G	Gain of the avalanche photodiode
h	Modulation index in CPFSK modulation
$I^k(t)$	Data modulation of user k
$[I^k_{-1}, I^k_0]$	Pair of symbols sent by user k in the interval $[0, T]$
K	Number of interfering users
$M_X(s)$	Moment generating function of the random variable X
N	Period of a pseudorandom sequence
N_i	Period of the inner sequence, in a Kronecker sequence
N_0	Period of the outer sequence, in a Kronecker sequence
P	Number of branches in a coherent, or incoherent, transversal filter
P_e	Average bit error probability
R_b	Bit rate
R	Repetition rate of a mode-locked laser
$R_k(\tau)$	Continuous-time partial crosscorrelation
T	Symbol duration
T_c	Chip duration
T^0	Equivalent noise temperature
Tr	Decision threshold

w	Radius of an optical beam
z_i	Decision variable at the photodetector i
$\beta(w)$	Propagation constant, as a function of frequency
$\delta\lambda$	Spectral width of an optical source
$1/d$	Grating resolution (lines/mm)
η	Quantum efficiency
$\theta_k(l)$	Periodic crosscorrelation function
$\widehat{\theta_k}(l)$	Odd crosscorrelation function
λ	Wavelength of the optical signal
$\lambda(t)$	Rate of a Poisson point process
τ_k	Time delay of user k compared to the reference
ϕ_k	Phase shift of user k compared to the reference
σ^2	Noise variance
APA	Almost perfect autocorrelation
ASE	Amplified spontaneous emission
ASK	Amplitude shift keying
ATM	Asynchronous transfer mode
CDMA	Code division multiple access
COTF	Coherent optical transversal filter
CPFSK	Continuous frequency shift keying
CPM	Colliding pulse mode-locking
CRD	Contention resolution device
EE-LED	Edge emitting light emitting diode
FDDI	Fiber distributed data interface
FE-CDMA	Frequency encoded code division multiple access
GQR	Gauss quadrature rule

GVD	Group velocity dispersion
HDTV	High definition television
ISI	Intersymbol interference
LAN	Local area network
LCTV	Liquid crystal television
LD-FSK	Large deviation frequency shift keying
LPF	Lowpass filter
MAI	Multiple access interference
MZ	Mach-zender
NOLM	Nonlinear optical loop mirror
OC	Orthogonal coding
OOC	Optical orthogonal code
PDF	Probability density function
PG	Processing gain
PPM	Pulse position modulation
SE-LED	Surface emitting light emitting diode
SLD	Superluminescent diode
SLM	Spatial light modulator
SMF	Single mode fiber
TDMA	Time division multiple access
VLSI	Very large scale integration
WDMA	Wavelength division multiple access
WSK	Wavelength shift keying

Chapter 1

Introduction

1.1 Motivation

Optical fiber has been a transmission medium of choice for many years for point-to-point communications. This is primarily due to its low loss over a very large frequency bandwidth, approximately less than 0.2 dB/km for a window of 100 nanometers, around 1.55 μm. The advent of optical amplifiers and the development of soliton transmission techniques have led to experimental demonstrations of multiple Gbit/s signals transmitted over thousands of kilometers, without any electro-optic conversion.

However, for networking applications, the problems to solve are more challenging than only dispersion or attenuation. Realizing a photonic network requires an efficient multiple-access technique. Mainly three techniques can be identified: WDM (wavelength-division multiplexing), TDM (time-division multiplexing) and CDM (code-division multiplexing). What is the optimum multiple-access scheme is not an easy question to answer. Opinions in the scientific community are very diverse, research is going in many directions, responding probably to very different needs. Each one, of course, has advantages and drawbacks, depending on many parameters, such as the traffic characteristics one is expecting on the future photonic network is willing to build. Certainly, each one deserves to be studied. In this thesis, we study code-division as the multiple-access technique. Our work positions itself on the physical layer of the standard OSI reference model, and higher-layer protocols are not considered. A general criticism against code-division multiple-access is its poor spectral inefficiency. The bit-rate per user must be to some extent sacrified, to permit coding with relatively long codes. However, how high a bit rate is needed depends on the particular application, and can vary from a few kbit/s to many Gbit/s. For example, improvements in digital signal processing algorithms and their VLSI implemenations have resulted in "VCR-quality" video at 1.5 Mbit/s, "full NTSC-quality" video at 3-4 Mbit/s, and HDTV video at 20-40 Mbit/s [1]. On the other hand, LAN interconnections (e.g., FDDI) would require several Mbit/s, and supercomputer interconnects need several Gbit/s.

On a code-division multiple access (CDMA) system, the multiple-access capability is due primarily to coding. Each subscriber is associated with a unique minimally interfering address code, usually called a pseudorandom sequence. CDMA is an asynchronous transmission technique. Users who have information to transmit can therefore do so without any access delay. It allows many, possibly not-colocated, sources to operate independently and concurrently on the same channel, with a minimum amount of interference. In this respect, CDMA has an advantage over TDMA, which requires precise synchronization between the subscribers of a network. Moreover, for a network having bursty traffic characteristics, reservation of time slots for each subscriber, as in TDMA, is highly inefficient since only a small fraction of them would typically transmit at the same time.

Compared to WDMA, CDMA using incoherent sources and incoherent processing elements is tolerant to a wide variety of system inadequacies. Optical sources with precise frequency control, or with large tuning capability are not required. Standard direct detection receivers, that do not require narrow, possibly tunable, optical filters can be used. However, tapping the fiber bandwidth by means of CDMA would require ultra-short pulses and poses problems as well. The number of possible subscribers is also limited by the number of codes in a given set, which is typically smaller than standard bipolar codes such as Gold codes, Kasami sequences or others. CDMA using coherent sources, but direct detection, allows hybrid schemes such as WDMA/CDMA, where many subscribers, code-multiplexed, can share a single wavelength. This allows an increase in concurrency without requiring increased tuning capability from the optical sources, or from the optical filters at the receiving end. Many problems and open questions remain for CDMA systems using coherent or incoherent sources. In this thesis, we consider and solve some of them.

1.2 Contributions and Outline of the Thesis

In Chapter 2, we give a brief overview of different CDMA systems presented so far in the literature. The systems are categorized in terms of the types of sources they require (coherent or incoherent), the codes used, the architectures used for the encoders/decoders, the correlation principle (field or power addition), and finally on the types of receiver, direct detection or coherent detection. Our own contribution is outlined on a classification diagram. The technological requirements for optical CDMA systems are reviewed.

In Chapter 3, we review the properties of the codes that will be considered in this thesis. No new codes are designed in this thesis, one of our goals being to find efficient architectures for using bipolar codes in coherent or incoherent CDMA with direct detection. We recall the definitions of useful parameters such as the periodic and odd crosscorrelation functions. We mainly discuss a class of codes less widely used called Kronecker sequences, as they will find important applications in the subsequent chapters. A construction method to obtain ternary perfect autocorrelation codes are given. A simple way to encode bipolar codes into unipolar ones is presented and will find an important application in Chapter 4.

In Chapter 4, we present new and efficient architectures for the encoders and the decoders in optical CDMA using coherent and incoherent sources. We show

how to combine electro-optic elements and pure optical processing elements such as delay lines to obtain structures with minimum complexity. We also propose the use of Kronecker sequences to obtain even simpler structures, while maintaining a high efficiency. To the best of our knowledge, Kronecker sequences were never proposed in the past in the context of optical CDMA systems. We show that they allow complete connectivity (each user being able to reach any other user in a network) *without requiring programmable delay lines.* We further show how incoherent sources can be used with bipolar codes, using a simple 2-PPM encoding of each chip. Detailed architectures for the encoders/decoders are given, and we show that unipolar codes can have the same crosscorrelation properties as bipolar ones, using a simple balanced receiver. The particularity of our architectures is that *they do not require a fast optical switches at the receiver.* Part of the work reported in this chapter has been presented in [2-3].

In Chapter 5, we proceed with a detailed performance analysis of coherent CDMA using bipolar codes and direct detection. This is the first detailed analysis of such systems, and it was published in [4]. We propose several calculation methods, for modulation shemes such as amplitude-shift-keying (ASK), continuous-phase frequency-shift-keying (CPFSK) and wavelength-shift-keying. Numerous results, in terms of the number of active users that can be supported for a given probability of bit error are given, for many different codes such as Gold codes and Kronecker sequences with different choices for the inner and outer sequences.

In Chapter 6, the performance evaluation of incoherent systems using a 2-PPM encoding of bipolar sequences is provided. The major sources of interference are considered, e.g. the dominating Multiple-Access-Interference (MAI), the shot noise and the thermal noise. Detailed results of the probability of error as a function of the number of active users is given, for the same codes used with coherent systems (Chapter 5), to allow comparison.

In Chapter 7, we study optical CDMA systems in which the coding is done in the frequency domain. We first review a system proposed by Salehi and Wiener

[5], based on coherent sources. We then present a new type of frequency-encoded system that we have designed, based on simple incoherent sources such as LED's. We believe that this design is one of the major contributions of our thesis. We discuss the advantages of our system compared to the previous systems. Suitable codes are studied, and a detailed performance analysis is done. We show that our system allows more than 100 simultaneous active users, each transmitting with a probability of error less than 10^{-9}. We further show that our design has a spreading gain independent of the bit rate, and therefore allows multiple types of services to be used on the same network without any performance degradation. Practical considerations are discussed in detail and their effects are quantitatively studied. Its application as the routing technique for ATM switches using optical interconnects is also considered. Part of the work in this chapter was presented in [6] and [7]. Finally, in Chapter 8, we give a summary of results and suggestions for future work.

Chapter 2

Optical CDMA Systems: A Brief Review

2.1 Introduction

In this chapter, we review some of the different types of optical CDMA systems, their advantages and their drawbacks, and the technological requirements. The architectures are divided into two main categories, depending on whether the coding is done in the time domain or in the frequency domain. We position our work in comparison to the work done by other researchers.

2.2 Time-Encoded Systems

Time-encoded optical CDMA systems take advantage of the bandwidth of optical fibers to map relatively low-information rate signals, carrying the data, into high-rate optical pseudorandom sequences to achieve asynchronous communication access to many users. A simple block diagram is shown on Fig. 2.1a. It is desirable that the encoding and decoding operations be done optically, in order to avoid the speed limitations of the electronics. However, at each transmitter one should be able to modify its encoder quickly to generate suitable code sequences to reach particular destinations. To solve the question of addressability, one would likely be constrained to use electronics in some way. Two main categories of time-encoded systems can be identified, depending on the coherence properties of the optical sources used.

a) Incoherent optical CDMA systems:

This includes much of the work done until recently in optical CDMA systems, for example the work of Salehi [8-9] and Prucnal [10]. In this case, the optical encoder/decoder, and other processing elements, are modeled as positives, i.e., they cannot manipulate their signals to add to zero. Bipolar codes cannot, in general, be used, since incoherent processing is based on correlation by intensity rather than field superposition. New (0,1) codes had to be designed, such as prime codes, optical orthogonal codes (OOC) [11] and more recently quadratic congruence codes [12]. The equivalence between these codes and time-hopping patterns is studied in [13]. The number of 1's in these codes is relatively small and the coding can simply be done by using optical delay lines, as shown in Fig.2.1b. The number of delay lines should be small, in order to reduce the complexity and to minimize the recombining losses, which are proportional to $10\log(w)$, where w is the number of 1's (code weight). The main disadvantage is the reduced number of codes in a particular set compared to the usual bipolar codes, such as Gold codes. This will limit the number of possible subscribers, which can be very large in a packet-switched environment. Precise indications of the size depends on many factors, such as the code weight w, the code length n and the crosscorrelation values. For OOC having a maximum crosscorrelation value of 1, the code length must be larger than $n \geq mw(w-1)$, where m is the number of subscribers to be accommodated. For $n = 127$ and $w = 3$, only $m = 21$ subscribers can be accommodated compared to 128 for Gold codes of the same length. For prime codes, or quadratic congruence codes, there are P codes in a given set, for a code length $n = P^2$. Other values can be obtained for other designs. An alternative encoder, called a ladder network, is made from cascading 3dB couplers, and the recombination losses are 3 dB, independent of the code length. A ladder encoder is shown on Fig. 2.1c. Code design for such codes must take into account the symmetry of the coding architecture.

Advantages of incoherent CDMA systems include the simplicity of the receiver, simple direct detection, including possibly an optical threshold element, low-cost optical sources, no need for precise carrier frequency stabilization and no need for small bandwidth optical filter. The stability requirements for the processing elements is small and needs only to be in the order of the chip period when using delay lines. A major advantage compared to TDM is the absence for synchronization requirement between the different users. Between a pair of users communicating, only bit synchronization, and not chip synchronization is required for quadratic congruence codes, since all out-of-phase autocorrelation values are much smaller than the peak autocorrelation value.

b) Coherent optical CDMA systems:

Two types of coherent optical CDMA systems can be found, depending on whether they need a local oscillator or not. Coherent detection, using a local oscillator, allows in optical CDMA, the simple use of standard bipolar codes, and the correlation can be done in the electronic domain, following the scheme used in electronic systems. Performance evaluations for such systems appears in the literature [14-15]. A large number of users can be usually accommodated, but these systems

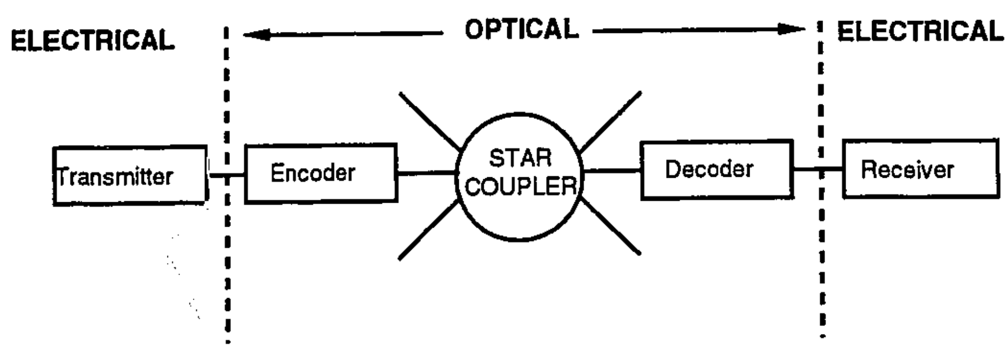

Fig.2.1a: General optical CDMA diagram.

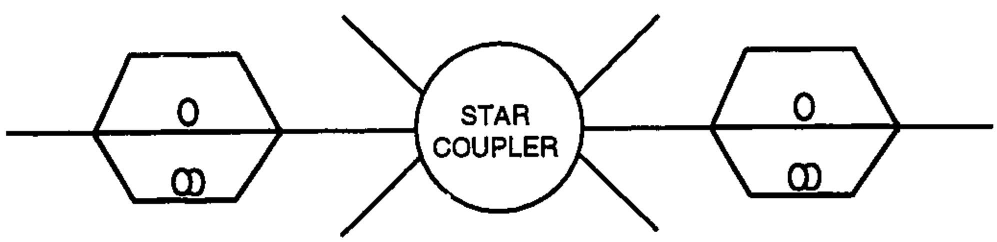

Fig.2.1b: Encoder/decoder using a splitter/combiner.

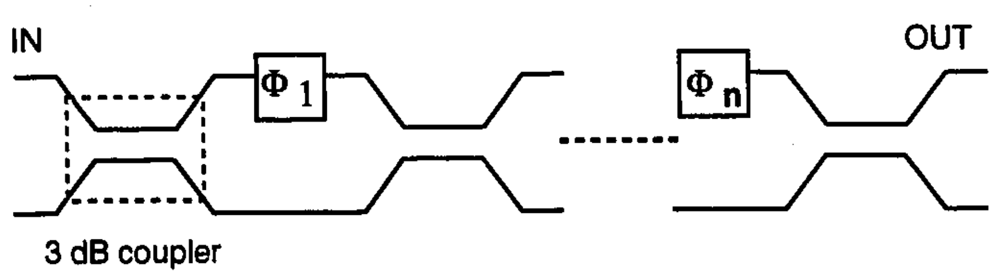

Fig.2.1c: Encoder/decoder using a ladder architecture.

have the same requirements and complexity of FDM systems with coherent detection, such as precise frequency tuning, low level of phase noise, polarization matching betweeen the incoming signal and the local oscillator. Hybrid FDMA-CDMA is a natural extension and allows to increase the concurrency.

Coherent optical CDMA using low-coherence sources is also studied in the literature [16-17]. The encoding/decoding can be done all optically using a ladder network. A necessary condition for coherent correlation to take place is that the receiver delays match those at the transmitter to within the coherence time of the source. Typical coherence time for these low-coherence sources, such as the gain-switched laser diode used in [18], is around 500 femtoseconds. Very precise control of delays in the coding architectures is therefore needed, but is not impossible, since experimentally demonstrated. Code design for this system is only at an early stage, represented in Fig. 2.2 by a question mark.

2.3 Frequency-Encoded Systems

All time-encoded optical CDMA systems, no matter which architecture is employed, suffer from one basic limitation. As the number of simultaneous active users, or subscribers has to be increased, the code length has to be increased. To do so, without sacrifying the bit rate, one is constrained to use shorter and shorter pulses. A remedy to this problem is to code in two different dimensions. In [5], temporal/frequency CDMA using mode-locked sources is suggested. Using the frequency dimension for the code is attractive in optics since optical sources with a large spectral width are available, should they be coherent or incoherent. In this thesis we explore frequency-encoded CDMA using incoherent sources, such as Light-Emitting Diodes (LED). Frequency-encoded systems using mode-locked sources still require short pulses and the coding has some effect on the temporal signal. As we will show, there are many advantages to use incoherent sources instead of mode-locked sources.

A general diagram of the different types of CDMA is given in Fig. 2.2. Our

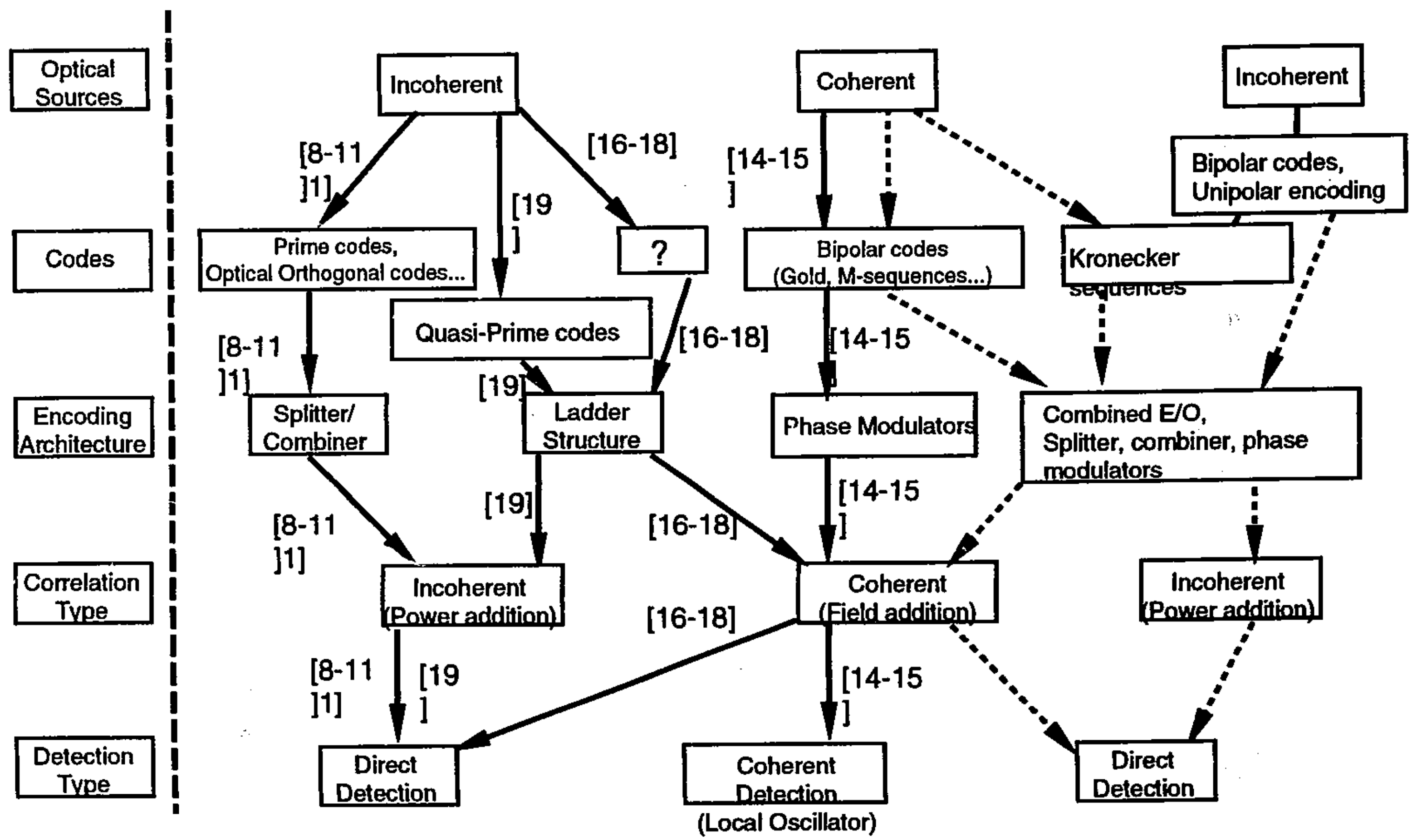

Our work;

Fig.2.2: Classification diagram for time-encoded optical CDMA systems.

intent is not to be complete, but to give a summary of the major systems suggested so far in the literature. We outline our own contributions, detailed in the next chapters. For the category of time-encoded systems, our work explores CDMA using coherent and incoherent sources, but always with the objective of using only direct detection and standard bipolar codes, or Kronecker sequences, since they are known to possess the best possible crosscorrelation properties. For frequency-encoded systems, we design a new system based on encoding incoherent optical sources. We now review the basic technological requirements for CDMA systems.

2.4 Technological Requirements

a) Optical sources

For time-encoded systems, sources generating picoseconds coherent pulses with a high-repetition rate are needed. DFB-LD's and mode-locked lasers are capable of generating high-repetition rate, transform-limited picoseconds pulses. For an overview of current capacity, see [20]. Pulses of duration in the order of $\approx$ 10 ps with repetition rate up to 20 GHz, have been achieved by many research teams [21], but shorter pulses in the femtoseconds range, or higher repetition rates (up to $\approx$ 40 GHz) were also obtained in many occasions. For example, colliding-pulse mode-locking (CPM) can output pulse train up to 350 GHz, and Er-doped fiber ring lasers producing 8 ps at repetition rate at 30 GHz have been reported. For incoherent CDMA systems, sources having a coherence time much shorter than the pulse duration, for incoherent summation, are required. As the pulse duration becomes shorter than $\approx$ 10 ps, this might be difficult. As a possible choice for incoherent systems, gain-switched laser diodes producing pulses of $\approx$ 50 ps with a coherence time in the femtosecond range are available.

b) Optical receivers

Ten-Gbit/s optical receivers have now been built, and demonstrated in many occasions, for example see [22]. In some cases [20], 20 Gbit/s receivers and decision circuits were demonstrated. In any case, the limit will come from the electronic amplifiers and associated electronics, and not from the PIN's or APD's, since they could have bandwidths in excess of 100 Gbit/s. One notes that there is a gap between the possible incoming pulses bandwidth, 100 GHz for 10 ps, and the receiver bandwidth. To solve this problem, one can use optical AND gates before photodetection.

c) Optical AND gates

Recent interest in optical time-divison multiplexing and demultiplexing has made the development of optical AND gates a very fast one. For TDM, optical AND gates are required to extract the desired signal from the intended slot, in the incoming frame. In the context of CDMA, optical AND gates will be in some cases required to extract the autocorrelation peak. Possible techniques include those based on the Kerr effect, the nonlinear optical loop mirror (NOLM), also called nonlinear Sagnac interferometer, four-wave mixing and cross-phase modulation [24]. All these techniques can achieve demultiplexing up to $\approx$ 64 Gbit/s, with state-of-the-art around 100 Gbit/s [25]. Another one, based simply on cascading ON/OFF gates, can achieve, to date, up to 49.6 Gbit/s by cascading only two Mach-Zender intensity modulators. This technique allows retention of the phase information of the pulses, which is important when one needs to further add on a field basis several previously extracted pulses.

d) Coherent optical delay lines

Encoding of pulses is usually done optically by the use of optical fibers. However, when the phase of such pulses need to be maintained, integrated optics is required since optical fibers are too sensitive to environmental effects. Remember that a change in the length of a delay line of $\lambda/2n$, n being the refractive index, would change a 0 phase into a π phase, destroying the code. Even for incoherent systems integrated optics will be required when the delays needed become very short. Coherent transversal filters, in integrated form, have been built with up to 16 branches [26]. Such structures were first made for realizing optical filters used in dense FDM systems. Such filters allow to have a frequency separation as small as 5 GHz between two FDM channels [27]. Arbitrary amplitude and phase coefficients can be used, and therefore coherent transversal filters with arbitrary impulse responses can be expressed. Such filters will be required in CDMA for encoding the pulses with phase information. They will serve as a complement to E/O phase modulators in our designs.

2.5 Summary

In this chapter we have briefly reviewed some of the optical CDMA systems suggested in the literature. The systems were divided into time-encoded and frequency-encoded systems. The former was further divided in two categories termed coherent or incoherent. Incoherent systems use (0,1) specially design codes such as Prime codes and Optical Orthogonal codes. They have the disadvantages of positive systems, but their implementation is relatively simple, since they are robust to optical sources or delay lines instabilities, and require only direct detection receivers. Coherent CDMA with coherent detection faces the same complexity as coherent FDM systems and are not therefore very attractive. Another kind of CDMA that achieves coherent correlation, although using low-coherence source and direct detection receiver was mentioned. They require tuning and stability of the delay lines to within the coherence time of the sources. Finally, we discussed another kind of CDMA system, in which case the coding and the information modulation are done respectively in the frequency and in the time domain.

Chapter 3

Codes for Optical CDMA Systems

3.1 Introduction

We briefly review in this chapter the basic properties of the codes we will use throughout our work. In this thesis, we do not design new codes, since our goal is to find efficient ways to use standard bipolar codes, such as M-sequences and Gold codes, in optical CDMA systems without using coherent detection. Definitions of the periodic and aperiodic properties of these codes are reviewed. We then present how bipolar codes can be used in CDMA systems using incoherent delay lines and sources, by using a simple Pulse Position Modulation (PPM) encoding. We review a special class of sequences termed Kronecker sequences, as they will find an important application in subsequent chapters. Finally, we discuss the construction of perfect ternary autocorrelation sequences.

3.2 Basic properties of bipolar codes

In a network using code-division as the multiple-access technique, many asynchronous users occupy the same channel simultaneously. The set of codes attributed to the subscribers must obey the following properties:

1) each code in the set can be distinguished from a time-shifted version of itself;
2) each code in the set can be distinguished from a possibly time-shifted version of every other code in the set;

The code set is written as $\{a_0(t), a_1(t), \cdots, a_K(t)\}$ where the subscript refers to the user. We assume the codes to be periodic with period $N = T/T_c$, where T is the bit period and T_c is the chip period. There is therefore one code period $\{a_0^k, a_1^k, \cdots, a_{N-1}^k\}$ per data bit, and $a_j(t) = a_j(t+T)$ for all t. Considering without loss of generality the time interval $0 < t \leq T$, user k transmits the following baseband signal:

$$I^k(t) = I_0^k \sum_{j=0}^{N-1} a_j^k p(t - jT_c) \tag{3.1}$$

where I_0^k is the transmitted information bit. Its contribution at a correlation receiver whose intended signal is from user "0", is simply:

$$z^k = \left[I_{-1}^k R_k(\tau) + I_0^k \widehat{R_k}(\tau)\right] \mathrm{Cos}(\phi_k) \tag{3.2}$$

where ϕ_k is the phase difference between user k and 0, and $R_k(\tau)$ and $\widehat{R_k}(\tau)$ are the continuous-time partial crosscorrelation functions defined by:

$$R_k(\tau) = \int_0^{\tau} a_0(t) a_k(t-\tau) dt \qquad \text{for} \qquad 0 \leq \tau \leq T \tag{3.3a}$$

$$\widehat{R_k}(\tau) = \int_{\tau}^{T} a_0(t) a_k(t-\tau) dt \qquad \text{for} \qquad 0 \leq \tau \leq T \tag{3.3b}$$

τ is the delay between the users, and $[I_{-1}^k, I_0^k]$ is the pair of symbols sent by user k in $[0, T]$. For $0 \leq lt_c \leq \tau \leq (l+1)T_c \leq T$, the crosscorrelation functions can be expressed as:

$$R_k(\tau) = C_{k,0}(l-N)T_c + \left[C_{k,0}(l+1-N) - C_{k,0}(l-N)\right](\tau - lT_c) \tag{3.4}$$

$$\widehat{R_k}(\tau) = C_{k,0}(l)T_c + [C_{k,0}(l+1) - C_{k,0}(l)]\,(\tau - lT_c) \tag{3.5}$$

where the discrete aperiodic crosscorrelation function $C_{k,0}(n)$ for the sequences $a_0(t)$ and $a_k(t)$ is defined by:

$$C_{k,0}(n) = \begin{cases} \sum_{j=0}^{N-1-n} a_j^k a_{j+n}^0 & 0 \le n \le N-1 \\ \sum_{j=0}^{N-1+n} a_{j-n}^k a_j^0 & -(N-1) \le n \le 0 \\ 0 \quad \text{else} & \end{cases} \tag{3.6}$$

The periodic crosscorrelation $\theta_{k,0}(l)$ is defined by:

$$\theta_{k,0}(l) = \sum_{j=0}^{N-1} a_j^0 a_{j+l}^k \tag{3.7}$$

Notice that $\theta_{k,0}(l) = C_{k,0}(l) + C_{k,0}(l-N)$ for $0 \le l \le N$. The odd crosscorrelation is defined by $\widehat{\theta}_{k,0}(l) = C_{k,0}(l) - C_{k,0}(l-N)$. We notice from Eqn(3.2) that when the interfering bits are equal, i.e. $I_{-1}^k = I_0^k$ we simply have:

$$z^k = I_0^k \left[\theta_{k,0}(l)T_c + \left(\theta_{k,0}(l+1) - \theta_{k,0}(l)\right)(\tau - lT_c)\right] \mathrm{Cos}(\phi_k) \tag{3.8}$$

The above functions are the main parameters needed in studying CDMA systems. We will now present their specific values for specific codes that will be used in the following chapters.

A) M-sequences

Maximal-length sequences (M-sequences) are probably the most widely known pseudorandom sequences. A binary shift-register with n stages cannot generate sequences whose period will exceed $N = 2^n - 1$. If the period of the sequence is effectively N, the sequence is an M-sequence and $h(x)$, its generator polynomial of degree n, is termed a primitive polynomial. A sequence $a(x)$ is said to be generated by $h(x)$ if for all integers j:

$$h_0 a_j \oplus h_1 a_{j-1} \oplus h_2 a_{j-2} \oplus \cdots \oplus h_n a_{j-n} = 0 \tag{3.9}$$

where $\oplus$ denotes modulo 2 addition. Replacing j by $j+n$ and using the fact that $h_0 = 1$ we have:

$$a_{j+n} = h_n a_j \oplus h_{n-1} a_{j+1} \oplus \cdots \oplus h_1 a_{j+n-1} \tag{3.10}$$

In this thesis, $N = 255$ is one of the code length used. To obtain a large set of sequences with a good crosscorrelation property one can use a well-known theorem [28]. Since $N = 2^8 - 1$, $n = 8$ and is a multiple of 4, with the sequence $\mathbf{b} = a(-1 + 2^{(n+2)/2})$, where $a(s)$ is the decimation of the sequence $\mathbf{a}$ by s, the periodic crosscorrelation $\theta_{a,b}$ has a four-valued spectrum:

$$\begin{array}{rll} -1 + 2^{(n-2)/2} & \text{occurs} \quad \dfrac{2^{n-1} - 2^{(n+2)/2}}{3} & \text{times} \\ -1 + 2^{n/2} & \text{occurs} \quad 2^{n/2} & \text{times} \\ -1 & \text{occurs} \quad 2^{n-1} - 2^{(n-2)/2} - 1 & \text{times} \\ -1 - 2^{n/2} & \text{occurs} \quad \dfrac{2^n - 2^{n/2}}{3} & \text{times} \end{array} \tag{3.11}$$

For $N = 255$, the values taken by the crosscorrelation are $\{31, 15, -1, -17\}$. The code set contains 257 sequences for which any pair of sequence will have the cross-correlation in (3.11). These sequences are simply:

$$G(a,b) = \{a, b, a \oplus b, a \oplus Tb, a \oplus T^2 b, \cdots, a \oplus T^{N-1} b\} \tag{3.12}$$

where T^j is the operator which shifts vectors cyclically to the left by j places. For our computations the generator polynomial H in octal is given by $H = 435$, and $\mathbf{b} = a(31)$.

B) Gold codes

When $n \neq 0 \bmod 4$, there exist pairs of M-sequences with three-valued croscorrelation functions, where the three values are $\{-t(n), -1, t(n) - 2\}$, with:

$$t(n) = 1 + 2^{\lfloor (n+2)/2 \rfloor} \tag{3.13}$$

where $\lfloor x \rfloor$ is the integer part of the real number x. The number of occurences is given by:

$$\begin{array}{rlll} t(n)-2 & \text{occurs} & 2^{n-2}+2^{(n-3)/2} & \text{times} \\ -1 & \text{occurs} & 2^{n}-2^{n-1}-1 & \text{times} \\ -t(n) & \text{occurs} & 2^{n-2}-2^{(n-3)/2} & \text{times} \end{array} \qquad (3.14)$$

Let $\{a, b\}$ denote a preferred pair of M-sequences of period $N = 2^n - 1$ generated by the primitive polynomials $h(x)$ and $\widehat{h}(x)$, respectively. Then the set of $N + 2$ sequences given in (3.12) is a set of Gold codes, and any pair in the set has the three-valued crosscorrelation given above. Every code in the set can be generated by the polynomial $f(x) = h(x)\widehat{h}(x)$. In our computations we will use Gold codes for $N = 63$, $N = 127$ and $N = 511$, with the following parameters:

$$\begin{array}{lll} N = 63 : H = 103 & \widehat{H} = 147 & \theta(l) \in \{-17, -1, 15\} \\ N = 127 : H = 211 & \widehat{H} = 217 & \theta(l) \in \{-17, -1, 15\} \\ N = 511 : H = 1021 & \widehat{H} = 1131 & \theta(l) \in \{-33, -1, 31\} \end{array} \qquad (3.15)$$

C) Small set of Kasami sequences

For $N = 255$, one can obtain a small set of $2^{n/2} = (N+1)^{1/2} = 16$ sequences called small set of Kasami sequences. For these sequences the crosscorrelation function is also three-valued, these values being $\{-s(n), -1, s(n) - 2\}$, with:

$$s(n) = 1 + 2^{n/2} = \frac{1}{2}\left(t(n) + 1\right) \qquad (3.16)$$

For $N = 255$ we have $\theta(l) \in \{-17, -1, 15\}$, which is smaller than the values obtained by combining M-sequences, as in A). However, the number of sequences is small and when one considers the large set of Kasami sequences, the same values for the crosscorrelation as in A) are obtained. The small set of Kasami sequences will therefore only be sparsely used in this work. The generator polynomial in octal will be $H = 11367$.

3.3 Kronecker sequences

In this section, we consider the correlation properties of sets of sequences in which each sequence is constructed by taking the Kronecker product of two short sequences [29]. The interest for these sequences for electronics systems has been quite moderate since their correlation properties are usually not as good as the other sequences considered previously. However, they will allow the design of very simple encoder and decoder architectures for optical CDMA, as we will show in the next chapter. To our knowledge they have never been considered so far for optical CDMA.

Let us consider two sequences $\mathbf{u}$ and $\mathbf{v}$ constructed as follows. Let $\mathbf{x}$ and $\mathbf{y}$ be sequences of length N_i, and $\mathbf{d}$ and $\mathbf{e}$ be sequences of length N_0, then:

$$u_k = d_l \times x_m \qquad k = lN_i + m, \qquad \begin{array}{l} 0 \leq l \leq N_0 - 1 \\ 0 \leq m \leq N_i - 1 \end{array} \tag{3.17a}$$

$$v_k = e_l \times y_m \qquad k = lN_i + m, \qquad \begin{array}{l} 0 \leq l \leq N_0 - 1 \\ 0 \leq m \leq N_i - 1 \end{array} \tag{3.17b}$$

Sequences $\mathbf{u}$ and $\mathbf{v}$ are of length $N = N_0 N_i$ and can be thought as being the Kronecker product of $\mathbf{d}$ with $\mathbf{x}$ and $\mathbf{e}$ with $\mathbf{y}$, respectively. As an example, if $\mathbf{d} = (+\mathbf{1}, +\mathbf{1}, -\mathbf{1})$, and $\mathbf{x} = (+\mathbf{1}, -\mathbf{1}, +\mathbf{1}, +\mathbf{1})$ then

$$\mathbf{u} = (+\mathbf{1}, -\mathbf{1}, +\mathbf{1}, +\mathbf{1}, +\mathbf{1}, -\mathbf{1}, +\mathbf{1}, +\mathbf{1}, -\mathbf{1}, +\mathbf{1}, -\mathbf{1}, -\mathbf{1}) \tag{3.18}$$

Sequences $\mathbf{d}$ and $\mathbf{e}$ will be called the outer sequences, while sequences $\mathbf{x}$ and $\mathbf{y}$ will be called the inner sequences. The advantage of using these sequences in the context of optical CDMA systems can be seen by noting that all the bits in $\mathbf{x}$ are successively encoded by the same bit of $\mathbf{d}$. It can be shown that the periodic and odd crosscorrelations for sequences $\mathbf{u}$ and $\mathbf{v}$ are given by:

$$\theta_{\mathbf{u},\mathbf{v}}(k) = \theta_{d,e}(l)C_{x,y}(m) + \theta_{d,e}(l+1)C_{x,y}(m - N_i) \tag{3.19}$$

$$\widehat{\theta}_{\mathbf{u},\mathbf{v}}(k) = \widehat{\theta}_{d,e}(l)C_{x,y}(m) + \widehat{\theta}_{d,e}(l+1)C_{x,y}(m - N_i) \tag{3.20}$$

If $\mathbf{d}$ and $\mathbf{e}$ are chosen to be Gold codes, we have for many l values that $\theta_{d,e}(l) = \theta_{d,e}(l+1)$, so that $\theta_{u,v}(k) = \theta_{d,e}(l)\theta_{x,y}(m)$. Suppose now that $\mathbf{x}$ and $\mathbf{y}$ are such that $\theta_{x,y}(m) = 0$ for N_i^* values of m, $(N_i^* < N_i)$. In this case, it appears that $\mathbf{u}$ and $\mathbf{v}$ will be uncorrelated sequences for many k values. For example, let $\mathbf{x} = \mathbf{y} = (1, 1, -1, 1)$ be the Barker sequence of length 4; in this case $\theta_{x,y}(m) = 0\, for\, m \neq 0$. It can also be seen that if $\mathbf{d}$ and $\mathbf{e}$ are chosen to be Barker sequence, instead of $\mathbf{x}$ and $\mathbf{y}$ then:

$$\theta_{u,v}(k) = \begin{cases} 4C_{x,y}(m) & l = 0 \\ 0 & l = 1, 2 \\ 4C_{x,y}(m - N_i) & l = 3 \end{cases} \tag{3.21}$$

It is therefore desirable, when using Kronecker sequences, to have as inner sequences perfect autocorrelation sequences. When different users have different cycle-shifts of such sequences, the periodic crosscorrelation would be zero for many values of the delay τ. In the next section we present some possible choices for perfect autocorrelation sequences.

3.4 Perfect Autocorrelation Sequences

Perfect autocorrelation sequences are periodic sequences such that all of the out-of-phase autocorrelation coefficients are zero

$$\theta_{a,a}(l) = \sum_{i=0}^{N-1} a_i a_{i+l} = 0 \qquad \text{for} \qquad l \neq 0 \tag{3.22}$$

In the case of binary sequences, where each chip takes the values $(-1, 1)$, it has been proven that there is no solution if $4 < N \leq 12100$, and for $N = 4$ the sequence is the Barker sequence given previously. One possibility is to use Almost Perfect Autocorrelation (APA) sequences as designed in [30], for which all the out-of-phase autocorrelation coefficients are zero except one. Another solution is to use perfect *ternary* autocorrelation sequences, where each chip $a_j \in \{-1, 0, 1\}$. One thing to take into account is the implementation practicality for optics. Binary chip ± 1 requires simple phase modulation of the laser. Chips taking on values $\{-1, 0, 1\}$ are also easily implementable by using combined phase and intensity modulations by an external phase modulator. Multilevel complex perfect autocorrelation sequences can be designed in many ways, but will be unsuitable for optical systems because of the difficulty in the implementation. The stability requirements for the optical processing elements such as the optical encoder/decoders would also be very difficult to obtain.

In our work, we will consider almost perfect binary autocorrelation sequences designed in [30], and perfect ternary autocorrelation sequences. We now review one of the simplest techniques for designing such sequences. Other techniques can be found in [31]. Let $\mathbf{x}$ and $\mathbf{y}$ denote sequences of period N, such that $\theta_{x,x}(l) = A_x$ if $l = 0 \bmod N$ and $\theta_{x,x}(l) = B_x$ otherwise, and that $\theta_{y,y}(l) = A_y$ if $l = 0 \bmod N$ and $\theta_{y,y}(l) = B_y$, otherwise. Then the autocorrelation function $\theta\left[\theta_{x,y}(l)\right]$ for the *sequence* $\theta_{x,y}(l)$ is given by:

$$\theta\left[\theta_{x,y}(l)\right] = \begin{cases} A_xA_y + (N-1)B_xB_y & l = 0 \bmod N \\ A_xB_y + A_yB_x + (N-2)B_xB_y & l \neq 0 \bmod N \end{cases} \tag{3.23}$$

When $\mathbf{x}$ and $\mathbf{y}$ are M-sequences, $A_x = A_y = N$ and $B_x = B_y = -1$. Furthermore, if they form a preferred-pair, the crosscorrelation function is three-valued $\theta_{x,y}(l) \in \{-t(n), -1, t(n)-2\}$. It can be seen then that the sequence $\theta_{x,y}(l) + 1$ will be a balanced, ternary sequences. Dividing each element by $t(n) - 1$, we obtain a simple way to get ternary (-1,0,1) sequences of length N. The important point is that it can be proven [32] that the sequence $\theta_{x,y}(l)+1$ is a perfect autocorrelation sequence. We now give an example.

Let $N = 7$, and x and y be the two M-sequences $x = \{-1,-1,-1,1,-1,1,1\}$ and $y = \{-1,1,1,-1,1,-1,-1\}$. The sequence $\theta_{x,y}(l)$ then has values $\{-5,-1,3\}$. The sequence $\theta_{x,y}(l) + 1$, divided by 4 is the following ternary sequence $\theta_{x,y} + 1 = \{-1,0,0,1,0,1,1\}$. We will use this sequence in our computation in the following chapters. Another useful ternary sequence of length $N = 6$, having higher energy efficiency (less 0's) is given by $\{1,0,-1,1,0,1\}$.

3.5 Unipolar Sequences

The use of bipolar codes is straightforward in electronics CDMA systems since the oscillators used have no, or negligable, phase noise and can be easily phase modulated. In optics, although many kinds of lasers used as transmitters have now a long coherence time, such as DFB lasers or mode-locked lasers, limitations to using the phase as an information parameter can arise from the optical processing elements in the systems, such as the encoder/decoder or the nonlinear optical gates. As we will discuss in the next chapter, processing elements, now built in waveguides, have the required stability for allowing the phase information to be used. However, in situations where the source is too noisy, or simply when the stability requirements cannot be met, bipolar codes as presented before are not directly usable. As mentioned in the previous chapter, many researchers directed their efforts to design new (0,1) codes where the power level is of concern only, and therefore are suitable for positive systems.

We propose an alternative which is a simple Manchester, or 2-PPM, encoding of standard bipolar codes. Consider a bipolar code $U = (u_0, u_1, \cdots, u_{N-1})$ for which each chip is mapped into $(1,0)$ if $u_j = 1$ and $(0,1)$ if $u_j = -1$. The unipolar code obtained is denoted as U^p. A balanced receiver is required for the unipolar codes to have the same crosscorrelation properties as the bipolar ones. At the receiver, the interfering signals coincident with a "1" ("0"), of the intended sequence, have to be routed to a positively (negatively) biased detector. Efficient architectures for doing this without optical switches working at the chip rate are presented in the next chapter. For unipolar codes, $\theta_{u^p,v^p}(l)$ has to be considered for $l = 0, 1, \cdots, 2N$, while for real bipolar codes, l goes from 0 to $N-1$. The periodic crosscorrelation for unipolar codes is written as:

$$\theta_{u^p,v^p}(l) = \sum_{i=0}^{2N-1} u_i^p v_{i+l}^p - \sum_{i=0}^{2N-1} (1 - u_i^p) v_{i+l}^p \tag{3.24}$$

It is easy to see that for l even, this is equivalent to the periodic crosscorrelation obtained between bipolar codes. However, for l odd, the values obtained slightly differ since u_i^p and v_{i+l}^p originate from different "bipolar" chips. As an example, for a Gold code of period $N = 127$, $\theta_{u^p,v^p}(l) = (\pm 1, -7, 9, \pm 15, \pm 17)$ while for the real bipolar case $\theta_{u,v}(l)$ is three-valued $(15, -1, -17)$. The maximum value is the same in both cases, so it can be expected that the BER performance should be similar. It will be shown in Chapter 6 that this is effectively the case. We show on Fig. 3.1 the periodic crosscorrelation obtained for the unipolar and bipolar codes, as a function of l, for a Gold code with $N = 127$.

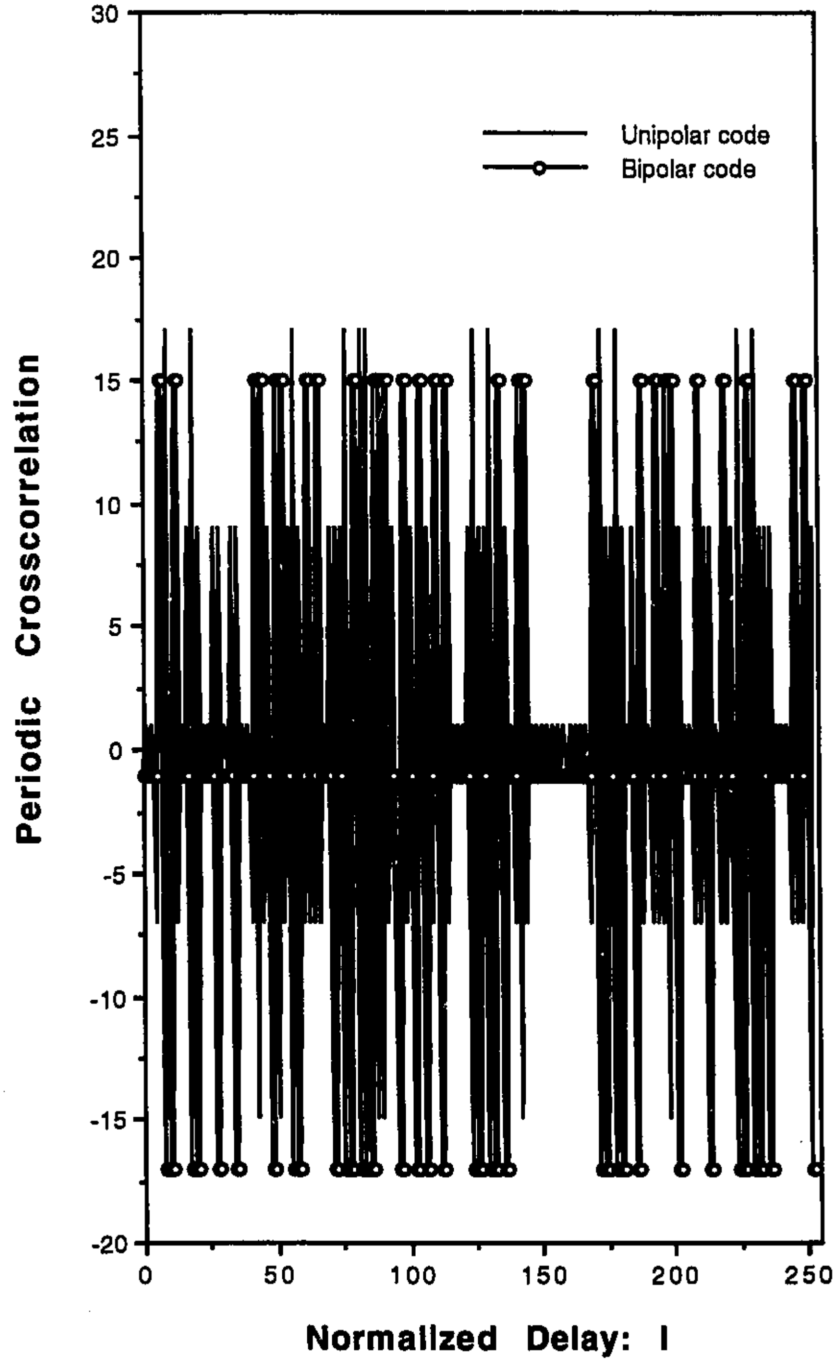

Fig.3.1: Comparison of the periodic crosscorrelation for unipolar and bipolar codes; Gold code, N=127.

3.6 Summary

In this chapter we reviewed the basic properties of some class of codes that will be used in this thesis, such as M-sequences, Gold codes and Kasami sequences. Kronecker sequences were discussed since they will find an important application in the architecture design of the encoders and decoders in the following chapter. Perfect, or almost perfect autocorrelation sequences were shown to be a good choice as the inner sequences in the construction of Kronecker sequences. We therefore reviewed a simple technique to obtain perfect ternary autocorrelation sequences. Finally, we showed a simple way to use bipolar codes in positive systems, based on a 2-PPM encoding of each chip. Efficient decoding architectures, that do not require fast optical switches, for unipolar codes, are presented in the next chapter.

Chapter 4

New Architectures for Bipolar Optical CDMA

4.1 Introduction

In this chapter, we propose several architectures for using bipolar codes in optical CDMA systems, that require only direct detection. We show that combining E/O elements and all optical processing elements allow the use of arbitrary bipolar sequences while requiring a small number of delay lines. The encoder/decoder architectures are such that the crosscorrelation properties of the codes are maintained, although requiring only direct detection. We also propose the use of Kronecker sequences in order to simplify the designs. We show that when the subscribers use Kronecker sequences, and share the same inner sequence, programmability of the delay lines is not required, which allows simple encoder/decoder architectures. We then modify the proposed architectures so they can be used with incoherent sources, and incoherent optical processing elements. Although the optical sources can now be only modulated in power, we show that bipolar codes can still be used, and that their properties are maintained.

4.2 A General Bipolar CDMA System

To use the bipolar codes in a CDMA system, one can simply copy the architecture employed in the electronic domain. However, since a photodetector responds only to the power of an optical incident signal, and discards all the phase information, coherent detection as used in optical FDM systems is required. The correlation is then donc in the electronic domain and a variety of modulation types can be used such as PSK or DPSK. Such systems were studied in [14-15]. Since the receiver architecture is the same as in FDM systems, hybrid FDMA-CDMA is a natural extension.

A CDMA system with coherent detection would however face the same complexity as an FDM system. A good alternative is to choose a hybrid WDMA-CDMA system. In such cases, multiple groups of users would typically be wavelength multiplexed with a wavelength spacing larger than 1 nanometer, and separated at the receiver by an optical filter. Multiple users can then share a single-carrier wavelength by using their own unique code. The system diagram is shown in Fig. 4.1. At the transmitter, the laser is phase modulated by the bipolar pseudorandom code by a simple E/O phase modulator. The signal is then broadcast to each receiver by a star coupler. At the receiver, a phase modulator is used to despread the intended signal. Perfect time synchronization is required between a pair of communicating users. At this point in the system, the interfering users are spread in frequency due to the phase modulation by the sequences, and the use of an optical filter is essential to reject most of the interfering power. This is in contrast with incoherent CDMA systems in which the correlation could be as well done in the electronic domain, but where encoder/decoders made of optical delay lines are usually used to take advantage of the fiber bandwidth.

If ten users can share a wavelength, the concurrency of the system would be multiplied by ten, with no need for more precise tuning from the optical sources, or for increased tuning capability of the optical filter. The system shown in Fig. 4.1.

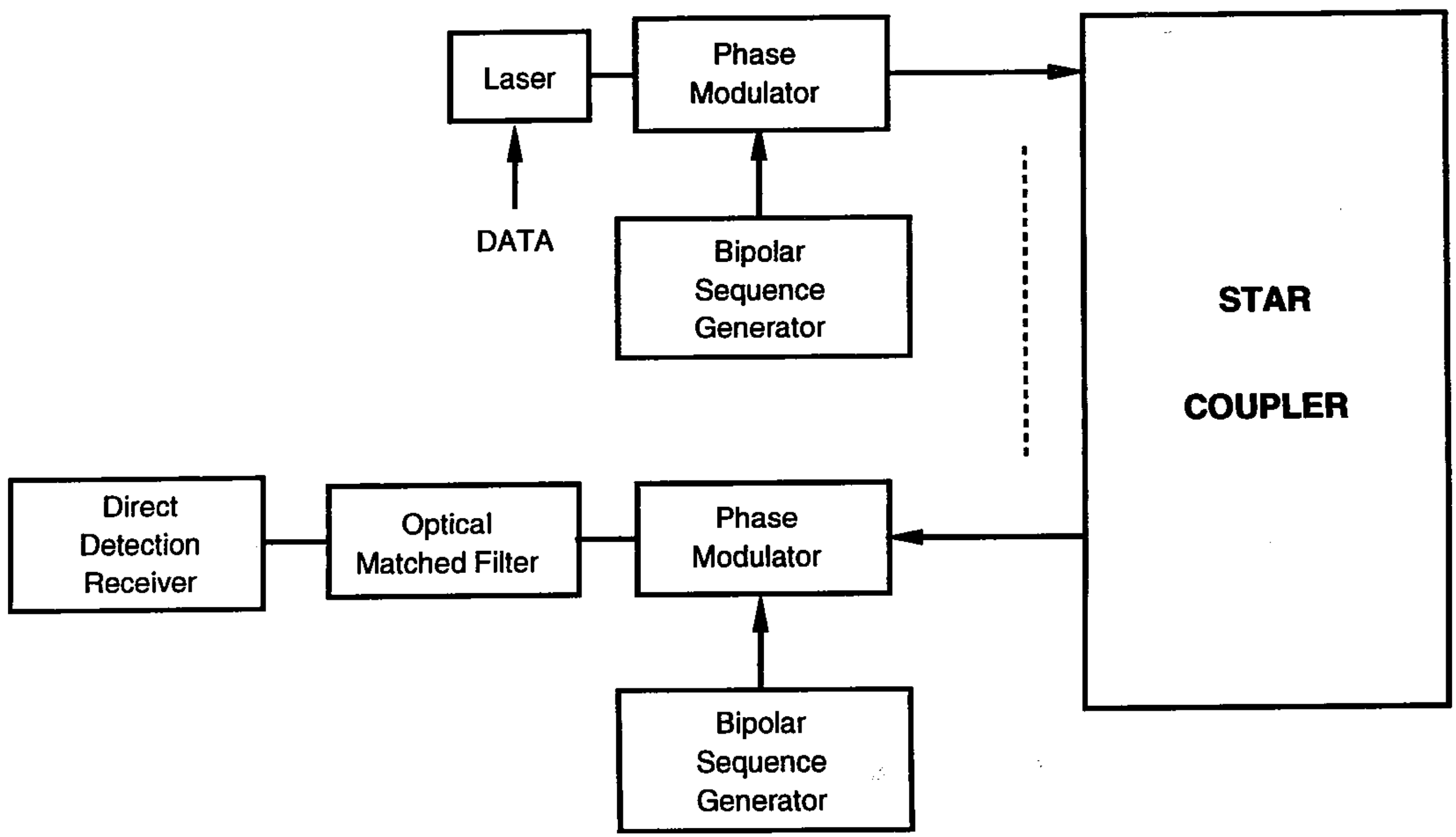

Fig.4.1: Conceptual diagram for an optical bipolar CDMA system using direct detection

was first proposed in [33], and experimental spreading, despreading using phase modulators was demonstrated in [34]. The main requirements for such a system are:

1) Good carrier frequency stabilization and small spectral linewidth for the optical source;

2) The optical filter must act as an optical matched filter;

The first requirement comes from the fact that if the carrier frequency of the incoming intended signal is unstable, it could be detuned compared to the optical filter central frequency. The phase noise should be small as it would degrade the system performance. Optical sources having these characteristics will be called in this thesis *coherent optical sources*, and the associated CDMA systems, *coherent CDMA systems*, although only direct detection receivers are used. The correlation must be done optically, and an optical filter with the $\sin x/x$ shape must be found, assuming a rectangular pulse shape. This is discussed in the next section.

We believe that the main limit for the system to be attractive is from the speed of the E/O phase modulators. The bandwidth limit for these devices, as well as the electronics to drive them is around 10 Gbit/s, and the spreading gain will be constrained to values between 100 and 250, for bit rates ranging from 100 Mbit/s to 40 Mbit/s. Efficient means to either increase the bit rate for a given code length, or to increase the code length for a fixed bit rate are needed. Our main contributions in this chapter are as follows. We first present different solutions to the speed-limit problem, and we then remove the requirement for coherent sources by proposing architectures for unipolar codes.

4.3 Optical Matched Filters

An optical matched-filter can be approximately realized by cascading Mach-Zender interferometers, as shown in Fig. 4.2b. A k stage filter has a frequency response given by:

$$H(f) = \prod_{i=1}^{k} \cos\left(2^{-i}\pi fT\right) = \frac{\sin(\pi fT)}{2^k \sin(2^{-k}\pi fT)} \tag{4.1}$$

In Fig. 4.3, we compare this frequency response for a $k = 3$ stage filter with a truely matched-filter with transfer function:

$$H_M(f) = \frac{\sin(\pi fT)}{\pi fT} \tag{4.2}$$

The approximate filter is almost ideal for $|fT| \leq 3$, which is where the signal energy lies for the desired signal. However, because the filter is periodic with a period $2^k/T$, special attention must be given to the spreaded interfering signals. For a code period $N = 512$, $k = 9$ stages are needed to remove most of the interfering power. One implementation had $k = 7$ [35] and $T = 0.1$ns, so $k = 9$ is realistic. As mentioned in [36], another filter with double-sided bandwidth $2^{k+1}/T$ should be cascaded with the matched-filter to remove the periodic peak at $f = 2^k/T$. At $\lambda = 1.5\mu$m and for $k = 10$, $1/T = 100$ Mbit/s, the bandwidth needed is $1.5nm$, which is easily achieved, for example, by using Fabry-Perot filters.

Silica-based integrated cascaded Mach-Zenders were first used for coarse multi-demultiplexer for FDM systems, and more recently [37], as a time multiplexer for TDM systems. Let consider Fig. 4.2b. When a single input pulse of amplitude A and duration Tc, Tc being the chip duration, is launched at the input, the output is a train of non-overlapping output pulses of amplitude $A/2^n$, spaced by $T/2^n$, which is taken to be Tc. *There is no losses other than the insertion losses.* There is no recombination losses when the sources are coherent. The same function can be achieved by cascading 3-dB couplers, as shown in Fig. 4.2c. However, in this case there is an intrinsic 3 dB loss. We note that this last architecture is proposed in some cases for optical CDMA encoders/decoders, for example [38], and is usually called ladder networks. However, due to the symmetry of the architecture, only specially designed codes can be accommodated. To our knowledge, the design of such codes is only in the early stage, and their efficiency is still to be proved. Due

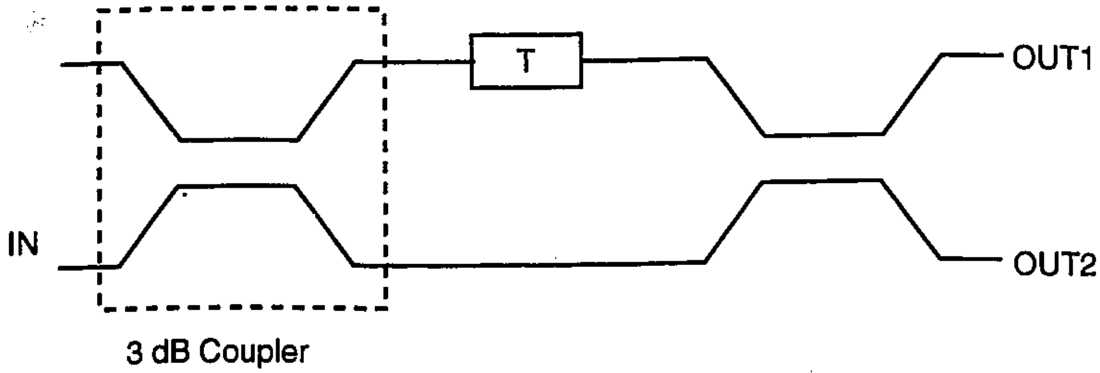

Fig.4.2a: Ideal single stage Mach-Zender filter
with differential delay T.

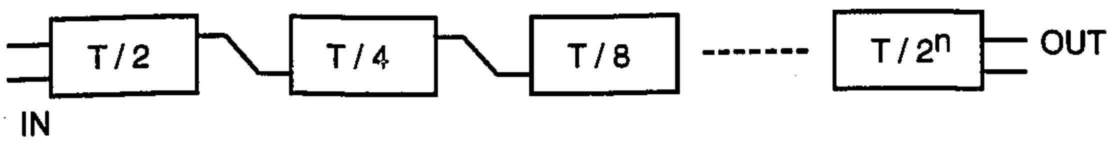

Fig.4.2b: Optical matched-filter from an n stage cascaded MZ.

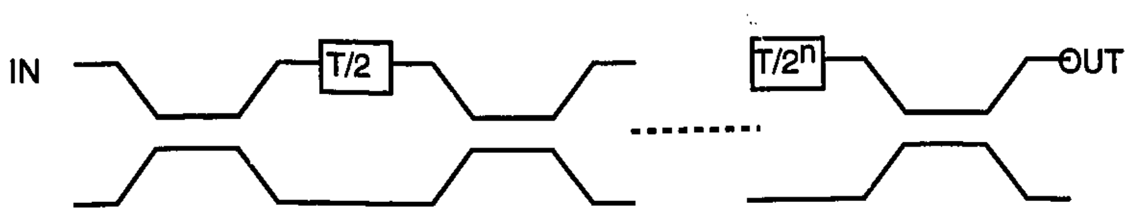

Fig.4.2c: Optical matched-filter by cascading n 3-dB couplers.

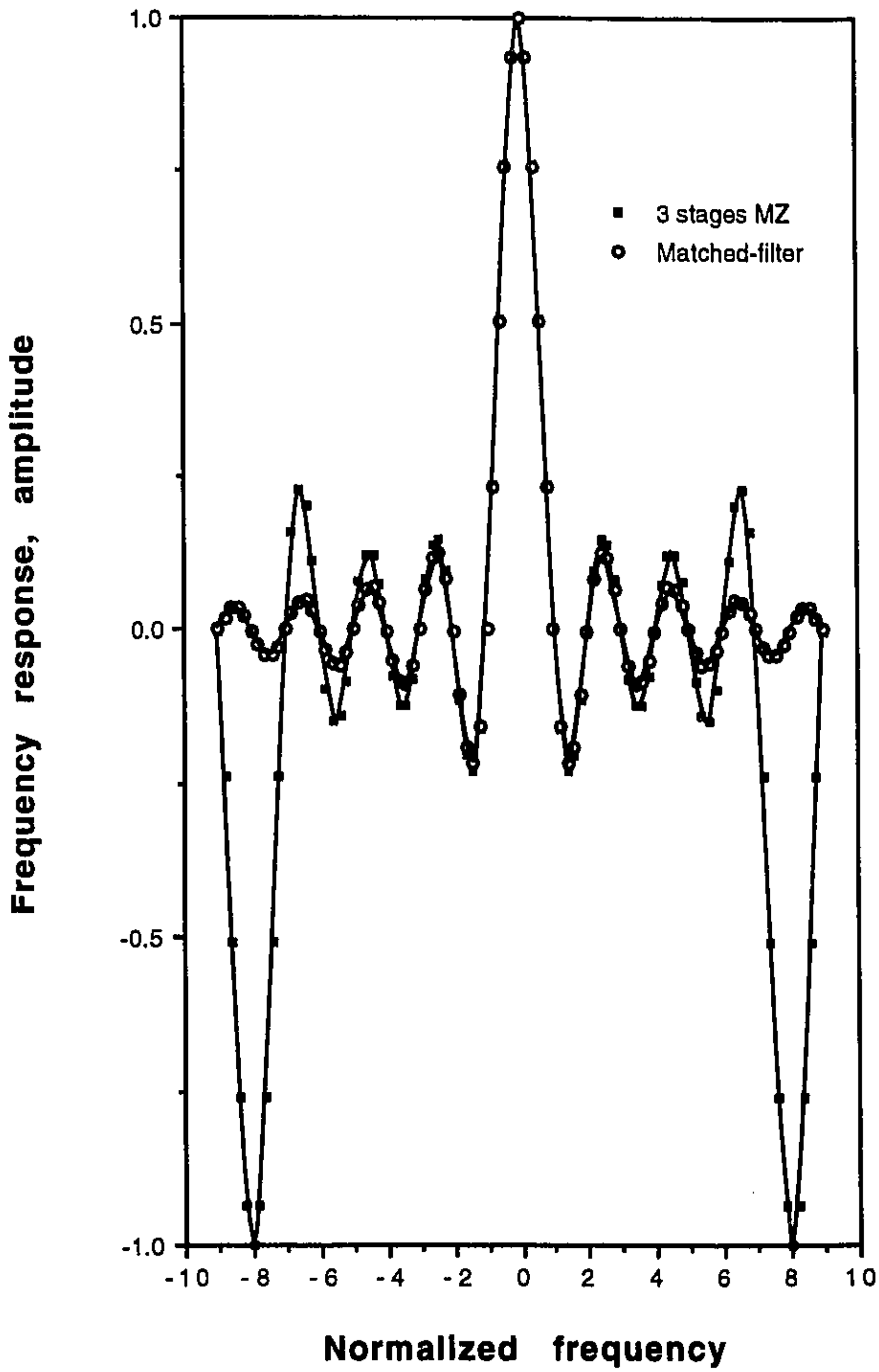

Fig.4.3: Frequency response of a 3-stage cascaded MZ vs real matched-filter response.

to the symmetry of the structure, we note that the class of codes and the number of codes in a given set could be severly limited.

In our opinion, it is better to separate the matched filtering operation from the encoding/decoding ones. We will show that this allows completely arbitrary codes to be used. In the next section, we present efficient architectures for coherent optical sources.

4.4 Architectures for Coherent Optical Sources

4.4.1 Encoders for Continuous-wave Sources

When using continuous-wave optical sources, a simple way to increase the code length for a given bit rate is illustrated in Fig. 4.4a. Assume P phase modulators are cascaded in serie. Different sequences drive each of them. This would be done by using a single dielectric waveguide of appropriate length, to which a serie of P electrodes is applied. When each sequence has a period N_a and a chip duration T_a, the resulting sequence at the output of the phase modulators has a chip duration $T_a/P = T_c$, provided that the modulating voltages are properly synchronized. The length of that sequence is $N = N_a \times P$ so that the bit rate is still $1/(N_a T_a)$. For example, using 3 cascaded phase modulators, and 10 GHz electronics, a code length $N = 3 \times 341 = 1023$ is achieved for a bit rate of 29.3 Mbit/s. It should be noted that a delay of T_c must be obtained between the modulating sequences. We believe the easiest way of doing so is to synchronize the applied voltages, while leaving a waveguide length $\delta L = cT_c/n$ between the phase modulators.

Alternatively, instead of increasing the code period, one can increase the bit rate by using the same configuration but designing the codes in a different way. We believe the principal drawback of the above technique is, for the resulting sequence to be a Gold or Kasami sequence, the basic sequences $a_1(t), a_2(t), ...$ could probably not be generated by shift registers.

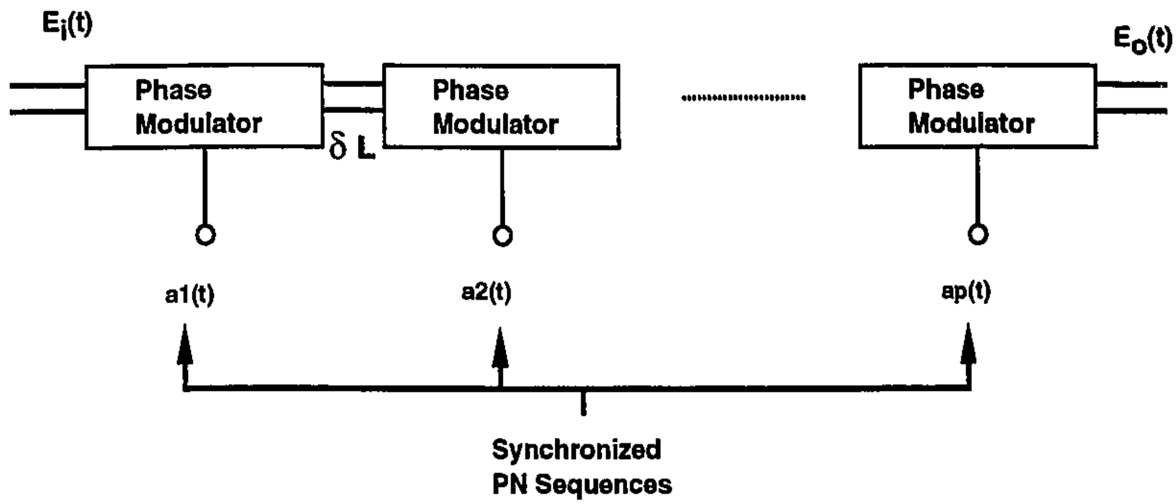

Fig.4.4a: Cascaded Phase Modulators.

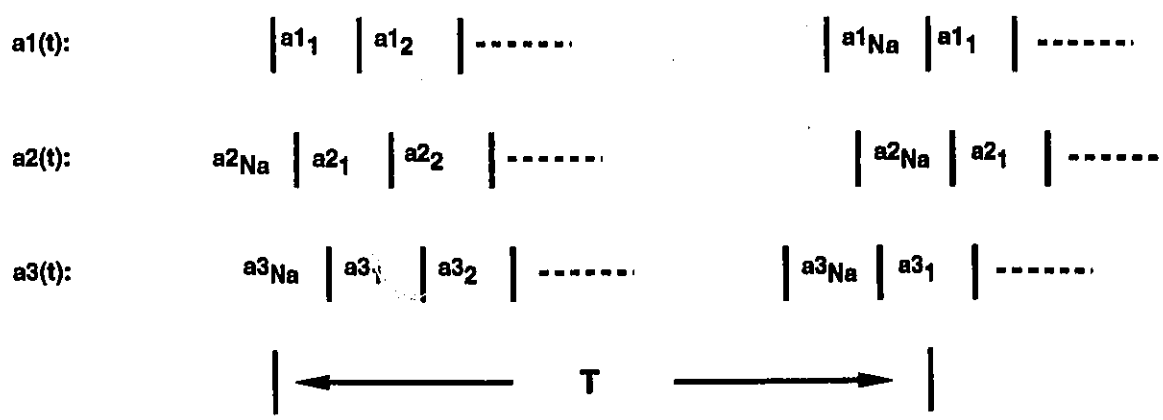

Fig.4.4b: Schematic of the sequences for P=3

4.4.2 Encoders for Short Optical Pulses

With the development of mode-locked lasers capable of generating picosecond and femtosecond pulses, ultrafast code-division multiple access systems become feasible. Consider for example a mode-locked laser delivering pulses of width Tc at a repetition rate R. Taking R as being the bit rate, a code length $N = 1/(RTc)$ is theoretically feasible. Since R is in the range of Mbit/s to low Gbit/s, and Tc takes values from a couple of picoseconds to hundreds of femtoseconds, a processing gain of 1000 to 10000 appears possible, but certainly the question is how it can be achieved. Production of hundreds of pulses from a single pulse, all of them being independently phase modulated is a challenging task.

We believe an efficient technique to achieve a high spreading gain for bipolar CDMA systems is by proper combination of electro-optic components and coherent all optical delay lines. Electro-optic components such as modulators are being extensively used and studied as demultiplexers for optical time-division multiplexed networks [39]. However, they seem to have been overlooked for CDMA systems, researchers generally looking for *pure* optical techniques. On the other hand, coherent optical transversal filters, with a number of taps up to 16 have been developed for highly-selective FDMA systems. Such integrated waveguides keep the phase information of the optical signals so that they seem very well suited for bipolar CDMA systems. We now show how to combine E/O components and coherent transversal filters to obtain fast phase modulation of optical pulses. Later on, we improve the design by using special codes known as Kronecker sequences.

In Fig. 4.6, a train of pulses of width Tc, with a period T is first split into $P = T/Tc$ branches. The variable T represents the period of the mode-locked pulses and will not usually be the bit period Tb. We take $Tb/T = K$, and therefore the total code length is given by $Tb/Tc = K\,P$. The P obtained pulses are independently phase modulated by P electro-optic modulators driven by independent sequences. All the branches are then recombined with a delay of Tc between each of them. The resulting signal is a train of pulses phase modulated at a rate of $1/Tc$ while using electronics at a frequency $1/T$, that is at a P-fold increase. In order to see how the phase relationship can be maintained among all the pulses in the different branches, we show in Fig. 4.5 a coherent optical transversal filter, acting also as a 1×4 splitter followed by a 4×1 combiner. This design is from [40], where it was proposed for dense FDMA systems and was experimentally demonstrated. The use of coherent optical sources, combined with the ability of changing the phase of the signals in the different branches allow the filter to be free of losses (other than insertion losses). Silica-based integrated-optic devices are needed for precise delay control. In [40], phase shifters are incorporated in each arm to provide a continuous phase change capability, and therefore to express arbitrary impulse responses. A phase shifter is a waveguide with a thin-film heater attached to it. The thermo-optic effect changes the carrier phase of the optical signal. For silica glass, the change in the refractive index with temperature is $\frac{\delta n}{\delta T^o} = 10^{-5}$ so that a 5mm waveguide heated by 30°C causes a phase shift of 2π for $1.5\mu m$ signals [41]. Phase shifters are also necessary to compensate for path length differences in the filter.

Instead of using the thermo-optic effect, one can use the faster electro-optic effect, as shown in our architecture of Fig. 4.6. We note that recently, IBM has also been working on combining coherent transversal filters and the E/O effect to obtain fast tunable optical filters for FDM applications [42]. In order to see what realistic values are for T, Tc and P, let us consider a numerical example. We want the repetition rate of the mode-locked pulses ($1/T$) to coincide with the bandwidth capacity of the electro-optic phase modulators, so we need $1/T \approx 5 - 10\,GHz$. The number of branches in the coherent transversal filter should be equal to T/Tc. A sixteen branch filter was experimentally demonstrated, so if we take $T = 1/10\,GHz = 100\,ps$, we need $T_c = 100\,ps/16 = 6.25\,ps$. With the above chip period and with a bit rate of 100 Mbit/s, this gives an impressive spreading gain of 1600, or $N = 160$ for a bit rate of 1 Gbit/s.

The principal drawback with the design described above is the number of phase

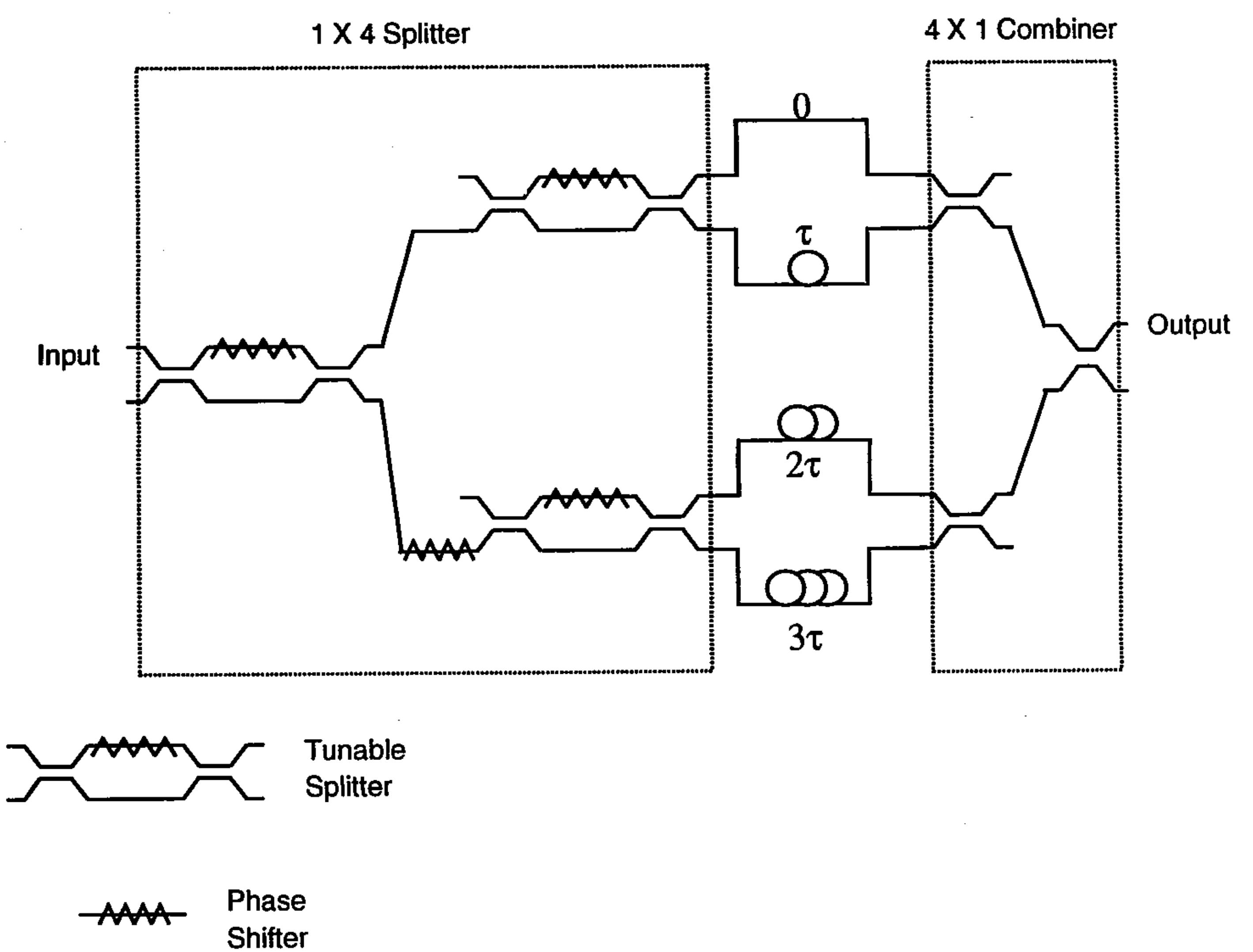

Fig.4.5: A coherent transversal filter with 4 taps

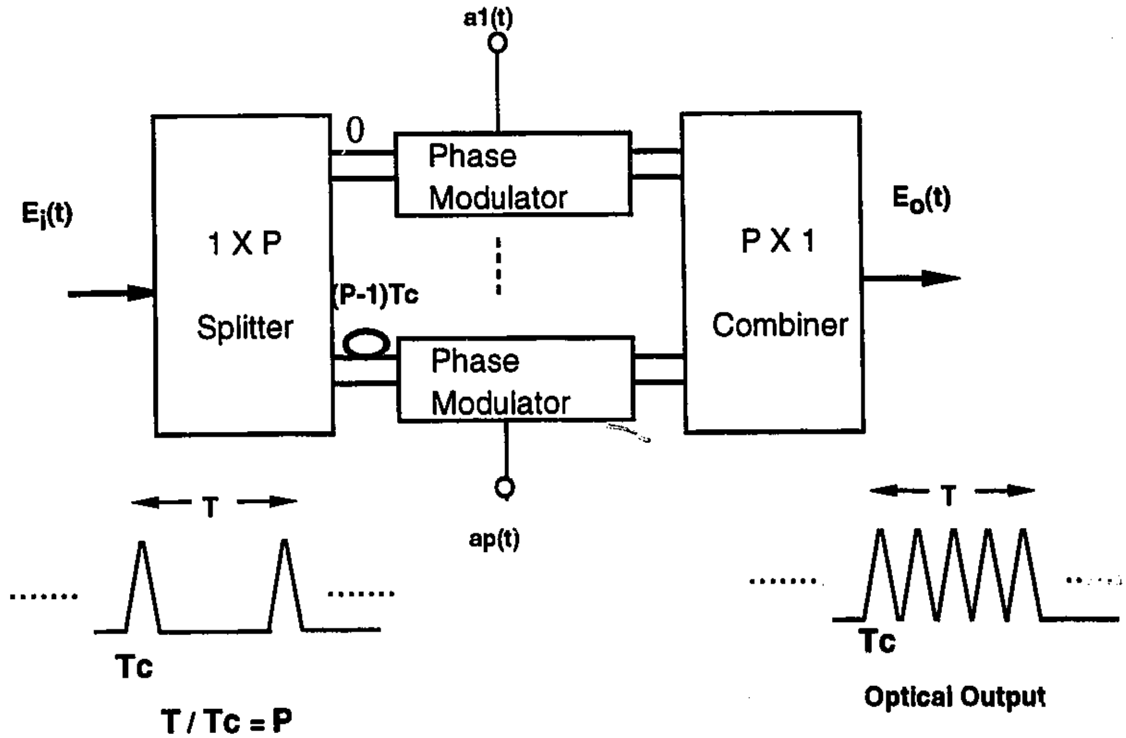

Fig.4.6: Encoder for coherent optical sources and arbitrary sequences, using a P-branch programmable, coherent transversal filter.

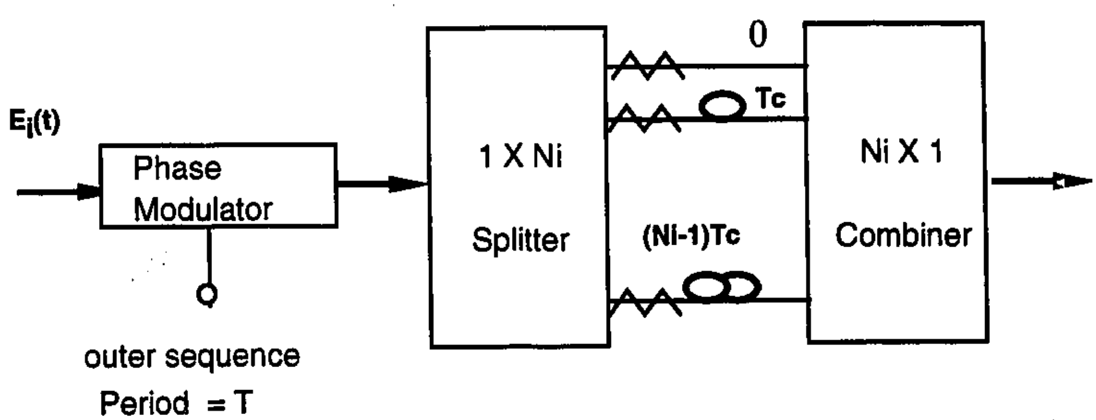

Fig.4.7: Encoder for coherent optical sources and Kronecker sequences, using a phase modulator and a non-programmable, coherent transversal filter.

modulators needed, typically from 4 to 16. We now propose, for the first time, the use of Kronecker sequences for efficient phase modulation of mode-locked pulses. We show that one can eliminate all but one of the phase modulators. As explained in Chapter 3, Kronecker sequences are constructed via the Kronecker product operation of an inner and an outer sequence of different chip durations, and with periods respectively of Ni and No. Each chip of the outer sequence encodes the entire period of the inner sequence. The architecture of Fig. 4.7 is therefore proposed. An optical pulse train with repetition rate $R = 1/T$, where T is the chip duration for the outer sequence, is incident on a modulator where it is phase modulated by the outer sequence. Each optical pulse is then split into Ni branches. Since all the chips of the outer sequence phase modulate the same inner sequence, the phase modulators are no longer necessary, and the coherent optical transversal filter (COTF) does not have to be programmable. The thermo-optics phase shifters can, for example, provide the fixed phases needed for the inner sequence. The limit on the size of the COTF limits the period of the inner sequence. There is no limit on the outer sequence, other than that longer sequences will limit the bit rate.

4.4.3 Decoders for Short Optical Pulses

The decoder architectures for arbitrary sequences and Kronecker sequences are shown on Fig. 4.8 to Fig. 4.10. Consider first Fig .4.8. The signal arriving from the network first goes to a Programmable Coherent Transversal Filter (PCOTF), as shown on Fig. 4.6, the delay between each branch being Tc. The impulse response of this filter needs to be the time reversal of that shown on Fig.4.6, and the signal $a1(t)$ is therefore used on the branch with the longest delay $(P-1)Tc$. For one bit period, the output of this filter is a serie of K correlation peaks spaced by T. These peaks need to be added before photodetection, since otherwise one would incoherently add the results of K partial cross-correlations, resulting on a performance degradation.

Field addition of the pulses can be done by using a $\log_2(K) - stages$ cascaded

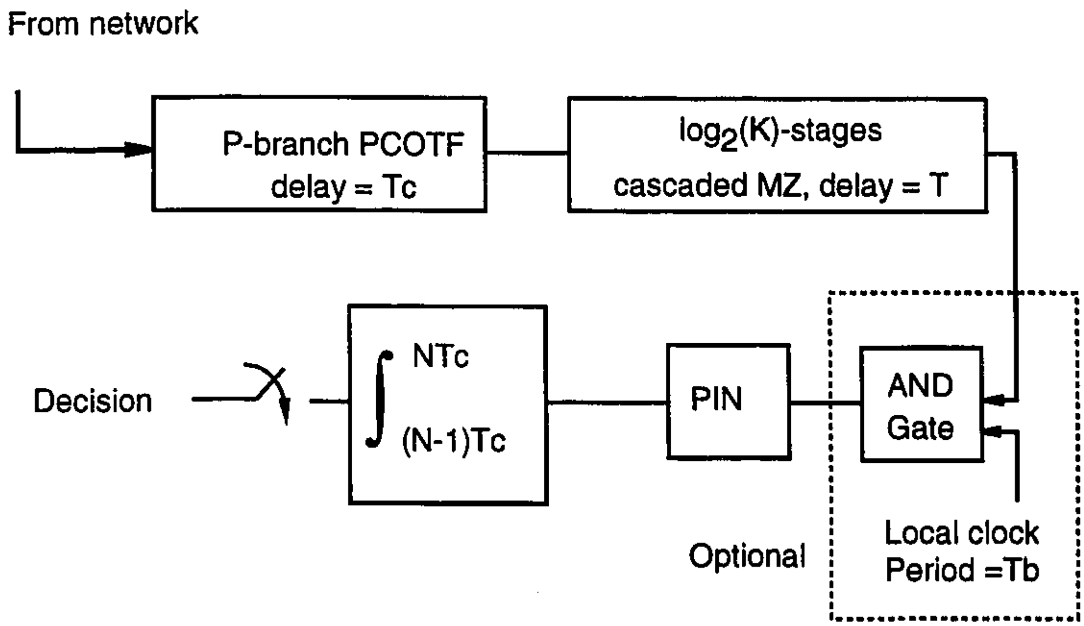

Fig.4.8: Decoder for coherent optical sources and arbitrary sequences.

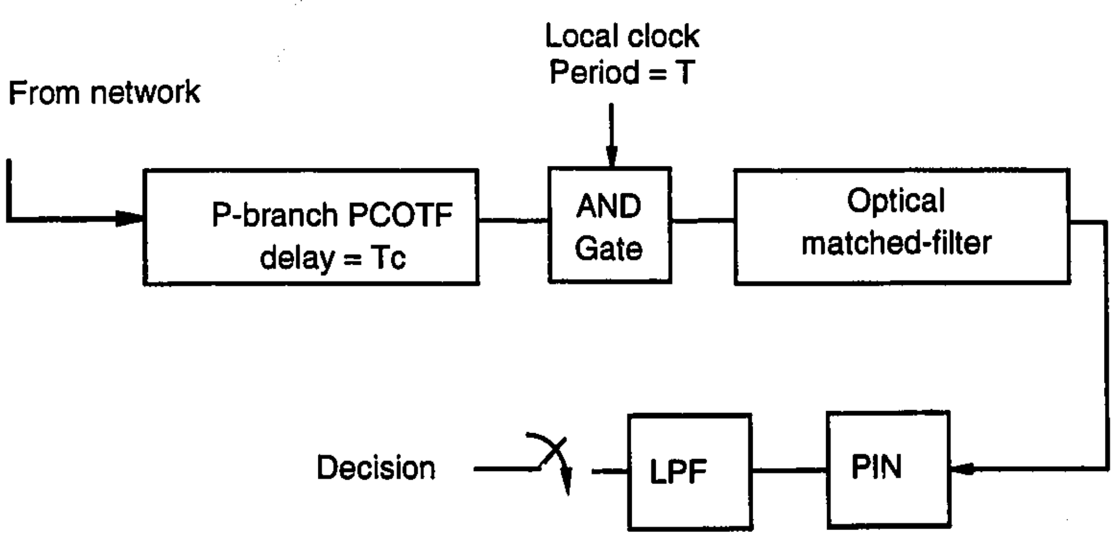

Fig.4.9: Alternative decoder for coherent optical sources and arbitrary sequences.

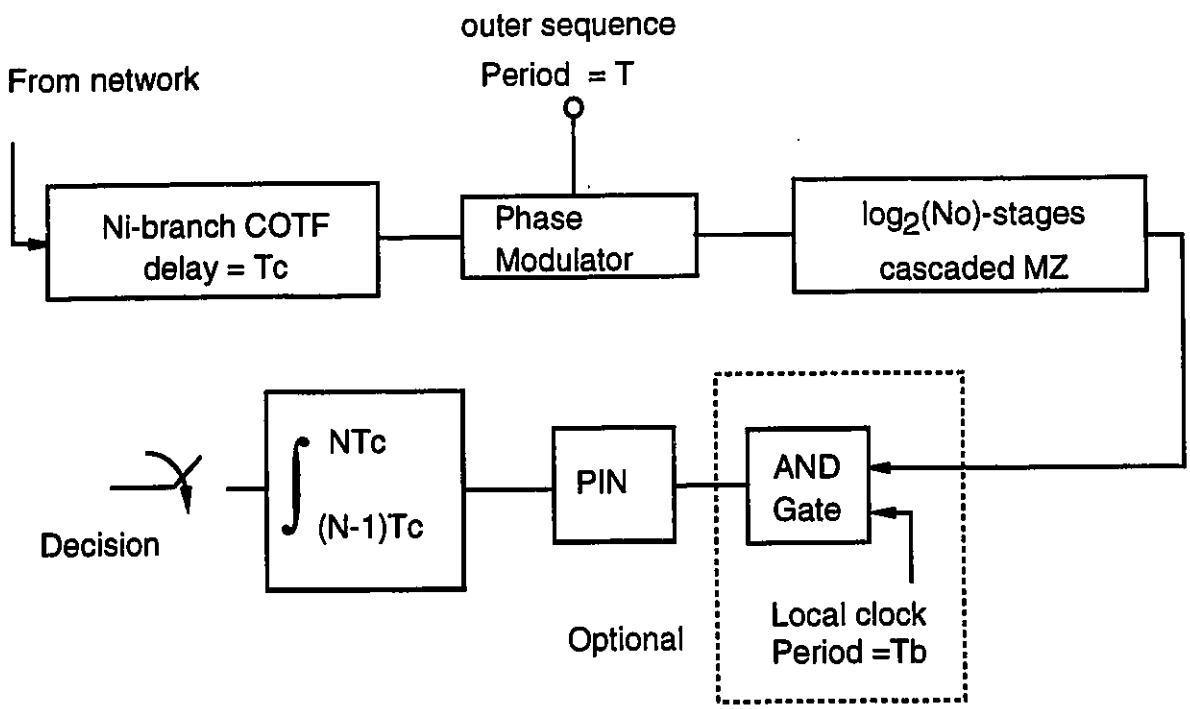

Fig.4.10: Decoder for coherent optical sources and Kronecker sequences.

MZ, as shown on Fig. 4.2b. If K is odd, a simple solution is to pad one zero to the sequence, which will not change the system performance, since ASK modulation is used. One can also tolerate the interference of one chip from the previous transmitted bit. After the cascaded MZ structure, we have performed the complete correlation, the results being an autocorrelation peak of time duration Tc, plus crosscorrelation. If $1/Tc$ is larger than the photodetector and associated electronics bandwidth, an optical AND gate can be used before photodetection, to avoid interference from the out-of-phase autocorrelation and crosscorrelation values. With the post-detection filter being an integrate-and-dump filter with integration time τ, the signal-to-noise Ratio (SNR), neglecting multiple-access interference is simply:

$$SNR = \frac{PT_c}{No\tau} \tag{4.3}$$

The optical AND gate allows τ to be larger than Tc, in case the post-detection electronics have a bandwidth smaller than $1/Tc$. However, since the signal power is fixed to PTc, a decrease of the SNR is unavoidable.

The Fig. 4.9 proposes a slightly modified structure. This time, the optical AND gate is used right after the PCOTF, to extract the K autocorrelation peaks, and filter out all out-of-phase autocorrelation and crosscorrelation values. One can then use an optical matched filter to complete the correlation before photodetection. The difference between Fig. 4.8 and Fig. 4.9 is that in Fig. 4.8 exactly $2^n = K$ cascaded MZ stages with delay T have to be used to *sum* the autocorrelation peaks. In Fig. 4.9, the number of stages can be arbitrarily increased so as to reach the $sinx/x$ shape. There is therefore more flexibility in the choice of bandwidth of the optical matched filter and the post-detection filter (LPF). In Fig. 4.8, without the optical AND gate, one is constrained to use as the post-detection filter an integrate-and-dump filter of duration T_c, which might not be the optimum choice.Fig.4.10 shows the decoder architecture when using Kronecker sequences. The only difference with Fig. 4.6 is the phase modulator used to despread the outer sequence, the COTF being used to despread the inner sequence. Fig. 4.11 shows the output of the COTF

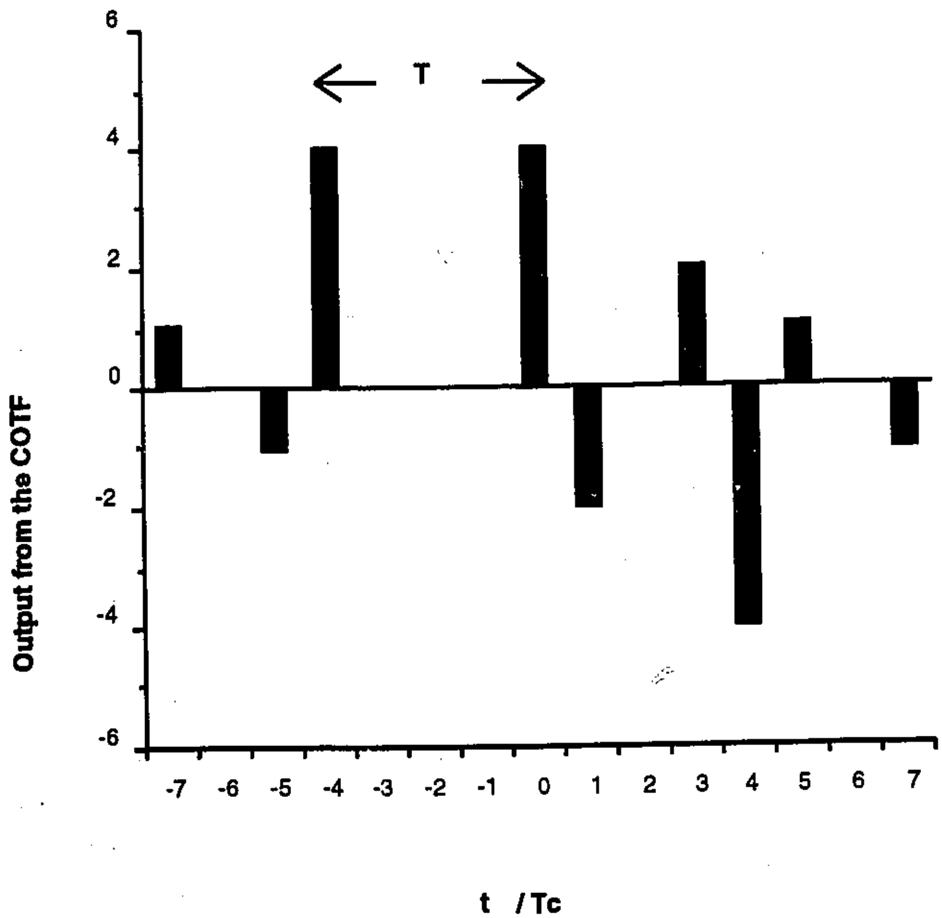

Fig.4.11: Optical output from the COTF.

when the inner sequence is $\{1, -1, 1, 1\}$ and the outer sequence is $\{1, 1, -1\}$. We suppose a transmitted information bit 1 is surrounded by two 0's. As seen we have $No = 3$ autocorrelation peaks. The phase modulator, driven by the outer sequence with chip period T, will make these peaks to have the same polarity. Suitable modulation schemes, due to the non-coherent nature of the detection, are limited to ASK, CPFSK or Large-Deviation FSK (LD-FSK), also sometimes called Wavelength-Shift-Keying (WSK). When using LD-FSK, a second branch as shown in Fig. 4.8 is required, for the other carrier frequency.

4.5 Architecture for Incoherent Optical Sources

When using the architecture proposed in the previous sections, lasers with a narrow linewidth are required. When one needs short optical pulses, this inevitably translates into the use of still quite expensive optical sources such as mode-locked lasers. The stability requirements for the optical processing elements is crucial to keep the phase information, and therefore simple optical fibers can not be used as the delay elements. Structures made in waveguides are needed.

Incoherent optical CDMA systems have the advantages of requiring less stability requirements for the optical encoders/decoders than the coherent ones, and need only sources with a small coherence time. However, since the correlation is based on power summation, they have the limitations of positive systems. It is usually believed that bipolar codes such as Gold codes, can not be used in incoherent systems, and as said in Chapter 2, new (0,1) codes such as Prime codes or Optical Orthogonal codes were designed. However, compared to bipolar codes, unipolar codes can usually support a smaller number of simultaneous active users and, if used in a packet-switched environment, the number of possible subscribers will be severly limited by the size of the code set. As an example, from a preferred-pair of M-sequences of length N, N+2 Gold codes can be constructed, while there is only $\sqrt{N}$ codes of period N for Prime codes.

We now propose an efficient way to use standard bipolar codes in optical systems, although requiring only incoherent delay lines and direct detection receivers, using the code construction given in Chapter 3, Section 3.5.

4.5.1 Encoder/Decoder for Arbitrary Unipolar Codes

The encoder architecture is shown in Fig. 4.12. The principle is similar to the one presented previously. When using a 2-PPM encoding of each bipolar chip to get unipolar chips, the code obtained necessarily contains N ones, where N is the period of the code. The code length is however $2NT_c$. It will therefore be totally impractical to use N delay lines for the encoder, and we believe that this aspect has probably directed researchers to other directions. As before, an easy way to counter this problem is by combination of E/O components and optical delay lines. Consider a laser with a repetition rate $R = K \times R_b$ where R_b is the bit rate. A pulse width of $T_c = T_b/(2N) = T_b/(2PK)$ allows to use P delay lines for a total code period of $K \times P = N$. As an example, for $T_b = 100ns$, a repetition rate of $R = 1\,GHz$, a code period of 500 is possible with only 5 delay lines, and a pulse width of $T_c = 100ps$. For incoherent systems, the delay lines can be simple optical fibers, and $1 : P$ splitters and combiners are easily constructed, such that P can be much larger than that in the coherent case. For arbitrary sequences, two optical switches such as shown in Fig.4.13, are inserted in each delay line, since the sequence $\{1, 0\}$ or $\{0, 1\}$ needs to be produced depending on if the chip in the bipolar code is a 1 or a -1. The speed requirement of the switches is *not* the chip rate, but is only $1/T_cP$. By increasing P, one can use relatively slow switches. However, increasing P will increase the recombining losses.

The decoder architecture is shown in Fig. 4.14. To maintain the bipolar properties of the codes, a balanced receiver is needed, even for ASK modulation. Any signal coinciding with a time slot asssociated with a "1" of the desired code is routed to the positively biased detector. By using in the lower branch the complement $\bar{a_1}(t)$, the signal will be routed to the negatively biased detector if it coincides in time with a "0" of the desired code. As before, cascaded M.Z. can be used to

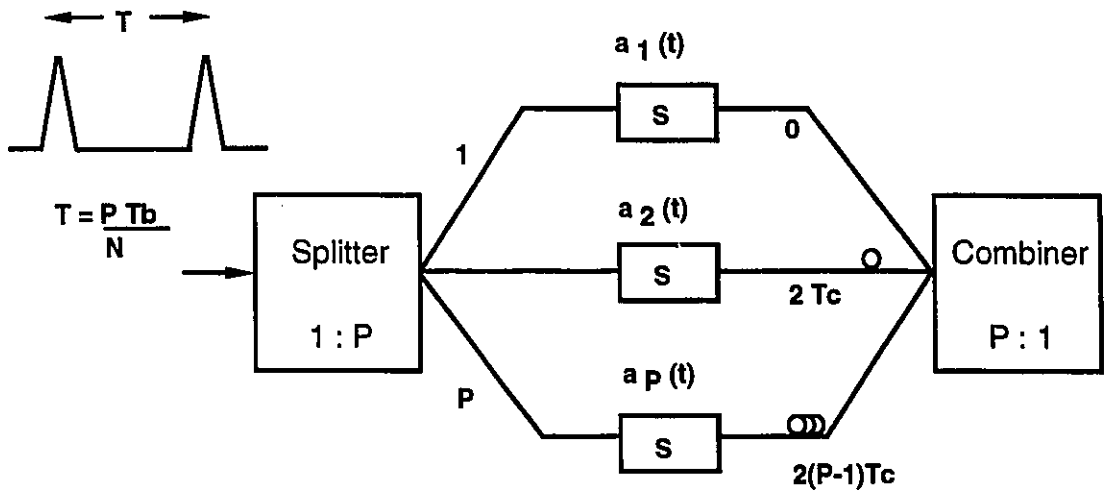

Fig.4.12: Encoder for incoherent optical sources and arbitrary sequences.

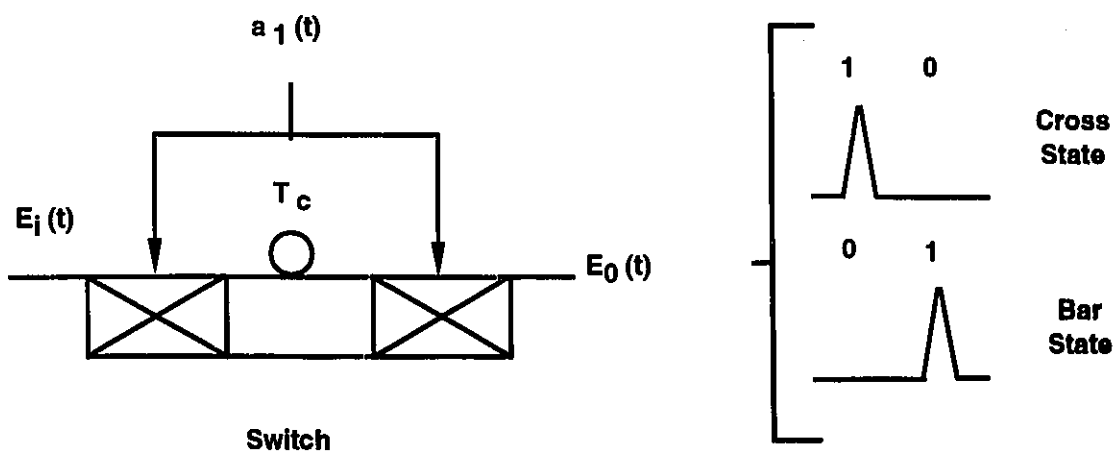

Fig.4.13: Optical switch configuration.

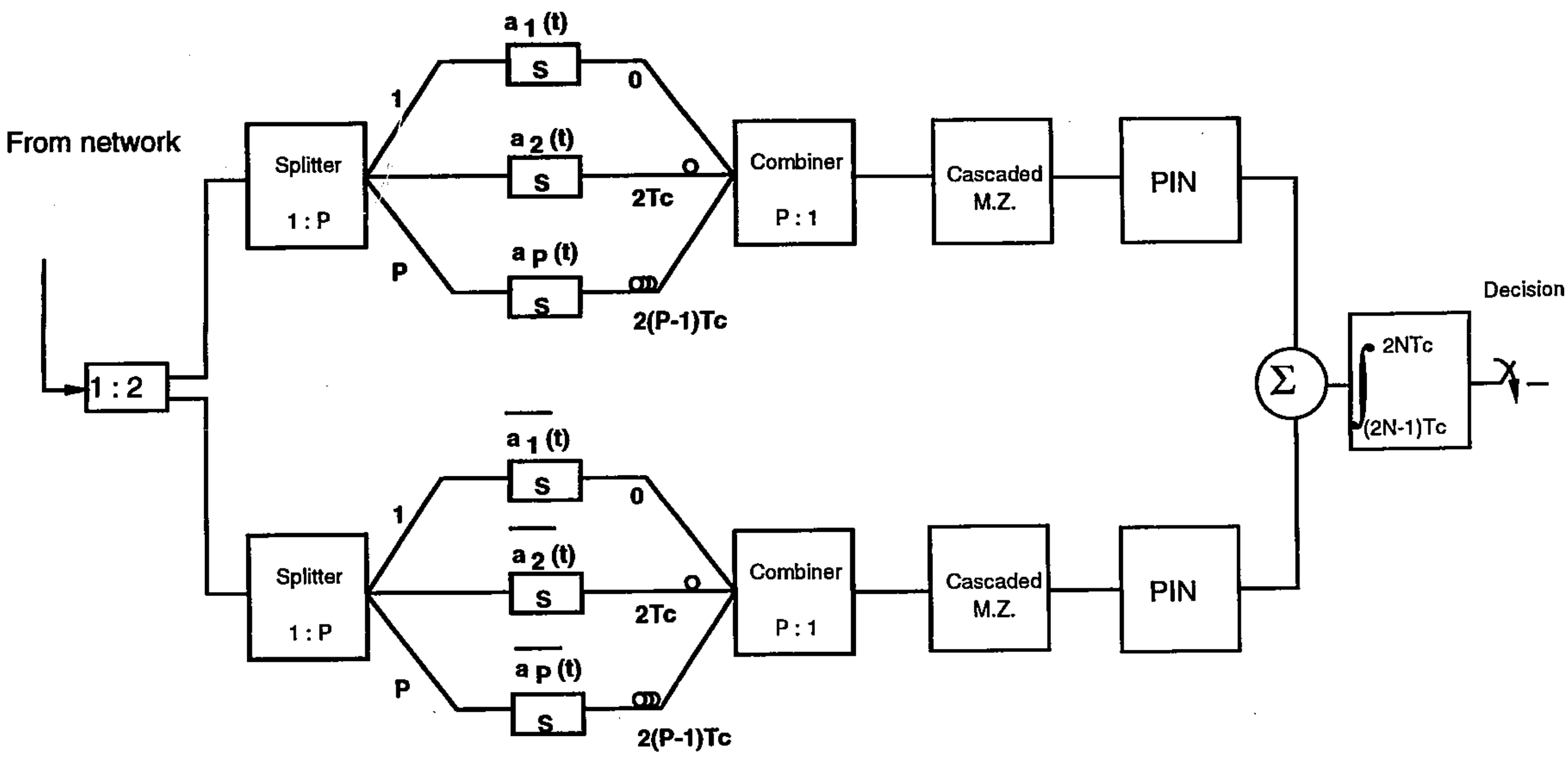

Fig.4.14: Decoder for incoherent optical sources and arbitrary sequences.

sum the autocorrelation peaks, in each branch. However, contrary to the coherent case, it is also possible to sum the peaks after photodetection.

4.5.2 Encoder/Decoder for Kronecker Unipolar Codes

When using Kronecker sequences, the encoder/decoder can be simplified considerably. They are shown in Fig. 4.15 and Fig. 4.16. The P optical switches in the delay lines of Fig. 4.12 are replaced by a single switch in front of two sets of N_i delay lines. At the transmitter, an incoming pulse is directed by an optical switch to one of the two sets of delay lines, according to the chip value of the outer sequence. The delays in the two sets correspond to the positions of the "1"s and the "0"s of the inner sequence. As an example, taking the inner sequence to be the Barker code $\mathbf{X} = (1, 1, -1, 1)$, the unipolar codes $\mathbf{X}^{\mathrm{P}} = (1, 0, 1, 0, 0, 1, 1, 0)$ and $1 - \mathbf{X}^{\mathrm{P}} = (0, 1, 0, 1, 1, 0, 0, 1)$ are needed. The two sets of delay lines in the encoder of Fig.1 will therefore be $(0, 2T_c, 5T_c, 6T_c)$ and $(T_c, 3T_c, 4T_c, 7T_c)$.

The same inner sequence can be used by all the susbscribers, and therefore a major advantage of the proposed system is that *the delay lines do not need to be programmable.* At the receiver, the signal is directed to two sets of delay lines matched to those at the transmitter. The bipolar nature of the codes is maintained by using two photodetectors inversely biased. *Note that no optical switch is needed at the receiver.* The output of the delay lines is a serie of autocorrelation peaks plus multiple-access interference, spaced by T, with out-of-phase cross-correlation and autocorrelation values in between. If $1/T_c$ is smaller than the photodetector and post-electronics bandwidth, the optical signal is directly detected. Otherwise, an optical AND gate must be used before detection. The resulting electrical signal is multiplied by a bipolar version of the outer sequence for the final despreading operation. A filter is then used to sum autocorrelation peaks and to filter the thermal noise. Suitable modulation schemes include ASK and orthogonal coding (OC). We will see in Chapter 6 that OC leads to a much better system performance in terms of the number of users it allows, and requires the same architecture as for

ASK. It can be used as follows. When a data bit "1" is sent, the pulse is directed to the upper set of delay lines, when the bit of the outer sequence is "1". The lower set is used when the bit of the outer sequence is "-1" (see Fig. 4.15). When a data bit "0" is sent the opposite is true. No dynamic threshold optimization is required since it is fixed at 0. As for the coherent case, WSK can also be used, in which case, for Kronecker sequences, one encoder and decoder as shown on Fig. 4.15 and Fig. 4.16 is needed for each wavelength. In terms of performance, there would however be no advantage compared to OC.

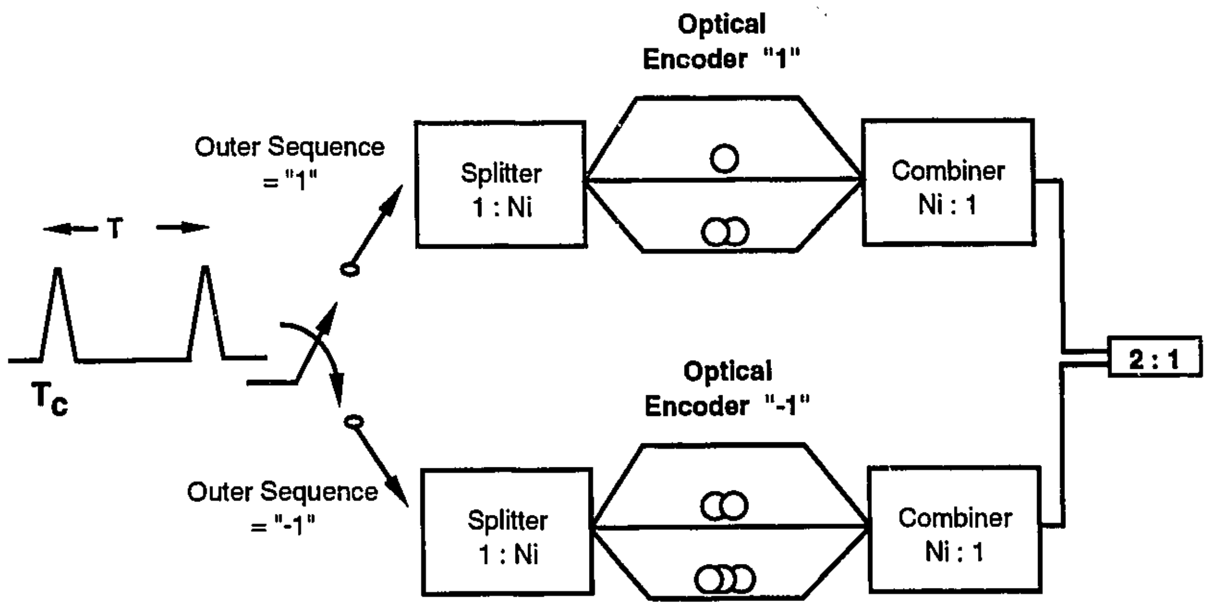

Fig.4.15: Encoder for incoherent optical sources and Kronecker sequences.

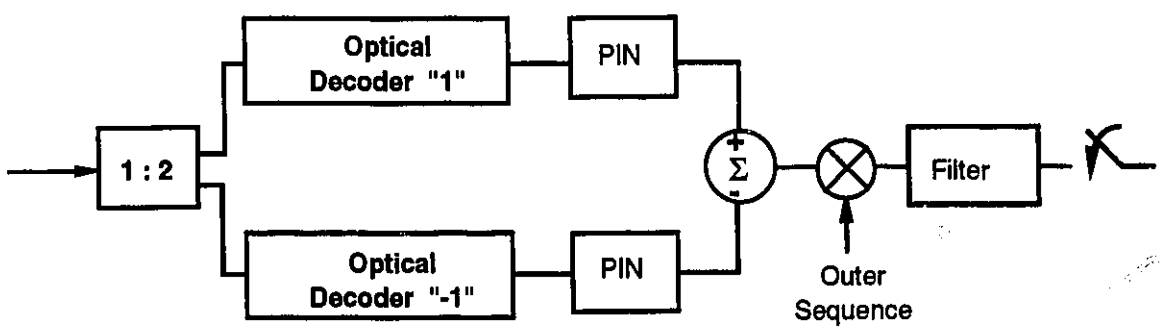

Fig.4.16: Decoder for incoherent optical sources and Kronecker sequences.

4.6 Conclusion

In this chapter, we have proposed new architectures for using bipolar codes in optical CDMA systems, that require only direct detection. We showed that combining E/O elements and all optical processing elements allow using arbitrary bipolar sequences and solve the speed limit imposed by the bandwidth of the phase modulators. The encoder/decoder architectures are such that the croscorrelation properties of the codes is maintained, although requiring only direct detection. Using a pulse width of 10 ps, and a mode-locked source with a repetition rate of 10 GHz, a code length of 10000 is possible for a bit rate of 10 Mbit/s, or $N = 1000$ for 100 Mbit/s. In both cases, only 10 delay lines are needed. The use of Kronecker sequences were proposed, as they allow to use only one phase modulator and non-programmable delay lines. We then modify the proposed architectures so they can be used with incoherent sources, and incoherent optical processing elements. Using a simple 2-PPM encoding of each pulse allows the use of standard bipolar codes. The size of the set for these codes is around $N + 2$ for a code length of N, for most of them, so that many more subscribers can be accommodated than when usign Prime codes. The number of 1's in the code must be N, but only P delay lines are required for the proposed architectures, where typically $P/N \approx 0.01$. In the next two chapters we proceed with the performance evaluation of the proposed architectures.

Chapter 5

Performance Evaluation of Coherent Optical CDMA Systems

5.1 Introduction

In this chapter we evaluate the performance of coherent optical CDMA systems using the architectures presented in the previous chapter. Our criterion will be the average bit error probability and our goal is to evaluate how many simultaneous active users can be supported by the proposed systems. Except for Section 5.5, we will assume that interfering users are solely responsible for the performance degradation. Shot noise and thermal noise will not be considered. Our results are therefore an indication of the performance obtained when the received optical power is sufficiently high that the system is not thermal noise or shot noise limited. They furthermore allow us to quickly identify the bit error rate floors that would be observed as the transmitted power is sufficiently increased.

Since the system model as well as the techniques used for the evaluation of the probability of error are very different for the noncoherent case, we will report these calculations in the next chapter.

5.2 System Model

A suitable model for the purpose of performance evaluation is shown in Fig. 5.1. As explained in the previous chapter, the optical filter acts as a correlator and is realized in practice by cascaded Mach-Zender interferometers. A low-pass filter would also be needed after photodetection. However, in a Multiple Access Interference (MAI) limited environment, the model of Fig. 5.1 is adequate. Section 5.5 will consider a more general situation including partial cross-correlation due to optical filtering, and electronics low-pass filtering.

We consider the following modulation types: Amplitude-Shift-Keying (ASK), Continuous-Phase-Frequency-Shift-Keying (CPFSK), Large-deviation FSK (LD-FSK). In this last case, a data bit "1" is transmitted on λ_1 while for a data bit "0", λ_0 is used. We assume orthogonal modulation, that is, for the desired signal, power is only received on the photodetector associated with the optical filter centered on λ_1 (λ_0) when a "1" ("0") is transmitted. This scheme corresponds to noncoherent orthogonal FSK, and is appropriately called in optics Wavelength-Shift-Keying. Note that, to obtain this orthogonality, we need $c/\lambda_1 - c/\lambda_0 = f_1 - f_0 > 1/T_c$, where T_c is the chip duration. The signal received from the network can be expressed for ASK as:

$$\vec{E}(t) = \sum_{k=0}^{K} \sqrt{2P} I^k(t-\tau_k) a_k(t-\tau_k) \cos(2\pi f_1 t + \phi_k) \tag{5.1}$$

where, for the kth user, $I^k(t)$ is the data modulation, $a_k(t)$ is the spreading waveform, τ_k is the delay that accounts for unsynchronized transmission between the users, $\phi_k = \theta_k - 2\pi f_1 \tau_k$ is the total phase term, θ_k being an initial random phase term. We consider that τ_k is uniformly distributed on $[0, T]$. The data modulation $I^k(t)$ has the form:

$$I^k(t) = \sum_{i=-\infty}^{\infty} I_i^k s(t - iT) \tag{5.2}$$

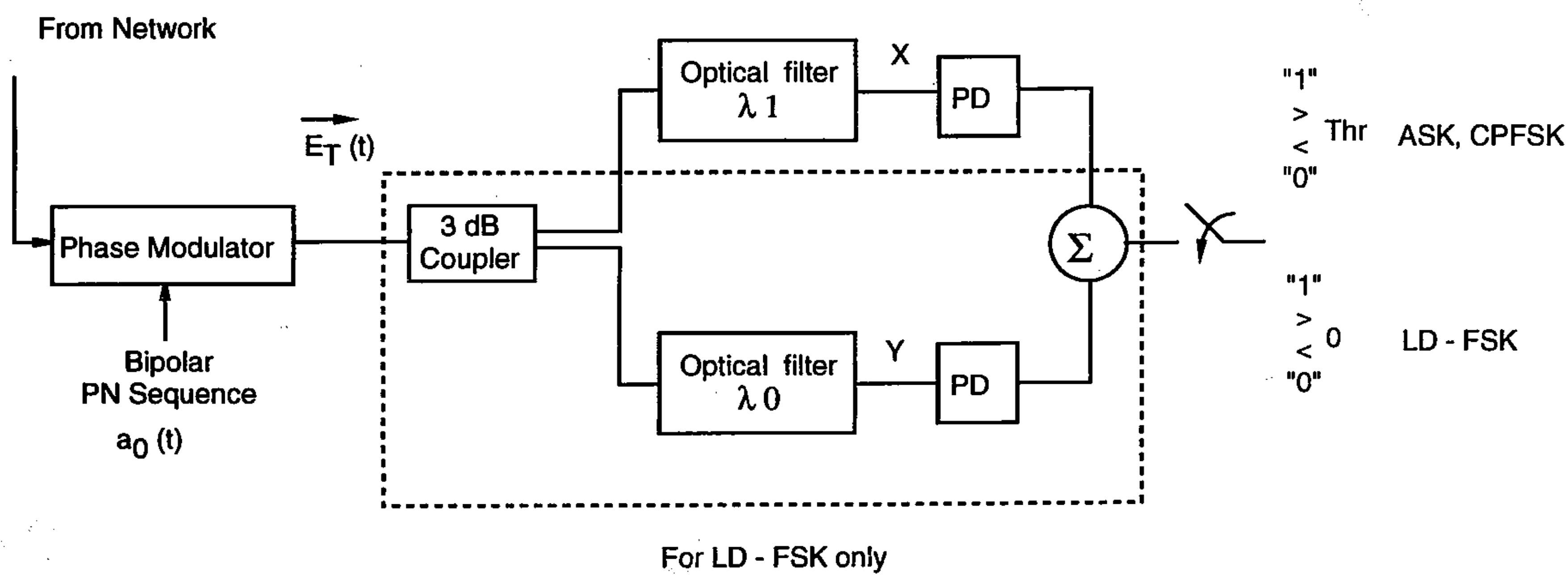

Fig. 5.1: Block diagram of the receiver for coherent CDMA system.

where I_i^k is a 1 or a 0, T is the symbol duration and $s(t) = 1$ for $0 \leq t \leq T$, and 0 otherwise. We therefore assume that no power is transmitted when sending a 0. For practical extinction ratios of ≈ 30 dB, this is reasonable. The spreading waveform is expressed as

$$a_k(t) = \sum_{j=-\infty}^{\infty} a_j^k p(t - jT_c) \qquad (5.3),$$

where a_j^k is a periodic pseudorandom sequence of period N, with $a_j^k \in [-1, 1]$. We take $T = NT_c$, T_c being the chip duration, and $p(t) = 1$ for $0 \leq t \leq T_c$. We therefore choose a rectangular chip waveform.

Without loss of generality, we consider the receiver for a reference user, e.g. $k = 0$. The electro-optic phase modulator of Fig. 5.1 is used to despread the desired signal. The total received signal is therefore phase modulated by $a_0(t)$. Assuming that perfect code synchronization has been established between the pair of communicating users, we have at the output of the modulator, and for ASK modulation:

$$\vec{E}_T(t) = \sqrt{2P} I^0(t) \cos(2\pi f_1 t + \phi_0) + \sum_{k=1}^{K} \sqrt{2P} I^k(t - \tau_k) a_0(t) a_k(t - \tau_k) \cos(2\pi f_1 t + \phi_k) \qquad (5.4)$$

The first term in (5.4) represents the desired signal and the second term represents the interference coming from other users. It is important to note that in noncoherent detection only the delay τ_0 is tracked by the receiver, in order to achieve synchronization and complete despreading, but not the phase.

For CPFSK modulation the desired signal, for $nT \leq t \leq (n+1)T$ is:

$$\vec{E}_0(t) = \sqrt{2P} \cos\left[2\pi \left(f_1 + \frac{hI_n^0}{2T}\right) t + \pi h \sum_{i=0}^{n-1} I_i^0 + \phi_0\right] \qquad (5.5)$$

Each interfering signal is written, for $nT \leq t \leq nT + \tau_k$ as:

$$\vec{E}_k(t-\tau_k) = \sqrt{2P}a_0(t)a_k(t-\tau_k)\cos\Bigg[2\pi f_1(t-\tau_k) + \pi h\sum_{i=0}^{n-2} I_i^k + 2\pi h I_{n-1}^k\left(\frac{t-\tau_k-(n-1)T}{2T}\right) + \theta_k\Bigg] \tag{5.6}$$

and for $nT + \tau_k \le t \le (n+1)T$:

$$\vec{E}_k(t-\tau_k) = \sqrt{2P}a_0(t)a_k(t-\tau_k)\cos\Bigg[2\pi f_1(t-\tau_k) + \pi h\sum_{i=0}^{n-1} I_i^k + 2\pi h I_n^k\left(\frac{t-\tau_k-nT}{2T}\right) + \theta_k\Bigg] \tag{5.7}$$

where h is the modulation index and I_i^k is the symbol sent in the ith interval by the kth user, $I_i^k \in [-1, 1]$. At this point in the system, the desired user is despread and has a bandwidth of about $1/T$ while other users, due to the spreading waveforms, have a bandwidth value in the order of N/T. A filter bandwidth of $1/T$ will therefore reject most of the interfering power. Note that, since the codes are bipolar, the optical filter acting as a correlator is essential. Without this filter, all users would appear despread at the photodetector output. This is in contrast with optical CDMA systems using unipolar codes. In this case, incoherent optical delay lines are used as a correlator in order to take advantage of the large bandwidth of optical fiber. In principle, however, the correlation process can be as well done in the electronic domain.

5.2.1 Optical Filter Output

A) The ASK Modulation Format

From now on we consider the first interval $0 \le t \le T$, and we use a complex low-pass representation for the signals. The optical filter is a matched-filter for the signal shape $I^0(t)$. It takes the form of a filter with impulse response:

$$h(t) = \begin{cases} \frac{2}{T}\cos(2\pi f_1 t) & \text{for} \quad 0 \le t \le T; \\ 0 & \text{otherwise.} \end{cases} \tag{5.8}$$

The complex envelope of the desired signal at the output of the filter at the decision time $t = T$ is

$$X_0(T) = \sqrt{P} b_0 e^{j\phi_0}, \tag{5.9}$$

where b_0 is a 1 or a 0 depending on the transmitted symbol. For the interfering signals we get

$$X_k(T) = e^{j\phi_k} \frac{\sqrt{P}}{N} (I_{-1}^k \frac{R_k(\tau_k)}{T_c} + I_0^k \frac{\widehat{R_k}(\tau_k)}{T_c}) \tag{5.10}$$

where $R_k(\tau_k)$ and $\widehat{R_k}(\tau_k)$ are the continuous-time partial crosscorrelation functions defined in Chapter 3, Equations (3.4) and (3.5).

B) The LD-FSK Modulation Format

Following the notation of Fig. 5.1, the outputs X_k and Y_k of the two optical filters for the kth user are easily found to be given by:

$$X_k(T) = e^{j\phi_k^1} \frac{\sqrt{P}}{N} (I_{-1}^k \frac{R_k(\tau_k)}{T_c} + I_0^k \frac{\widehat{R_k}(\tau_k)}{T_c}) \tag{5.11}$$

$$Y_k(T) = e^{j\phi_k^2} \frac{\sqrt{P}}{N} ((1 - I_{-1}^k) \frac{R_k(\tau_k)}{T_c} + (1 - I_0^k) \frac{\widehat{R_k}(\tau_k)}{T_c}) \tag{5.12}$$

where $I_0^k, I_{-1}^k \in \{0, 1\}$.

C) The CPFSK Modulation Format

The impulse response of the optical filter is described by (5.8) with f_1 replaced by $f_1 + \frac{h}{2T}$. We therefore assume that when using CPFSK modulation, a "1" is transmitted by the filter while a "0", corresponding to $I_0 = -1$, is blocked. The

CPFSK signal is therefore converted into an ASK signal ready for direct detection. This will be true if we choose $h = m$, with $m \geq 1$ an integer. For the desired signal, (5.9) holds provided that the phase term is written as:

$$\phi_0 = \pi h \sum_{i=0}^{-1} I_i^0 + \theta_0 + \pi h - 2\pi f_c \tau_0$$

It can be shown that ϕ_0 modulo 2π is uniformly distributed on $[0, 2\pi]$. This follows from a theorem for the modulo y values of the sum of independent processes [43]. For the interfering signals we get:

$$X_k(T) = e^{j\phi_{-1}^k} \frac{\sqrt{P}}{T} \int_0^{\tau_k} a_0(t) a_k(t-\tau_k) e^{j\frac{\pi h t}{T}[I_{-1}^k - 1]} dt$$

$$+ \quad \frac{\sqrt{P}}{T} e^{j\phi_0^k} \int_{\tau_k}^{T} a_0(t) a_k(t-\tau_k) e^{j\frac{\pi h t}{T}[I_0^k - 1]} dt, \qquad (5.13)$$

where:

$$\phi_{-1}^k = \theta_k + \pi h \sum_{i=-\infty}^{-2} I_i^k - \pi h I_{-1}^k \frac{\tau_k}{T} + \pi h I_{-1}^k - 2\pi f_1 \tau_k$$

$$\phi_0^k = \phi_{-1}^k + \frac{\pi h}{T} \tau_k [I_{-1}^k - I_0^k]$$

For the same reasons, we take ϕ_{-1}^k to be uniformly distributed on $[0, 2\pi]$, while ϕ_0^k is expressed directly in terms of ϕ_{-1}^k. We see that if the delay between user k and user 0 is zero, $\phi_{-1}^k = \phi_0^k$, which is also true if the two consecutive symbols transmitted by the user k are the same, i.e. $I_{-1}^k = I_0^k$.

5.2.2 The Photodetector Output

At the photodetector output, our decision variable for ASK and CPFSK is:

$$z_1(T) = R \left| \sqrt{P} b_0 e^{j\phi_0} + \sum_{k=1}^{K} X_k(T) \right|^2 \qquad (5.14)$$

. while for LD-FSK we have:

$$z_1(T) = R\left|\sum_{k=1}^{K}\frac{\sqrt{P}}{N}(I_{-1}^k\frac{R_k(\tau_k)}{T_c} + I_0^k\frac{\widehat{R_k}(\tau_k)}{T_c})e^{j\phi_k^1} + \sqrt{P}I_0e^{j\phi_0}\right|^2 \tag{5.15}$$

$$z_2(T) = R\left|\sum_{k=1}^{K}\frac{\sqrt{P}}{N}((1-I_{-1}^k)\frac{R_k(\tau_k)}{T_c} + (1-I_0^k)\frac{\widehat{R_k}(\tau_k)}{T_c})e^{j\phi_k^2} + \sqrt{P}(1-I_0)e^{j\phi_0}\right|^2 \tag{5.16}$$

where R are the responsivity of the photodiodes (assumed identical). In order to compute the probability of error for ASK and CPFSK, we have to find the probability that $z_1(T) \leq Tr$ or $z_1(T) \geq Tr$ for $b_0 = 1$ and $b_0 = 0$ respectively, with Tr being the detection threshold. For LD-FSK, we have to find the probability that $z_1(T) - z_2(T)$ is larger or smaller than 0, for $I_0 = 0$ and $I_0 = 1$ respectively. It can be seen from the preceding equations that the decision variable, for a given value of the desired data bit sent, is a function of the bits transmitted by the interfering users, $\mathbf{I} = (\mathbf{I^1}, \mathbf{I^2}, \ldots, \mathbf{I^K})$, the delays $\tau = (\tau_1, \tau_2, \ldots, \tau_K)$ and the phase angles $\phi = (\phi^1, \phi^2, \ldots, \phi^K)$. The symbol $\mathbf{I^K}$ represents the pair of transmitted symbols $[I_{-1}^k, I_0^k]$ sent by user k in $[0, T]$.

Many good techniques are available in the literature for evaluating the performance of CDMA in the case of electronic systems that use coherent detection, or for optical CDMA with unipolar codes [44]. However, as stated before, the case of bipolar codes followed by noncoherent direct detection has only been briefly studied in the literature. Furthermore, to the best of our knowledge, no performance results of optical CDMA systems using Kronecker sequences are available in the literature. We believe the following presents efficient and accurate techniques for evaluation of the performance of the systems considered.

5.3 Probability of Error for ASK and CPFSK

We will first consider the case of ASK and CPFSK, since for both these cases we have to find the probability that $z_1(T)$ is larger or smaller than a given threshold.

For reasons explained later, the case of LD-FSK will be only briefly covered in Section 5.3.4. In order to facilitate the computation of the probability of error from the expression of $z_1(T)$ in (5.14) we wish to express each complex $X_k(T)$ in terms of its amplitude and phase: $X_k(T) = A_k e^{j\varphi_k}$, where φ_k is uniformly distributed over $(0, 2\pi)$. The decision variable would then be:

$$z = \left| b_o e^{j\varphi_0} + \sum_{k=1}^{K} A_k e^{j\varphi_k} \right|^2 \tag{5.17}$$

Since we do not consider near-far effects, the power P has been normalized to 1. If A_k's were fixed values instead of being random variables, the problem would reduce to finding the distribution of the sum of randomly phased components. Much has been written about this distribution over the past years; for example, [45]. An additional degree of complexity is present here since each A_k is a function of the random delay τ_k and the data bits I_0^k and I_{-1}^k. In order to make the problem tractable we will therefore seek the probability density function of the A_k's.

5.3.1 Probability Density Function of the Interfering Signals

A) Chip-Synchronism Assumption

Under chip-synchronous assumption, it is assumed that each delay τ_k is a discrete random variable taking values $\tau_k = l_k T_c$, for $l_k = 0$ to $N-1$, instead of being uniformly distributed on $[0, T]$. It corresponds to the situation where the transmitting users are chip-synchronous. In the literature this assumption is often made to facilitate the calculations, and it is usually found that the performance obtained is an upper bound compared to the truly random case where τ_k is continuously uniform on $[0, T]$. This is also equivalent to assuming that the channel is slotted, and might correspond to some transmitting protocol constraints. Under the chip-synchronism assumption, it is obvious that each A_k can take only a finite number of different values, and it is straightforward to get their discrete probability density function. The explicit expression for the A_k's in the case of ASK is simply found from (5.10):

$$A_k = \left|I_{-1}^k \frac{R_k(\tau_k)}{N} + I_0^k \frac{\widehat{R_k}(\tau_k)}{N}\right|, \tag{5.18}$$

where the delay τ_k have been normalized, $\tau_k = \tau_k/T_c$. The absolute value is taken here since a random phase can be included in φ_k. For the case of CPFSK some manipulations are necessary. Starting from (5.13), we get

a) for $I_{-1}^k = I_0^k = 1$:

$$A_k = \frac{\sqrt{P}}{N} \sum_{n=0}^{N-1} a_n^0 a_{N+n-l_k}^k \tag{5.19}$$

b) for $I_{-1}^k = I_0^k = -1$:

$$A_k = \frac{\sqrt{P}}{\pi h} \sin\left(\frac{\pi h}{N}\right)$$

$$\times \left\{ \left[\sum_{n=0}^{N-1} a_n^0 a_{N+n-l_k}^k \cos(\frac{2\pi hn}{N})\right]^2 + \left[\sum_{n=0}^{N-1} a_n^0 a_{N+n-l_k}^k \sin(\frac{2\pi hn}{N})\right]^2 \right\}^{\frac{1}{2}} \tag{5.20}$$

c) for $I_{-1}^k = -1, I_0^k = 1$:

$$A_k = \left\{ \left[U\cos(\frac{\pi h}{N} + tg^{-1}(W)) + Q\cos(\frac{2\pi h l_k}{N})\right]^2 + \right.$$

$$\left. \left[U\sin(\frac{\pi h}{N} + tg^{-1}(W)) + Q\sin(\frac{2\pi h l_k}{N})\right]^2 \right\}^{\frac{1}{2}} \tag{5.21}$$

where:

$$U = \frac{\sqrt{P}}{\pi h} \sin\left(\frac{\pi h}{N}\right) \left\{ \left[\sum_{n=0}^{l_k-1} a_n^0 a_{N+n-l_k}^k \cos(\frac{2\pi hn}{N})\right]^2 \right.$$

$$\left. + \left[\sum_{n=0}^{l_k-1} a_n^0 a_{N+n-l_k}^k \sin(\frac{2\pi hn}{N})\right]^2 \right\}^{\frac{1}{2}}$$

$$Q = \frac{\sqrt{P}}{N} \sum_{n=l_k}^{N-1} a_n^0 a_{N+n-l_k}^k$$

$$W = \frac{\sum_{n=0}^{l_k-1} a_n^0 a_{N+n-l_k}^k \sin(\frac{2\pi hn}{N})}{\sum_{n=0}^{l_k-1} a_n^0 a_{N+n-l_k}^k \cos(\frac{2\pi hn}{N})}$$

d) and for $I_{-1}^k = 1, I_0^k = -1$:

$$A_k = \left\{ U^2 + Q^2 + 2UQ\cos\left(\frac{\pi h}{N} + tg^{-1}(W) + \frac{2\pi h l_k}{N}\right)\right\}^{\frac{1}{2}} \tag{5.22}$$

where U and W are defined as previously except that the summations go from $n = l_k$ to $N-1$, and Q is defined as previously with the summation going from $n = 0$ to $l_k - 1$.

In the above, case a) corresponds to the situation where two consecutive interfering bits are transmitted at the detected frequency while case b) is the case where the two bits are transmitted at the opposite frequency. We see that if $h = N$, no interference is produced for $I_{-1}^k = I_0^k = -1$, corresponding to the case in ASK modulation where the interfering user is not transmitting. However, this case will be covered by LD-FSK, so for CPFSK we will limit the value of h to $h = 1, h = 2$. The maximum number of values taken by each A_k is $4N$ in the case of CPFSK since there are four possible values for the pair $\{I_{-1}^k, I_0^k\}$. In the case of ASK modulation this number is reduced to $3N + 1$ since for $I_{-1}^k = I_0^k = 0$, $A_k = 0$ for all values of τ_k. However, it is expected that this number will in fact be much smaller, since the set of values that the crosscorrelation can take for pseudorandom sequences is limited. For Gold sequences of period $N = 127$ and ASK modulation, it was found that each A_k would take 22 to 24 different values depending on the exact sequence used. In the case of CPFSK modulation and $N = 127$, the number of values is in the order of 200.

An example of the pdf obtained for a Gold code of period 127 and ASK modulation is shown in Fig. 5.2a. We see that $A_k = 0$ with a probability ≥ 0.25 since the probability of having the interfering user sending two consecutive 0's is 0.25, for equally-likely emitted symbols. Fig. 5.2b shows the pdf of A_k for a particular m-sequence of period $N = 63$ while Fig. 5.2c shows the result for a Kasami sequence of period $N = 255$. As seen from these figures, increasing the code length decreases the maximum value that A_k can take, as expected. For $N = 63$, the maximum value with a significant probability is around 0.27, while it is only 0.08 in the case of $N = 255$.

B) Chip-Asynchronism Assumption

In the case of chip-asynchronism, each τ_k is a continuous random variable and, therefore, so is each A_k. We propose to approximate the probability density function of each A_k using the Gauss Quadrature Rule (GQR) technique, whose details can be found in [46]. Usually this technique is used to calculate integrals of the type:

$$Q = \int_R g(u)p(u)du \tag{5.23}$$

by approximating it by

$$Q \approx \sum_{k=1}^{T} w_k g(u_k), \tag{5.24}$$

where $g(u)$ is, e.g., a conditional probability of error, and $p(u)$ is a weighting function, e.g., a probability density function. When $p(u)$ is not known but $2T + 1$ moments of the random variable u can be calculated, one obtains the set $(w_j, u_j)|_{j=1}^{T}$ by a technique outlined in [46]. Looking at (5.24), we see that the GQR technique provides a set of appropriately chosen samples u_k of the pdf of a random variable. These samples are weighted by the values w_k. This technique seems therefore suitable for approximating the probability density function (pdf) of a random variable. From the expression for A_k in (5.18), it is straightforward for ASK to compute the moments needed. Given the moment of each A_k, we calculate the set $(w_j, u_j)|_{j=1}^{T}$ and approximate the pdf by $\sum_{i=1}^{T} w_i \delta(A_k - u_i)$. Once the pdf of each A_k is made discrete, the case of chip-synchronism and chip-asynchronism can be treated the same way, as far as the probability of error calculation is concerned. An important remark is that the GQR technique can also be used to reduce the number of samples needed in the chip-synchronous case. This would be particularly useful in the case of CPFSK where each A_k can take approximately 200 different values. An example of the pdf obtained for a Gold code of period $N = 127$ and ASK modulation is shown on Fig. 5.3, where we took T=16. This number of samples was sufficient to obtain convergence of the probability of error. As it can be seen by comparing the Fig. 5.2a and Fig. 5.3 the maximal value that A_k takes in the chip-asynchronism case is 0.12 while it is 0.15 in the chip-synchronous case. One can therefore suspect that a better performance should be obtained in the former case. The results will show that this is in fact the case.

5.3.2 Series expansion of the probability of error

To compute the probability of error we will make use of two techniques applicable for two different ranges of K, the number of interfering users. These techniques will allow us to take into account the random nature of A_k's. When K is small, say $K < 6$, we will use a series expansion developed by Bennet in [45]. For a fixed set of $\{A_k\}$, we will calculate the conditional probability of error, for $b_0 = 1$ and $b_0 = 0$. To remove conditioning we average over all possible $\{A_k\}$ sets. For example, if each A_k can take ≈ 30 values, in theory 30^K conditional error probability values have to be computed, for each value of b_0 and different thresholds. In practice however, it is obvious that only the combination of $A_k's$ such that $\sum A_k \geq Tr$ or $1 - \sum A_k < Tr$ have to be considered. It was found that this leads to a substantial decrease in the computation time. For a large number of interfering users, say $K > 6$, such an exercise however is likely to be futile because it leads to an exponentially growing computational complexity as K grows. In Section 5.3.3 we therefore propose a very fast and efficient technique when $K > 6$.

In this section, since all the detailed derivations can be found in [45], we will just state the main results. When $b_0 = 0$ is sent, we have to compute the probability $Pr(z \geq Tr)$. From now on, we consider z to be the modulus instead of the modulus

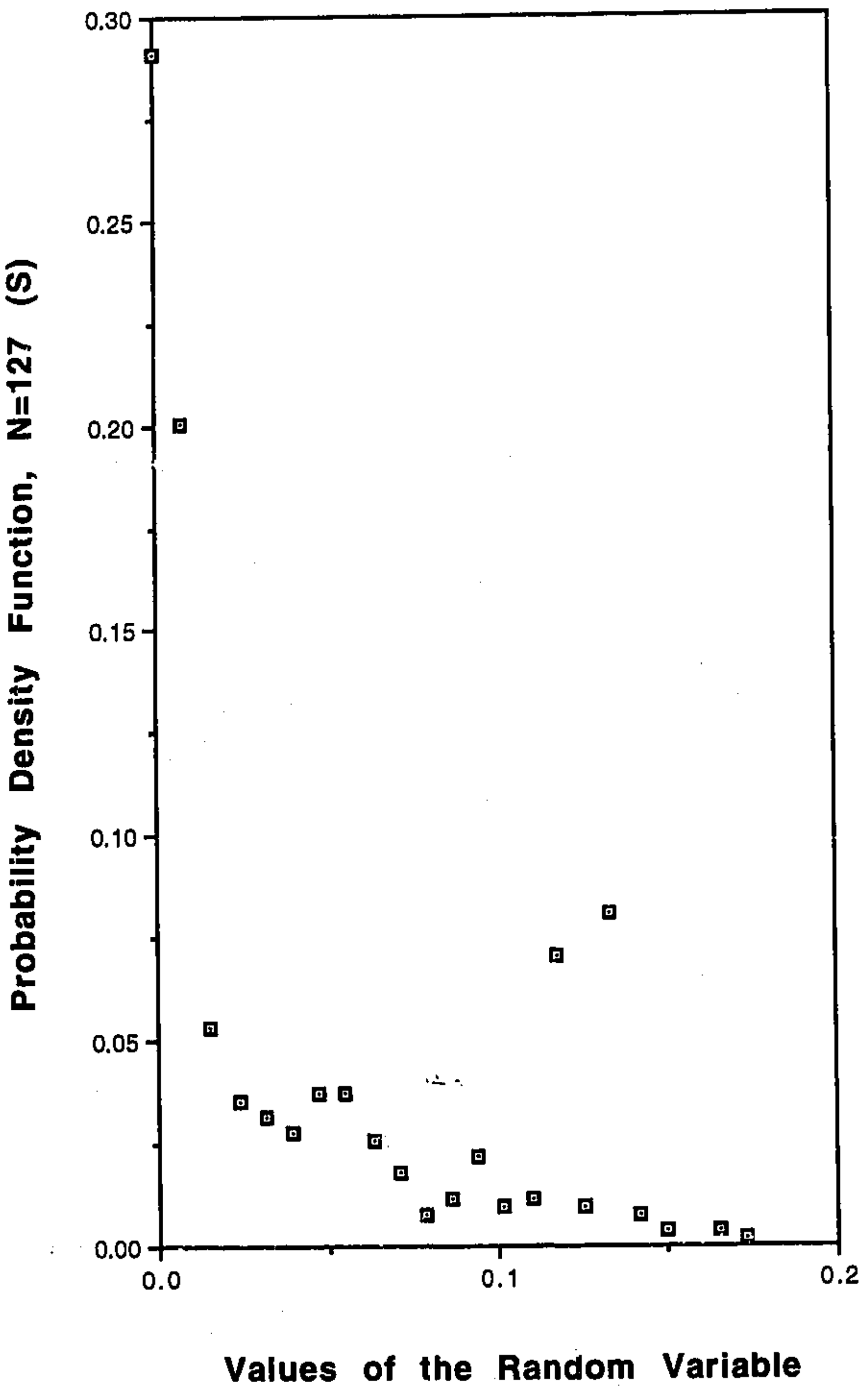

Fig.5.2a: Pdf of one user, ASK, N=127, chip-synchronous assumption.

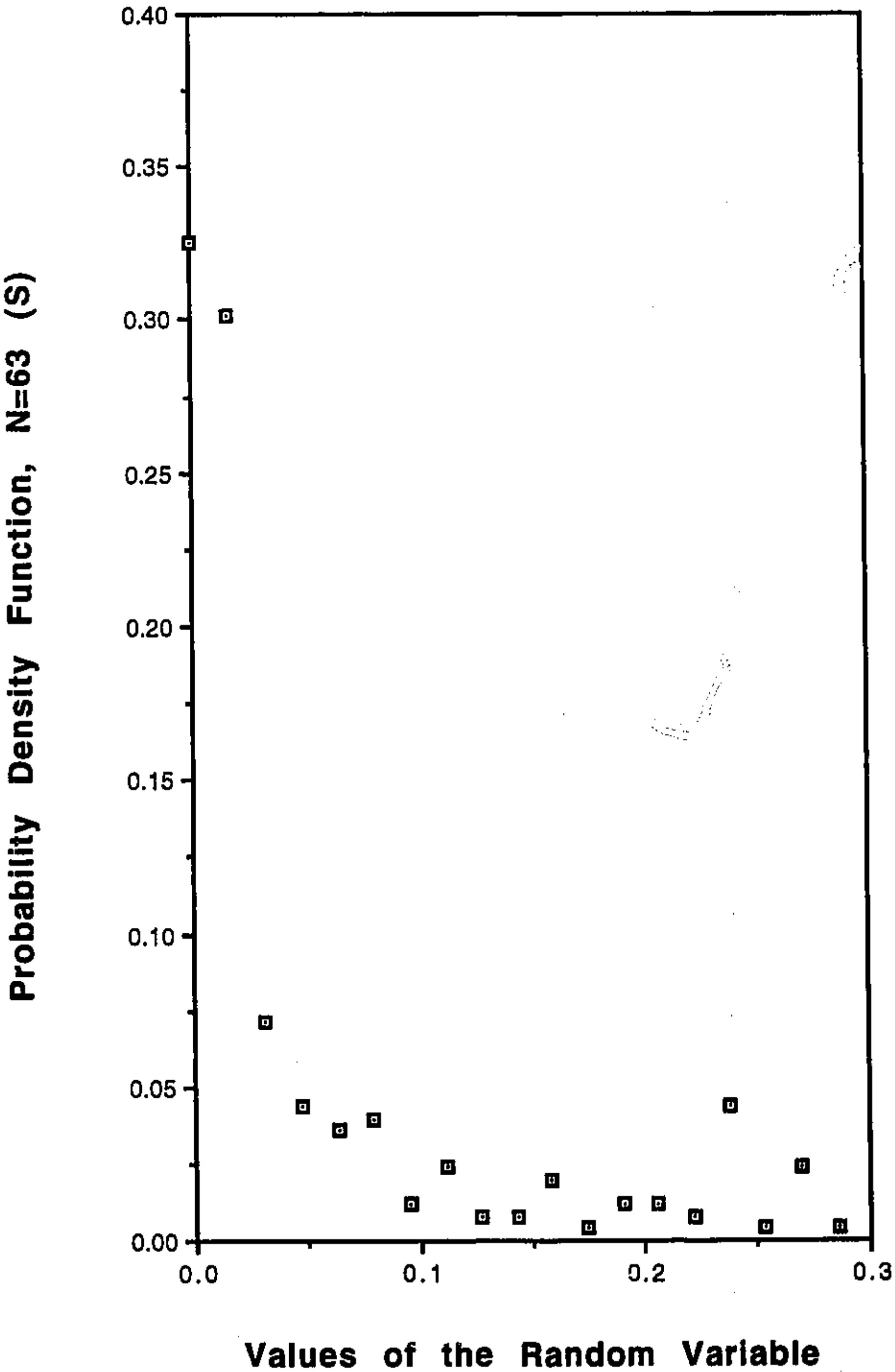

Fig.5.2b: Pdf of one user, ASK, N=63, chip-synchronous assumption.

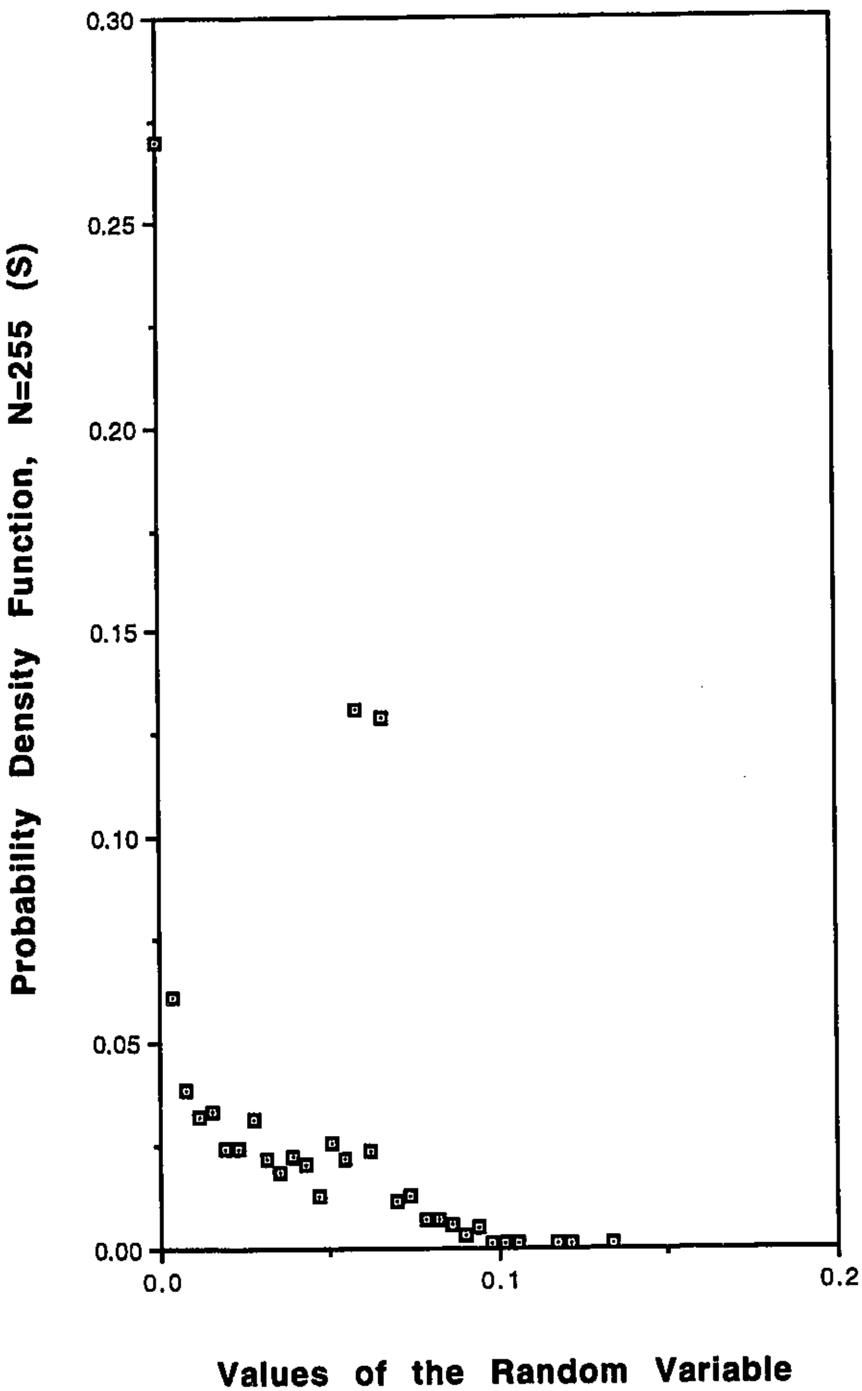

Fig.5.2c: Pdf of one user, ASK, N=255, chip-synchronous asssumption.

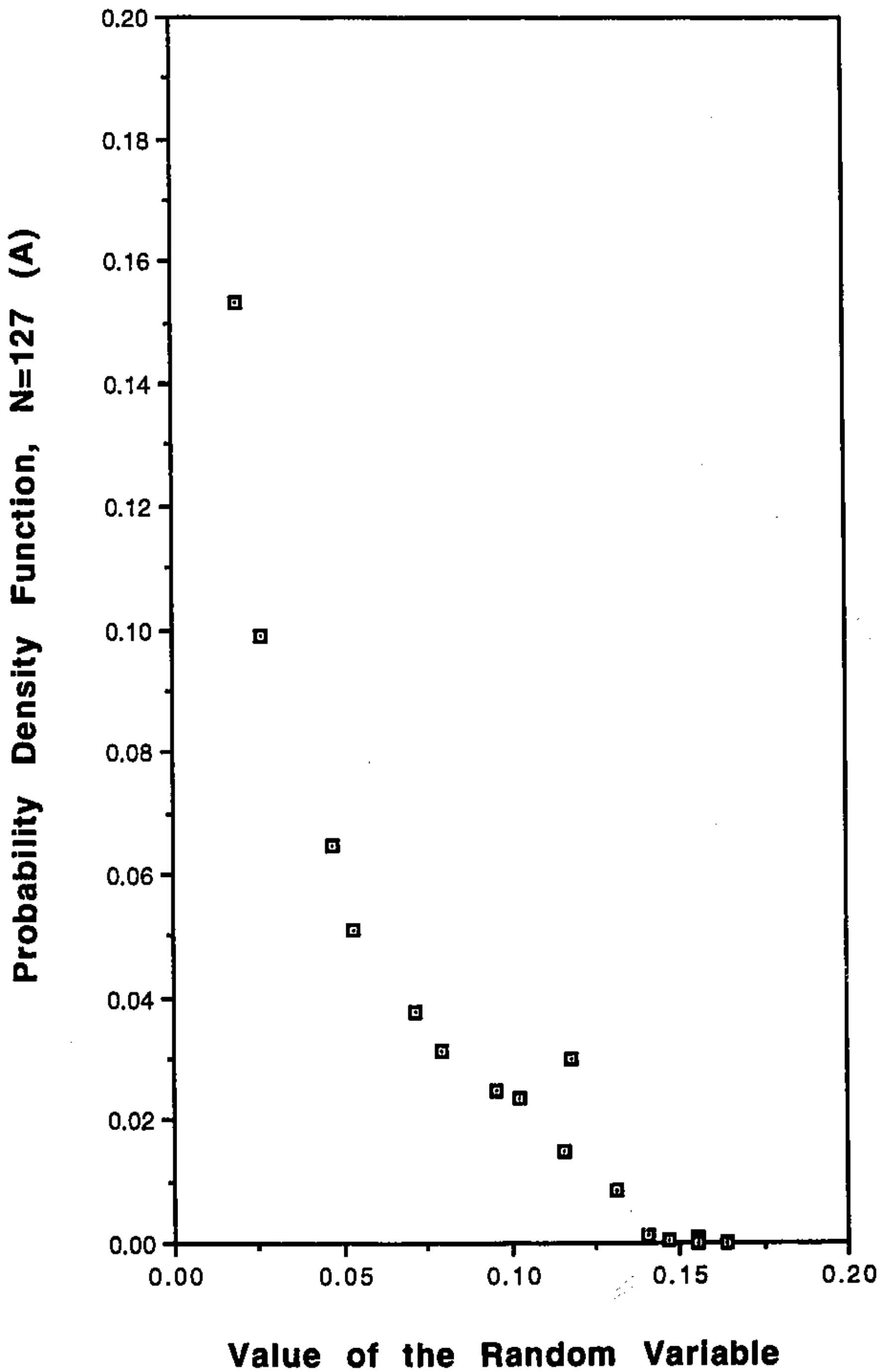

Fig.5.3: Pdf of one user, ASK, N=127, chip-asynchronous asssumption.

squared, and Tr will represent the square root of the actual threshold in the system. Furthermore, capital letters will represent random variables while lower case letters will be a particular outcome of the random variable. For example, A_1 is the random amplitude of the vector corresponding to user 1 while a_1 is a particular outcome that the variable can take on. Starting with the characteristic function of $\sum A_k e^{j\varphi_k}$, it can be shown that:

$$\Phi_{K|\{A_1,A_2,\ldots,A_K,b_0=0\}} = Pr(z \geq Tr) = 1 - Tr \int_0^\infty J_1(Tr \cdot u) \times E_x(u)\, du, \quad (5.25)$$

where

$$E_x(u) = J_0(a_1 u) J_0(a_2 u) \ldots J_0(a_K u) \quad (5.26)$$

and $J_0(x), J_1(x)$ are Bessel functions of orders 0 and 1. The expansion in series is given by:

$$\Phi_{K|\{A_1,A_2,\ldots,A_K,b_0=0\}} = \frac{2}{S} \sum_{m=1}^{\infty} \frac{b_m c_m J_0(Tr \cdot j_m/S)}{j_m J_1^2(j_m)}, \quad (5.27)$$

where $S = \sum_{k=1}^{K} a_k$ and:

$$b_m = \prod_{s=1}^{K} J_0(a_s j_m/S),$$

$$c_m = \sum_{s=1}^{K} \frac{a_s J_1(a_s j_m/S)}{J_0(a_s j_m/S)}.$$

The term j_m is the mth root in ascending order of magnitude of the equation $J_0(x) = 0$. To remove the conditioning over the set of vector amplitudes $\{A_1, A_2, \ldots, A_K\}$, we weight $\Phi_{K|\{A_1,A_2,\ldots,A_K,b_0=0\}}$ by the probability of the particular outcome $\{a_1, a_2, \ldots, a_K\}$ and go over all the possibilities:

$$Pe_{|b_0=0} = \sum_{a_1} \sum_{a_2} \cdots \sum_{a_K} p_{a_1} p_{a_2} \cdots p_{a_K} \Phi_{K|\{A_1,A_2,\ldots,A_K,b_0=0\}}, \quad (5.28)$$

and $p_{a_1} = Pr(A_1 = a_1)$. For a transmitted "1", we proceed in the same way:

$$Pe_{|b_0=1} = 1 - \sum_{a_1}\sum_{a_2}\cdots\sum_{a_K} p_{a_1}p_{a_2}\cdots p_{a_K}\Phi_{K|\{A_1,A_2,\ldots,A_K,b_0=1\}}. \qquad (5.29)$$

However, for numerical precision in the calculations, we found that one should compute the following equivalent formula:

$$Pe_{|b_0=1} = \sum_{a_1}\sum_{a_2}\cdots\sum_{a_K} p_{a_1}p_{a_2}\cdots p_{a_K}\left(1 - \Phi_{K|\{A_1,A_2,\ldots,A_K,b_0=1\}}\right), \qquad (5.30)$$

and $E_x(u)$ in that case is given by:

$$E_x(u) = J_0(u)J_0(a_1u)J_0(a_2u)\ldots J_0(a_Ku). \qquad (5.31)$$

The final probability of error Pe, is given by:

$$Pe = \frac{1}{2}\left(Pe_{|b_0=0} + Pe_{|b_0=1}\right). \qquad (5.32)$$

5.3.2.1 Using an approximate probability density function

Equations (5.28) and (5.29) show how to average the probability of error by going over all the values that each A_k can take from its probability density function. In the chip-synchronous case, we remember that for each user, A_k takes about $Y \approx 200$ in the case of CPFSK. Even when the number of users is smaller than 5, it is quite inefficient to consider all the samples in the pdf of the A_k, since this would require approximately 200^K conditional probability of error calculations. Furthermore, the optimum threshold has to be found. A way to reduce the amount of computation is therefore needed. This can be simply done by approximating the real pdf of the random variable using the GQR technique. Fig. 5.4 shows an example of the utility of this technique. It gives the probability of error for CPFSK modulation, code length $N = 127$, modulation index $h = 2.0$, for 4,5 and 6 interfering users. The case of ASK, $N = 127$ and four users is also given. For ASK,

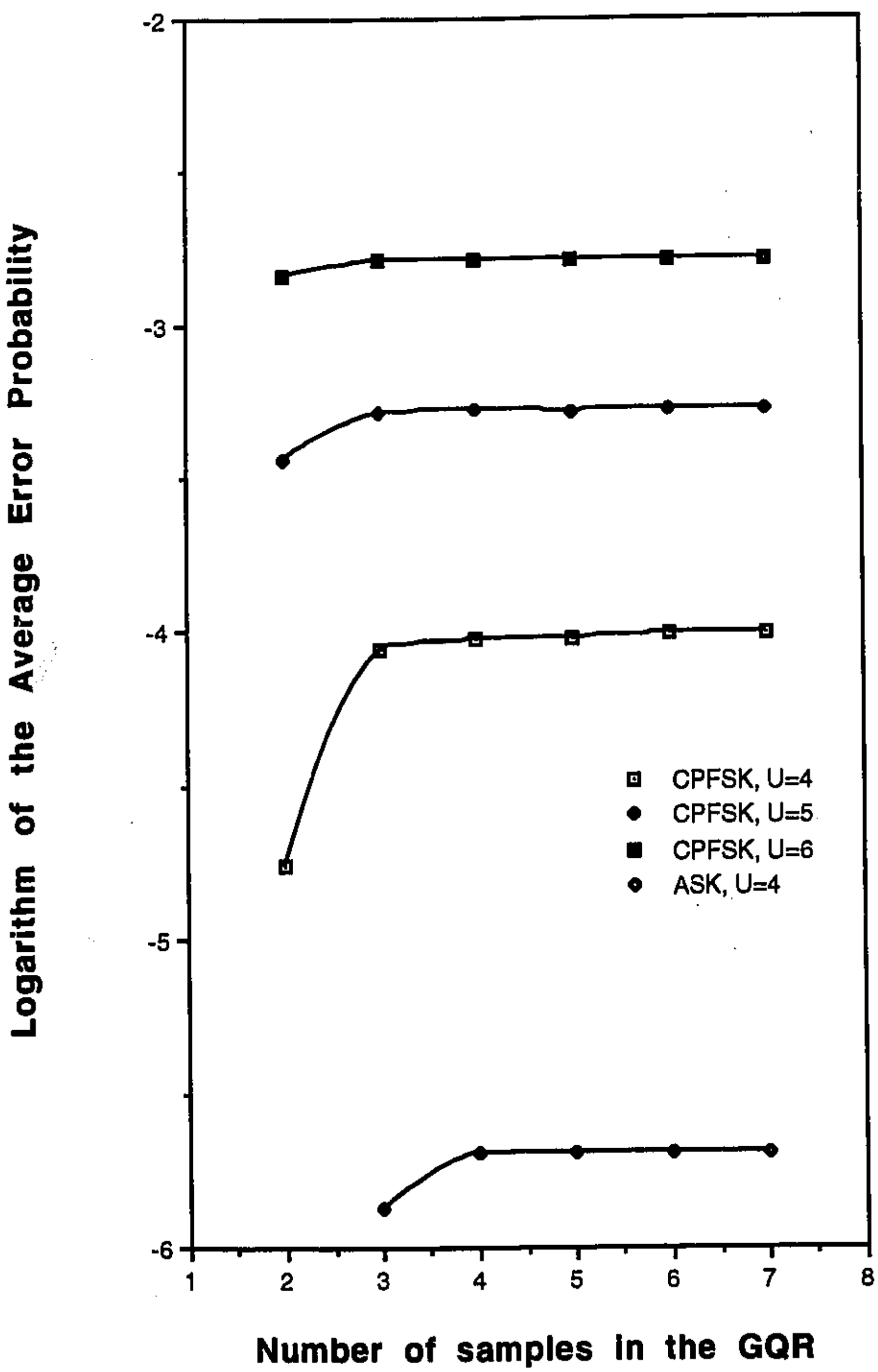

Fig.5.4: Convergence of the error probability as the number of samples is increased in the G.Q.R.

each A_k before using the GQR takes about 24 values so that 24^4 averaging of the error probability values are needed. We see that with the GQR technique, only 7 nodes (T=7) are needed to obtain a good convergence, so that the number of averaging reduces to 2400, a tremendous reduction. The exact probability of error calculated in this case is $P_e = 2.0221 \times 10^{-6}$, while the approximation with the GQR produces an average $P_e = 2.0258 \times 10^{-6}$. For CPFSK and $K < 6$, we use the approximate pdf at all times since the exact pdf would require an unrealistic number of averages. In the next section, we will present an optimum technique for $K > 6$.

5.3.3 Numerical Integration

One possibility for $K \geq 6$ is to use a numerical integration technique, similiar to the one used by Rice [47] in the case of deterministic A_k's. We generalize the technique for random A_k and show its efficiency in the context of noncoherent optical CDMA. We recall that for a "0" transmitted, we have to compute the following probability of error:

$$\Phi_{K|\{A_1,A_2,\ldots,A_K,b_0=0\}} = 1 - Tr \int_0^\infty J_1(Tr \cdot u) \times \prod_k J_0(a_k u) \quad du \tag{5.33}$$

and for a "1" transmitted:

$$\Phi_{K|\{A_1,A_2,\ldots,A_K,b_0=1\}} = Tr \int_0^\infty J_1(Tr \cdot u) J_0(u) \times \prod_k J_0(a_k u) \quad du \tag{5.34}$$

Since each random variable A_k is decoupled in this equation, we can first average the probability of error before performing the integration, that is:

$$\begin{aligned} Pe_{|b_0=0} &= 1 - Tr \int_0^\infty J_1(Tr \cdot u) \int \sum_{a_1} J_0(A_1 u) p_{a_1} \delta(A_1 - a_1) dA_1 \\ &\times \int \sum_{a_2} J_0(A_2 u) p_{a_2} \delta(A_2 - a_2) dA_2 \ldots \times \int \sum_{a_K} J_0(A_K u) p_{a_K} \delta(A_K - a_K) dA_K \quad du \\ &= 1 - Tr \int_0^\infty J_1(Tr \cdot u) \left[\sum_{a_1} p_{a_1} J_0(a_1 u)\right] \ldots \left[\sum_{a_K} p_{a_K} J_0(a_K u)\right] du \end{aligned} \tag{5.35}$$

For a "1" transmitted, the same type of equation is obtained. We see that in (5.35) the interfering users appear as a product of sums in the integral. For each value of the integration variable u, a sum is calculated for each interfering user according to the different values a_k that the amplitude A_k of the vector can take on. The product of all the sums is then taken; adding more interfering users only adds the number of terms in the product and therefore no exponential increase is encountered as in the preceding technique. However, as already pointed out in [47], when the number of Bessel functions $J_0(a_k u)$ is smaller than 5, it is very difficult, if not impossible to have reliable results and good convergence properties by numerical integration. This is due to the fact that the rate of convergence follows $J_0(t) = O(t^{-1/2})$. We then use the series expansion technique previously described. The complementary of both techniques is therefore obvious and very useful. In order to compute (5.35) a numerical integration needs be done. We have used a simple trapezoidal rule method.

5.3.4 Gaussian approximation for ASK and CPFSK

It is interesting to see how the precise calculation of the probability of error compares with the results obtained when the interfering signals at the input of the photodetector are treated as Gaussian noise. For this we write (5.17) as:

$$\begin{aligned} z &= \left[b_0 + \sum A_k \cos\varphi_k\right]^2 + \left[\sum A_k \sin\varphi_k\right]^2 \\ &= \left[b_0 + nc\right]^2 + ns^2 \end{aligned} \tag{5.36}$$

where $nc = \sum A_k \cos\varphi_k$ and $ns = \sum A_k \sin\varphi_k$ are respectively taken as the inphase and quadrature components of the Gaussian noise. In that case $z^{\frac{1}{2}}$ is a Rician random variable when $b_0 = 1$ and a Rayleigh random variable when $b_0 = 0$. The variance is calculated by:

$$\sigma_{nc}^2 = \sigma_{ns}^2 = E\left(\sum A_k^2 cos^2\varphi_k\right) = \frac{1}{2}\sum_k\left(\sum_i \left(a_k^i\right)^2 p_{a_k^i}\right), \tag{5.37}$$

since $E(\cos\varphi_i \cos\varphi_j) = 0$ for $i \neq j$. The P_e calculated when using a Rician or a Rayleigh pdf will be compared to the results obtained with the actual distribution in Section 5.5.

5.4 Probability of Error for LD-FSK

Going back to (5.15) and (5.16) we recall that we seek the following probability:

$$Pr\Big(z = z_1(T) - z_2(T) \underset{\text{"0"}}{\overset{\text{"1"}}{\gtrless}} 0\Big)$$

One possible way to calculate this probability is first to expand the modulus of $z_1(T)$ and $z_2(T)$ to get:

$$\begin{aligned}
&z = (2I_0 - 1) + \\
&\frac{1}{N^2}\sum_k \Big[R_k^2(\tau_k)(2I_{-1}^k - 1) + \widehat{R_k}^2(\tau_k)(2I_0^k - 1) + 2(I_0^k + I_{-1}^k - 1)R_k^2(\tau_k)\widehat{R_k}^2(\tau_k)\Big] \\
&+ \frac{2I_0}{N}\sum_k \Big(I_{-1}^k R_k(\tau_k) + I_0^k \widehat{R_k}(\tau_k)\Big)\cos(\varphi_k) \\
&+ \frac{2(1-I_0)}{N}\sum_k \Big((1 - I_{-1}^k)R_k(\tau_k) + (1 - I_0^k)\widehat{R_k}(\tau_k)\Big)\cos(\varphi_k^2) \\
&+ \frac{2}{N^2}\sum_k\sum_j \Big(I_{-1}^k R_k(\tau_k) + I_0^k \widehat{R_k}(\tau_k)\Big)\Big(I_{-1}^j R_j(\tau_j) + I_0^j \widehat{R_j}(\tau_j)\Big)\cos(\varphi_{k,j}) \\
&+ \frac{2}{N^2}\sum_k\sum_j \Big((1 - I_{-1}^k)R_k(\tau_k) + (1 - I_0^k)\widehat{R_k}(\tau_k)\Big) \\
&\qquad\qquad \Big((1 - I_{-1}^j)R_j(\tau_j) + (1 - I_0^j)\widehat{R_j}(\tau_j)\Big)\cos(\varphi_{k,j}^2)
\end{aligned} \tag{5.38}$$

The first term represents the desired signal and has the value $1, -1$ when λ_1, λ_0 are transmitted, respectively. The interfering terms have random and independent phases, but their amplitudes clearly are not independent. One possible way to evaluate the probability of error is to find an expression for the case of fixed amplitudes and random phases, and then to average the results. Note, however, that for LD-FSK, using the GQR technique means finding the joint density of $R_k(\tau_k)$, $\widehat{R_k}(\tau_k)$, for all k, since they are not independent. In the case of chip-synchronism this is straightforward, but in the case of chip-asynchronism this is more involved. A two-dimensional quadrature rule technique has to be used. Although this poses no conceptual problems, one might wonder if it is worthwhile going over all these calculations. In the following we will only briefly study the case of LD-FSK and therefore we seek only an approximation of the error probability. The reason is that we believe that LD-FSK is unlikely to be a popular modulation choice when combined with CDMA. LD-FSK requires either a fast tunable laser, from λ_1 to λ_0, or two lasers. If one posseses the former the question might arises as why not using wavelength division multiplexing alone. On the other hand, providing each subscriber with two transmitters might be too costly and an unviable option when compared to ASK. Note that, the same comments can be made concerning CPFSK while in this case the range of tunability needed is much smaller. In the next section we will therefore present more results using the ASK modulation format than with the other modulation formats.

An approximation of the error probability for LD-FSK can be obtained as follows. First, by symmetry we only need to compute either the probability of error when $I_0 = 0$ or $I_0 = 1$; we choose $I_0 = 0$. Second, since chip-synchronism leads to an upper bound, take $\tau_k = l_k T_c$. We now have to evaluate:

$$Pe_{|I_0=0} = Pr\Big(\sum_k B_k \cos\varphi_k \geq X + 1\Big),$$

where X is the second term in Eqn(5.38) and the sum groups all the cosine terms. From there we may use a numerical integration technique. The conditional probability of error is given by:

$$Pe_{|I_0=0} = \frac{1}{2} - \frac{1}{\pi}\int_0^\infty \prod_k J_0(B_k u) \quad \frac{\sin\big((1+X)u\big)}{u} du \tag{5.39}$$

Probability of error comparison		
Bit values, user 1	Bit values, user 2	Bit error probability
0 0	0 0	2.95e-6
0 0	0 1	1.63e-6
0 0	1 0	1.88e-6
0 0	1 1	4.0e-7
0 1	0 0	1.50e-6
0 1	0 1	8.25e-7
0 1	1 0	9.62e-7
0 1	1 1	1.84e-7
1 0	0 0	1.54e-6
1 0	0 1	8.41e-7
1 0	1 0	9.84e-7
1 0	1 1	1.81e-7
1 1	0 0	4.55e-7
1 1	0 1	2.35e-7
1 1	1 0	2.94e-7
1 1	1 1	2.85e-8

Table 5.1 Pe as a function of the interfering bit values

Note that, in this case the amplitudes B_k are not independent so that the averaging can not be performed before the integration, as it was done in Section 5.3.3. We are therefore constrained to face an exponentially growing computational complexity as the number of interfering users increases. If, for each user, the number of samples in the joint density of $\left(R_k(\tau_k),\ \widehat{R_k}(\tau_k)\right)$ is $\approx M$, M^K averaging will be needed. We will bring the simplification a step further by assuming for each user that $I_{-1}^k = I_0^k$. In this case it is easy to see that the density we need is simply the density of

$$R_k(\tau_k) + \widehat{R_k}(\tau_k) = \Theta_k(l_k).$$

The number of values taken by $\theta_k(l_k)$ is small in the case of appropriately chosen pseudorandom sequences. For the case of Gold sequences of period $N = 127$, it is only three, $\theta_k(l_k) \in \{15, -1, -17\}$, and for appropriately chosen m-sequences of period 255, only four, i.e. $\theta_k(l_k) \in \{31, 15, -1, -17\}$. In order to see what would be the *degree* of approximation obtained with this assumption, we evaluate the conditional probability of error for two interfering users, and $N = 127$, for all possible combinations of $\{I^k_{-1}, I^k_0\}_{k=1,2}$. To facilitate the convergence of the numerical integration we included a thermal noise with variance σ^2, so that the signal-to-noise ratio would be $S/N = 1/\sigma^2 = 25$. The integrand in (5.39) must then be multiplied by $e^{-\sigma^2 u^2/2.0}$. As it can be seen, considering only the cases $I^k_{-1} = I^k_0$ for all users will give both the maximum and the minimum probability of error. If the probability of error observed with $I^k_{-1} = I^k_0 = 1$ is negligeable compared to $I^k_{-1} = I^k_0 = 0$ as it is the case here, the final result will therefore constitute an upper bound on the real probability of error. Choosing the chip-synchronous assumption for this modulation scheme will further help to make the results an upper bound.

5.5 Results and Discussion

The results we present give the probability of error as a function of the number of active users for ASK, CPFSK and LD-FSK. As shown in Fig. 5.5, operating the system at the optimum threshold is crucial since small variations (± 0.1) in the threshold level would lead to a large increase in the probability of error. We also note that the optimum threshold increases as the number of users is increased. This is not surprising since it is well known that in binary ASK modulation, as the variance of the noise increases (more users), the optimum threshold level becomes larger. Operating the system with a noise power much smaller than the signal power always leads to an optimum threshold value of 0.5. Fig. 5.6 shows the optimum threshold as a function of the number of active users for CPFSK modulation, $h = 2.0$ and code lengths $N = 127$ and $N = 255$. The values with the Gaussian approximation are very close to those obtained with the exact probability density function. It can also be seen that for $N = 255$, the optimum threshold value for a given number of active users is always smaller than the one for $N = 127$. This of course confirms the fact that a longer code period reduces the interfering power going through the optical filter and therefore the noise variance in the system.

Figure 5.7 shows the probability of error for ASK as a function of the number of active users for different code lengths, and for the chip-synchronous assumption. We see that $N = 63$ gives an unsatisfactory performance, while $N = 127$ allows ≈ 5 simultaneous transmitting users with a probability of error of 10^{-6}. Doubling the code length to $N = 255$, using Kasami sequences, allows 11 active users for the same probability of error, so approximately twice the number. Using $N = 255$ with M-sequences, leads to a less satisfactory performance, since as seen in chapter 3, the cross-correlation is higher than with Kasami sequences. Since the set of Kasami sequences is too small to be practical, we will in the following consider only the M-sequences.

Figure 5.8 shows that CPFSK leads to a worse performance. A code length $N = 255$ for that modulation allows only 6 active users instead of the 11 possible with ASK. We found that the probability of error was almost insensitive to the modulation index value, for the practical range $1 < h < 10$. The worse performance of CPFSK compared to ASK is expected since for CPFSK, no matter which bit is transmitted by the interfering users, almost the same interfering power will be transmitted through the optical filter. The power spectral density for these users is governed by the pseudorandom sequence and not by the data. Finally, we see that the Gaussian approximation gives an unsatisfactory precision for $N = 63$ and $N = 127$ for ASK modulation (it gives a lower bound) , but very good results in the case of $N = 255$. It should be remembered however that the variance used in these calculations is from the exact pdf found with our technique, and that the white Gaussian noise approximation is not used. In Fig. 5.9 we show the P_e for LD-FSK. The results show better results than ASK, but of course there is an increase in the receiver complexity, and in the source requirements. In Fig. 5.10, a comparison is made between the chip-synchronous and the chip-asynchronous assumptions. As stated previously, the chip-synchronous assumption yields an upper bound. Finally in Fig. 5.11, the results when using Kronecker sequences are shown. We assume that all users have the same inner sequence, so that the delay lines are not programmable. The case of using standard M-sequences of period $N = 511$, is now compared to the

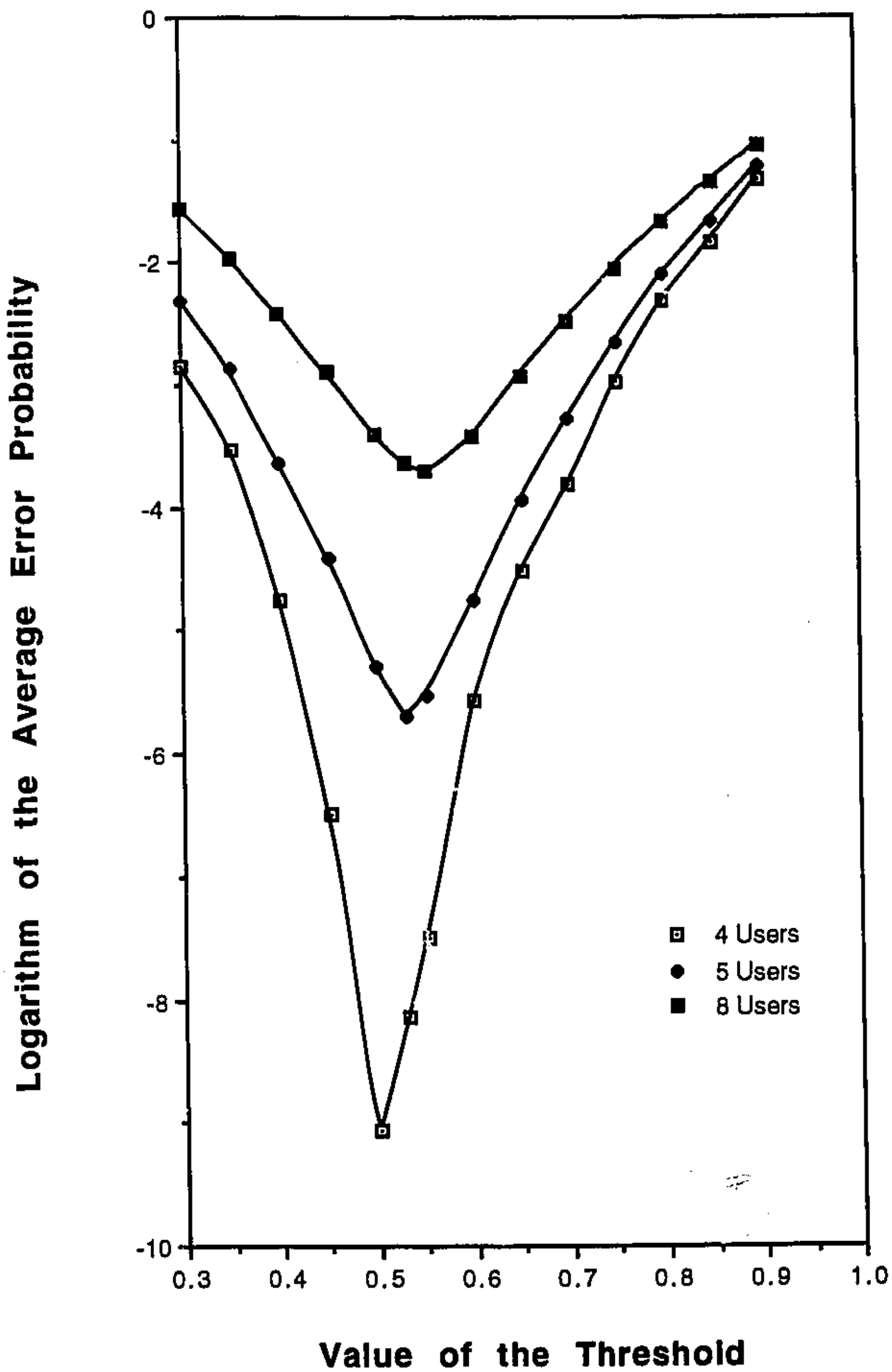

Fig.5.5: Pe vs threshold, ASK, N=127.

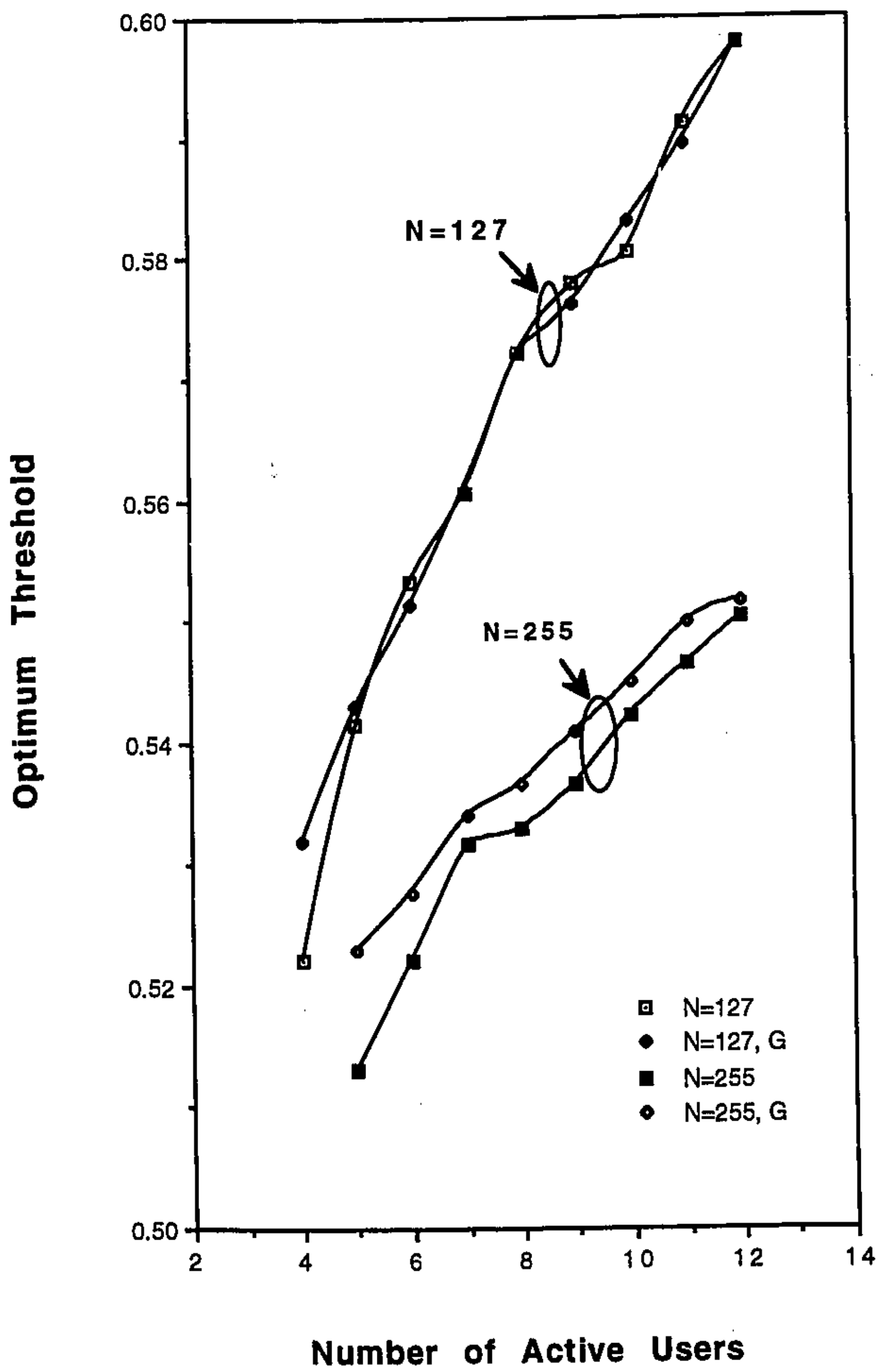

Fig.5.6: Optimum threshold vs the number of active users, CPFSK, h=2.0.

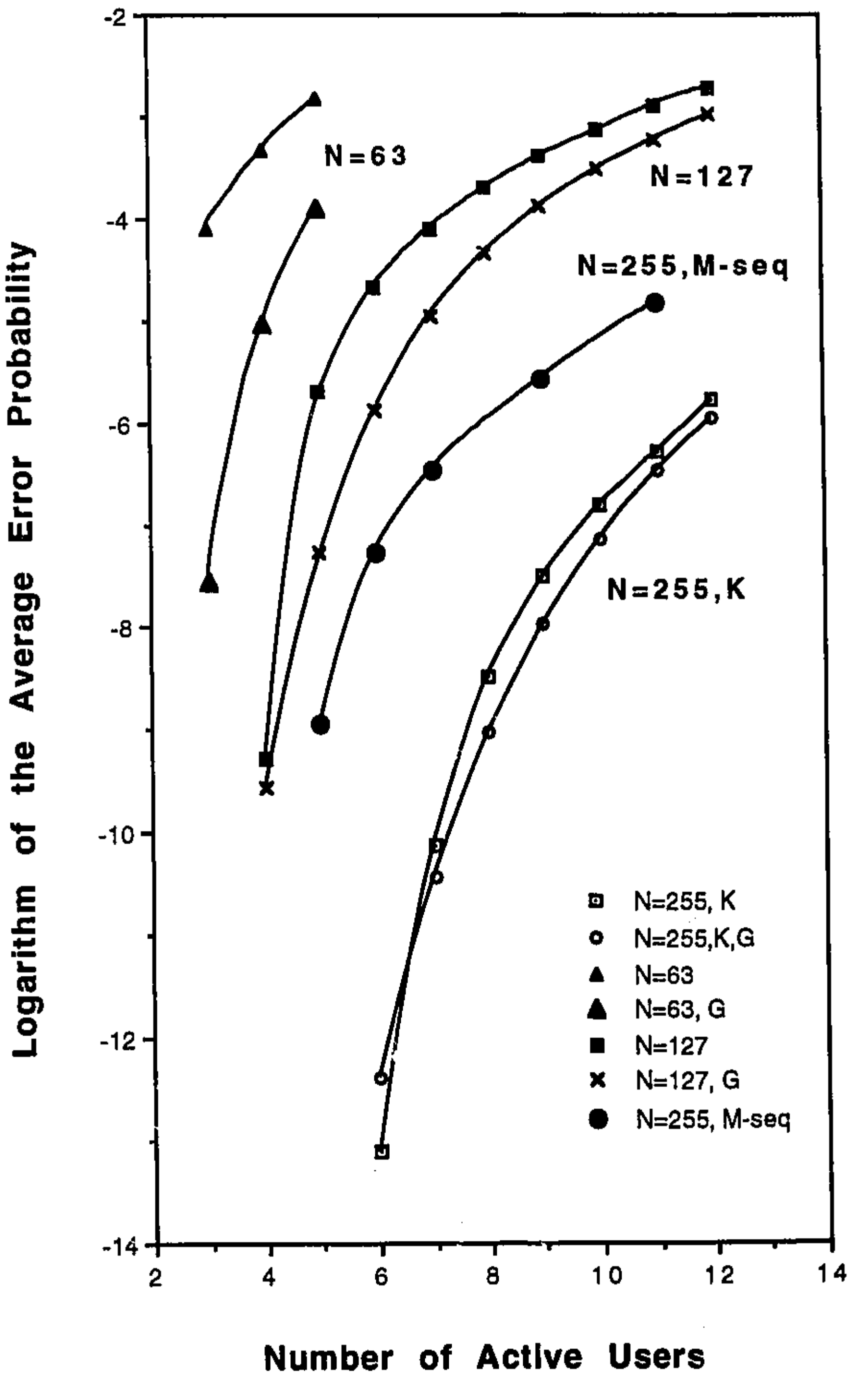

Fig.5.7: Pe vs number of active users, ASK, chip-synchronous assumption.

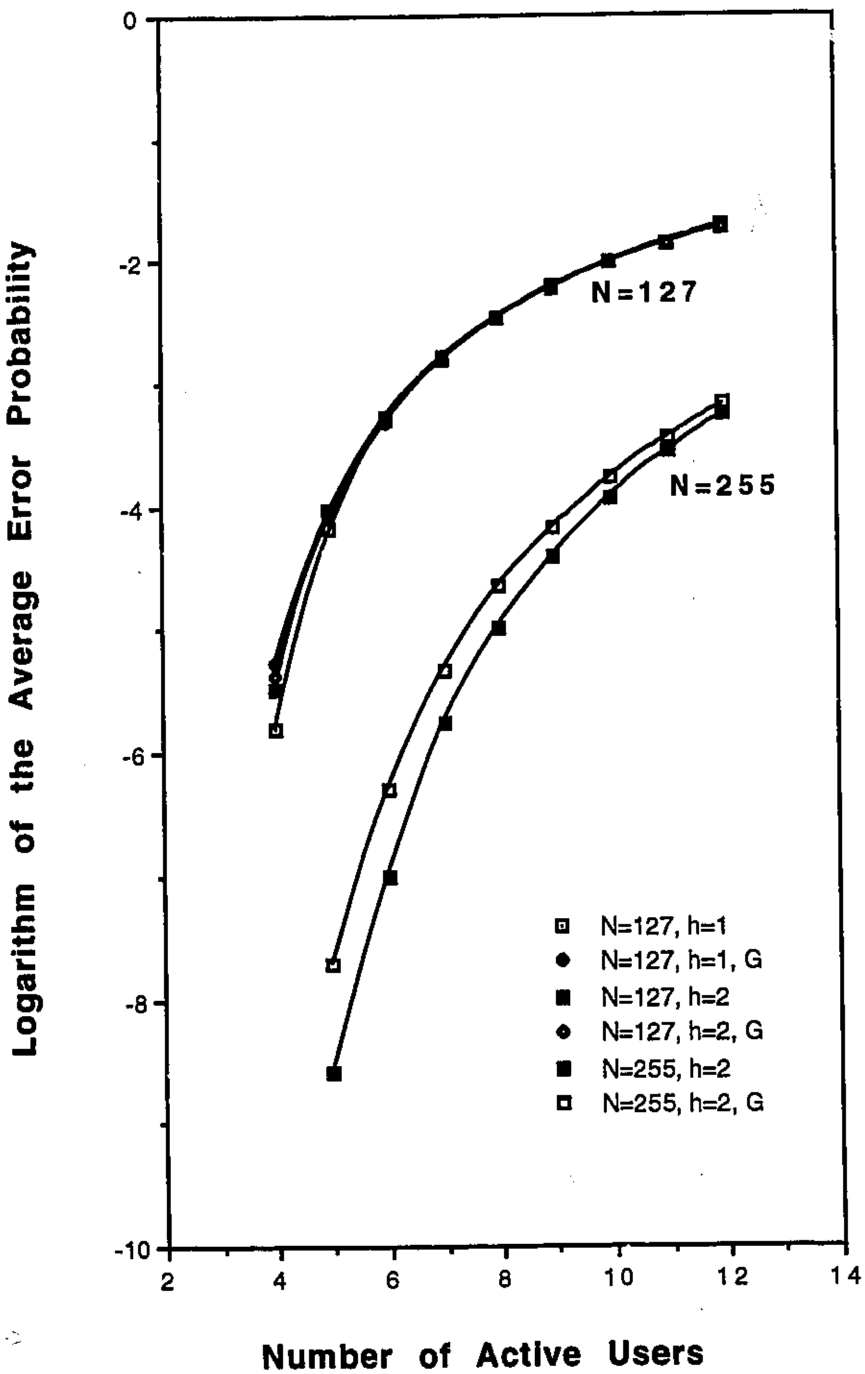

Fig.5.8: Pe vs number of active users, CPFSK, chip-synchronous assumption.

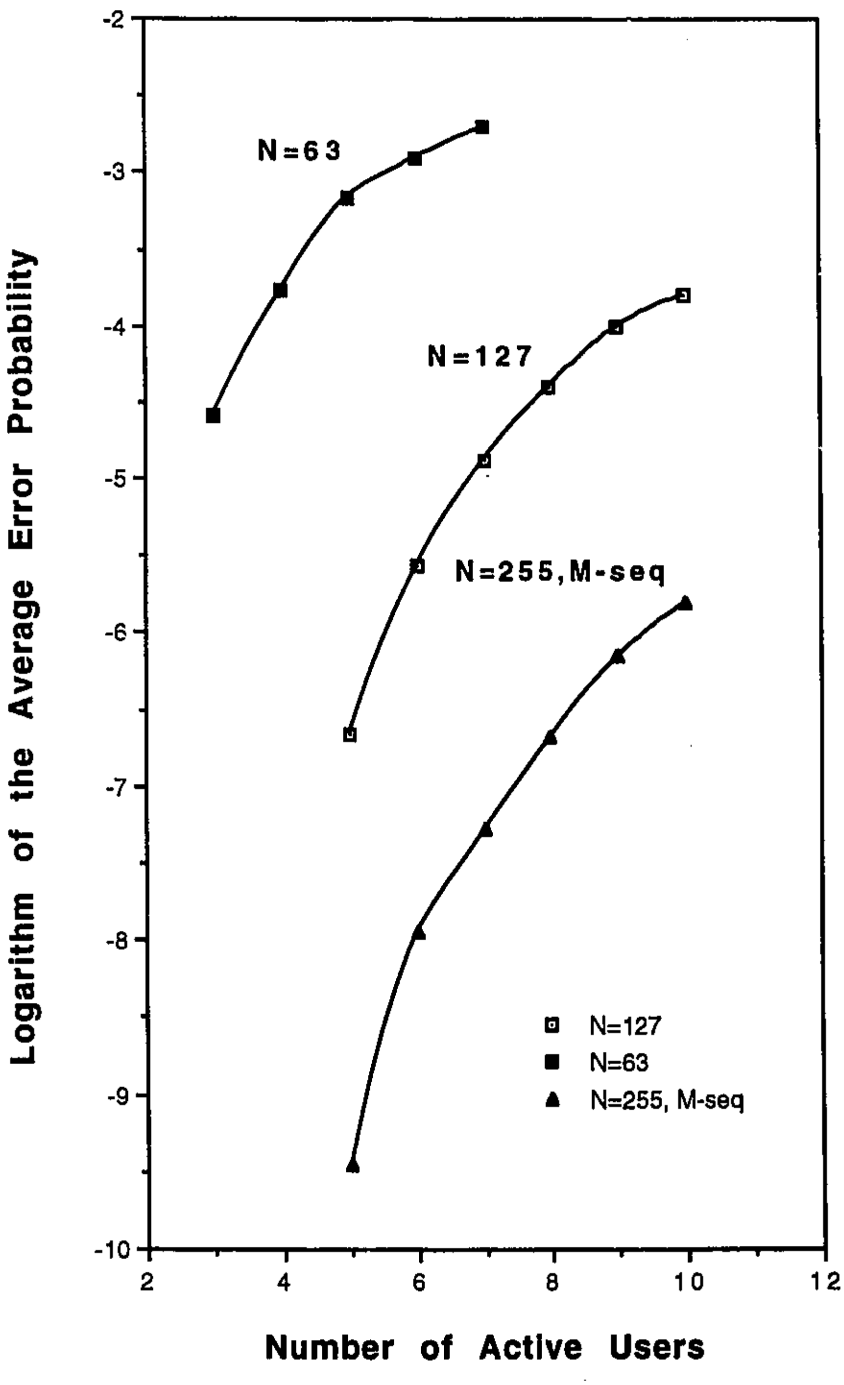

Fig.5.9: Pe vs number of active users, LD-FSK, chip-synchronous assumption.

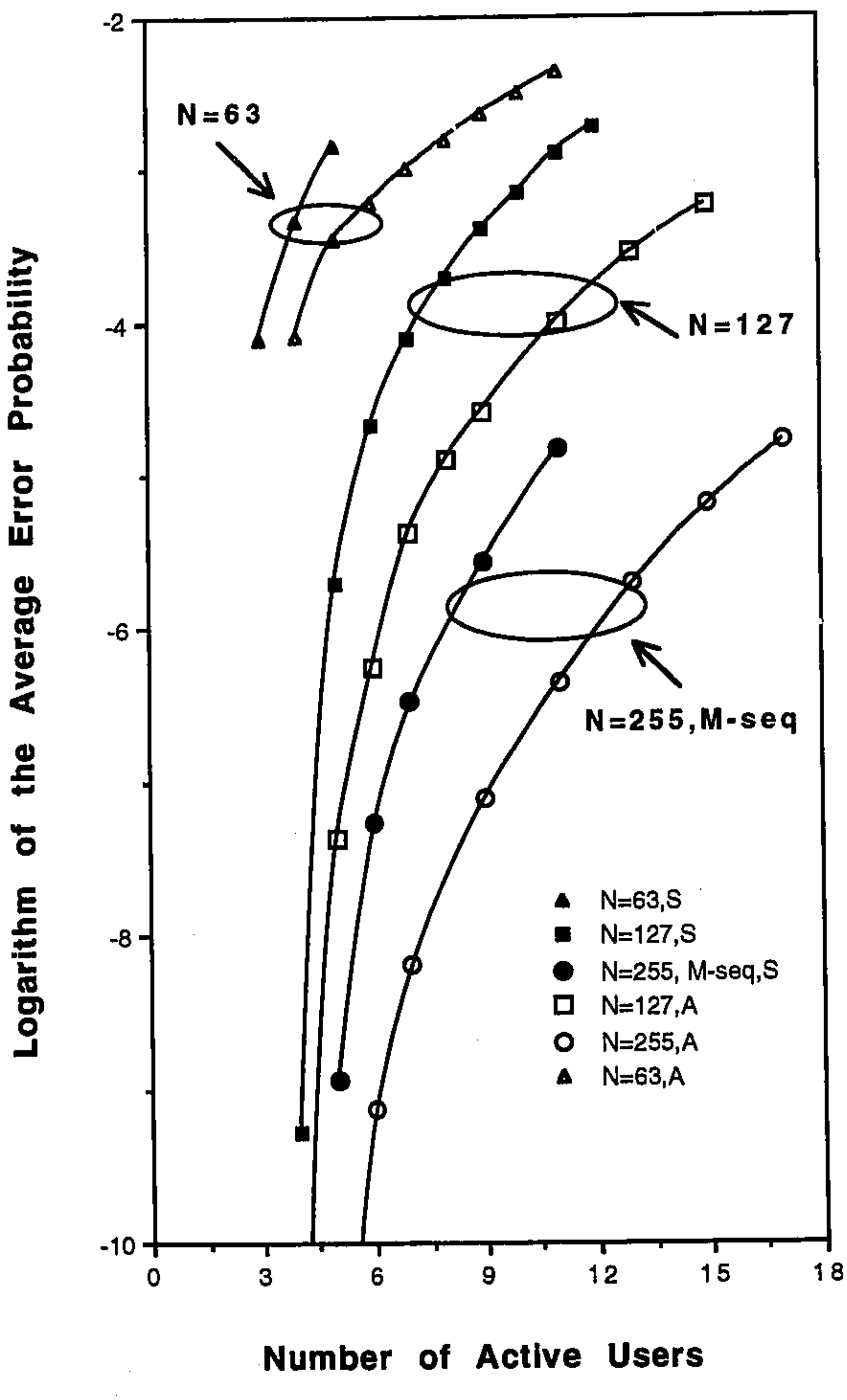

Fig.5.10:Pe vs number of active users, ASK, chip-syn. & chip-asyn. comparison.

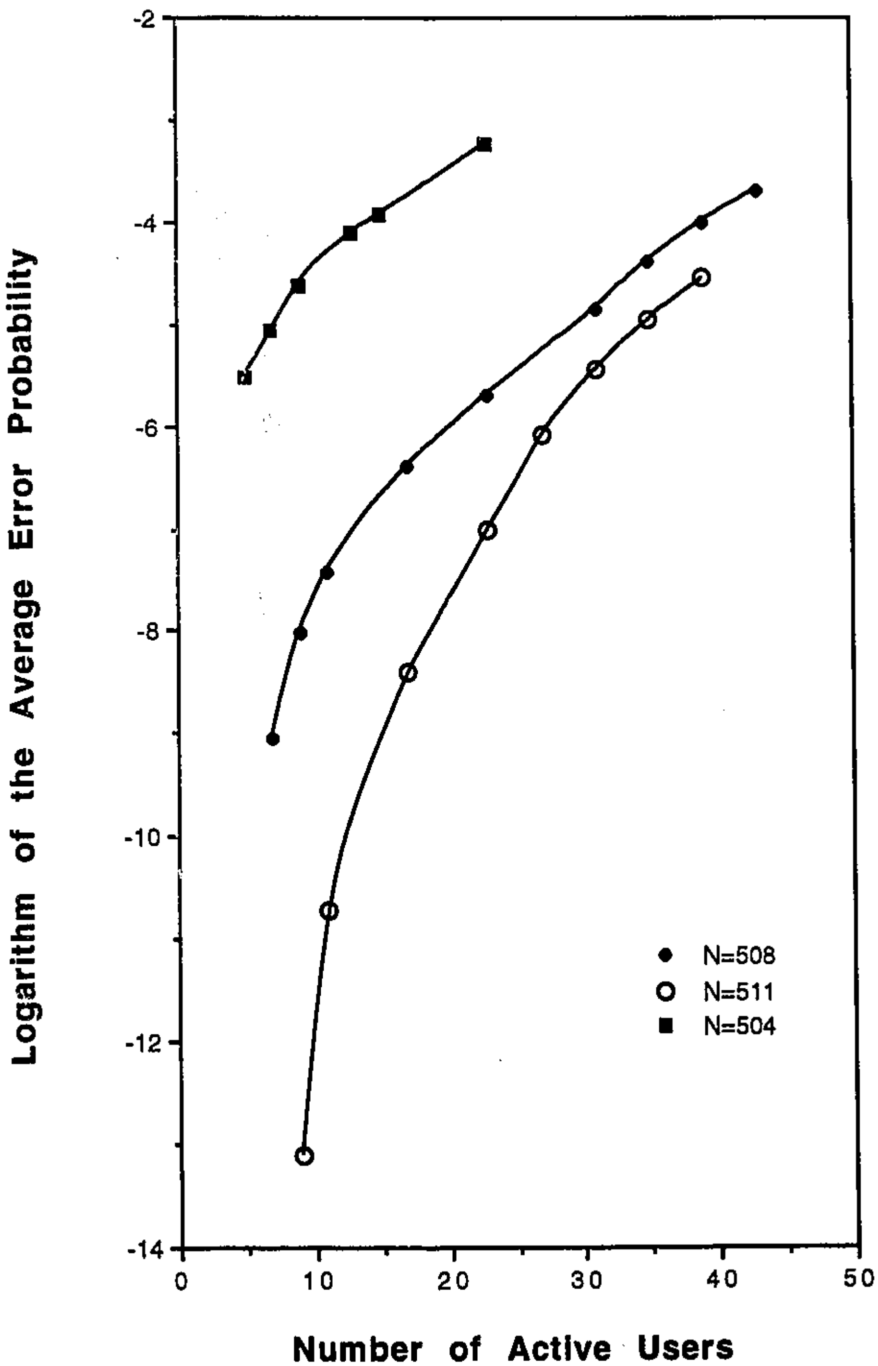

Fig.5.11: Pe vs number of active users, ASK,
N=511, N=508 (No=127,Ni=4), N=504 (No=63,Ni=8);

performance of a system using an outer sequence of length $No = 127$ and an inner sequence of length $Ni = 4$ (the Barker sequence), giving $N = 508$. The case of a system using a Gold sequence of length $No = 63$ and an almost perfect sequence of length $Ni = 8$, giving $N = 504$, is also shown. As seen, using Kronecker sequences give a worse performance, but allow simpler encoding architectures. Using a longer period outer sequence seems to give a better performance than using a longer one. More results, using different combinations of these will be provided in Chapter 6.

5.6 Partial Cross-Correlation Effects

Although the model of Fig. 5.1 is adequate in a MAI limited environment, a filter is used in practice after photodetection to filter the shot noise and the thermal noise. The combined impulse response of the optical filter and the post-detection filter should not exceed the bit duration T to avoid intersymbol inteference (ISI). The optimum bandwidth of both filters will depend on the relative power of the different interfering sources. In this section we present a first step in studying these effects.

5.6.1 Dual-Filter Model

The Fig. 5.12 shows the model considered. Compared to Fig. 5.1, an optical filter with a larger bandwdith than $1/T$ is used before the detector. We model it as an integrator with integration time T', with $T' < T$. The post-detection filter is modeled as an integrate-and-dump filter with integration time $T - T' = T''$. Only the case of ASK will be considered. Our goal is to find an expression for the optical field $\vec{E}_T(t)$ incident on the photodetector. If $\vec{E}(t)$ is the field at the input of the optical filter then:

$$\left|\vec{E}_T(t)\right|^2 = \left|\frac{1}{T'}\int_{t-T'}^{t} \vec{E}(\tau)d\tau\right|^2 \qquad T' < t < T \tag{5.40}$$

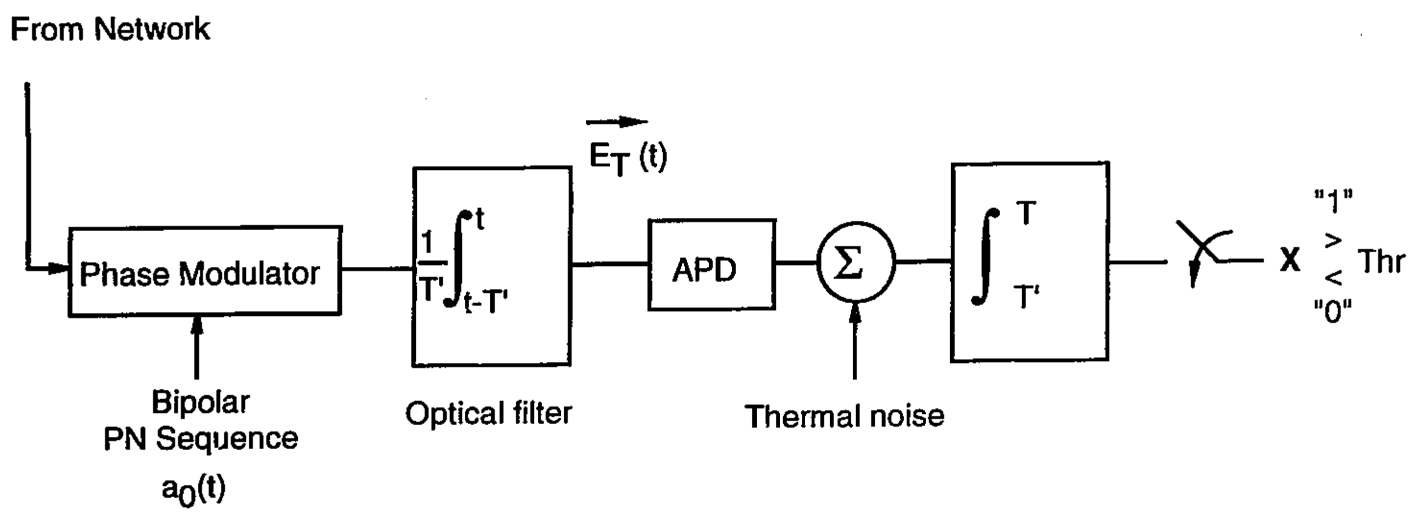

Fig. 5.12: Receiver model for coherent CDMA system including a post-detection filter.

Following the notation of Section 5.2.2. we have:

$$\begin{aligned}\vec{E}_T(t) &= \sqrt{P}b_0e^{j\Phi_0} + \sum_{k=1}^{K} X_k(t) \\ &= \sqrt{P}b_0e^{j\Phi_0} + \sum_{k=1}^{K} e^{j\Phi_k}\frac{\sqrt{P}}{T'} R_k(t)\end{aligned} \tag{5.41}$$

Due to the partial integration time of the optical filter compared to the bit duration T, only a partial cross-correlation will be performed optically for the interfering signals. The usual cross-correlation terms no longer hold and new expressions have to be found. The cross-correlation expressions we get are necessarily functions of time. We will assume $T' = MT_c$, where M is an integer. For $l_kT_c \leq \tau_k \leq (l_k+1)T_c$, where τ_k is the delay between the desired signal and interfering signal k, and code period N (such that $T = NT_c$), one can derive the following. For $yT_c \leq t \leq yT_c + \tau_k - l_kT_c$ and with $M \leq y \leq (N-1)$,

$$\begin{aligned}R_k(t) =& a_j^0 a_{N-l_k-1+j}^k\left[yT_c + \tau_k - l_kT_c - t\right] + a_{j+M}^0 a_{N-l_k-1+j+M}^k\left[t - yT_c\right] + \\ &\sum_{n=j+1}^{y-1} a_n^0 a_{N-l_k-1+n}^k\left[\tau_k - l_kT_c\right] + \sum_{n=j}^{y-1} a_n^0 a_{N-l_k+n}^k\left[(l_k+1)T_c - \tau_k\right]\end{aligned}, \tag{5.42}$$

while when $yT_c + \tau_k - l_kT_c \leq t \leq (y+1)T_c$,

$$\begin{aligned}R_k(t) =& a_j^0 a_{N-l_k+j}^k\left[(y+1)T_c - t\right] + a_{j+M}^0 a_{N-l_k+j+M}^k\left[t - yT_c - (\tau_k - l_kT_c)\right] + \\ &\sum_{n=j+1}^{y} a_n^0 a_{N-l_k-1+n}^k\left[\tau_k - l_kT_c\right] + \sum_{n=j+1}^{y-1} a_n^0 a_{N-l_k+n}^k\left[(l_k+1)T_c - \tau_k\right]\end{aligned}, \tag{5.43}$$

where $j = y - M$. Each term gets multiplied by I_0^k if we have a_i^0 such that $i \geq l_k$ and a_i^k such that $i \neq N-1$, and by I_{-1}^k otherwise. Note that, the first two terms in (5.42) and (5-43) are functions of only time. In calculating the probability of error in the next section, we will need the rate $\lambda(t)$ of the inhomogeneous Poisson point process, which is simply related to the intensity of the field $\vec{E}_T(t)$ by:

$$\begin{aligned}\lambda(t) &= \frac{\eta P}{hf}\left|\vec{E}_T(t)\right|^2 \\ &= \frac{\eta P}{hf}\left|b_0 e^{j\Phi_0} + \sum_{k=1}^{K} e^{j\Phi_k}\frac{}{T'} R_k(t)\right|^2\end{aligned} \tag{5.44}$$

The post-detection filter being an integrate-and-dump filter, the mean value of the process is then:

$$\begin{aligned}\lambda &= \frac{\eta P}{hf}\int_{T'}^{T} \lambda(t)dt \\ &= \frac{\eta P}{hf}\int_{MT_c}^{NT_c}\left|b_0 e^{j\phi_0} + \sum_{k=1}^{K} X_k(t)\right|^2 dt \\ &= \frac{\eta PT_c}{hf}\sum_{y=M}^{N-1}\int_y^{y+1}\left|b_0 e^{j\phi_0} + \sum_{k=1}^{K}\frac{R_k(t)}{M}e^{j\phi_k}\right|^2 dt \\ &= \frac{\eta PT_c}{hf}\Bigg(b_o(N-M) + \sum_{k=1}^{K}\frac{1}{M^2}\sum_y\int_y^{y+1} R_k^2(t)dt \\ &+ \sum_{k=1}^{K}\frac{2b_0}{M}\cos\varphi_k\sum_y\int_y^{y+1} R_k(t)dt \\ &+ \frac{2}{M^2}\sum_{k=1}^{K-1}\sum_{j=k+1}^{K}\cos\varphi_{k,j}\sum_y\int_y^{y+1} R_k(t)R_j(t)dt\Bigg)\end{aligned} \tag{5.45}$$

In the above, $\frac{\eta PT_c}{hf}$ is the number of received photons/chip and $R_k(t)$ is given by (5.42) and (5.43). One can see that as the bandwidth of the electronic filter is decreased (M increases), the collected desired signal power $b_o(N-M)$ is decreased. We now proceed to the evaluation of the average bit error probability.

5.6.2 Computation of the Error Probability

There are many ways to evaluate the error probability of systems including shot noise and thermal noise. The saddlepoint aproximation developed by Helstrom [48] is convenient when one has the moment generating function (MGF) of the decision variable. It is known to give excellent accuracy in the tail of the distributions. Let us call the decision variable X, and write its MGF, conditioned on the interfering users parameters $\{\tau_k\}_{k=1}^{K}$ and $\{I_{-1}, I_0\}_{k=1}^{K}$:

$$M_X(s) = exp\left(e^{\int_{-\infty}^{\infty} \lambda(\alpha) \left[M_g\left(sh_e(T-\alpha)\right) - 1 \right] d\alpha} \right) \quad e^{\sigma^2 s^2/2} \tag{5.46}$$

where $M_g(s)$ is the MGF of the APD gain. In the case considered, $h_e(t) = 1$ for $0 \leq t \leq T - T'$, and 0 otherwise, which yields:

$$M_X(s) = e^{\left[M_g(s)-1 \right] \int_{T'}^{T} \lambda(\alpha) d\alpha} \quad e^{\sigma^2 s^2/2}, \tag{5.47}$$

where σ^2 is the thermal noise variance given by:

$$\sigma^2 = \frac{2kT^o(N-M)T_c}{Rq^2} \tag{5.48}$$

where k is the Boltzmann constant, q is the electronic charge, T^o is the equivalent noise temperature, R is the equivalent input resistance and T_c is the chip period.

In order to get the average probability of bit error by using $M_X(s)$, one would like to average the MGF over the statistics of λ:

$$\overline{M_x(s)} = \int_0^{\infty} M_X(s) p(\lambda) d\lambda \tag{5.49}$$

This would require either a knowledge of the pdf of λ, or its moments. Neither approach is an easy task here since we can not express λ as $\lambda = \sum \lambda_k$, i.e. as a sum of terms contributed by the different users. We will therefore develop a simple upper bound on the bit error. Our results therefore should not be considered as giving absolute values of the power needed in some particular situation, but they give a good basis for comparing the power required as the optical filter bandwidth is varied. To simplify the calculations, we consider the chip-synchronous case $\tau_k = l_k T_c$ so that only (5.43) is necessary. It is also suitable to decouple $R_k(t)$ and $R_j(t)$ in the last term of (5.45). This is easily done by using the Schwartz inequality. Noting that an arbitrary phase term can be included in the phases ϕ_k, we can take the modulus of the amplitudes in (5.45) and get:

$$\begin{aligned}\Big|\sum_{y=M}^{N-1}\int_y^{y+1} R_k(t)R_j(t)dt\Big| \leq \\ \int_M^N |R_k(t)||R_j(t)|dt \quad &\leq \quad \left[\int_M^N R_k^2(t)dt\right]^{1/2} \quad \left[\int_M^N R_j^2(t)dt\right]^{1/2}\end{aligned} \tag{5.50}$$

Therefore we can rewrite (5.45) as:

$$\begin{aligned}\lambda \leq \frac{\eta P T_c}{hf}\Bigg(& b_o(N-M) + \sum_{k=1}^{K}\frac{1}{M^2}B_k \\ &+ \sum_{k=1}^{K}\frac{2b_0}{M}A_k\cos\varphi_k + \frac{2}{M^2}\sum_{k=1}^{K-1}\sum_{j=k+1}^{K} B_k^{1/2}B_j^{1/2}\cos\varphi_{k,j}\Bigg)\end{aligned} \tag{5.51}$$

where:

$$A_k = \int_M^N R_k(t)dt \qquad\qquad B_k = \int_M^N R_k^2(t)dt$$

Note that each A_k and B_k are function of τ_k through Eqn(5.43). The conditional probability of error for $b_0 = 1$ and $b_0 = 0$ can be expressed respectively as:

$$Pe_{b_0=1} = \int_{-\infty}^{V} f_1(u)du = -\int_{c-i\infty}^{c+i\infty}\frac{M_{X1}(s)}{s}e^{-Vs}\frac{ds}{2\pi i} \quad c<0 \tag{5.52a}$$

$$Pe_{b_0=0} = \int_{V}^{\infty} f_0(u)du = \int_{c-i\infty}^{c+i\infty}\frac{M_{X0}(s)}{s}e^{-Vs}\frac{ds}{2\pi i} \quad 0<c<s_* \tag{5.52b}$$

The integrand for $b_0 = 1$, ($b_0 = 0$) possesses saddlepoint s_1 and s_0 respectively, on the real axis and one takes $c_0 = s_0$ and $c_1 = s_1$ so that the integration passes through the saddlepoint. The integrands are then written as: $e^{\Psi_{0,1}(s)}$ with:

$$\Psi_0(s) = \ln\left(M_{X0}(s)\right) - \ln(s) - sV \tag{5.53a}$$

$$\Psi_1(s) = \ln\left(M_{X1}(s)\right) - \ln(s) - sV \tag{5.53b}$$

The conditional probability of bit error is written as:

$$Pe_{0,1} = \frac{e^{\Psi_{0,1}(s_{0,1})}}{\left(\Psi''_{0,1}(s_{0,1})\right)^{1/2}} \tag{5.54}$$

Detailed expressions for $M_X(s)$, $\Psi(s)$ and its derivatives are given in Appendix 5-B.

An Upper Bound on P_e

We will first remove the conditioning on the set $\tau = (\tau_1, \tau_2, \ldots, \tau_K)$, that is we evaluate the probability of error conditioned on the set $\{I_{-1}^k, I_0^k\}_{k=1}^K$, and then average the results over the 4^K possible combinations. The strategy is as follows:

a) When calculating P_e for $b_0 = 0$:

1) find the approximate discrete pdf of each B_k by using the GQR, τ_k being the random variable;

2) for each possible combination of $\{b_1, b_2, \cdots, b_K\}$, ($b_1$ being a realization of B_1), substitute in the expression for λ and calculate the $Pe_{bo=0}$;

b) When calculating P_e for $b_0 = 1$:

1) find the approximate discrete pdf of each A_k by using the GQR;

2) find the minimum value $\underset{l_k}{MinB_k}$ and substitute in (5.51), second term;

3) find the maximum value $\underset{l_k}{MaxB_k}$ and substitute in (5.51), fourth term;

4) for each possible combination of $\{a_1, a_2, \cdots, a_K\}$, substitute in the expression for λ and calculate the $Pe_{bo=1}$;

When calculating $Pe_{bo=1}$, the third term in (5.51) is likely to dominate (see the amplitude factor) so it is better to accurately approximate A_k and take the worst case situation for each B_k. Obviously, for an upper bound, the second term has to be minimized while the amplitude of each interfering factor (fourth term) has to be maximized. For $bo = 0$, the third term is zero, so we simply need to approximate each B_k. It is expected however that the upper bound so obtained will be quite loose, but will still allow us to observe the effect of M on the system performance.

5.7 Results and Discussion

The results are shown on Fig. 5.13 and Fig. 5.14. On Fig. 5.13, the APD gain is taken to be $G = 55$, while on Fig. 5.14, $G = 35$. For both cases, the effects of partial crosscorrelation is easily seen, although the number of users is taken to be only three. A floor on the P_e is observed, which shows the effect of MAI, and not the effect of thermal noise or shot noise. For $M > 110$, no floor is observed. The P_e is reduced by increasing the power since the main interference sources in these cases are thermal noise and shot noise. Choosing M too large ($M = 125$), causes a large power penalty since the power collected by the electronic filter is inversely propertional to M, and becomes very small for $M = 125$. However, from these results, one can expect that as the number of interfering signals is increased, larger values than $M = 110$ would be required to avoid P_e floors, since the MAI will dominate.

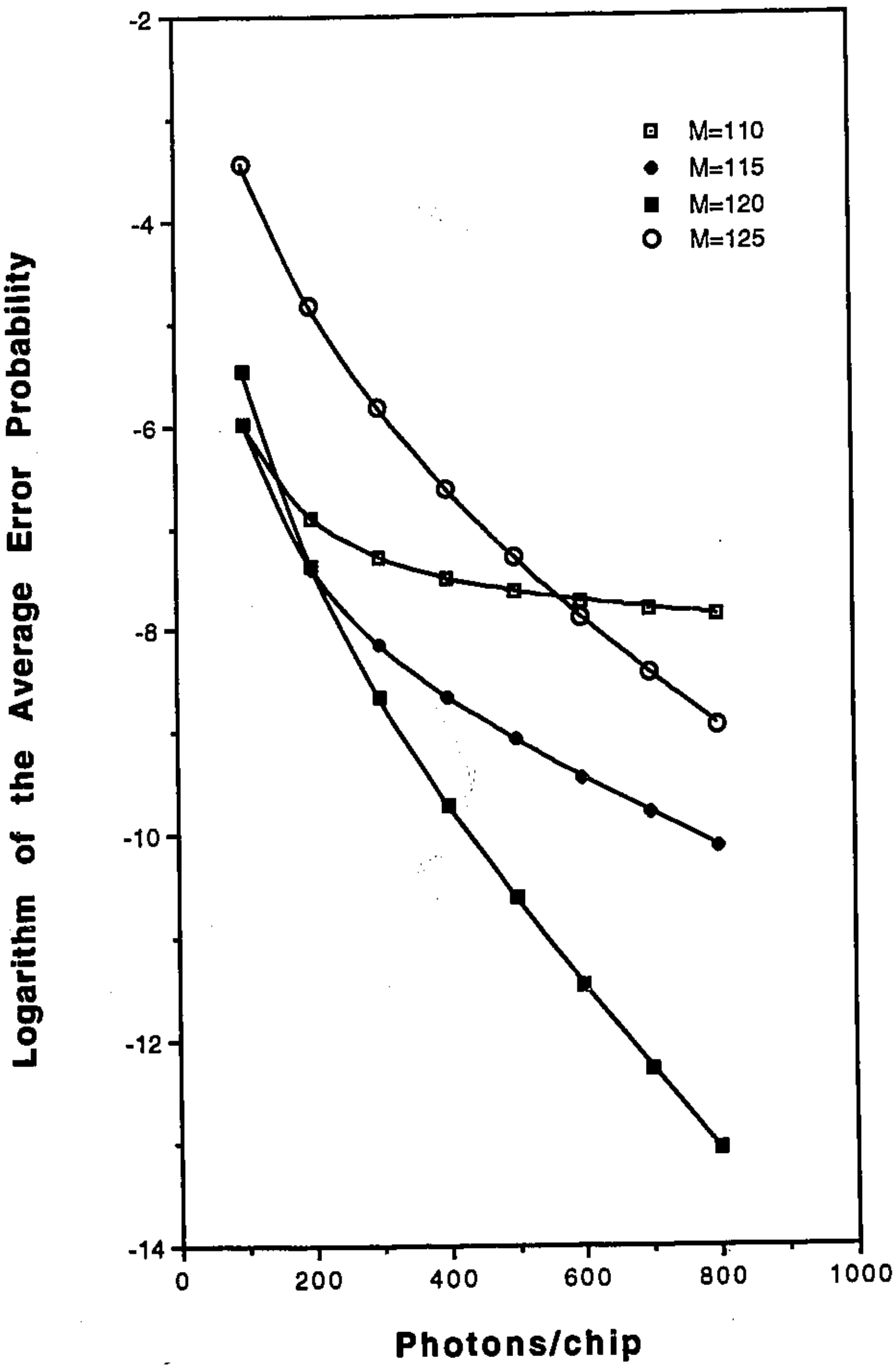

Fig.5.13: Optical filter bandwidth effect on the Pe; G=55.0, k=0.1, N=127, ASK.

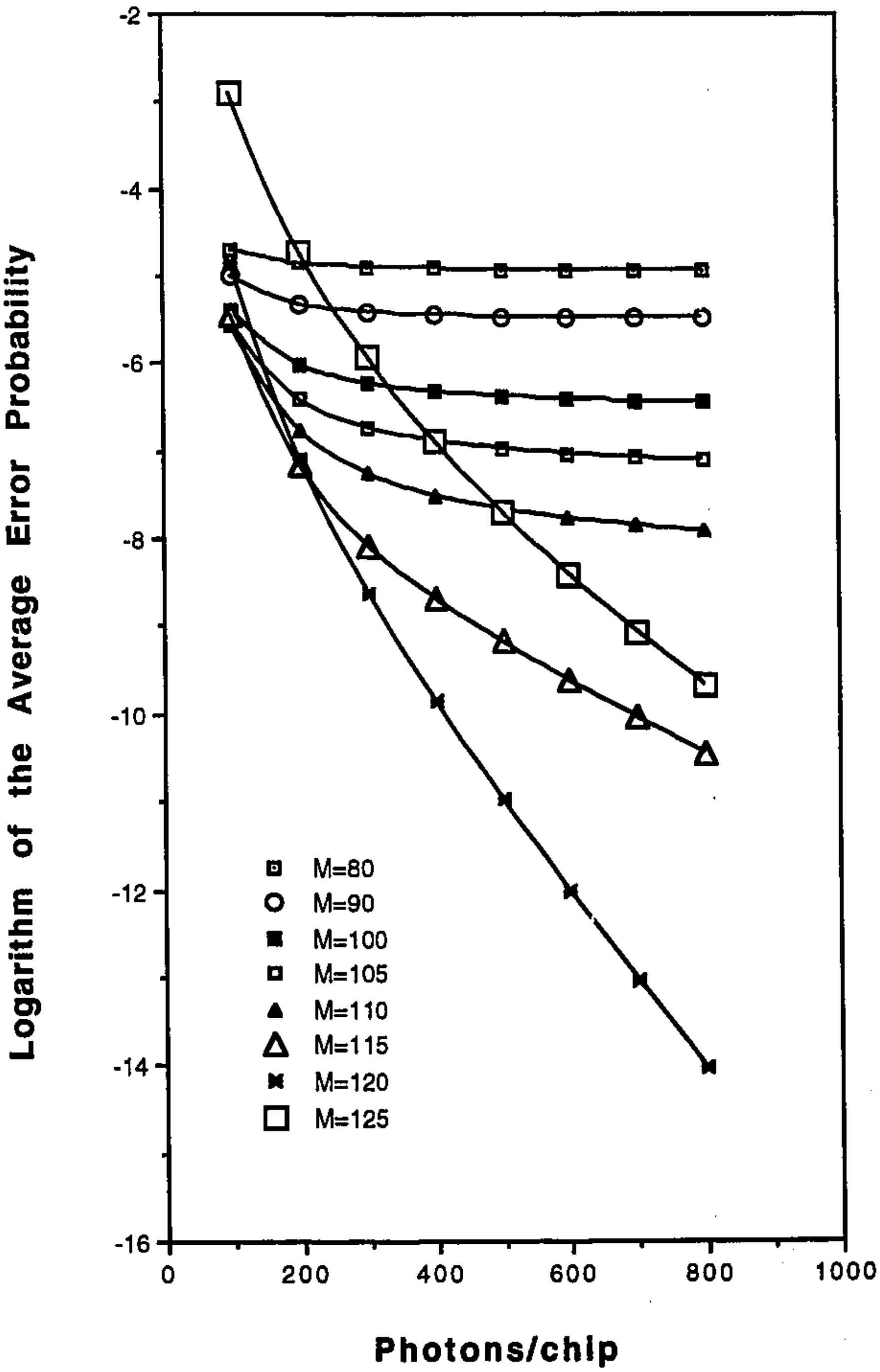

Fig.5.14: Optical filter bandwidth effect on the Pe; G=35.0, k=0.1, N=127, ASK.

5.8 Conclusion

In this chapter, we presented an accurate analysis of an optical CDMA system using bipolar codes and noncoherent detection. Electro-optic phase modulators are used to modulate the laser with the bipolar codes, and may be combined with coherent transversal filters, as shown in Chapter 4, to increase the code length. An optical filter in front of the photodetector allows to reject most of the interfering power coming from the other active users in the network. We showed that it is possible to write the signal at the input of the photodetector as modulus of the sum of randomly phased components. Chip-synchronous and chip-asynchronous assumptions were both studied, the former resulting in an upper bound. By finding the probability density function of the decision variable, we were able to compute the probability of error using two different techniques, depending on the number of active users. We showed that by using a simple trapezoidal rule for numerical integration, a computational complexity growing linearly with the number of active users is possible, even if the photodetector introduces a nonlinearity in the system model. The number of active users that can be supported for different code lengths was given, for ASK and CPFSK modulations. Comparison with a Gaussian approximation was made for the chip-synchronous case, and shown to give very good results for $N = 255$. Three modulation schemes, ASK, CPFSK and LD-FSK were studied. Standard codes such as Gold codes were compared with Kronecker sequences. Although the former yields a better performance, the latter allows simpler architectures for the encoder/decoders. More results, with different choices for the inner and outer sequences will be given in Chapter 6.

Appendix 5.A: Avalanche Photodiode Characteristics

Using the model of [48], the MGF $M_g(s)$ of the APD gain, defined as:

$$M_g(s) = \sum_{l=0}^{\infty} Pr\,(g = l)\, e^{ls} \tag{5.A.1}$$

is given by the relation:

$$s = \ln\Big(M_g(s)\Big) - b\ln\Big(1 + a\big[M_g(s) - 1\big]\Big) \tag{5.A.2}$$

where:

$$b = (1-k)^{-1} \qquad\qquad a = (1-k)\,(1 - G^{-1})$$

where k is the collision-ionization probability of holes to that of electrons, and G is the mean gain of the APD $G = E(g)$. We also have:

$$M_g'(s) = M_g(s)\frac{f_1}{f2} \qquad\qquad M_g''(s) = M_g'(s)\frac{f_1^2 - a^2 b M_g^2(s)}{f_2^2}$$

where:

$$f_1 = 1 + a(M_g(s) - 1) \qquad\qquad f_2 = f_1 - abM_g(s)$$

Appendix 5.B: Saddlepoint Approximation of the Pe

Starting from the expression $M_X(s)$ and the expression of λ in Eqn(5.51) we remove the conditioning over the independent phase terms to get:

$$\begin{aligned} M_X(s) = exp &\left(PhD(s)\, b_0(N - M) + PhD(s) \sum_{k=1}^{K} \frac{B_k}{M^2} \right) \\ &\times \prod_k I_0\Big[\frac{2b_0}{M} A_k PhD(s)\Big] \prod_{k,j} I_0\Big[\frac{2}{M^2} B_k^{1/2} B_j^{1/2} PhD(s)\Big] e^{\frac{\sigma^2 s^2}{2}} \end{aligned} \tag{5.B.1}$$

where $D(s) = M_g(s) - 1$. We have then:

$$\Psi(s) = D(s)\left[Phb_0(N-M) + Ph\sum_{k=1}^{K}\frac{B_k}{M^2}\right] + \sum_k \ln\left(I_0\left[\frac{2b_0}{M}A_k PhD(s)\right]\right) + \sum_k\sum_j \ln\left(I_0\left[\frac{2}{M^2}B_k^{1/2}B_j^{1/2}PhD(s)\right]\right) + \frac{\sigma^2 s^2}{2} - Vs - \ln(\pm s) \tag{5.B.2}$$

where $\pm s = s\,(-s)$ for $b_0 = 0\,(b_0 = 1)$. Let call $g(x) = I_1(x)/I_0(x)$ so:

$$\Psi'(s) = D'(s)\left[Phb_0(N-M) + Ph\sum_k\frac{B_k}{M^2}\right] + \sum_k g\Big(\frac{2b_0}{M}A_k PhD(s)\Big)\Big(\frac{2b_0}{M}A_k PhD'(s)\Big) + \sum_k\sum_j g\Big(\frac{2}{M^2}B_k^{1/2}B_j^{1/2}PhD(s)\Big)\Big(\frac{2}{M^2}B_k^{1/2}B_j^{1/2}PhD'(s)\Big) + \sigma^2 s - V - \frac{1}{s} \tag{5.B.3}$$

Now with $g'(x) = 1 - x^{-1}g(x) - [g(x)]^2$:

$$\Psi''(s) = D''(s)\left[Phb_0(N-M) + Ph\sum_k\frac{B_k}{M^2}\right] + \sum_k g'\Big(\frac{2b_0}{M}A_k PhD(s)\Big)\Big(\frac{2b_0}{M}A_k PhD'(s)\Big)^2 + \sum_k g\Big(\frac{2b_0}{M}A_k PhD(s)\Big)\Big(\frac{2b_0}{M}A_k PhD''(s)\Big) + \sum_k\sum_j g'\Big(\frac{2}{M^2}B_k^{1/2}B_j^{1/2}PhD(s)\Big)\Big(\frac{2}{M^2}B_k^{1/2}B_j^{1/2}PhD'(s)\Big)^2 + \sum_k\sum_j g\Big(\frac{2}{M^2}B_k^{1/2}B_j^{1/2}PhD(s)\Big)\Big(\frac{2}{M^2}B_k^{1/2}B_j^{1/2}PhD''(s)\Big) + \sigma^2 + \frac{1}{s^2} \tag{5.B.4}$$

The saddlepoint s_0 is found by solving the nonlinear equation $\Psi'(s_0) = 0$ using a simple numerical method. In the above equations, Ph is the number of photons/chip.

Chapter 6

Performance Evaluation of Incoherent Optical CDMA Systems

6.1 Introduction

In this chapter, we evaluate the performance of incoherent optical CDMA systems using the architectures presented in Chapter 4. As in Chapter 5, we seek how many simultaneous active users can be supported by the proposed systems for a given probability of error. The technique used allows us to take into account the main sources of interference: Multiple-Access-Interference (MAI), shot noise and thermal noise. As before, however, we will mainly consider the MAI, since this would be the limiting factor in a LAN environment where the power is sufficiently increased. We will study the performance using Kronecker sequences and we will try different choices of outer and inner sequences in order to see what the good combinations are. The computation of the probability of error is simply done using the saddlepoint approximation.

6.2 System Model

The model we use for the performance evaluation is shown in Fig. 6.1. Remember that in practice the implementation would be similar to that shown in Chapter 4. In this chapter, since the sources are incoherent, the whole system, from modulation to detection, can be regarded as being linear in power, and therefore all phase terms can be discarded. This simplifies the performance evaluation considerably. We consider two modulation schemes: ASK and Orthogonal Coding (OC). For ASK, the sequence $\mathbf{a_k} = \{a_0, a_1, a_2, \cdots, a_{N-1}\}$ is generated when a "1" is transmitted, while nothing is sent for a data bit "0". In the case of OC, $\mathbf{a_k}$ is generated for a data bit "1" while $1 - \mathbf{a_k}$ is sent for a data bit "0". The received signal from the network, for the time interval $0 < t < T$ can be readily expressed as:

$$S(t) = \sum_{k=0}^{K} S_k(t) = \sum_{k=0}^{K} X_k(t - \tau_k) \tag{6.1}$$

where:

$$X_k(t) = \sum_{j=0}^{N-1} X_j^k p(t - jT_c) \tag{6.2}$$

and $p(t) = 1$ for $0 < t < T_c$ and 0 elsewhere. The sequence $X_k(t)$ is either $a_k(t), 1 - a_k(t)$ or the zero sequence, according to the bit transmitted and the modulation scheme used. Note that, for unipolar codes obtained from a 2-PPM encoding of bipolar codes, the length of the code is N but its period is really the period of the bipolar code, $N/2$. As explained in chapter 4, to maintain the bipolar nature of the codes, the correlation process needs two sets of orthogonal optical delay lines. A balanced receiver is needed then even for ASK modulation. The correlator made of optical delay lines is followed by photodetection, and by an integrate-and-dump filter of integration time T_c, with the impulse response:

$$h(t) = \frac{1}{T_c} \qquad \text{for} \qquad (N-1)T_c < t < NT_c \tag{6.3}$$

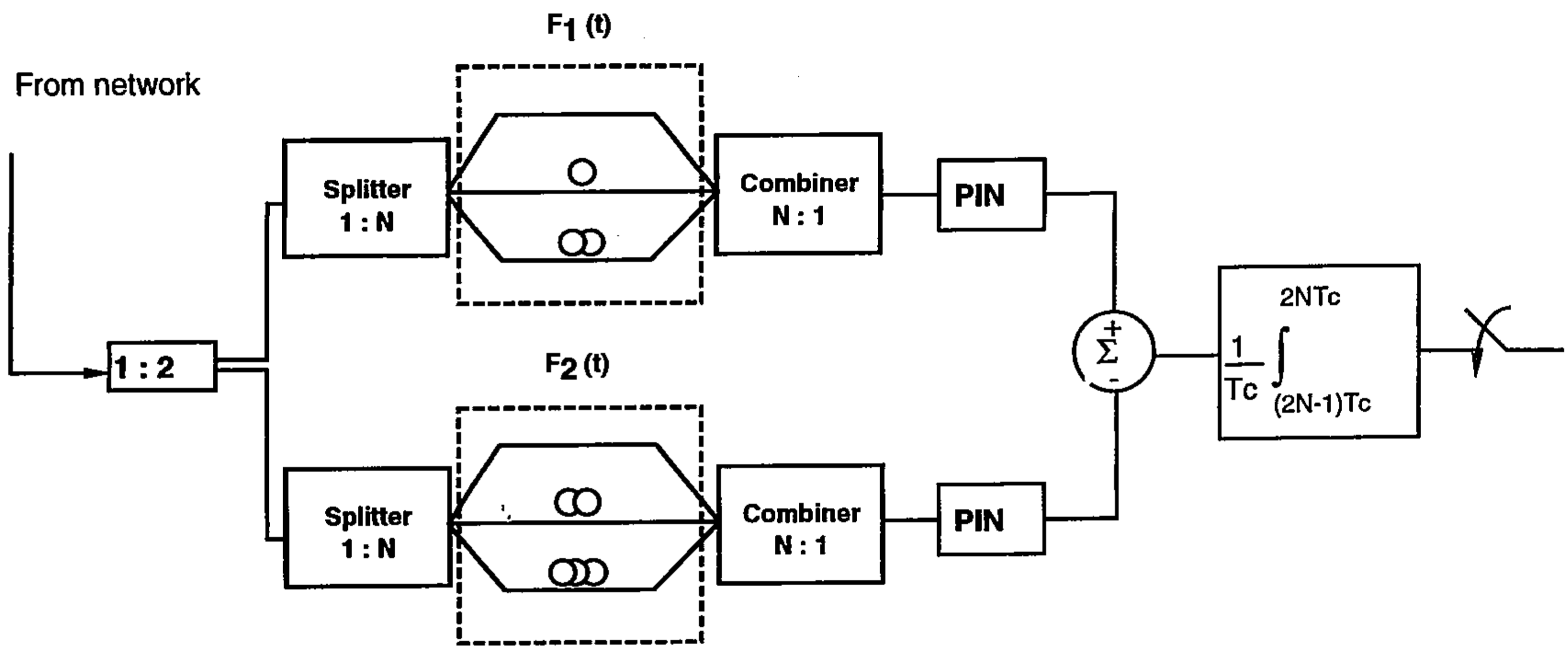

Fig.6.1: Conceptual block diagram of the receiver for incoherent optical CDMA system.

An optical AND gate can be used before detection if $1/T_c$ is larger than the bandwidth of the photodetector and the associated electronics. The first set of delay lines $F_1(t)$ is a filter matched to the intended sequence $a_0(t)$ and has therefore an impulse response corresponding to the time reversal of $a_0(t)$:

$$F_1(t) = \sum_{i=0}^{N-1} f_i \delta(t - iT_c) = \sum_{i=0}^{N-1} a_{N-1-i} \delta(t - iT_c) \tag{6.4}$$

The impulse response of $F_2(t)$ (see Fig. 6.1) is then simply:

$$F_2(t) = \sum_{i=0}^{N-1} (1 - a_{N-1-i}) \delta(t - iT_c) \tag{6.5}$$

Most of the results presented consider only the MAI so we first develop the equations for the situation where the shot noise and the thermal noise are absent. Generalization to include these noise sources is straightforward and will be given in Section 6.4

Since the system is linear, and in the absence of noise, the two filters of Fig. 6.1 and the substractor can be replaced, for the purpose of performance evaluation, by a simple filter $F(t)$ with transfer function:

$$F(t) = F_1(t) - F_2(t) = \sum_{i=0}^{N-1} \left[2a_{N-1-i} - 1\right] \delta(t - iT_c) \tag{6.6}$$

At the output of this filter and for the desired signal $S_0(t)$ we have:

$$\begin{aligned} z_0(t) &= S_o(t) * F(t) \\ &= \sum_{j=0}^{N-1} X_j^0 p(t - jT_c) * \sum_{i=0}^{N-1} \left[2a_{N-1-i} - 1\right] \delta(t - iT_c) \\ &= \sum_{j=0}^{N-1} \sum_{i=0}^{N-1} X_j^0 \left[2a_{N-1-i} - 1\right] p\left(t - (j+i)T_c\right) \end{aligned} \tag{6.7}$$

Since we are interested in the time interval $(N-1)T_c < t < NT_c$ we then have:

$$z_0(t) = \sum_{j=0}^{N-1} X_j^0 \left[2a_j - 1\right] p\left(t - (N-1)T_c\right) \tag{6.8}$$

The output $z_0(t)$ is then integrated from $(N-1)T_c$ to NT_c and we finally get:

$$z_0 = \frac{1}{T_c}\int_{(N-1)T_c}^{NT_c} z_0(t) = \sum_{j=0}^{N-1} X_j^0\left[2a_j - 1\right] \tag{6.9}$$

We already see that:

$$\begin{aligned} z_0 =& N_1 \qquad \text{for} \qquad X_0(t) = a_0(t) \\ z_0 =& -N_1 \qquad \text{for} \qquad X_0(t) = 1 - a_0(t) \end{aligned} \tag{6.10}$$

where N_1 is the number of chips taking the value "1", and it is $N/2$ for the case where the unipolar sequence is generated from sequences taking only values ± 1. In the case of a Kronecker sequence whose inner sequence of period N_i is a ternary sequence with N_b "0"s, then $N_1 = \frac{N_o}{2}(N_i - N_b)$ where N_o is the period of the outer sequence. An interfering signal $S_k(t)$ can be expressed as:

$$\begin{aligned} S_k(t) &= \sum_{j=-1}^{l_k-1} X_{N-l_k+j}^k p\left(t - jT_c - \left[\tau_k - l_k T_c\right]\right) \quad \text{for} \quad 0 < t < \tau_k \\ S_k(t) &= \sum_{j=0}^{N-l_k-1} Y_j^k p\left(t - jT_c - \tau_k\right) \quad \text{for} \quad \tau_k < t < T \end{aligned} \tag{6.11}$$

where $X_k = Y_k$ if $I_{-1}^k = I_0^k$. After correlation with the filter $F(t)$, the output for $(N-1)T_c < t < (N-1)T_c + \tau_k - l_k T_c$:

$$\begin{aligned} z_k^1(t) = & \sum_{j=-1}^{l_k-1} X_{N-l_k+j}^k\left[2a_{j+1} - 1\right] p\left(t - (N-2)T_c - \left[\tau_k - l_k T_c\right]\right) \\ & + \sum_{j=0}^{N-l_k-2} Y_j^k\left[2a_{j+l_k+1} - 1\right] p\left(t - (N-2)T_c - \left[\tau_k - l_k T_c\right]\right) \end{aligned} \tag{6.12}$$

and for $(N-1)T_c + \tau_k - l_k T_c < t < NT_c$:

$$\begin{aligned} z_k^2(t) = & \sum_{j=0}^{l_k-1} X_{N-l_k+j}^k\left[2a_j - 1\right] p\left(t - (N-1)T_c - \left[\tau_k - l_k T_c\right]\right) \\ & + \sum_{j=0}^{N-l_k-1} Y_j^k\left[2a_{j+l_k} - 1\right] p\left(t - (N-1)T_c - \left[\tau_k - l_k T_c\right]\right) \end{aligned} \tag{6.13}$$

One can see that by using two orthogonal filters $F_1(t)$ and $F_2(t)$, and subtracting their outputs, an interfering pulse will be given the weight 1, or -1 depending on, if it coincides with $a_j = 1$ or $a_j = 0$, i.e., if there is a delay corresponding to position j in $F_1(t)$ or in $F_2(t)$. The output of the integrate-and-dump filter for an interfering signal is then simply expressed as:

$$
\begin{aligned}
z_k &= \frac{1}{T_c}\int_{(N-1)T_c}^{NT_c} \left[z_k^1(t) + z_k^2(t)\right] dt = \\
& C_{X^k(2a^0-1)}(l_k - N) + \left[C_{X^k(2a^0-1)}(l_k + 1 - N) - C_{X^k(2a^0-1)}(l_k - N)\right]\left(\tau_k - l_k\right) \\
& + C_{Y^k(2a^0-1)}(l_k) + \left[C_{Y^k(2a^0-1)}(l_k + 1) - C_{Y^k(2a^0-1)}(l_k)\right]\left(\tau_k - l_k\right)
\end{aligned}
\tag{6.14}
$$

where the delay τ_k has been normalized $\tau_k = \tau_k/T_c$. For OC, remembering that X^k and Y^k are either a^k or $1 - a^k$, it is easy to show that this can be simply written in the following way, similar to the expression found for bipolar coherent CDMA systems:

$$
z_k = I_{-1}^k R_k(\tau_k) + I_0^k \widehat{R_k}(\tau_k) + D^k(\tau_k) \tag{6.15}
$$

where I_{-1}^k, $I_0^k \in \{-1, 1\}$ and $R_k(\tau_k)$, $\widehat{R_k}(\tau_k)$ are defined as usual. The last term does not appear in a real bipolar case. Its expression is:

$$
D^k(\tau_k) = \left|\frac{I_{-1}^k - I_0^k}{2}\right| \left(\frac{1 - I_{-1}^k}{2} D_1^k(\tau_k) + \frac{1 - I_0^k}{2} D_2^k(\tau_k)\right) \tag{6.16}
$$

with:

$$
\begin{aligned}
D_1^k(\tau_k) &= \left[2a_l^k - 1\right]\left(\tau_k - l_k\right) + \left[2a_{l-1}^k - 1\right] \quad \text{for} \quad l_k \text{ odd} \\
&= \left[2a_l^k - 1\right]\left(\tau_k - l_k\right) \quad \text{for} \quad l_k \text{ even} \\
D_2^k(\tau_k) &= -\left[2a_l^k - 1\right]\left(\tau_k - l_k\right) + \left[2a_l^k - 1\right] \quad \text{for} \quad l_k \text{ odd} \\
&= -\left[2a_l^k - 1\right]\left(\tau_k - l_k\right) \quad \text{for} \quad l_k \text{ even}
\end{aligned}
$$

For ASK, the last term of (6.15) is zero and I_{-1}^k, $I_0^k \in \{0, 1\}$. It was found that the contribution of the last term $D^k(\tau_k)$ is negligeable in the probability of error computations, so for notational simplicity we will simply assume it to be zero in the following. The decision variable can then be simply expressed as:

$$
\begin{aligned}
z &= boN_1 + \sum_{k=1}^{K} z_k \\
&= boN_1 + \sum_{k=1}^{K} \left[I_{-1}^{k} R_k(\tau_k) + I_0^k \widehat{R_k}(\tau_k) \right]
\end{aligned}
\tag{6.17}
$$

where bo and $(I_{-1}^k,\, I_0^k)$, take the values $\{0,1\}$ and $\{-1,1\}$ for ASK and OC, respectively. The expression obtained for the decision variable confirms what was stated in Chapter 4. By using unipolar codes of length N, constructed from a 2-PPM encoding of bipolar codes of period N/2, an incoherent optical CDMA system can behave like a coherent CDMA system (electronic or optical) using bipolar codes and PSK modulation. Of course, the performance when considering shot noise and thermal noise will be different in terms of the power penalties incurred. Finally, note that a bipolar coherent CDMA system in the electronic domain, or in the optical domain using coherent detection, would have the additional factor $\cos\varphi_k$ in the expression of the decision variable, reducing the variance by a factor of two compared to our situation.

The ouput in the incoherent case is therefore a simple sum of independent variables and the probability of error calculation is straighforward. We present the main steps in the next section.

6.3 Computation of the Error Probability

The moment generating function of z can be expressed as the product of the individual MGF since the variables are independent. From the MGF, it is then easy to compute the probability of error using the saddlepoint approximation. Another possibility would be to use a GQR technique by finding the global moments of z, from its cumulants. However, in the absence of shot noise and thermal noise, it was found that to obtain convergence, a very large number of moments (more than 40) is needed, making the technique unsuitable. The conditional probability of error

$Pe_{b_o=1}$ and $Pe_{b_o=0}$ are expressed for ASK as:

$$Pe_{b_0=1} = \int_{-\infty}^{V} f_1(u)du = -\int_{c-i\infty}^{c+i\infty} \frac{M_{Z1}(s)}{s} e^{-V_s} \frac{ds}{2\pi i} \quad c < 0 \tag{6.18a}$$

$$Pe_{b_0=0} = \int_{V}^{\infty} f_0(u)du = \int_{c-i\infty}^{c+i\infty} \frac{M_{Z0}(s)}{s} e^{-V_s} \frac{ds}{2\pi i} \quad 0 < c < s_* \tag{6.18b}$$

As in Section 5.5, the integrand for $b_0 = 1(b_0 = 0)$ possesses saddlepoints s_0 and s_1 respectively, on the real axis and one takes $c_0 = s_0$ and $c_1 = s_1$ so that the integration passes through the saddlepoints. In the above, V is the threshold and $V = 0$ for OC signaling. The final probability of error is simply $Pe = \frac{1}{2}\left(Pe_{b_0=1} + Pe_{b_0=0}\right)$. For OC, by symmetry, $Pe = Pe_{b_0=1} = Pe_{b_0=0}$. The integrands are then written as $e^{\Psi_{0,1}(s)}$ with:

$$\Psi_0(s) = \ln\left(M_{Z0}(s)\right) - \ln(s_0) - sV \tag{6.19a}$$

$$\Psi_1(s) = \ln\left(M_{Z1}(s)\right) - \ln(-s_1) - sV \tag{6.19b}$$

The conditional probability of bit error is then written as:

$$Pe_{0,1} = \frac{e^{\Psi_{0,1}(s_{0,1})}}{\left(\Psi''_{0,1}(s_{0,1})\right)^{1/2}} \tag{6.20}$$

Contrary to Section 5.5, the above moment generating functions $M_{Z1}(s)$ and $M_{Z0}(s)$ are already averaged over the statistics of the interfering users. Expressions for $M_Z(s)$, $\Psi(s)$ and its derivatives are now given. The moment generating function is expressed as:

$$M_Z(s) = \prod_k M^k(s)\, e^{b_0 N_1 s} \tag{6.21}$$

We first rewrite z_k as:

$$\begin{aligned} z_k = I_{-1}^k &\left[C_k(l_k - N) + \left[C_k(l_k + 1 - N) - C_k(l_k - N)\right]\left(\tau_k - l_k\right)\right] \\ + I_0^k &\left[C_k(l_k) + \left[C_k(l_k + 1) - C_k(l_k)\right]\left(\tau_k - l_k\right)\right] \end{aligned} \tag{6.22}$$

where C_k represents the discrete aperiodic correlation between the sequence $2a^0 - 1$ and a^k. We further group terms in the following way to get:

$$z_k = p_1 + p_2 (\tau_k - l_k) \tag{6.23}$$

where:

$$p_1 = I_{-1}^k C_k(l_k - N) + I_0^k C_k(l_k)$$

$$p_2 = I_{-1}^k [C_k(l_k + 1 - N) - C_k(l_k - N)] + I_0^k [C_k(l_k + 1) - C_k(l_k)]$$

Of course p_1 and p_2 are functions of l_k but we do not write it for notational simplicity. At this point, the MGF for one user is written as:

$$\begin{aligned} M^k(s) &= \sum_{I_{-1}^k, I_0^k} \frac{1}{N} \int_0^N e^{s[p_1 + p_2(\tau_k - l_k)]} d\tau_k \\ &= \sum_{I_{-1}^k, I_0^k} \frac{1}{N} \sum_{l_k=0}^{N-1} \int_0^1 e^{s[p_1 + p_2 \tau_k]} d\tau_k \\ &= \sum_{I_{-1}^k, I_0^k} \frac{1}{N} \sum_{l_k=0}^{N-1} \left(\frac{e^{s[p_1+p_2]}}{p_2 s} - \frac{e^{sp_1}}{p_2 s} \right) \end{aligned} \tag{6.24}$$

It is easy to see that $\Psi(s)$ of Eqn(6.19) is given by:

$$\Psi(s) = \sum_k Log \left[\sum_{I_{-1}^k, I_0^k} \frac{1}{N} \sum_{l_k=0}^{N-1} \left(\frac{e^{s[p_1+p_2]}}{p_2 s} - \frac{e^{sp_1}}{p_2 s} \right) \right] + boN_1 s - ln(s) - sV \tag{6.25}$$

Furthermore:

$$\Psi'(s) = \sum_k \frac{dM^k(s)/ds}{M^k(s)} + boN_1 - 1/s - V \tag{6.26}$$

$$\Psi''(s) = \sum_k \frac{d^2 M^k(s)/ds^2}{M^k(s)} - \frac{\left(dM^k(s)/ds\right)^2}{\left(M^k(s)\right)^2} + \frac{1}{s^2} \tag{6.27}$$

Detailed expressions for the derivatives of $M^k(s)$ are given in Appendix 6-A. The probability of error calculation is simply done by finding s such that $\Psi'(s) = 0$ and replacing in the expression (6.20). In the next section, we modify the equations presented so far as to include the shot noise and the thermal noise. The previous analysis allows to calculate the BER floors that would ultimately be observed. The following is useful in finding the power penalty incurred for a given Pe when the number of active users is increased.

6.4 Performance including shot noise and thermal noise

Following the notation of Section 6.2, the rates $\lambda(t)$ of the Poisson process for the photodetectors 1 (positively biased) and 2 (negatively biased) are expressed as:

$$\lambda_1(t) = \sum_k \lambda_1^k(t - \tau_k) + bo\lambda^0(t) \tag{6.28}$$

$$\lambda_2(t) = \sum_k \lambda_2^k(t - \tau_k) + (1 - bo)\lambda^0(t) \tag{6.29}$$

where we make use of the fact that for incoherent optical CDMA, the system is linear in power. For ASK, the second term in (6.29) is zero. It is straightforward to see that the mean intensity λ_1^k for each interfering user is expressed as:

$$\begin{aligned}\lambda_1^k = \int_{(N-1)T_c}^{NT_C} \lambda_1^k(t)dt = \frac{\eta P T_c}{hf}\Big[I_{-1}^k\Big(C_{a^k a^0}(l_k - N)\\
+ \Big[C_{a^k a^0}(l_k + 1 - N) - C_{a^k a^0}(l_k - N)\Big]\Big(\tau_k - l_k\Big)\Big)\\
+ I_0^k\Big(C_{a^k a^0}(l_k) + \Big[C_{a^k a^0}(l_k + 1) - C_{a^k a^0}(l_k)\Big]\Big(\tau_k - l_k\Big)\Big)\Big]\end{aligned} \tag{6.30}$$

$$\begin{aligned}\lambda_2^k = \int_{(N-1)T_c}^{NT_C} \lambda_2^k(t)dt = \frac{\eta P T_c}{hf}\Big[I_{-1}^k\Big(C_{a^k(1-a^0)}(l_k - N)\\
+ \Big[C_{a^k(1-a^0)}(l_k + 1 - N) - C_{a^k(1-a^0)}(l_k - N)\Big]\Big(\tau_k - l_k\Big)\Big)\\
+ I_0^k\Big(C_{a^k(1-a^0)}(l_k) + \Big[C_{a^k(1-a^0)}(l_k + 1) - C_{a^k(1-a^0)}(l_k)\Big]\Big(\tau_k - l_k\Big)\Big)\Big]\end{aligned} \tag{6.31}$$

Note that, here the correlation is done between the unipolar sequences a^k and a^0 or $1 - a^0$ depending on the photodetector. As explained before, when an interfering pulse is coincident with a chip value $a_j^0 = 1$, it is directed to the positively biased photodetector while when it is coincident with $a_j^0 = 0$ it is routed to the negatively biased photodetector. The routing is automatically done by the delays in the optical filters and no optical switches are needed. In the absence of noise, the correlation in (6.30) is done between a^k and $2a^0 - 1$ since the two branches could be grouped together. In the presence of noise, the shot noise processes produced by the photodetectors are independent and both outputs must be treated separately. As before, the term $\frac{\eta PT_c}{hf}$ is the number of photons/chip. The MGF of the decision variable can be written as:

$$M_z(s) = \prod_k M^k(s) e^{\frac{\eta PT_c}{hf} b_0 N_1 (e^s - 1)} e^{\sigma^2 s^2/2} \tag{6.32}$$

where σ^2 is the variance of the thermal noise. Its expression is given by:

$$\sigma^2 = \frac{2kT^o N_0 T_c}{q^2 R} \tag{6.33}$$

For our calculations we choose $T^o = 293$, $R = 100$, $T_c = 1$ns and $N_0 = 127$. The factor N_0 is one in the case where the sequences used are ordinary, but is the period of the outer sequence in the case where Kronecker sequences are being used. We have to remember that for Kronecker sequences the electronic filter is not a simple integrate-and-dump filter, but is an accumulator of the N_0 correlation peaks observed after the final despreading operation in the electronic domain. The MGF for one interfering signal is easily expressed as:

$$M^k(s) = \sum_{I_{-1}^k, I_0^k} \frac{1}{N} \sum_{l_k=0}^{N-1} \int_0^1 e^{(c1 + c2\tau_k)(e^s - 1)} e^{(c3 + c4\tau_k)(e^{-s} - 1)} \, d\tau_k \tag{6.34}$$

where:

$$c1 = \frac{\eta PT_c}{hf} \left[I_{-1}^k C_{a^k a^0}(l_k - N) + I_0^k C_{a^k a^0}(l_k) \right] \tag{6.35}$$

$$c3 = \frac{\eta PT_c}{hf} \left[I_{-1}^k C_{a^k (1-a^0)}(l_k - N) + I_0^k C_{a^k (1-a^0)}(l_k) \right] \tag{6.36}$$

$$\begin{aligned} c2 = \frac{\eta PT_c}{hf} \Big[& I_{-1}^k \left(C_{a^k a^0}(l_k + 1 - N) - C_{a^k a^0}(l_k - N) \right) \\ & + I_0^k \left(C_{a^k a^0}(l_k + 1) - C_{a^k a^0}(l_k) \right) \Big] \end{aligned} \tag{6.37}$$

$$c4 = \frac{\eta PT_c}{hf}\Big[I_{-1}^k \left(C_{a^k(1-a^0)}(l_k+1-N) - C_{a^k(1-a^0)}(l_k-N)\right)$$
$$+ I_0^k \left(C_{a^k(1-a^0)}(l_k+1) - C_{a^k(1-a^0)}(l_k)\right)\Big] \tag{6.38}$$

The probability of error is simply calculated using Eqn(6.20), where in this case the phase function $\Psi(s)$ is slightly modified to be:

$$\Psi(s) = \sum_k \ln M^k(s) + \frac{\eta PT_c}{hf} boN_1(e^s - 1) - \ln(s) - sV + \frac{\sigma^2 s^2}{2} \tag{6.39}$$

$$\Psi'(s) = \sum_k \frac{dM^k(s)/ds}{M^k(s)} + \frac{\eta PT_c}{hf} boN_1 e^s - 1/s - V + \sigma^2 s \tag{6.40}$$

$$\Psi''(s) = \sum_k \frac{d^2M^k(s)/ds^2}{M^k(s)} - \frac{\left(dM^k(s)/ds\right)^2}{\left(M^k(s)\right)^2} + \frac{\eta PT_c}{hf} boN_1 e^s + \frac{1}{s^2} + \sigma^2 \tag{6.41}$$

Detailed expressions for the above functions and their derivatives are provided in Appendix 6-B. Using the above analysis, several computations were performed using both ordinary sequences and Kronecker sequences, for ASK and for OC. In the next section we present the results obtained.

6.5 Results and Discussion

We have calculated the probability of error using the above equations for the case of Orthogonal Codes (Fig. 6.2 to Fig. 6.5, and Fig. 6.8 to Fig. 6.9) and for Amplitude Shift Keying (Fig. 6.6 and Fig. 6.7). The abbreviations in the figures have the following meaning:

We first show on Fig. 6.2 the performance using Gold codes of period $N = 63$, $N = 127$ $N = 255$ and $N = 511$, without an inner sequence. Respectively 4, 9, 19 and 38 users can be accommodated for a probability of error of 10^{-9}. Doubling the code length therefore approximately doubles the number of possible users. Fig. 6.3 compares the performance when the Barker sequence of length $Ni = 4$ is used with $No = 127$ to form a Kronecker sequence of length $N = 508$. When the delay lines are non-programmable, 21 users can be accommodated, more than two times

N : period of the bipolar sequences, termed $N/2$ in the text;

$M - seq$: sequences are M-sequences and not Kasami sequences;

AP : the inner sequence is the Almost Perfect autocorrelation sequence given by $\{-1,-1,1,-1,1,1,1,1\}$;

np : when using Kronecker sequences, all users have the same inner sequence, and the delay lines are non-progammable;

p : when using Kronecker sequences, the delay lines are allowed to be programmable, and the active users share the Ni possible cycle-shifts of the inner sequence;

$mixed$: when using Kronecker sequences, the first Ni active users use the Ni cycle-shifts of the inner sequence, while all other users use the same cycle-shift.

the number with $N = 127$ alone. When the delay lines are made programmable, this number increases to 31 users. Remember that in this case the phase needs only be changed, in the worst case, on a per-call basis. One can see that it is really worthwhile to add 2 blocks of 4 delay lines to the system since it will increase the concurrency of the CDMA system by more than 300 percent. The jumps in the case of $N = 508, p$ are easily explained. The performance is calculated every two users (from one dot to the next) while there is only four cycle-shifts for Ni=4. Therefore, every four active users, the same cycle-shift is used and a jump is seen on the P_e. When the users added have different cycle-shifts, the increase in the P_e is small since the different cycle-shifts of the Barker code are orthogonal to each other.

We next show on Fig. 6.4 the performance obtained when using a Gold code of period $No = 63$ as the outer sequence. A Kronecker sequence of length $N = 441$ is obtained when the inner sequence is the M-sequence of length $Ni = 7$ given by $\{-1,-1,-1,1,-1,1,1\}$. A Kronecker sequence of length $N = 504$ is obtained when this time the inner sequence is the AP sequence given above. This combination has a length comparable to the previous case $No = 127$ and $Ni = 4$ and allows to study the effect of decreasing the length of the outer sequence while increasing the length of the inner one. The case $N = 504\,(Ni = 8)$ or $N = 441\,(Ni = 7)$ with non-programmable delay lines both allow 9 active users for $P_e = 10^{-9}$ while $N = 508\,(Ni = 4)$ allows 21 users. It is therefore more advantageous to have fewer delay lines, and a two times higher speed optical switch at the transmitter and work with $No = 127$. Since there is no performance difference when using as the inner sequence an M-sequence of lenght $Ni = 7$ or the AP autocorrelation sequence with length $Ni = 8$, it is slightly more advantageous to use the former. For the same bit rate it allows somewhat longer pulses (therefore diminishing the effect of dispersion in the fiber) and allows to spare one delay line. Depending on the bit rate considered, and the speed of the optical switch, one can be constrained to use $No = 63$. Using $N = 63$ alone allows only 4 users for $P_e = 10^{-9}$, while using $N = 504$ and programmable delay lines increases this number to 17. Note that, the jumps in the P_e curve occurs every 8 users this time, since there are eight possible cycle-shifts for the inner sequence.

The performance difference observed when using a Barker code of length 4 as the inner sequence or the AP autocorrelation sequence of length 8 seemed at first quite surprising. We then decided to change the outer sequence length while using the same type of sequence as the inner sequence. As there is no perfect *binary* autocorrelation sequence for length $4 < Ni \leq 12100$ we moved to perfect autocorrelation *ternary* sequences. Fig. 6.5 shows the results when using the ternary sequence $\{-1, 0, 0, 1, 0, 1, 1\}$ of length $Ni = 7\,(N = 441)$ and the ternary sequence $\{1, 0, -1, 1, 0, 1\}$ of length $Ni = 6\,(N = 378)$. For the former case, the case of programmable or non-programmable delay lines is studied. As it can be seen, using $N = 441$ is slightly more advantageous over N=378. Comparing $N = 441\,(No = 63, Ni = 7)$ and $N = 504\,(No = 63, Ni = 8)$, both with programmable delay lines, shows that the former allows 20 active users compared to 17. However this has to be put in perspective. The ternary sequence has 3 chips over 7 which are 0's. It would therefore require higher peak power from the pulses when considering shot noise and thermal noise. Note that the case of $No = 127, Ni = 4$ is still the best combination so that using sequences with longer outer period is better. The curve labeled *mixed* is obtained by giving to the first 7 users a different cycle-shift of the inner sequence, and to all others the same cycle-shift.

In Fig. 6.6 and Fig. 6.7 the case of ASK is studied. The advantage of ASK is that of using only one set of delay lines at the transmitter, while the architecture of the receiver is the same. As it can be seen, the performance of ASK is much worse than OC. A code length $N = 127$ with OC is better than $N = 255$ with ASK. Results using Kronecker sequences of length $N = 508$ and $N = 504$ are shown on Fig. 6.7, using the same combination as for OC. The best performance is with $N = 508$ and programmable delay lines, but allows only 10 users compared to the 31 with OC. It is therefore advantageous to use OC in the incoherent case since it requires only a small added complexity compared to ASK. Finally, in Fig. 6.8 and Fig. 6.9, the performance is shown as a function of the number of received photons/chip, for 10, 20, 30 and 40 *interfering* users. The performance of a single active user is also shown. We also show the P_e floors for K=30 and K=40. As predicted the performance converges to the floors calculated previously. The penalty in dB, for different P_e values is shown in Table 6.1. However, these numbers are of course affected by the choices of equivalent input resistance, equivalent temperature and chip duration in (6.33). Studying the performance while neglecting shot noise and thermal noise is therefore practical, since it allows to see the performance limit in the power range of interest.

Sensitivity Penalties,in dB		
Interfering users, K	Log(Pe) = -7	Log(Pe) = -8
10	0.71	0.65
20	1.49	1.62
30	2.52	3.54
40	4.56	-

Table 6.1 Sensitivity Penalties for two different Pe values as a function of the number of interfering users

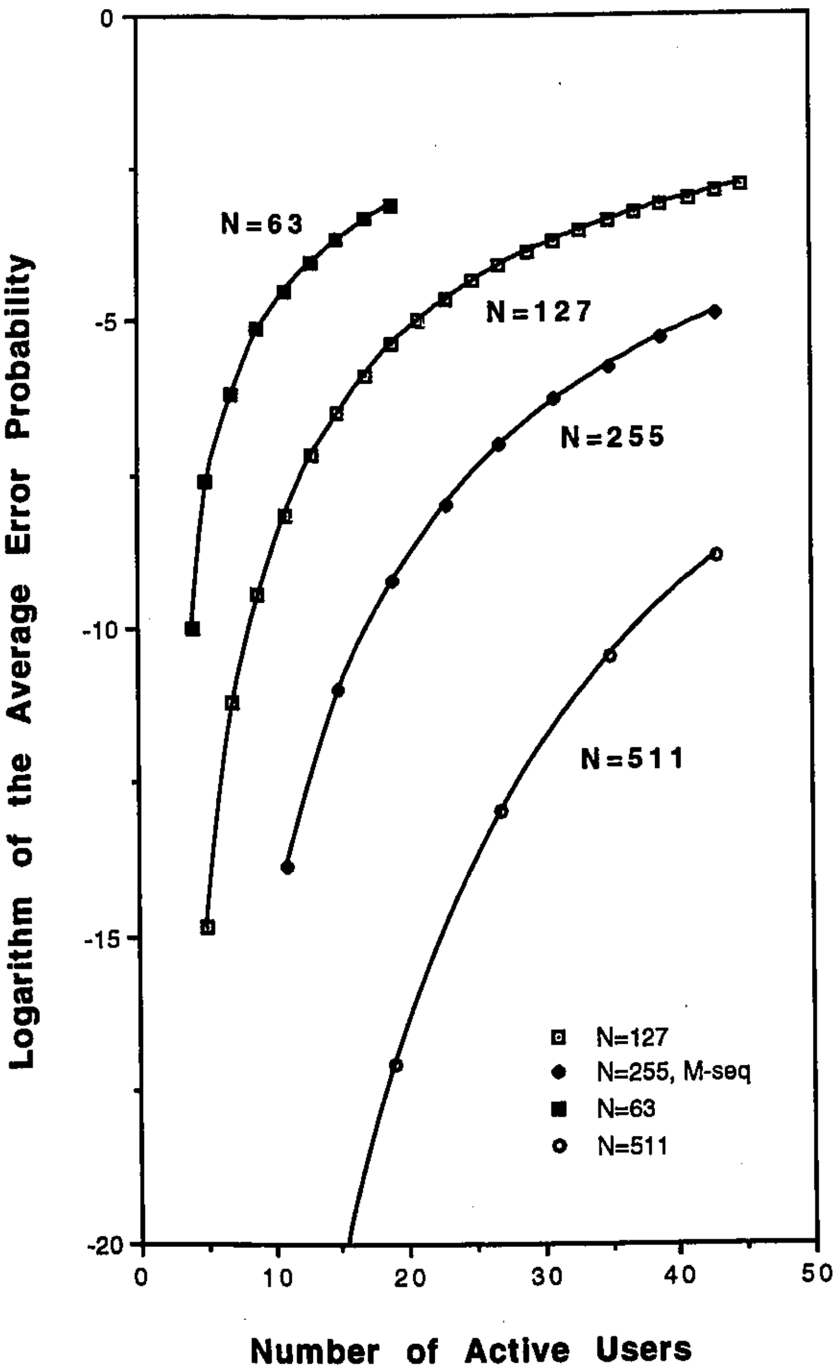

Fig.6.2: Pe vs number of active users, OC;

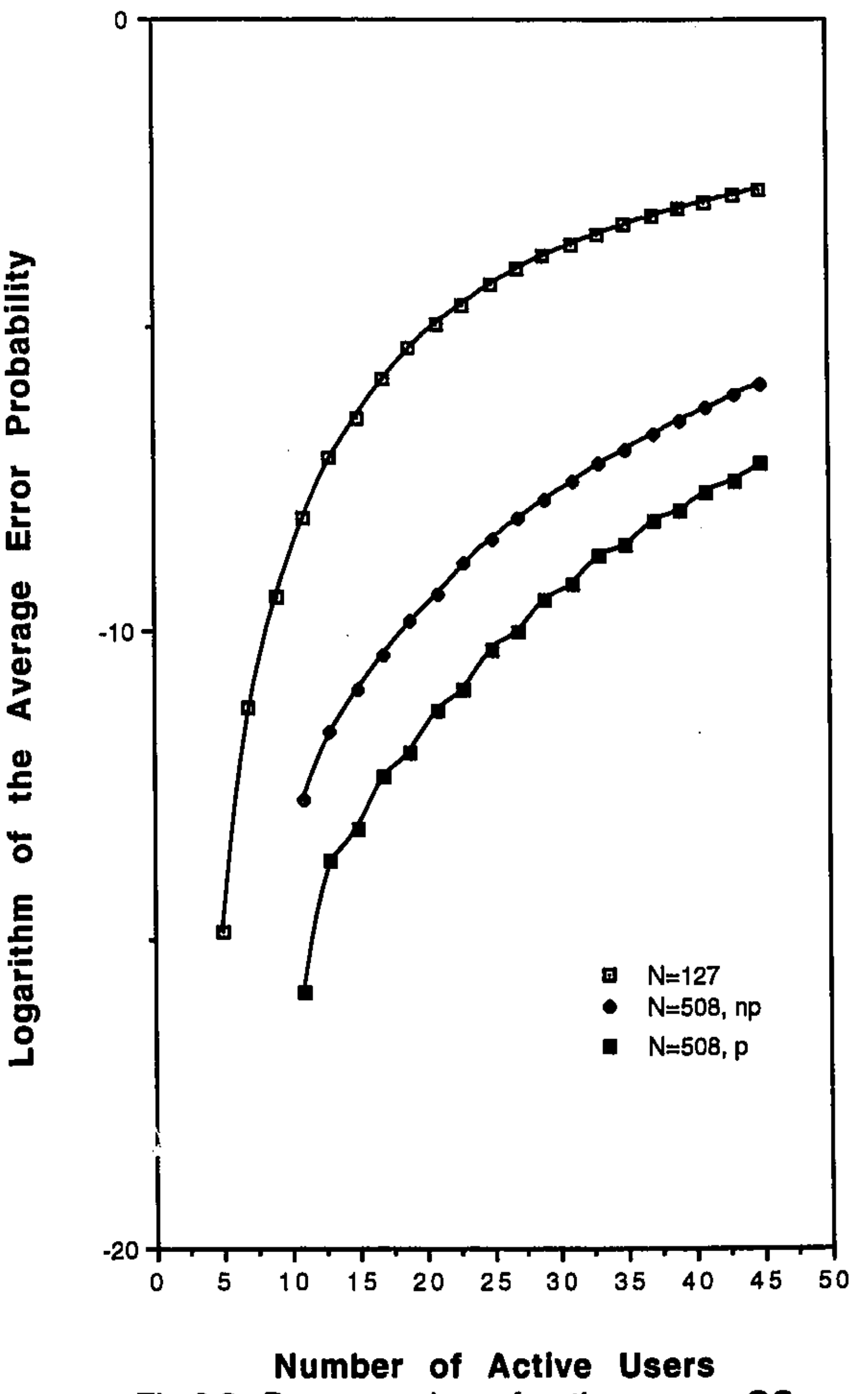

Fig.6.3: Pe vs number of active users, OC,
No = 127 , Ni = 4 , N=508 , np;
No = 127 , Ni = 4 , N=508 , p;

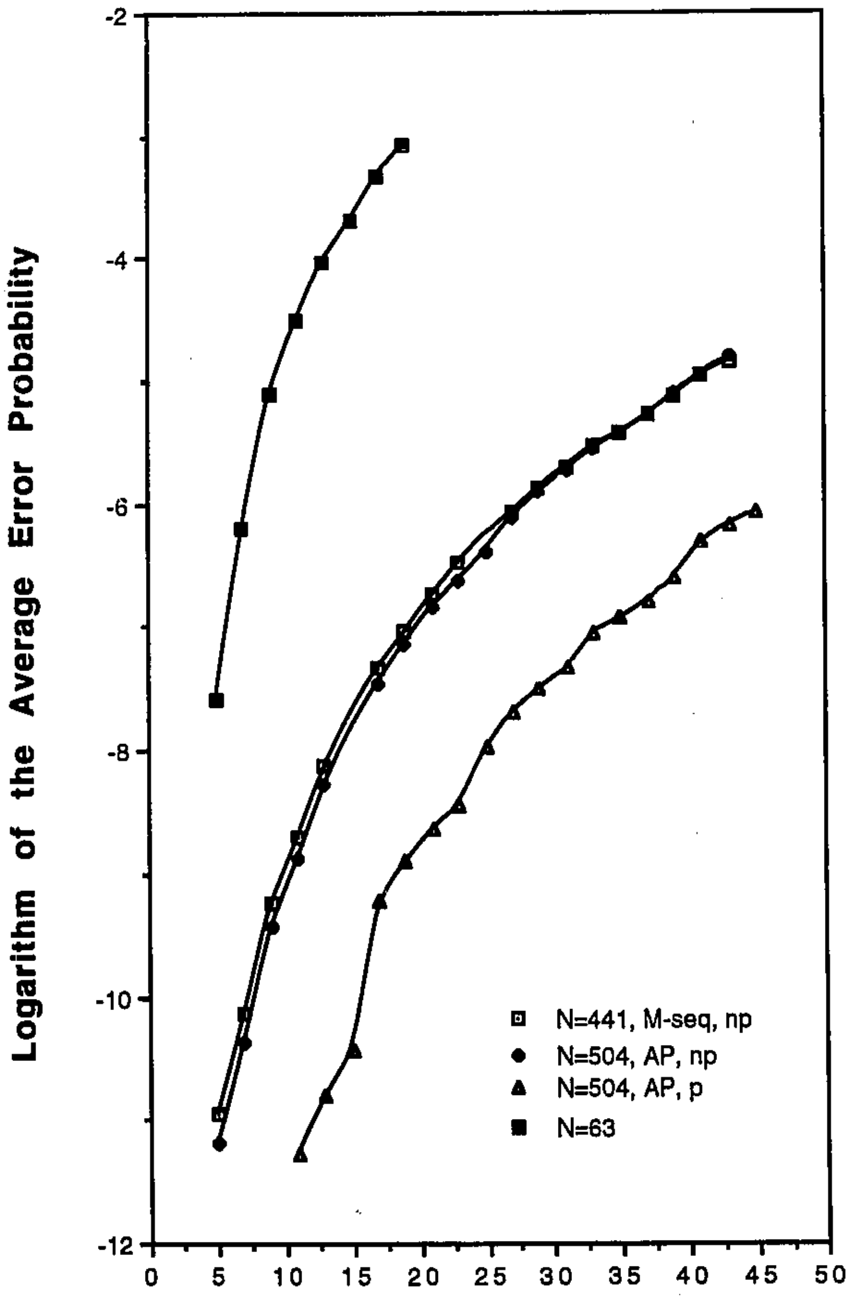

Number of Active Users

Fig.6.4: Pe vs number of active users, OC, No = 63, Ni = 8 and Ni = 7;

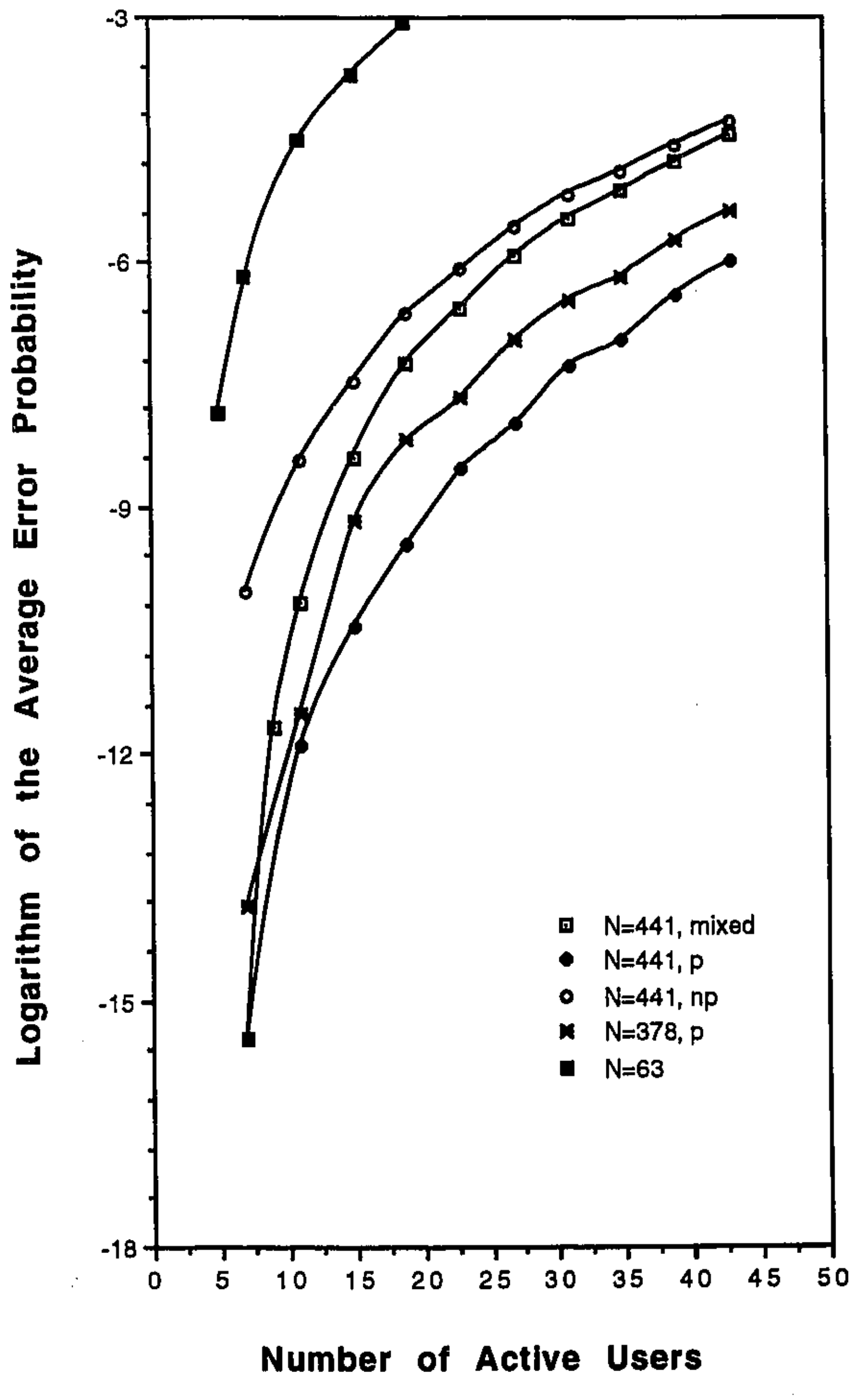

Fig.6.5: Pe vs number of active users, OC,
No = 63, Ni = 7 and Ni = 6, Ternary sequences;

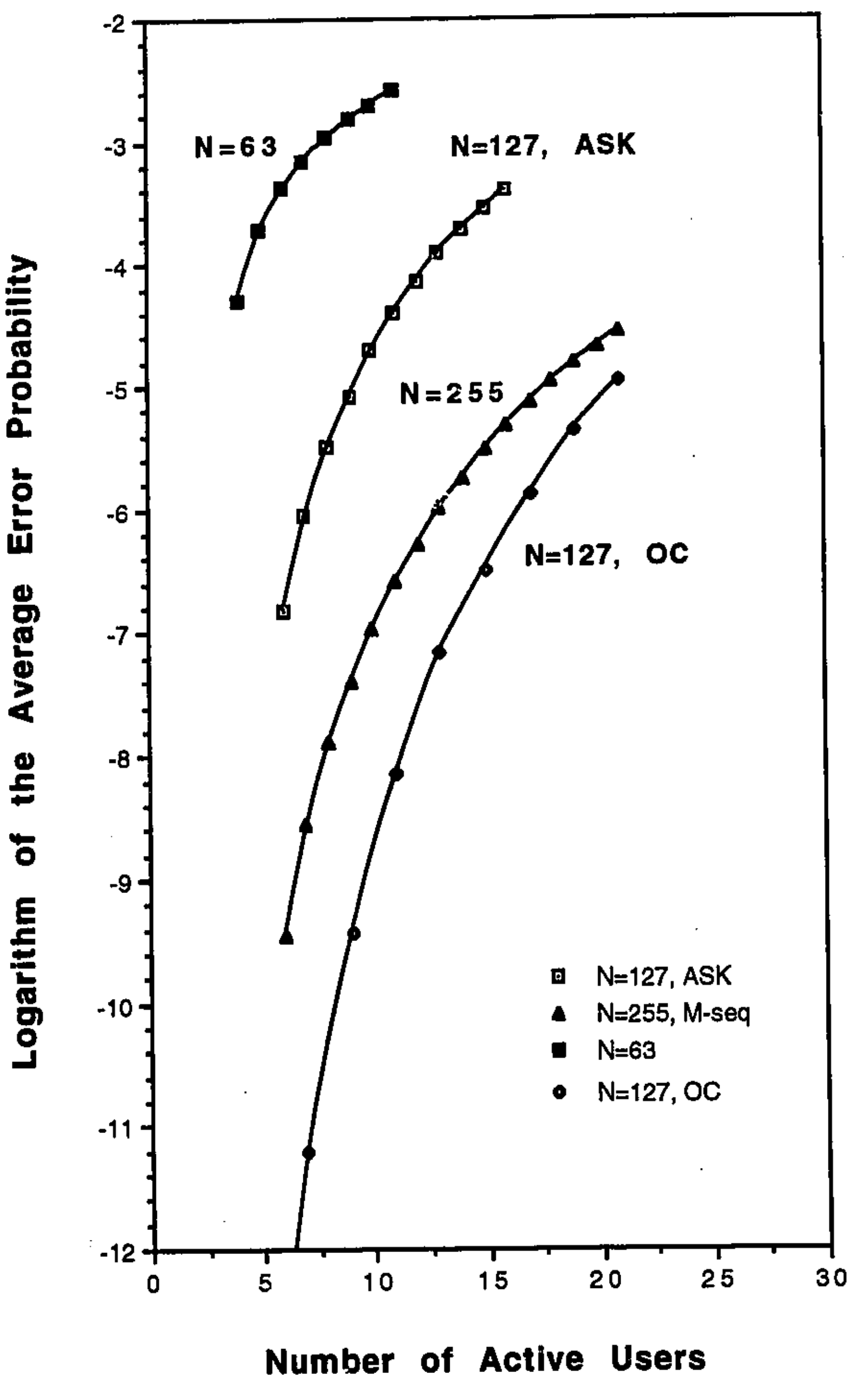

Fig.6.6: Pe vs number of active users, ASK

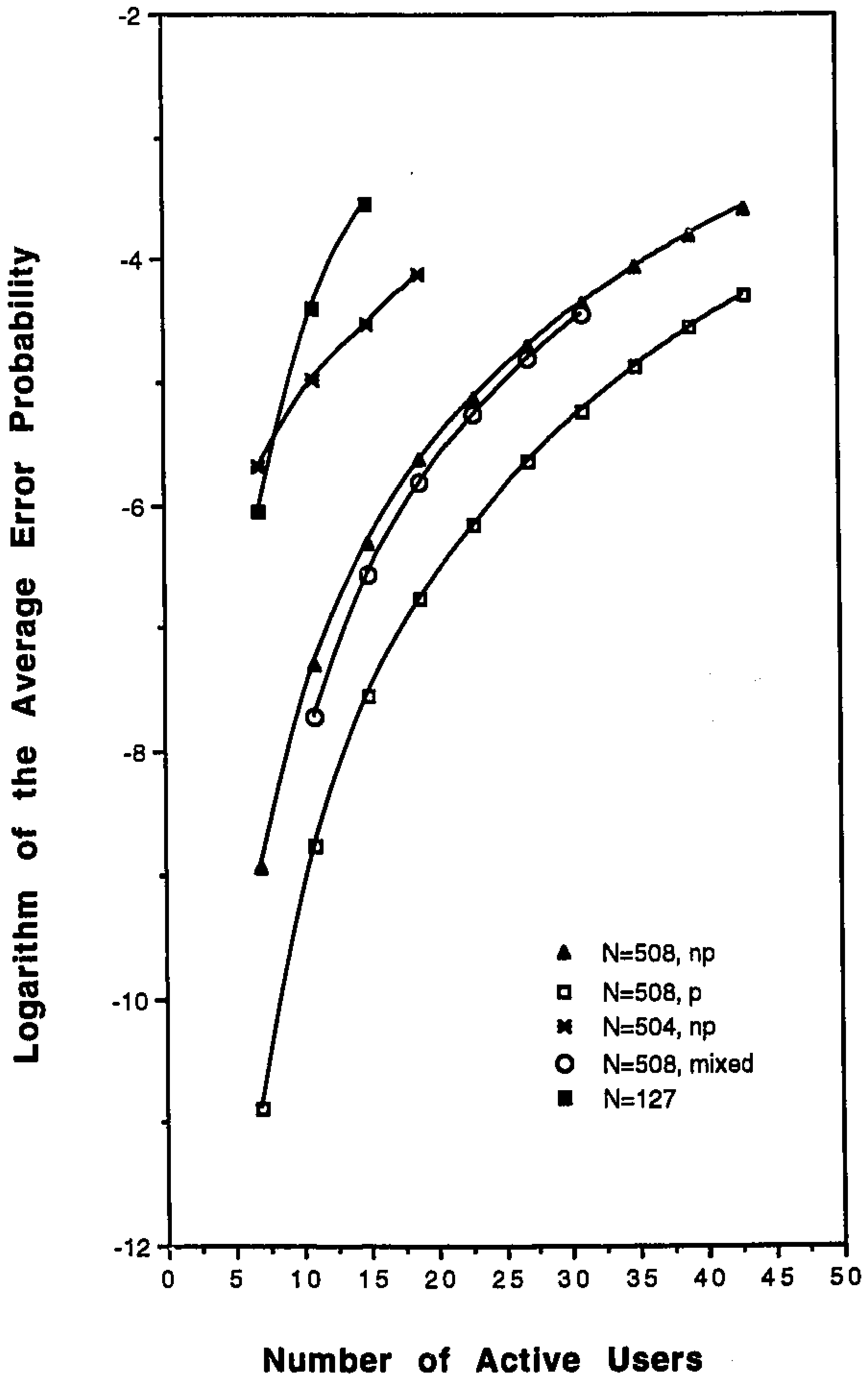

Fig.6.7: Pe vs number of active users, ASK,
No = 127, Ni = 4; No = 63, Ni = 8;

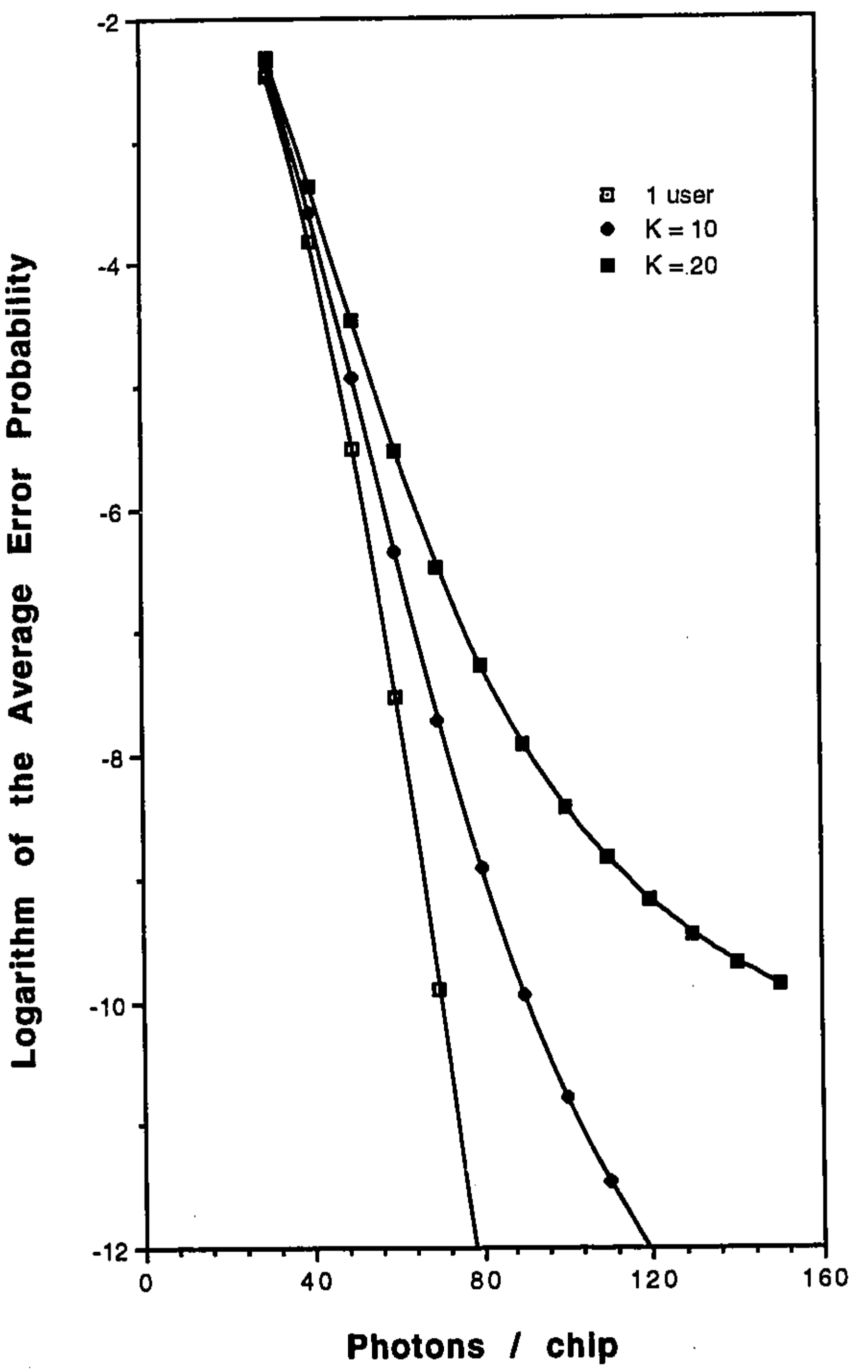

Fig.6.8: Pe vs number of photons/chip, OC, N=508 (No=127, Ni=4);

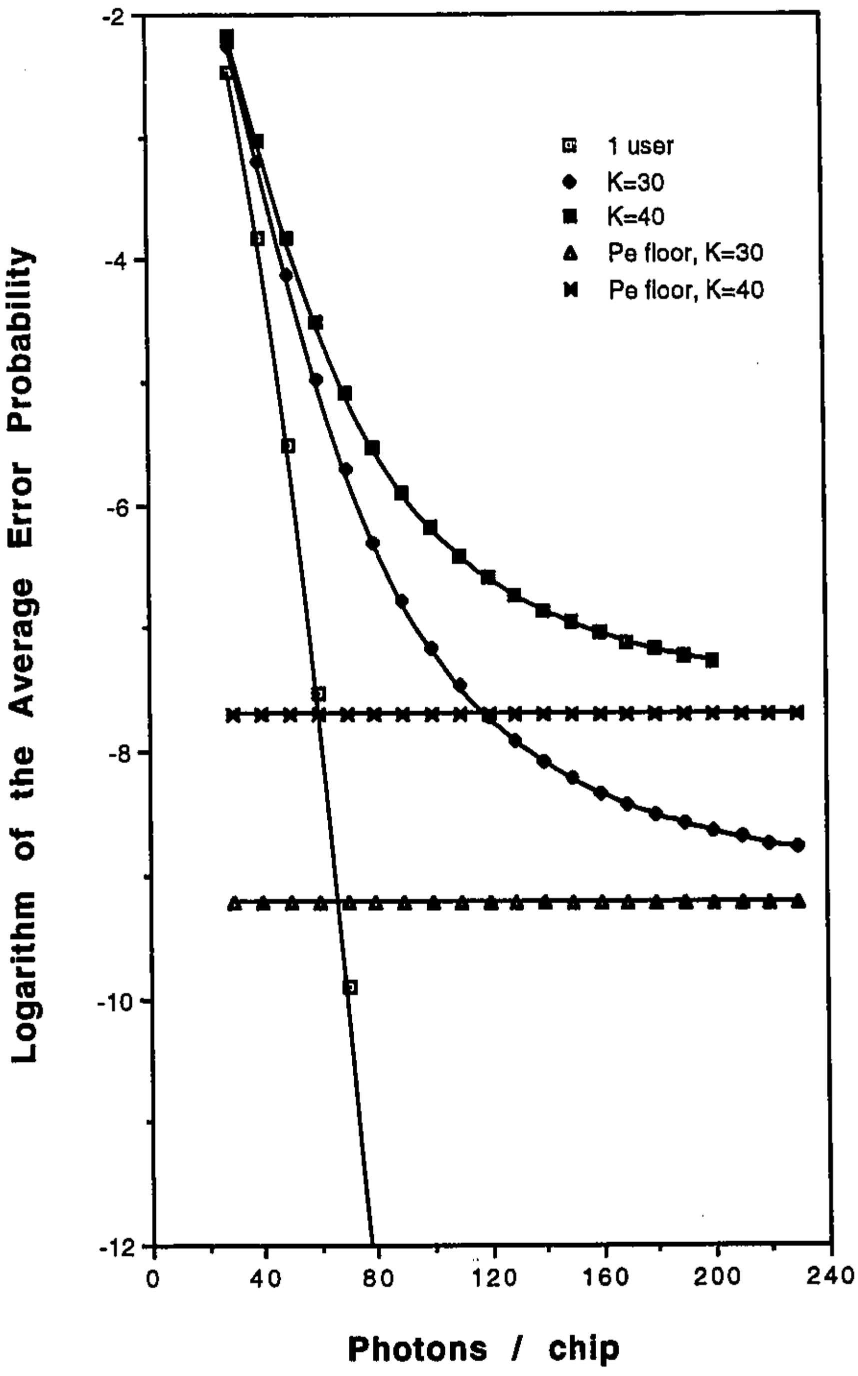

Fig.6.9: Pe vs number of photons/chip, OC, N=508 (No=127, Ni =4);

6.6 Conclusion

In this chapter we have presented a detailed theoretical performance analysis of incoherent optical CDMA system using unipolar codes, obtained from a 2-PPM encoding of standard bipolar codes. The equations derived allowed to take into account the main sources of interference, MAI, shot noise and thermal noise, and to identify the bit error rate floors that would be observed as the power is increased. The technique used to calculate the P_e was the saddlepoint approximation. It was shown that OC is much better than ASK, and that combining Gold codes of period 127 and the Barker sequence of period 4 allows 21 or 31 active users for non-programmable and programmable delay lines respectively, for $P_e = 10^{-9}$. This is a large improvement compared to using only an outer sequence of length 127, in which case only 9 users can be accommodated.

Appendix 6.A: Derivatives of the Moment Generating Function

In this appendix we derive the expressions needed in (6.26) and (6.27). Starting with the expression for the MGF:

$$M^k(s) = \sum_{I_{-1}^k, I_0^k} \frac{1}{N} \sum_{l_k=0}^{N-1} \left(\frac{e^{s[p_1+p_2]}}{p_2 s} - \frac{e^{sp_1}}{p_2 s} \right) \tag{6.A.1}$$

the first derivative is found to be:

$$\frac{dM^k(s)}{ds} = \sum_{I_{-1}^k, I_0^k} \frac{1}{N} \sum_{l_k=0}^{N-1} \left[\frac{e^{s[p_1+p_2]} \left(p_1 p_2 s + p_2^2 s - p_2\right)}{\left(sp_2\right)^2} - \frac{e^{sp_1} \left(p_1 p_2 s - p_2\right)}{\left(sp_2\right)^2} \right] \tag{6.A.2}$$

and the second derivative is expressed as:

$$\frac{d^2 M^k(s)}{ds^2} = \sum_{I_{-1}^k, I_0^k} \frac{1}{N} \sum_{l_k=0}^{N-1} \left[\frac{\left(sp_2\right)^2 B - A\, 2sp_2^2}{\left(sp_2\right)^4} \right] \tag{6.A.3}$$

where A is the numerator in Eqn(6.A.2) and its derivative, $A' = B$ is:

$$\begin{aligned} B = {} & e^{s[p_1+p_2]} \left[p_2(p_1+p_2) + \left(p_1 p_2 s + p_2^2 s - p_2\right)\left(p_1+p_2\right) \right] \\ & - e^{sp_1} \left[p_2 p_1 + p_1 \left(p_1 p_2 s - p_2\right) \right] \end{aligned} \tag{6.A.4}$$

Appendix 6.B: M.G.F. expressions for a balanced, direct-detection receiver.

In this appendix we derive the general expressions of the M.G.F. and its derivatives in the case of a balanced, direct-detection receiver for PIN photodiodes and for incoherent optical sources. These equations are valid both for Chapter 6, Section 6.4 and Chapter 7, Section 7.4. The mean intensity of the Poisson process for photodetectors 1 (positively biased) and 2 (negatively biased) can be written in both cases in the general form:

$$\lambda_1 = c1 + c2\tau \tag{6.B.1}$$

$$\lambda_2 = c3 + c4\tau \tag{6.B.2}$$

The MGF of the contribution of one interfering signal contains the integral:

$$I(s) = \int_0^1 e^{(c1+c2\tau)(e^s-1)} e^{(c3+c4\tau)(e^{-s}-1)} \, d\tau \tag{6.B.3}$$

which is written, by grouping terms that multiply τ:

$$I(s) = \int_0^1 e^{A(s)+B(s)\tau} \, d\tau \tag{6.B.4}$$

where:

$$A(s) = c1(e^s - 1) + c3(e^{-s} - 1) \tag{6.B.5}$$

$$B(s) = c2(e^s - 1) + c4(e^{-s} - 1) \tag{6.B.6}$$

The delay τ is usually uniform on $[0, T]$, but we always work with the normalized delay $\tau = \frac{\tau - lkT_c}{T_c}$ so the new delay τ is uniform on $[0, 1]$. Performing the integration we have:

$$I(s) = \frac{e^{A(s)+B(s)} - e^{A(s)}}{B(s)} \tag{6.B.7}$$

The derivative of the integral $I(s)$ is also needed. It is easy to see that it is given by:

$$\frac{dI(s)}{ds} = \frac{e^{A(s)+B(s)} \left(B(s)\left[A'(s) + B'(s)\right] - B'(s)\right)}{B^2(s)} - \frac{e^{A(s)} \left(B(s)A'(s) - B'(s)\right)}{B^2(s)} \tag{6.B.8}$$

where:

$$A'(s) = c1e^{s} - c3e^{-s} \tag{6.B.9}$$

$$B'(s) = c2e^{s} - c4e^{-s} \tag{6.B.10}$$

To find the second derivative of $I(s)$ we first find the derivative of the numerator $N(s)$ of $I'(s)$ which is written as $N'(s)$:

$$\begin{aligned} N'(s) = {} & e^{A(s)+B(s)} \left(B(s)\left[A''(s) + B''(s)\right] + B'(s)\left[A'(s) + B'(s)\right] - B''(s)\right) \\ & + e^{A(s)+B(s)} \left(B(s)\left[A'(s) + B'(s)\right] - B'(s)\right)\left(A'(s) + B'(s)\right) \\ & - e^{A(s)} \left(B(s)A''(s) + A'(s)B'(s) - B''(s)\right) \\ & - e^{A(s)} \left(B(s)A'(s) - B'(s)\right) A'(s) \end{aligned} \tag{6.B.11}$$

The second derivative of $I(s)$ is then expressed as:

$$\frac{d^2 M_z(s)}{ds^2} = \frac{N'(s)}{B^2(s)} - \frac{2\,N(s)B'(s)B(s)}{B^4(s)} \tag{6.B.12}$$

and in the above:

$$A''(s) = c1e^{s} + c3e^{-s} \tag{6.B.13}$$

$$B''(s) = c2e^{s} + c4e^{-s} \tag{6.B.14}$$

Chapter 7

Frequency-Encoded Optical CDMA Systems

7.1 Introduction

In this chapter, we present a new category of optical CDMA systems which is based on spectral encoding of the sources. In these systems, referred to as Frequency-Encoded CDMA (FE-CDMA) systems, the coding is done in the frequency domain while in conventional CDMA systems the code multiplies the modulation signal in the time domain. We will first briefly review a system proposed by J.A.Salehi and A.Wiener [5]. We discuss the major problems and drawbacks of their system, in particular, we show how chromatic dispersion is likely to reduce the multiple-access capacity of their system seriously. In the second part we present a new type of FE-CDMA system that we have designed, based on the encoding non-coherent broadband sources. We believe that this is one of the major contributions of this thesis. We discuss the advantages of our system compared to the previous system and calculate its performance. It is shown that very efficient, low-cost, CDMA systems with aggregate network throughput in the Gbit/s range can be implemented.

7.2 Motivation

In all the previous chapters and in most of the studies in the literature, the CDMA systems designed are based on encoding the information signal in the time domain by a pseudorandom sequence. As shown, efficient systems for use in LAN environments can be obtained. However, no matter how the system is designed, it will always suffer from a basic limitation. As the number of simultaneous active users increases, the code length has to be increased. To do so, without sacrifying the bit rate, one is constrained to use shorter and shorter pulses. When being coherent, the required optical sources are likely to be mode-locked lasers producing transform limited pulses, rending the system expensive and possibly not cost competitive when compared with other access schemes. If an incoherent CDMA system is considered, it might be difficult, at some point, to find lasers for which the coherence time is much shorter than the chip period, a necessary condition for the systems to behave as computed. We should also note that as the pulses used become very short, the chip duration becomes incompatible with the bandwidth of the photodetector, and that optical non-linear elements, such as AND gates have to be used as in TDMA systems, increasing the cost and the complexity of the system.

It is therefore necessary to find other types of optical CDMA systems, for which increasing the multiple access capacity, i.e., the code length, will not necessarily mean using shorter pulses or lower bit rates. One possibility is to use different *"dimensions"* for the code and for the information. In [5], Wiener et al., proposed coding mode-locked pulses in the frequency domain. The information is transmitted using ASK in the time domain. However, as we will see, the coding in the frequency domain will affect the pulse in the time domain, putting some constraints on the bit rate. Moreover, short pulses are still required and mode-locked lasers have to be used, making the system expensive.

Inspired by their design, we propose an original solution based on encoding in the frequency domain incoherent optical sources such as Edge-Emitting Light-

Emitting Diodes (EE-LED) or Superluminescent Diodes (SLD). Our system has the advantage of being simple, inexpensive and posseses a spreading gain totally independent of the bit rate. In the next section, we first present how in practice coding optical sources can be done in the frequency domain. The coder is the well-known double-grating apparatus and is common to both our system and the system developed in [5]. In Section 7.4, we present a brief summary of their system and highlight some of its drawbacks. We then discuss in detail, starting in Section 7.5, the system we propose.

7.3 Frequency Encoding of Optical Sources

A well-known frequency-encoder for optical sources is shown in Fig. 7.1. It consists of a pair of diffraction gratings placed at the focal planes of a unit magnification, cofocal lens pair. This apparatus has been used with high efficiency by many research teams for temporal shaping of short pulses, for example,[49]-[50]. The first grating spatially decomposes with a certain resolution the spectral components present in the incoming optical signal. A spatially patterned mask is inserted midway betweeen the lenses at the point where the optical spectral components experience maximal spatial separation. After the mask, the spectral components are reassembled by the second lens and second grating into a single optical beam. The mask can modify the frequency components in phase and/or in amplitude, depending on the coherence property of the incident optical source. The number of frequency bands that can be resolved by the encoder will dictate the code length, and therefore the number of subscribers in the system. It has been shown [49] that this number is given approximately by:

$$N \approx 0.5 \frac{\delta\lambda}{\lambda} \frac{\pi w}{d \cos(\theta_r)} \tag{7.1}$$

where λ is the center wavelength of the optical source, $\delta\lambda$ is the spectral width being encoded, w is the input beam radius, d is the grating period and θ_r is the diffracted angle of the central wavelength. For $\delta\lambda = 60$nm, $\lambda = 1.3\mu$m, $w = 5$mm and $1/d =$

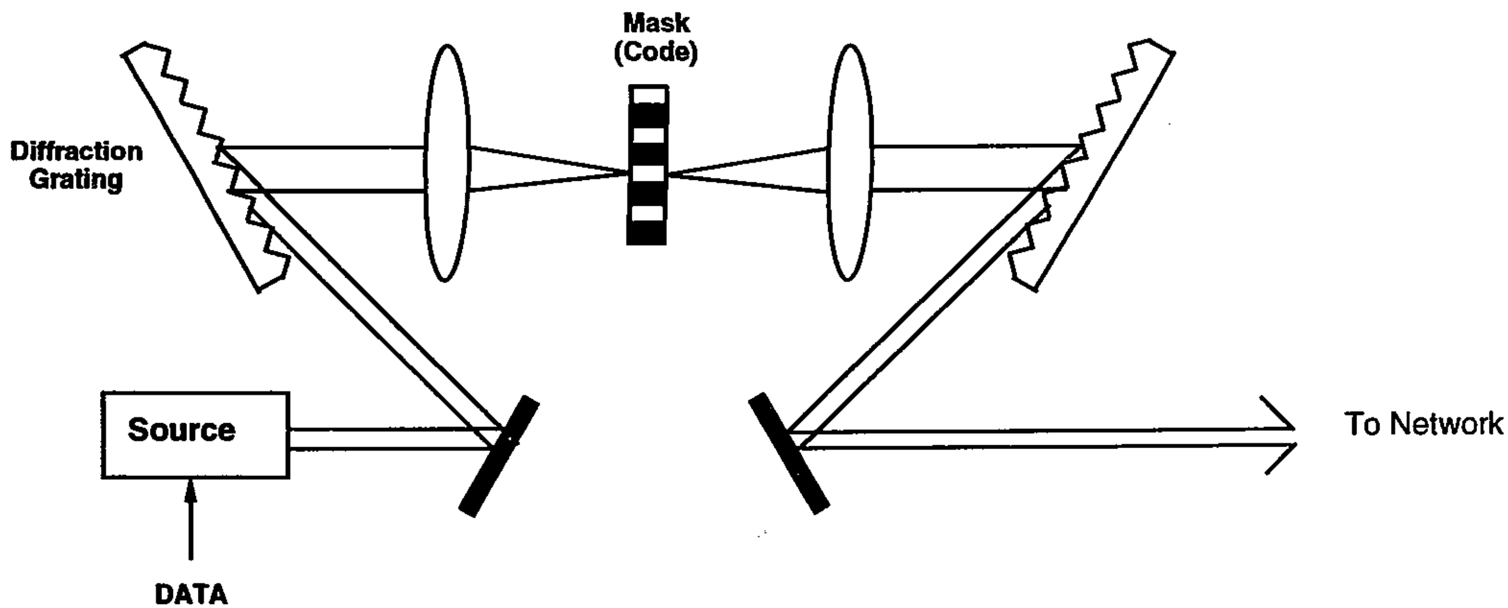

Fig.7.1: Frequency encoder for optical sources.

$1200 lines/\mathrm{mm}$ grating, with $\theta_r = 51^o$ (for Littrow configuration), we compute $N \approx 690$ subscribers. Such a spectral width is easily obtained when using incoherent optical sources such as LEDs. When using coherent optical sources, it requires pulse's duration of approximately 0.1 picosecond, at that wavelength.

7.4 FE-CDMA Systems with Temporally Coherent Sources

The behavior of FE-CDMA systems depends on the coherence properties of the optical source used. When the source is highly temporally coherent, such as mode-locked lasers, the direct relationship between the frequency and time domain allows to shape the temporal profile of a signal by modifying its Fourier transform. For example, consider a wave whose complex envelope and its Fourier transform are:

$$S(t) = A(t)e^{j\theta_0} \quad S(f) = e^{j\theta_0}\int_{-\infty}^{\infty} A(t)e^{-j2\pi ft}dt \tag{7.2}$$

When one multiplies $F_A(f)$, the Fourier transform of $A(t)$, by a weighting function $W(f)$, the resulting time signal $S_E(t)$ is:

$$S_E(t) = e^{j\theta_0}\int_{-\infty}^{\infty} F_A(f)W(f)e^{j2\pi ft}df \tag{7.3}$$

where the subscript E is for "encoded" wave. In a FE-CDMA system, $W(f)$ is the pseudorandom code:

$$W(f) = \sum_{k=-N_0}^{N_0} w_k p(f - kf_c) \tag{7.4}$$

where $p(f) = 1$ for $|f| \leq f_c$, W is the double-sided bandwidth to be encoded, $N = 2N_0 + 1$ is the code period, $f_c = W/N$ is the chip length and w_k is the code sequence. For coherent waves, w_k can be any complex number. However, in order to keep all the signal energy, it is preferable to choose $|w_k| = 1$.

As an example, consider for the temporal pulse before coding and its Fourier transform:

$$S(t) = (P_o)^{1/2}\mathrm{sinc}(Wt) \qquad S(f) = (P_o)^{1/2}/W \quad \text{for } |f| \leq W/2 \tag{7.5}$$

where P_o is the peak power of the mode-locked pulse of duration $\approx 1/W = \tau_c$. The encoded pulse is then written as:

$$S_E(t) = \frac{(P_o)^{1/2}}{N}\mathrm{sinc}(f_c t) \sum_{k=-N_0}^{N_0} e^{2\pi j(k f_c t + w_k)} \tag{7.6}$$

where we took the codes to be pure phase factors; for binary phase codes, $w_k = 0$ or π. The first factor is a real envelope function which determines the temporal width of the encoded pulse $1/f_c = N\tau_c$. The second factor determines the temporal shape of the pulse according to the sequence w_k.

At the receiver, the desired signal is despread by multiplying its spectrum by $W^*(f)$ such that $W(f)W^*(f) = 1$. The mode-locked pulses of the desired signal will be restored, while for the interfering signals the codes do not match and their time profile remains a low intensity pseudonoise burst. After the optical decoder and before the photodetector, an optical threshold element is used to filter the interfering signals. An optical threshold element is necessary since no photodectector is fast enough to match the bandwidth of the incoming pulses. For practical code lengths (more than 30), and achievable resolution in the spectral encoding apparatus, the pulse duration has to be less than 1 picosecond. Since the technology of optical threshold elements is not mature yet, a receiver for such a system will be quite expensive and complex, still for some time. This is in contrast with the system we propose later in this chapter, since in this case the bandwidth of the photodetector needs only to match the bit rate, as any simple point-to-point optical communication system. However, one should note that encoding of mode-locked pulses is a useful technique to avoid non-linear effects in single-mode fiber due to the reduced instantaneous intensity. One can see that this type of FE-CDMA system is in complete analogy with an ordinary spread-spectrum system. In the latter case, the desired signal is despread and has a small bandwidth compared to the interfering signals, which are spread in frequency. In a FE-CDMA system, the desired signal has a high peak power and a short duration, while the interfering signals are spread in time and have a low intensity. Fig. 7.2 gives the FE-CDMA system diagram for coherent sources.

The code design is governed by the detection method. The system proposed in [5] uses direct-detection with ASK as the modulation format. The multiple-access capacity is therefore achieved by designing the codes such that:

$$|S(t)|^2 >> |S_E(t)|^2 \tag{7.7}$$

It is shown in [51], that independent of the codes used, a lower bound on the peak intensity for an encoded signal is:

$$\max |S_E(t)|^2 \geq \frac{P_0}{N} \tag{7.8}$$

for all t. The performance evaluation of such systems was performed neglecting shot noise and thermal noise [51]. An upper bound was also obtained:

$$P_e \leq \sum_{l=1}^{K} \binom{K}{l} \left(\frac{1}{2M}\right)^l \left(1 - \frac{1}{2M}\right)^{K-l} e^{\frac{-PG}{4MT}} \tag{7.9}$$

where K is the number of interfering users and $M = T_b/T$, where T_b is the bit rate and T is the temporal width of the encoded pulse. The variable M accounts for the fact that the encoded pulse duration may be shorter than the bit period, and $PG = MN$ is the processing gain. The variable l has a binomial distribution and defines the number of interfering users transmitting a "1" in the same time slot as the desired signal. Note that, the individual bit rates can not exceed $1/\tau_c MN = 1/TM$. The above formula assumes that the detector looks at the optical threshold output in a time interval of duration τ_c, the pulse duration. This requires an unrealistically fast detector if τ_c is in the femtosecond range. In practice, the detector will observe

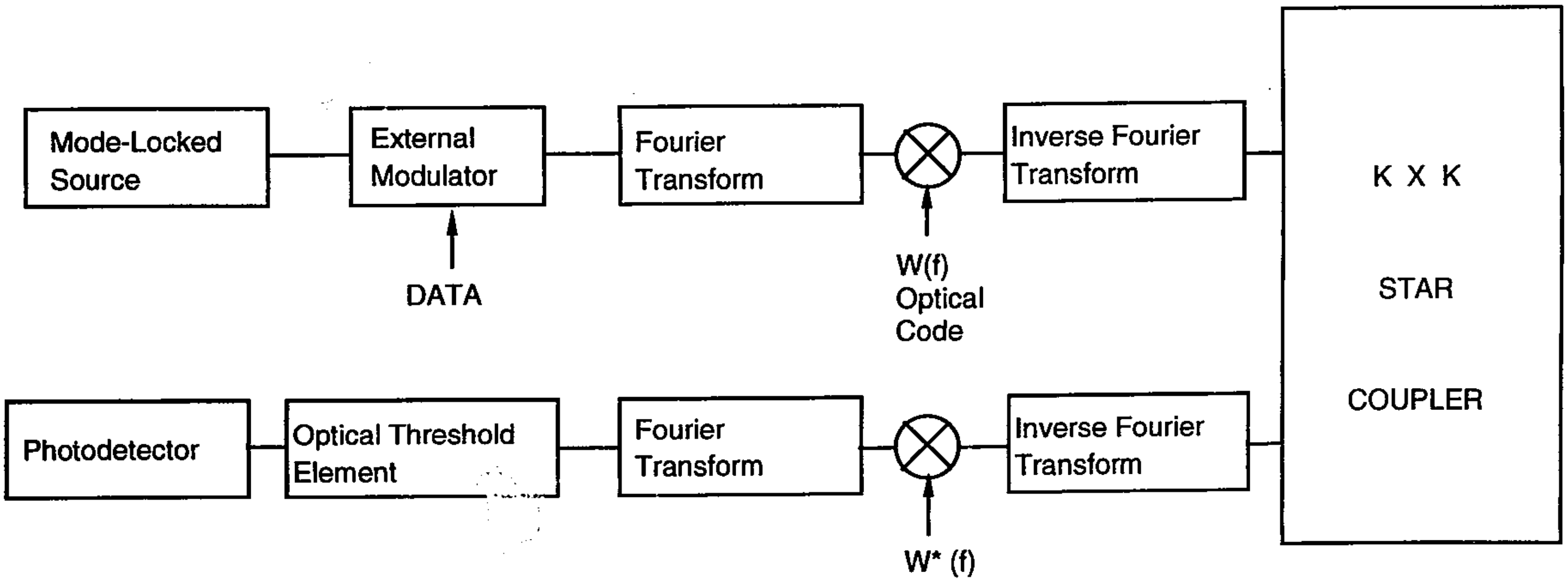

Fig.7.2: Block diagram of a coherent FE-CDMA system.

the output for a time $\beta\tau_c$, $1 \leq \beta \leq 100$. In such cases the performance degradation is about one order of magnitude. For example, with $N = 128$ code elements, $M = 100$ (a processing gain value of PG = 12800) and $\beta = 1$, $K = 100$ users gives $P_e = 2 \times 10^{-7}$, while for $\beta = 128$ we have $P_e = 3 \times 10^{-6}$[51].

It is shown that for a constant processing gain value, one is much better served by increasing N instead of M: for $M = 25, N = 510$ we have $P_e = 10^{-8}$, while for $M = 400, N = 32$, $P_e = 10^{-4}$. By increasing the code length, the intensity of the original pulse is spread over a longer time period and the instantaneous intensity is more effectively reduced. Encoding and decoding was experimentally demonstrated for $N = 127$, by using fixed phase masks and programmable Spatial Light Modulators (SLM) [52]. It was argued that $N = 2000$ should be feasible.

In the next section we discuss the main drawback of the system, namely the effect of fiber chromatic dispersion on the multiple access capacity.

7.4.1 Chromatic Dispersion Effects on a Coherent FE-CDMA System

Our goal in this section is to qualitatively discuss the possible performance degradation that one will encounter on the multiple access capacity due to fiber dispersion, and how it can be lightened. To be efficient, a FE-CDMA system must have a high value for N, and therefore the bandwidth to be encoded must be large; stated differently the pulses used must be very short. The different spectral components will propagate at different group velocities, creating pulse spreading at the output of the fiber. It should be noted that it is sometimes *wrongly* believed that since encoded pulses have a longer time duration, they have a smaller bandwidth and, therefore, that FE-CDMA systems will be less affected by chromatic dispersion than other systems using short pulses, such as optical TDMA. In fact, in the linear regime, a coded pulse will be affected by dispersion in the same way as an uncoded one. This is because the spectral phase shifts imparted by the encoding mask will be removed by the decoding mask after reconstruction to reveal the spectral phase shifts caused by fiber's dispersion alone.

In analyzing chromatic dispersion effects, it is customary to expand the propagation constant β in a Taylor series around the carrier frequency ω_0 [53]:

$$\beta(\omega) = \beta_0 + \beta_0^1 (\omega - \omega_0) + \frac{\beta_0^2}{2}(\omega - \omega_0)^2 + \frac{\beta_0^3}{6}(\omega - \omega_0)^3 \tag{7.10}$$

where:

$$\beta_0^1 = \frac{d\beta}{d\omega} = \frac{1}{c}\left(n - \frac{\lambda dn}{d\lambda}\right) s/m \tag{7.11a}$$

$$\beta_0^2 = \frac{d^2\beta}{d\omega^2} = \frac{\lambda^3}{2\pi c^2}\frac{d^2 n}{d\lambda^2} s^2/m \tag{7.11b}$$

$$\beta_0^3 = \frac{d^3\beta}{d\omega^3} = \frac{-\lambda^2}{4\pi^2 c^3}\left[3\lambda^3\frac{d^2 n}{d\lambda^2} + \lambda^3\frac{d^3 n}{d\lambda^3}\right] s^3/m \tag{7.11c}$$

The second and third derivatives of the refractive index with respect to the wavelength are responsible for the dispersion. It is known [53] that for an input Gaussian pulse shape with an rms pulse width $T/\sqrt{2}$, and for a monochromatic source, the output pulse width after a propagation distance z will be:

$$\sigma = \frac{T}{\sqrt{2}}\left(1 + \frac{(\beta^2 z)^2}{T^4} + \frac{(\beta^3 z)^2}{4T^6}\right)^{\frac{1}{2}} \tag{7.12}$$

For SMF with zero-dispersion wavelength at 1.3μm, the values of β^2 and β^3 at 1.55μm are typically $-20ps^2/km$ and $0.1ps^3/km$, respectively. When operating at the zero dispersion wavelength, one can eliminate the second order dispersion term, or as we will see in the next section, one can compensate it. We are therefore interested in studying the pulse shape when only the third order dispersion remains. In this case, the output pulse shape is not Gaussian so that the rms pulse width is not a useful criterion. It is known that for a Gaussian input pulse $e^{-4(t/\tau_0)^2} = e^{-4t^2}$ (by normalizing the time such that $t = t/\tau_0$), the output pulse is:

$$S(t,z) = 2\sqrt{\pi}|B|^{-1/3} e^{\frac{2-3(4t)B}{3B^2}} A_i\left[(1-(4t)B)B^{-4/3}\right] \tag{7.13}$$

where:

$$B = \frac{32\beta^3 z}{\tau_0^3} \tag{7.14}$$

and $A_i(x)$ is the Airy function. For example, at 1.55um, $B = 480$ for $\tau_0 = 0.1ps$ and $z = 100m$, and $B = 4.8$ for $\tau_0 = 1ps$ and $z = 1km$. The variation of B as a function of wavelength is given for a 1ps pulse and 1km distance on Fig. 7.3. The dispersion is of course larger for longer wavelengths.

In Fig. 7.4, we plot the normalized time for which the pulse amplitude has decreased to one tenth of its peak value, as a function of B. For $B = 50$ (1ps pulse over 10km) the pulse already occupies 20 times its orignal width.

Fig. 7.5a and Fig. 7.5b give the output pulse shape for different values of B. Note that, the output pulse is already largely distorted for $B = 10$, which is a 1ps pulse traveling 2 Km or 100 femtoseconds pulse (0.1ps) traveling only 2 meters of fiber ! Remember that in these curves, the second order dispersion is already assumed to be perfectly compensated. This type of pulse shape was experimentally observed in [54]. The effects on a FE-CDMA system are therefore basically:

1) A decrease in peak pulse intensity of a decoded pulse. This level might falls below the threshold level of the optical threshold element causing a decoding error.

2) An observation time $\beta\tau_0$ which must be larger since the position of the peak intensity is shifted in time. As seen before, larger observation times will deteriorate the performance of a coherent FE-CDMA system.

7.4.2 Partial Solution to Chromatic Fiber Dispersion: Grating-Pair Compressor

The use of a single grating pair for pulse compression is a very old concept, first proposed by Treacy in [55], and studied by Martinez in [56]. The goal is to find an optical arrangement which can provide the inverse phase function imposed by the fiber. The SMF is usually modeled as a phase factor $\Phi(w) = \beta(w)Z$ where

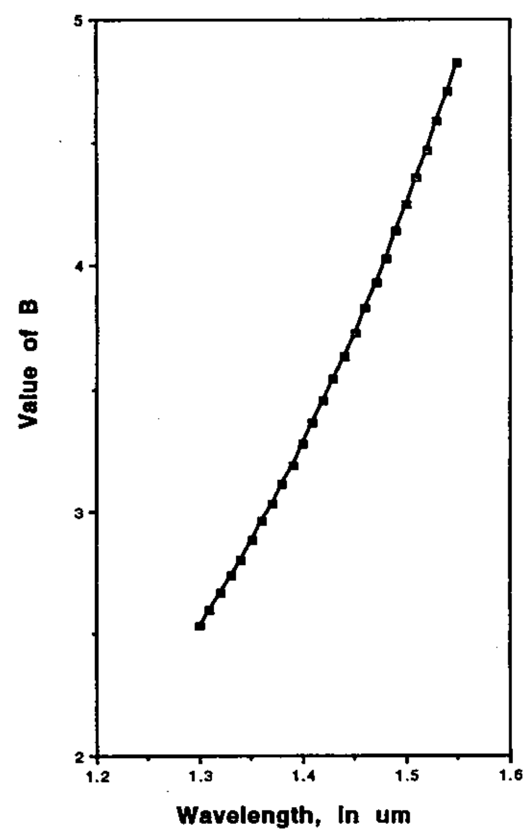

Fig.7.3: Value of B versus wavelength.

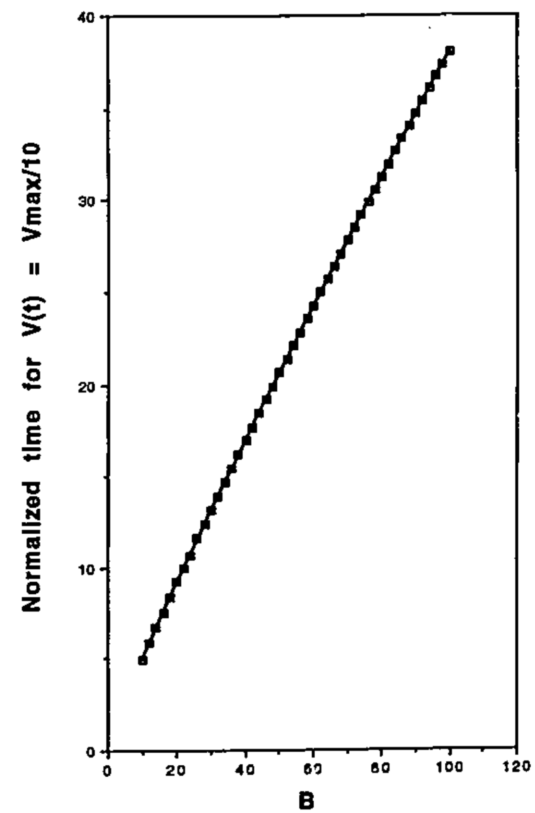

Fig.7.4: Spreading factor versus B.

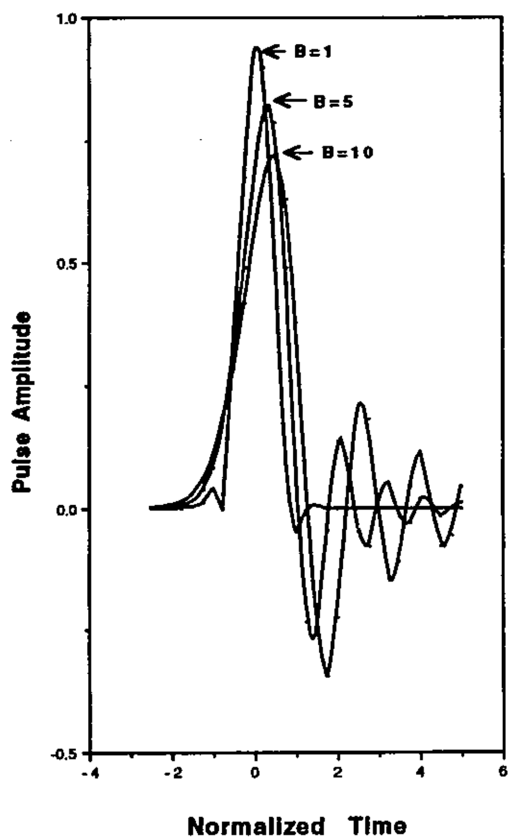

Fig.7.5a: Third order dispersion effect on a Gaussian input pulse.

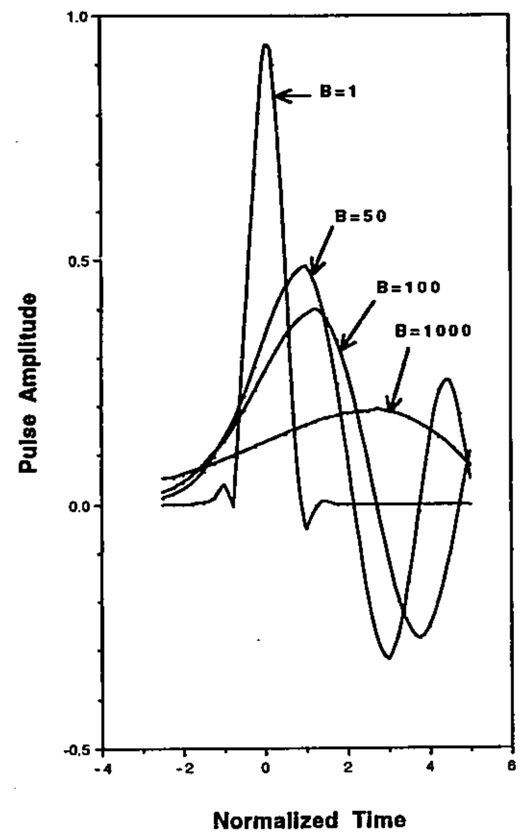

Fig.7.5b: Third order dispersion effect on a Gaussian input pulse.

$\beta(w)$ is given by (7.10), so the goal is to find a transfer function whose phase is $-\beta(w)Z$. In the anomalous dispersion region, the design proposed by Treacy is unusable since it also has a negative second-order Group-Velocity Dispersion (GVD), and would further broaden the pulse. However, it was recently shown [57] that a grating pair with a telescope, see Fig. 7.6, can provide negative as well as positive GVD. In that case the mask is transparent. Exactly the same set-up is used for frequency-encoding, with $z1 = z2 = 0$. The dispersion parameters for this arrangement are:

$$\frac{d^2\Phi}{d\omega^2} = \frac{\lambda_0^3 Z}{2\pi\Big(cS cos\Theta_0\Big)^2} \tag{7.15a}$$

$$\frac{d^3\Phi}{d\omega^3} = \frac{-3\lambda_0^4 Z\Big(cos^2\Theta_0 + \lambda_0/S sin\Theta_0\Big)}{4\pi^2 c^3 S^2 cos^4\Theta_0} \tag{7.15b}$$

where $Z = z1 + (f1/f2)^2 z2$, $z1$ and $z2$ are the distances between the grating and the external focal planes, S is the groove spacing, Θ_0 is the output diffraction angle and λ_0 is the carrier wavelength. The distances $z1$ and $z2$ are defined as positive in the configuration of Fig. 7.6 and negative when the gratings are after the external focal planes. Note that the sign of the second order β^2 and the third order β^3 GVD terms of the apparatus are always reversed. For $\lambda_0 > \lambda_S$, where λ_S is the zero dispersion wavelength of the fiber,the second and third order GVD terms are negative and positive respectively, so that this configuration can be used to compensate simultaneously for both dispersion terms. For $\lambda_0 < \lambda_S$ the fiber GVD terms have the same sign, and simultaneous compensation is not possible.

In theory, therefore, it is possible, if one knows the transmitted distance, to completely compensate fiber chromatic dispersion at 1.55μm in a SMF with $\lambda_S =$ 1.3μm. However, it is clearly shown in [57], that both simultaneous compensations is practical only if the transmitting wavelength is near zero dispersion, $1.307\mu m \leq \lambda_0 \leq 1.34\mu m$. One possible solution proposed in [54] is then to use dispersion-shifted fiber with $\lambda_S \approx 1.55\mu$m. They have conducted an experiment with $\lambda_0 = 1537$nm

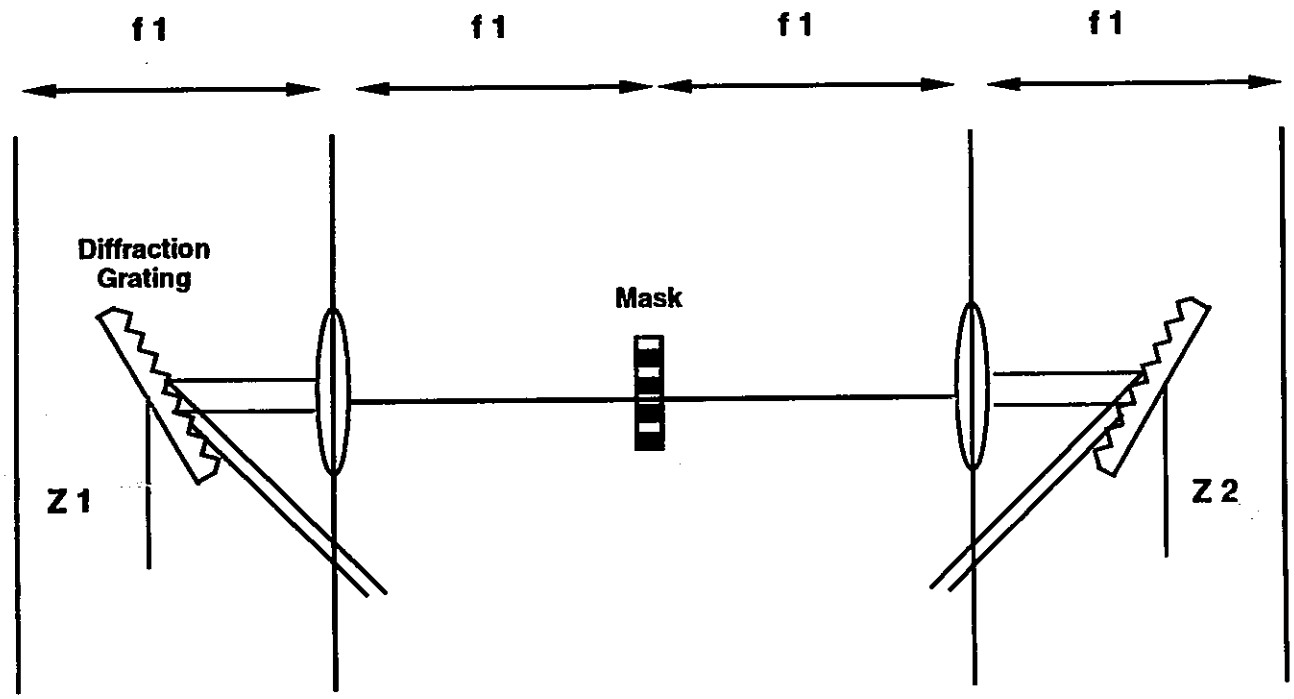

Fig.7.6: Double-Grating Compressor.

and λ_S = 1542nm which gives $\beta^2 = 0.52ps^2/km$ and $\beta^3 = 0.13ps^3/km$. They showed experimentally that in this case the third order dispersion dominates. By using the grating apparatus with $Z = -12.4$cm, they were able to largely compensate for chromatic dispersion after propagation over a fiber length of $3.2km$. They used an input pulse width of 500 femtoseconds with $\lambda_0 = 1573$nm. The compressed output pulse width was $\approx 1ps$; uncompensated pulse width would have been around 40ps. The conclusions to be drawn are as follow:

1) Both second and third order GVD can be compensated when operating near the zero dispersion wavelength. However, as shown recently [58], the fourth order dispersion term will in that case become important for pulses shorter than 0.2 picoseconds.

2) When one wishes to transmit at 1.55μm with a normal SMF with zero-dispersion wavelength at 1.3μm, the second order dispersion in the fiber dominates and can be compensated. In that case, the third order GVD will dictate the output pulse shape. Severe spreading and an asymmetry can be observed.

3) In order to be efficient, such pulse compressors must know within a certain accuracy, the fiber length to be compensated. In a network where the distance between users is varying, the distances between the gratings and lenses need to be adjusted on a per-call basis. In practice, this might prove to be difficult. We believe that more efficient solutions to fiber dispersion (that would not destroy the code) have to be found. One solution might be in the use of spectral holography, where the distorted pulse is first recorded, and then acts as a matched-filter for the incoming pulse at the time of information transmission [59].

7.5 FE-CDMA Systems with Temporally Incoherent Sources

Since FE-CDMA systems are based on encoding the spectrum of optical sources, natural alternatives to mode-locked lasers are non-coherent sources such as multimode lasers or LEDs. For these sources, the large frequency bandwidth, is caused by photons being produced with different energy, and is independent of the modulating signal. It is then clear that filtering the spectrum of these sources will not affect the temporal shape of the modulating signal. * Therefore the multiple-access capacity can not be based on the differences of intensity levels between the coded and uncoded waves. New coding strategies have to be found.

Polychromatic spatially coherent or incoherent sources have found many applications in the past in different areas such as spectrography, holography [61], optical processing [62] and image transmission [63-64]. In transform applications spatial incoherence allows to avoid coherent noise while the large spectrum is divided into many "wavelength channels" to achieve parallel capacity. Much effort is still being spent by the researchers to achieve achromatic transforms using broadband sources.

In communications applications however, broadband sources such as LEDs were until recently, considered as being undesirable, laser diodes being considered the right choice. Mainly three reasons explain this: 1) Lasers couple more light into SMF, 2) they allow a wide variety of modulation types such as DPSK of FSK and 3) they can be modulated at higher bit rates. A number of recent, experiments, however have demonstrated that light-emitting diodes can be used instead of laser diodes to satisfy many short to medium distance single-mode or multimode system requirements. When compared with laser diodes, LEDs offer the advantage of higher reliability, reduced temperature sensitivity, less complicated drive circuit requirements, immunity to optical feedback, and lower cost due to high yields in packaging technology. The cost factor is a very important one in bringing the optical fiber with transmission capacity of up to 600 Mbit/s to customers in the Subscriber Loop applications [65]. To answer this need, extensive research efforts are made to develop "new" types of LEDs such as Edge-Emitting LEDs (EE-LED) and Superluminescent Diodes (SLD). These LEDs are very strong competitors to laser diodes since they can couple high power level into SMF. As examples, SLDs with average output

* In fact the signal in the time domain will be only slightly modified [60].

power of $-5dBm$ at $1480nm$ have been reported [66]. EE-LEDs coupling $-6dBm$ into SMF are available. Such high coupling power is made possible by the fact that the output emission profile is a narrow beam, very similar to that of the lasers. Their modulation bandwidth is also very large compared to Surface-Emitting LED (SE-LED). The Amplified Spontaneous Emission noise (ASE) emitted by erbium-doped fiber amplifiers, usually called Broad-band Superluminescent Fiber Source [67], is also a good candidate for FE-CDMA systems. Recent experiments show that the ASE can be used as a broadband (more than 30 nm) source with a total output power of 5 mW (+ 7 dBm). The spectral density of the source has less than 5 dB variation over the 30 nm bandwidth. The coherence length was 210 μm. Recent experiments with EE-LED over 10 km and 20 km of SMF have been conducted at bit rates of $1.2Gbit/s$ and $600Mbit/s$ [65]. The FWHM of these devices is from $50nm$ to $\approx 120nm$ so that for CDMA applications, the bandwidth to be encoded is also very large.

All these factors make us believe that EE-LED and SLD could play an important role in future LAN applications. In the next section, we show how LEDs could outperform laser diodes in LAN applications using CDMA. This is accomplished by using the dimensionality of wavelength. Since the system configuration depends on the codes used, we first describe suitable codes for amplitude coding of LEDs.

7.6 Codes for Incoherent FE-CDMA Systems

Since LEDs are temporally incoherent sources, they can not in general retain phase information and the weighting function $W(f)$ in this case is constrained to be a unipolar real function. Since the masks used are passive devices we must have $W(f) \leq 1$, and it is immediately apparent that some power loss will occur. Note that, although we consider complete asynchronism between the users, only the periodic correlation parameters are of interest, since the frequency slots of the different users will always be aligned.

Let $(\mathbf{X}) = (\mathbf{x_0}, \mathbf{x_1}, \cdots, \mathbf{x_{N-1}})$ and $(\mathbf{Y}) = (\mathbf{y_0}, \mathbf{y_1}, \cdots, \mathbf{y_{N-1}})$ be two $(0,1)$

sequences. The periodic crosscorrelation is:

$$\Theta_{\mathbf{XY}}(k) = \sum_{i=0}^{N-1} x_i y_{i+k} \tag{7.16}$$

Define the complement of sequence $(\mathbf{X})$ by $(\bar{\mathbf{X}})$ whose elements are obtained from the elements of $(\mathbf{X})$ by $\bar{x}_i = 1 - x_i$. The periodic crosscorrelation sequence between $(\bar{\mathbf{X}})$ and $(\mathbf{Y})$ is similarly:

$$\Theta_{\bar{\mathbf{X}}\mathbf{Y}}(k) = \sum_{i=0}^{N-1} \bar{x}_i y_{i+k} \tag{7.17}$$

We look for sequences for which:

$$\Theta_{\mathbf{XY}}(k) = \Theta_{\bar{\mathbf{X}}\mathbf{Y}}(k) \tag{7.18}$$

A receiver that computes $\theta_{\mathbf{XY}}(k) - \theta_{\bar{\mathbf{X}}\mathbf{Y}}(k)$ will reject the interference coming from the user with the sequence $(\mathbf{Y})$. We first list some sequences that achieve this, and then explain how $\theta_{\mathbf{XY}}(k) - \theta_{\bar{\mathbf{X}}\mathbf{Y}}(k)$ can be computed optically.

a) M-sequences

An unipolar M-sequence of length N is obtained from the bipolar version by replacing each binary 1 by a 0 and each -1 by a 1. Consider the sequence $(\mathbf{Y})$ as being $(T^k\mathbf{X}) = (\mathbf{X})^{\mathbf{k}}$ where T is the operator that shifts vectors cyclically to the left by one place, that is $(TX) = (x_1, x_2, \ldots, x_{N-1}, x_0)$. In that case:

$$\Theta_{XY}(k) = \sum_{i=0}^{N-1} x_i x_{i+k} \tag{7.19}$$

which results in $\theta_{XY}(0) = \frac{N+1}{2}$ for $k = 0$ and to $\theta_{XY}(k) = \frac{N+1}{4}$ for $k = 1$ to $N-1$. The sum $i+k$ is taken modulo N. These results come from the shift-and-add property of m-sequences which says that the modulo-2 sum of an m-sequence and any cycle phase shift of the same m-sequence is another phase of the same sequence. In other words, half of the 1's in $(\mathbf{X})^k$ coincide with the 1's of $(\mathbf{X})$ while the other half coincide with the 0's, where $(\mathbf{X})^k$ is the k cycle shift of $(\mathbf{X})$. A receiver that computes:

$$Z = \Theta_{XY}(k) - \Theta_{\bar{X}Y}(k) = \sum_{i=0}^{N-1} x_i x_{i+k} - \sum_{i=0}^{N-1} (1 - x_i) x_{i+k},$$
$$= 2\Theta_{XY}(k) - \Theta_{XY}(0) = 2 \times (N+1)/4 - (N+1)/2 = 0 \tag{7.20}$$

will reject the signal coming from the interfering user having sequence $(\mathbf{X})^k$. This is true for any k, and by assigning the N cycle shifts of a single m-sequence to N subscribers, we have a network that can support N simultaneous users without any interference. Complete orthogonality between the users is theoretically achieved.

b) Hadamard Codes

A Hadamard Code is obtained by selecting as codes the rows of a Hadamard matrix. It is well known that an $(N \times N)$ Hadamard matrix of 1's and 0's has the property that any row differs from any other row in exactly $N/2$ positions. All rows except one contains $N/2$ 0's and $N/2$ 1's. As an example, for $N = 4$:

$$M_4 = \begin{pmatrix} 1 & 1 & 1 & 1 \\ 1 & 0 & 1 & 0 \\ 1 & 1 & 0 & 0 \\ 1 & 0 & 0 & 1 \end{pmatrix} \quad \bar{M}_4 = \begin{pmatrix} 0 & 0 & 0 & 0 \\ 0 & 1 & 0 & 1 \\ 0 & 0 & 1 & 1 \\ 0 & 1 & 1 & 0 \end{pmatrix}$$

Taking $(\mathbf{X})$ as being row i and $(\mathbf{Y})$ as being row j with $i \neq j$, it is easy to verify that:

$$\Theta_{\mathbf{XY}}(i,j) = \Theta_{\bar{\mathbf{X}}\mathbf{Y}}(i,j) \tag{7.21}$$

where $\bar{X}$ is from $\bar{M}_4$, therefore satisfying (7.18). In particular, we note that Hadamard codes allow orthogonal signaling in place of ASK. This is not possible with m-sequences. This allows to gain back a 3dB loss inherent to the previously designed system. Finally, note that for an $N \times N$ Hadamard matrix, $N - 1$ subscribers can be accommodated since the codeword containing all 1's can not be used.

c) Bipolar Codes

Any complex number can be represented as a combination of real, unipolar components. For practical reasons when designing the masks, we limit ourselves to (-1,1) codes. We recall from Chapter 4, that one can represent a bipolar sequence $(\mathbf{Y}) = (\mathbf{y_0}, \mathbf{y_1}, \cdots, \mathbf{y_{N-1}})$ by its unipolar version $(\mathbf{Y^u}) = (\mathbf{y_0^u}, \mathbf{y_1^u}, \cdots, \mathbf{y_{2N-1}^u})$. We note that:

$$
\begin{aligned}
y_{2i}^u &= 1 \quad y_i = 1 \\
&= 0 \quad y_i = -1 \\
y_{2i+1}^u &= 0 \quad y_i = 1 \\
&= 1 \quad y_i = -1
\end{aligned}
\tag{7.22}
$$

Therefore, the condition $Z = \theta_{\mathbf{X^u Y^u}}(k) - \theta_{\bar{\mathbf{X}}^u\mathbf{Y^u}}(k) = 0$ is equivalent to:

$$
\begin{aligned}
Z &= 2\Big[\sum_{i=0}^{2N-1} x_i^u y_i^u\Big] - \sum_{i=0}^{2N-1} y_i^u \\
&= 2\Big[\sum_{i=0}^{N-1} \frac{(x_i+1)}{2}\frac{(y_i+1)}{2} + \sum_{i=0}^{N-1} \frac{(1-x_i)}{2}\frac{(1-y_i)}{2}\Big] - \sum_{i=0}^{2N-1} y_i^u \\
&= \sum_{i=0}^{N-1} x_i y_i = \Theta_{\mathbf{XY}}(0) = 0
\end{aligned}
\tag{7.23}
$$

which is the usual bipolar crosscorrelation function. Therefore, all orthogonal ($\theta_{\mathbf{XY}}(0) = 0$) bipolar (-1,1) codes will satisfy (7.18) and can be applied to our system. For a unipolar sequence of length $2N$, only N subscribers however can be accommodated. This poses no problems when the number of resolvable frequency slots is large enough. Namely, we look at sequences for which $(\mathbf{Y}) = (\mathbf{X})^{\mathbf{k}}$:

$$
\Theta_{\mathbf{X}}(k) = \sum_{i=0}^{N-1} x_i x_{i+k} = 0 \quad \text{for all k} \neq 0
$$

These sequences are termed Perfect Autocorrelation Sequences (PAS). However, it has been proved that no solution exists for $4 < N \leq 12100$. Almost PAS which have all out-of-phase autocorrelation values equal to 0 except 1 were recently proposed [30] and could be used for our system. For a bipolar sequence of length N, 2N frequency slots would be necessary and N-1 subscribers could be supported. Note that, for all unipolar sequences obtained from bipolar sequences, orthogonal signaling can be used. We have mentioned these sequences for completeness. In the following however, we will consider only m-sequences and Hadamard codes since they utilize the source spectrum more efficiently.

7.7 Transmitter and Receiver Description

Consider Fig. 7.7 which shows the transmitter and the receiver needed for a pair of communicating users. At the transmitter, the data directly modulates the optical source, which is then directed to the temporally nondispersive lens and grating apparatus presented before, for the spectral encoding operation. At the receiver, the following needs to be realized: $\theta_{\mathbf{XY}}(k) - \theta_{\bar{\mathbf{X}}\mathbf{Y}}(k)$. This can be easily done using 2 photodetectors, one to receive $\sum x_i x_{i+k}$ and the other to receive $\sum(1 - x_i)x_{i+k}$ and substracting their outputs. One way of doing this, although probably not the most efficient, is to split the incoming signal in two parts, each one going through a separate lens and grating apparatus. Two masks that transmit complementary frequency bands are then needed. The notation $\bar{A}(w)$ in Fig. 7.7 simply means that the mask pattern in that branch is the opposite of the one used for $A(w)$. Another way which uses only one encoding apparatus, is to replace the spherical lenses by cylindrical lenses and to use a two-dimensional mask, where one dimension is still used for the frequency while the other is used to place the two complementary amplitude patterns. Of course, in a CDMA application, it is necessary that each user could communicate with any other user. Although the two masks at the receiver can usually be fixed, the mask at the transmitter needs to be

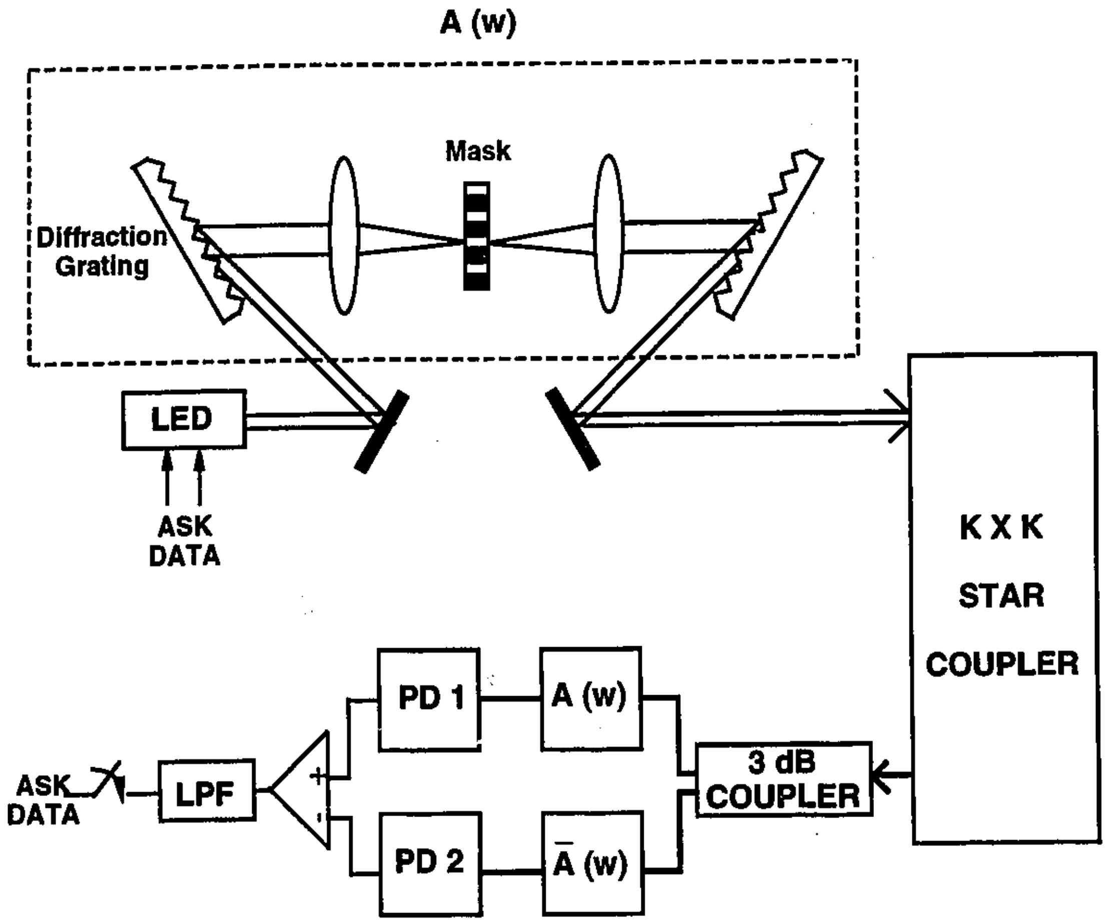

Fig.7.7: Diagram of a noncoherent FE-CDMA system.

programmable. This can be done, as already experimentally demonstrated, using Spatial-Light-Modulators based on liquid-crystal technology [52].

Note that, the desired signal is received only by photodetector 1, so that a 3dB loss due to the coupler is inherent to the detector when using m-sequences. One way to efficiently use the balanced receiver for the transmitted data would be to use orthogonal signalling. When transmiting a "0", the spectrum is encoded by $A(w)$, while to transmit a "1", the spectrum is encoded by $\bar{A}(w)$. However, as we will discuss later, this would require at the transmitter, programmable masks with a response time shorter than a bit period. For R_b in the Mbit/s range, this is still a challenging task with current technology.

Looking at the architecture of the proposed system, we see that it requires only low-cost broadband incoherent sources (compared to mode-locked sources) and simple direct detection receivers (no optical threshold element is needed). Furthermore, the spreading gain is independent of the bit rate since the coding in the frequency domain will not affect significantly the signal in the time domain. This is a major advantage for a network that supports different kinds of services with different bit rates. The bandwidth of the receiver and the associated electronics need only to match the bandwidth of the information signal, and not the chip rate, as in the previous chapters.

7.8 Practical Considerations

a) Spectral Shape of the Optical Sources

In the above discussion, it was implicitly assumed that all the 1's in the sequence will appear as 1's at the photodetector. However, the spectrum of an LED is not flat, but might exhibit for example a Gaussian shape, meaning that some 1's will be seen as different values depending on the position they take along the spectrum. The consequence of this will be a loss of perfect orthogonality between the users. There are basically three ways to counter this effect. The first is to use programmable

Spatial Light Modulators (SLM), such as liquid crystal devices, in order to obtain nonbinary amplitude transmissions. Alternatively, one can assign different lengths of frequency bands depending on the chips positions in the codes, so that the power transmitted in each band will be the same. This, however increases the complexity of mask fabrication. A second method is to equalize the LED spectrum, up to some degree, by using Acousto-Optical Tunable Filters, in the same way they have been used in optical systems with optical amplifiers [68]. Finally one can simply reduce the length of the total frequency band that is encoded to be in the center of spectrum, which is flatter. In this thesis, we concentrate on this solution. To see the effect of the spectral shape of the source, we have calculated the Signal-to-Interference Ratio (SIR) for different possibilities. We assume the code used is an M-sequence of length N=127, a different cycle-shift of the same sequence being attributed to each subscriber. The SIR can be written as:

$$SIR = \frac{\left(\sum_{i=0}^{N-1} x_i\, z_i\right)^2}{\sum_{k=1}^{K}\left(\sum_{i=0}^{N-1} x_i x_{i+k}\, z_i - \sum_{i=0}^{N-1}(1-x_i)x_{i+k}\, z_i\right)^2} \tag{7.24}$$

where z_i depends on the spectral shape of the source. We consider three cases:

1) Gaussian shape

$$z_i = \frac{1}{\left(2\pi\sigma^2\right)^{1/2}} \int_{(-B/2\alpha+iB/N\alpha)}^{(-B/2\alpha+(i+1)B/N\alpha)} e^{-f^2/2\sigma^2}\, df \tag{7.25}$$

where B is the 3 dB bandwidth of the source ($B = 2.354\sigma$), α is a design parameter related to the bandwidth encoded and $\alpha = 1$ when we encode the 3 dB band of the source. As α is increased, the encoded bandwidth is reduced and the code looks more binary at the receiver.

2) Cosinusoidal shape

$$z_i = \int_{-B/2}^{B/2} X + \frac{X}{Am}\mathrm{Cos}\left(\frac{2\pi T f}{B}\right) df \tag{7.26}$$

where X is the mean spectral height. This shape is chosen to see the effect of ripples of different amplitudes Am and different period T, on the SIR. It might correspond also to an unperfectly equalized spectrum.

3) Sinusoidal shape

$$z_i = \int_{-B/2}^{B/2} X + \frac{X}{Am} \mathrm{Sin}\left(\frac{2\pi T f}{B}\right) df \tag{7.27}$$

In this case, the spectrum is assymetric around the carrier frequency, and as it will be seen, the SIR is different from the cosinusoidal shape.

The results are shown on Fig. 7.8 and Fig. 7.9. On Fig. 7.8, the SIR (in dB) is plotted as a function of the number of active users for the three spectral shapes considered. Remember that for a perfectly flat spectrum the SIR would be infinite. The first observation is that the cosinusoidal and Gaussian spectra lead to approximately to the same SIR, although they are very different shapes. The sinusoidal shape leads to a worse performance which might be an indication that an asymmetry around the carrrier frequency is detrimental. As the period T of the cosinusoidal or sinusoidal shapes is changed from $T = 1$ to $T = 9$, the effect on the SIR is minor. However, as the amplitudes of the ripples is reduced, the SIR increases by more than 5 dB, for 40 users and a cosinusoidal shape. Note that, the value $Am = 2$ corresponds to a very badly equalized spectrum since the amplitudes of the ripples is the same as the mean value X. On Fig. 7.9, the SIR is plotted as a function of α, for 20, 60 and 100 interfering users, and for a Gaussian spectrum. As expected, increasing α leads to a higher SIR since the spectrum looks more flat. However, the power received would be smaller, since the encoded spectrum is reduced. This effect is not seen here, but will be observed in the next section when calculating the probability of bit error.

b) Programmable Amplitude Masks

In a CDMA network, it will usually be required that each user should be able to communicate with all other subscribers. In the context of an FE-CDMA system

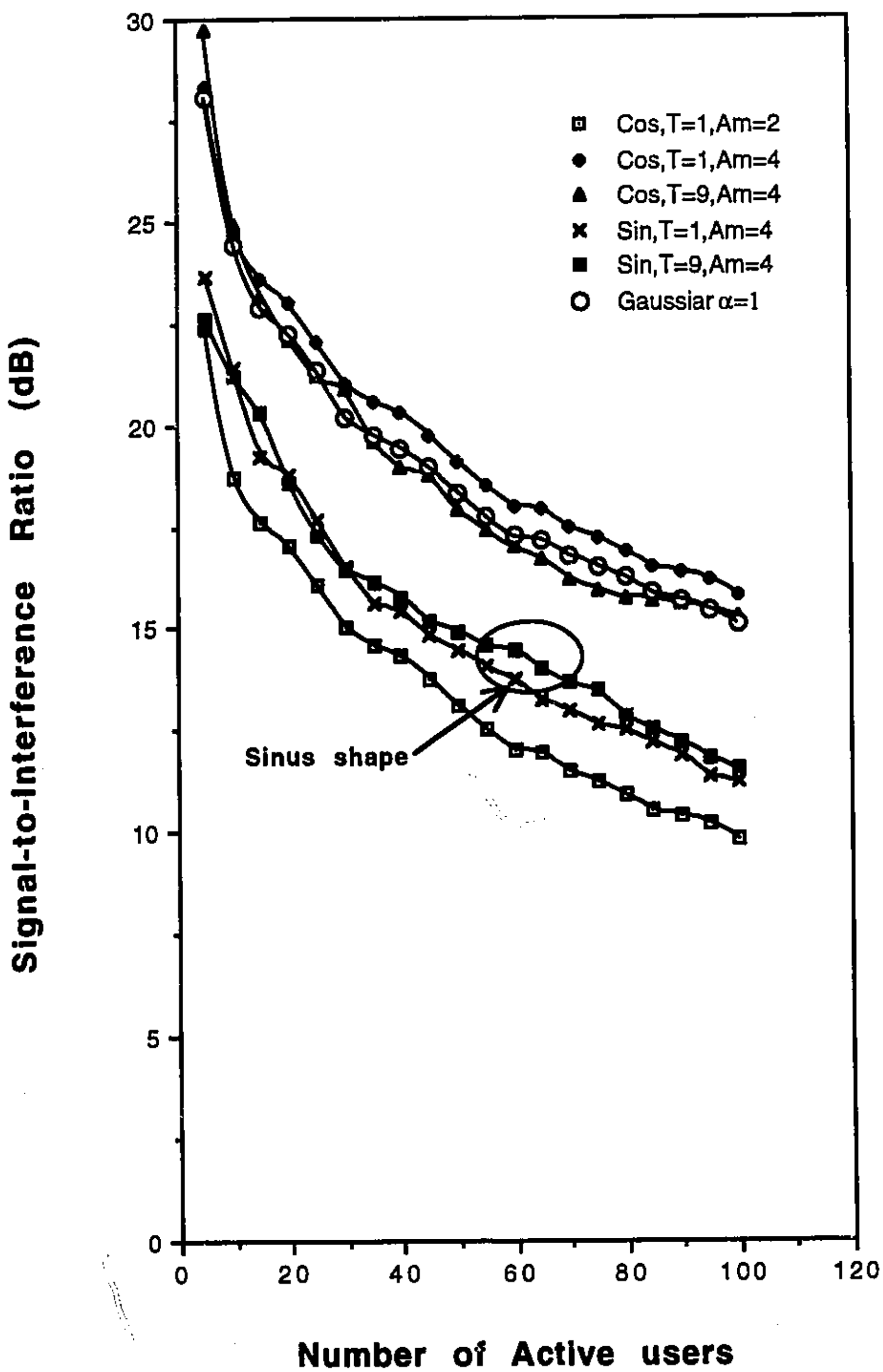

Fig.7.8: SIR vs number of active users, for different spectral shapes.

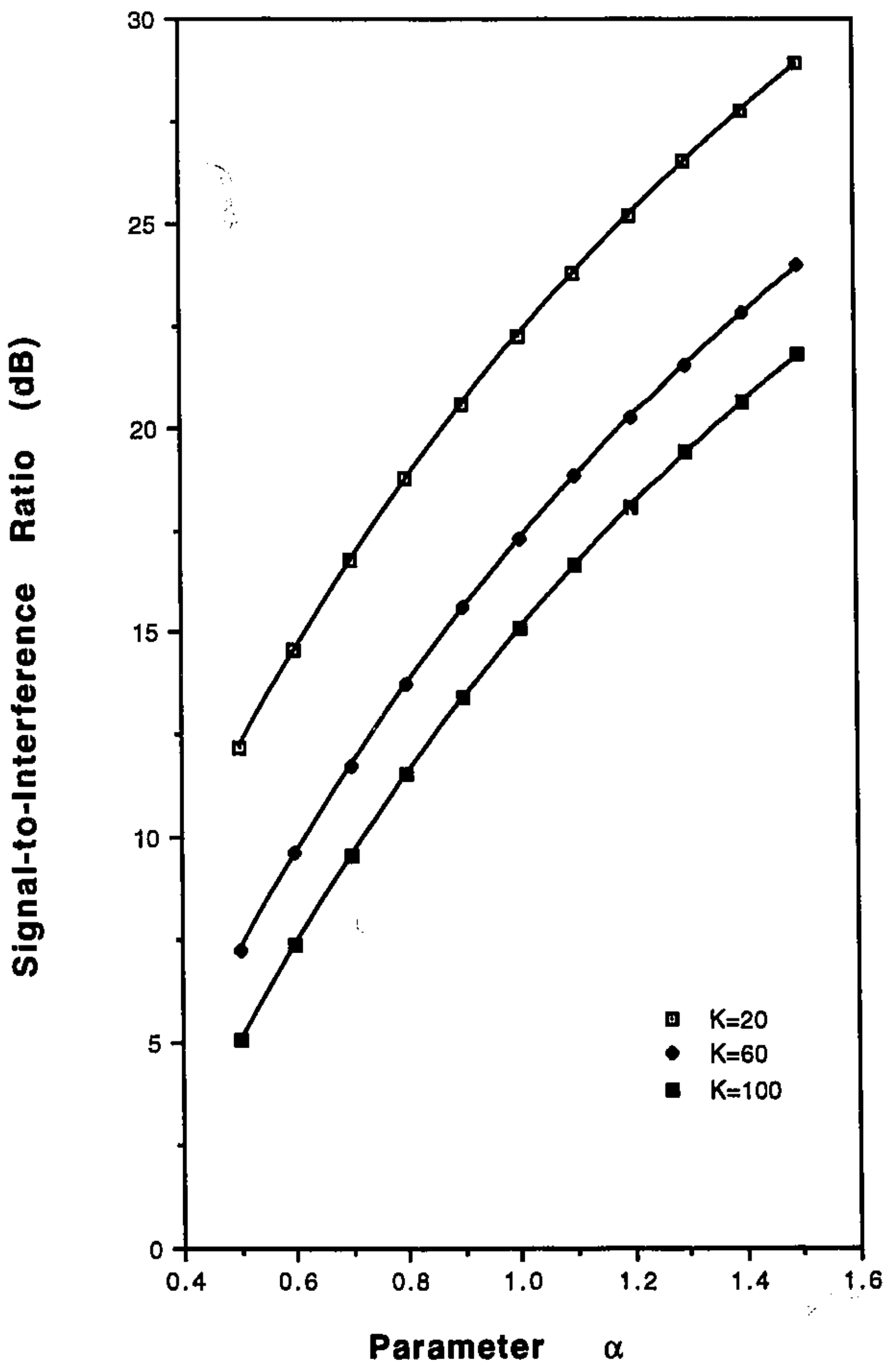

Fig.7.9: Effect of the encoded bandwidth on the SIR for a Gaussian spectral shape.

this imposes that the mask used to code the spectrum of the source at the transmitter should be programmable. Alternatively, the masks at the receiver could be made programmable. However, it is more convenient to make the mask at the transmitter programmable since there is only one mask, compared to two at the receiver. Programmable Spatial Light Modulators (SLM), electrically addressed or optically addressed, are useful in many applications in optics so that they have been available for a long time. Probably the type of electrically addressed SLM most commonly used is the Liquid Crystal Television (LCTV) panel, as it offers simplicity and low-cost. However, recent applications such as pulse shaping, dynamic space-variant optical interconnects [69], and spatial optical switches [70] require lower losses and higher speed, so they lead to the development of specially designed liquid crystal modulator array. One can find a summary of the state-of-the-art for smart-pixels, SLM based on liquid crystal technology in [71].

In our application, as well as in the case of coherent FE-CDMA, the main SLM parameters of interest are its speed and its optical contrast ratio, defined as the ratio of output optical power for a pixel being in the ON state to that of a pixel in the OFF state. For presently commmercially available devices, this ratio is usually larger than 10. Qualitatively, a finite contrast ratio will reduce the desired signal power at the receiver since the power of the OFF pixels at the transmitter will flow through the lower branch of the receiver. In the upper branch nothing is changed, since the masks used at the receiver are fixed plates (transparencies or others), having an infinite contrast ratio.

For an interfering signal, the effect will be minimal if approximately half of the power in the OFF pixels of the interfering code goes through the upper branch, and half goes through the lower branch. This will be indeed the case when using Hadamard codes, but not quite so when using M-sequences (the number of 0's is odd in this case). If the spectrum was flat, it is easy to see then that a finite contrast ratio would have little effect on the multiple-access capacity of the system. In the next section, we will show the quantitative effects when one is using an M-sequence of periode $N = 127$, and for a low contrast ratio value of 10.

The other major concern is the switching time required for a pixel to go from one state to another. One interesting application of the FE-CDMA system designed is its use as the routing technique for ultrafast Asynchronous Transfer Mode (ATM) switches. We will discuss this application in Section 7.10. For an ATM switch, a packet has a fixed length of 53 bytes and is called a cell. Assuming a bit rate of $500 Mbit/s$, a cell is transmitted in $0.85 \mu s$, so that the time to program a new address on the SLM should be a fraction of that value. For present SLMs, this is still challenging, although rapid progress is being made [72-73]. However, one should remember that SLMs are two-dimensional devices, having usually between 200 and 300 rows, most of them being independently programmable. Encoding the spectrum requires only one row. A possible solution to the speed limit, for a switch application, could be to program the other unused rows in advance, by reading the address of the waiting packets in the queue. An LED array whose elements are associated with different rows of the SLM could be used, as done in the context of a free-space optical interconnect.

7.9 Performance Calculation

In this section, we will calculate the probability of bit error taking into account the MAI, the shot noise and the thermal noise. We will present the results in a format different from the one used in the other chapters. Since for EE-LEDs or SLDs the transmitted power can be limited, we will not only plot the BER floors that would be observed. We will rather seek the number of photons/bit required for a given P_e, as a function of the number of active users.

As in Chapter 6, the entire system is linear in power, and the MGF can be easily found. We will therefore use the saddlepoint approximation to calculate the probability of error. However, as it will be shown, the Gaussian approximation gives results almost identical (it gives a tight upper bound) to those observed by using the saddlepoint technique. The Gaussian approximation is used for most of the results presented. The results will be presented assuming the spectral shape is Gaussian. Following chapter 6, the MGF of the decision variable z is simply:

$$M_z(s) = \prod_k M^k(s) e^{\lambda^0 (e^s - 1)} e^{\sigma^2 s^2/2} \tag{7.28}$$

For our calculations, we choose $T^o = 293$, $R = 1000$ and $1/T = 500 Mbit/s$. The M.G.F. for one interfering signal is easily expressed as:

$$M^k(s) = \sum_{I_{-1}^k, I_0^k} \frac{1}{T} \int_0^T e^{(c1+c2\tau)(e^s-1)} e^{(c3+c4\tau)(e^{-s}-1)}\, d\tau \tag{7.29}$$

where:

$$c1 = \lambda_1^k I_0^k T$$
$$c2 = \lambda_1^k \left[I_1^k - I_0^k\right]$$
$$c3 = \lambda_2^k I_0^k T$$
$$c4 = \lambda_2^k \left[I_1^k - I_0^k\right]$$

We will consider only ASK modulation and therefore bo, $I_1^k, I_0^k \in \{0, 1\}$. The delay τ is uniform over the bit period. The factors λ_1^k and λ_2^k are the mean intensities received on the positively and negatively biased photodetectors respectively, for interfering user k. Their expressions, and the expression for λ^0 are:

$$\lambda_1^k = \frac{\eta PT}{hf} \sum_{i=0}^{N-1} x_i x_{i+k} z_i \tag{7.30}$$

$$\lambda_2^k = \frac{\eta PT}{hf} \sum_{i=0}^{N-1} (1 - x_i) x_{i+k} z_i \tag{7.31}$$

$$\lambda^0 = \frac{\eta PT}{hf} \sum_{i=0}^{N-1} x_i z_i \tag{7.32}$$

the variable z_i being defined in (7.25).

When using the Gaussian approximation, it is sufficient to find the mean and the variance of the decision variable z. They are easily found to be:

$$\eta_z = \lambda^0 bo + \frac{1}{2} \sum_{k=1}^{K} (\lambda_1^k - \lambda_2^k) \tag{7.33}$$

$$\sigma_z^2 = \lambda^0 bo + \frac{1}{2}\sum_{k=1}^{K}(\lambda_1^k + \lambda_2^k) + \frac{1}{4}\sum_{k=1}^{K}\left(\lambda_1^k - \lambda_2^k\right)^2 + \sigma_{th}^2 \qquad (7.34)$$

Note that, the second term in (7.34) comes from the fact that the shot noise processes produced by the two photodetectors are independent, while the third term would be zero in the case of perfect cancellation of the interfering signals. As it can be seen, this would occur for a flat spectral density ($z_i = cte$). The factor 1/4 in front of the third term in (7.34) is true if we assume that all users are bit synchronized, ($\tau_k = 0$) for all k. For τ_k uniform on $[0, T]$ it would be 1/6. The reason for assuming bit synchronized users is from the ATM switching application discussed in Section 7.10. In this case, the packets at the input ports will be routed to their destination output ports at the same time, so there is no random delay among them.

7.10 FE-CDMA Systems for Ultrafast ATM Switching

Before presenting the results obtained from the performance calculation, we will briefly discuss one application of our system: routing in packet switches. The Asynchronous Transfer Mode (ATM) is considered a promising technique to switch different kinds of traffic in future broadband ISDN (B-ISDN). The switch capacity needed depends strongly on the application and can range from several Gbit/s in small Local Area Networks, up to a few Tb/s in B-ISDN exchange office. As an example, if 100 000 customers are served each with a STS-3c line (155.52 Mbit/s), a capacity of 1.5 Tb/s is already needed for a ten percent traffic load [74].

Electronic ATM switches have been extensively developed, but their throughput is limited by the operation speed limit of LSIs and signal transmission bandwidth limit. It is expected that the bottleneck of large capacity switching systems made up of electronic components will arise first in the interconnection of modules or boards. Optical interconnects with self-routing capability may be an efficient solution to this problem [74]. Switch architectures that combine the strength of electronics for contention resolution and buffering, and the strength of optics for routing and signal transmission are therefore suitable. Optical routing strategies include those based on wavelength [74-75] and time [76] domain multiplexing, as well as CDMA. A new optical routing strategy can be obtained from the incoherent FE-CDMA just discussed. Our routing technique can be used in many packet switch architectures, among them are the ones described in [74] and more recently in [77]. They both take the form shown in Fig. 7.10. In [77], m is larger than n and the structure generalizes the knockout principle to a group of n outputs. Buffering is only done at the output. In [74], $n > m$ and the structure uses shared input and output buffers based on memory chips developed by Hitachi [78]. Following is a list of the involved parameters:

1) $L = nK$ input and output lines;

2) K input and output modules;

3) m optical stars, each with K input and output ports;

4) m transmitters (receivers), e.g. number of LEDs in a LED array, for each of the K input (ouput) modules;

5) R: bit rate used in the input lines;

6) R_0: bit rate for the optical signals in the optical interconnect ($R \times n = R_0 \times m$);

For $n > m$, a Contention Resolution Device (CRD) is needed to resolve output contention. Its role is, for each of the m optical stars, to choose one cell for each output module. Detailed description of the CRD can be found in [74]. When the CRD is m times faster than the cell transmission time through one star, the m optical stars are busy at all times. Only up to m cells can be routed to the same output module in one cell transmission time and therefore there is a Head of Line Blocking (HOL) probability. This probability can be reduced by increasing m. However, for K fixed, m is limited by the speed limit of the CRD. On the other hand, K is limited by the power division occuring at the star couplers. The number

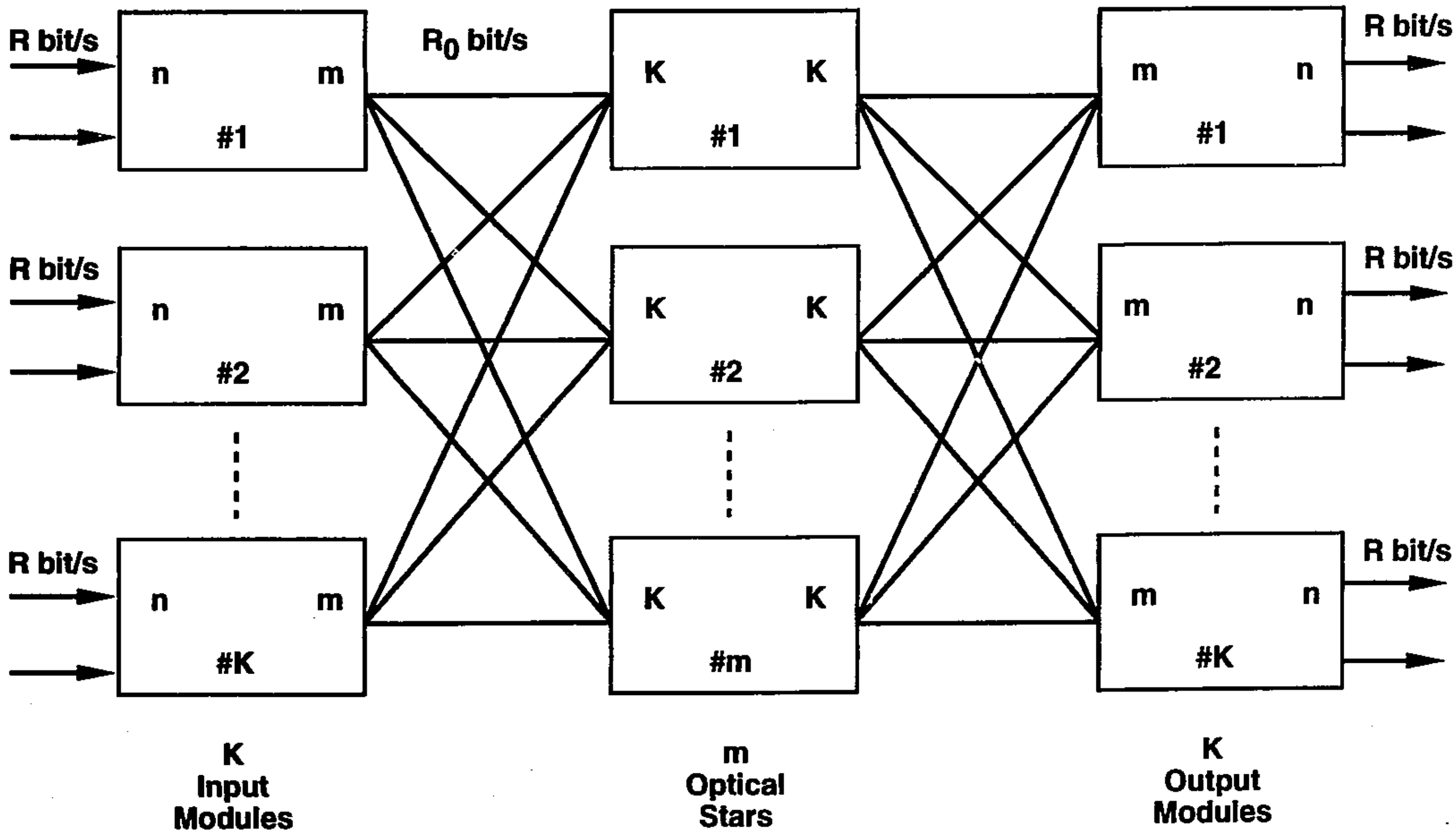

Fig.7.10: A Growable ATM Switch Architecture.

of photons/bit (Ph) available at a receiver is given by:

$$Ph = \frac{10^{(Ps - 10log\,K - 6)/10}}{R_0 h f} \tag{7.35}$$

where Ps is the source power in dB, $10\log K$ is the splitting loss due to the star coupler, a total of $6\,dB$ group other losses and R_0 is the bit rate. This will be plotted on the figures of the P_e shown in the next section, for Ps values of $0\,dBm$, $-2\,dBm$ and $-5\,dBm$. The crossing points of Ph with the Pe curves determine the maximum value of K that can be used.

7.11 Results and Discussion

The results obtained are given on Fig. 7.11 to Fig. 7.16. All these results assume a Gaussian shape, with $\alpha = 1.3$. The number of photons/bit required to get $P_e = 10^{-9}, 10^{-7}$ and 10^{-5} is given, as well as the number of photons/bit available, for three power source values, from (7.35). The reasons for considering different P_e values is that $P_e = 10^{-5}$ might lead to an acceptable probability of *packet* error. Unless stated otherwise, the results are calculated using the Gaussian approximation for the decision variable. The first thing to note is the number of interfering users (K), more than one hundred, that can be accommodated for $P_e = 10^{-9}$. This is much better than any architecture considered in the previous chapters. Note in Fig. 7.11 that, with up to 70 interfering users, the power penalty is less than 3 dB. However, if the incoherent optical source can launch less than $-2dBm$, the multiple-access capacity will be limited to around 40. This is for a reasonable code length of 127, for which a high-speed programmable SLM is already developed for pulse shaping. On Fig. 7.12, Hadamard codes are considered instead of M-sequences. As seen, a better performance is obtained. Less than 3 dB penalty is observed for up to 100 users. The improved performance can probably be explained by the fact that for a Hadamard code, the distribution of the 1's and 0's across the spectrum is more uniform than for an M-sequence of length $N = 2^r - 1$, which always contains a run of r 1's and $r-1$ 0's. On Fig. 7.13, we show the effect of increasing the code length N to 511. A code length N=127 is sufficient to accommodate 127 subscribers. However, by increasing the code length, the spectral length associated to each chip is smaller, and the power associated to each of them is therefore more uniform. As seen, the performance is better than with N=127, but the requirement on the resolution of the spectral filtering is much higher. Tolerance to misalignments would also be greatly reduced.

In Fig. 7.14, we show the effect of having a finite contrast ratio (labeled SLM), taken to be 10. As seen, 70000 photons/bit are needed for K=100, and $P_e = 10^{-9}$, compared to 54000 photons/bit needed when the contrast ratio is infinite. For the other values of P_e there is little difference between a finite value, and an infinte value of the contrast ratio. We, therefore, believe that a finite contrast ratio from a programmable SLM would not be too detrimental to our system. In Fig. 7.15, we compare the P_e obtained when using the saddlepoint approximation or the Gaussian approximation. As seen, the Gaussian approximation is very close to the "exact" values (curve labeled E). It gives a tight upper bound. We also give the performance obtained when using an APD with gain $G = 10$ and ionization coefficient $k = 0.1$. In this case the expressions for the mean and variance need to be modified as:

$$\eta_z = G\left[\lambda^0 bo + \frac{1}{2}\sum_{k=1}^{K}(\lambda_1^k - \lambda_2^k)\right] \tag{7.36}$$

$$\sigma_z^2 = G^3(1-a^2b)\left[\lambda^0 bo + \frac{1}{2}\sum_{k=1}^{K}(\lambda_1^k + \lambda_2^k)\right] + G^2\left[\frac{1}{4}\sum_{k=1}^{K}\left(\lambda_1^k - \lambda_2^k\right)^2\right] + \sigma_{th}^2 \tag{7.37}$$

An APD with the parameters considered would perform better only when the thermal noise dominates, which seems true for $K \leq 40$. When there are more interfering users, the shot noise dominates and a PIN is the right choice. It is interesting to see that the Gaussian approximation and the saddlepoint approximation give identical results in the range where thermal noise dominates, since it is Gaussian. Finally, in Fig. 7.16 we plot the P_e as a function of the number of photons/bit for different values of the parameter α, and for $K = 40$ interfering users. It was seen in Fig. 7.9 that reducing the encoded bandwidth (increasing α), will result in a higher SIR. One can see that taking into account the shot noise and the thermal noise, the highest α is not the best choice, since reducing the encoded bandwidth will reduce the received signal power and therefore, the Signal to Noise Ratio (SNR). Note that, for $\alpha = 0.8$, a floor is observed. In that case, the encoded bandwidth is too large and the spectrum is not *flat* enough. The multiple-access-interference dominates and the P_e can not be reduced by increasing the power.

Let us now estimate a possible achievable throughput for an ATM switch based on our encoding technique. Suppose $R_0 = 500 Mbit/s$, as achievable by EE-LEDs, M-sequences and $N = 511$ (Fig. 7.13). The cell transmission time is then $0.848\mu s$ ($53bytes \times 8 \,/\, R_0$). An arbitration cycle must therefore be over $0.848\mu s/m$, and a device that can achieve that in less than $22ns$ is described in [74]. Taking a conservative value of $22ns$ we therefore get $m \leq 42$. The total throughput T_R of the switch is given by :

$$T_R = R_0 \times K \times m \tag{7.38}$$

Assuming $Pe = 10^{-9}$ is needed and a value of $Ps = -2\,dBm$, K is limited to 72, from Fig. 7.13, and the achievable throughput is $T_R = 500Mbit/s \times 42 \times 72 = 1.5\,Tb/s$. To reduce the number of transmitters and receivers needed per module, we might choose $m = 10$ and the throughput decreases to $T_R = 360\,Gbit/s$. For $m = 20$, and assuming a $Pe = 10^{-7}$ is sufficient, one can achieve $T_R = 840\,Gbit/s$.

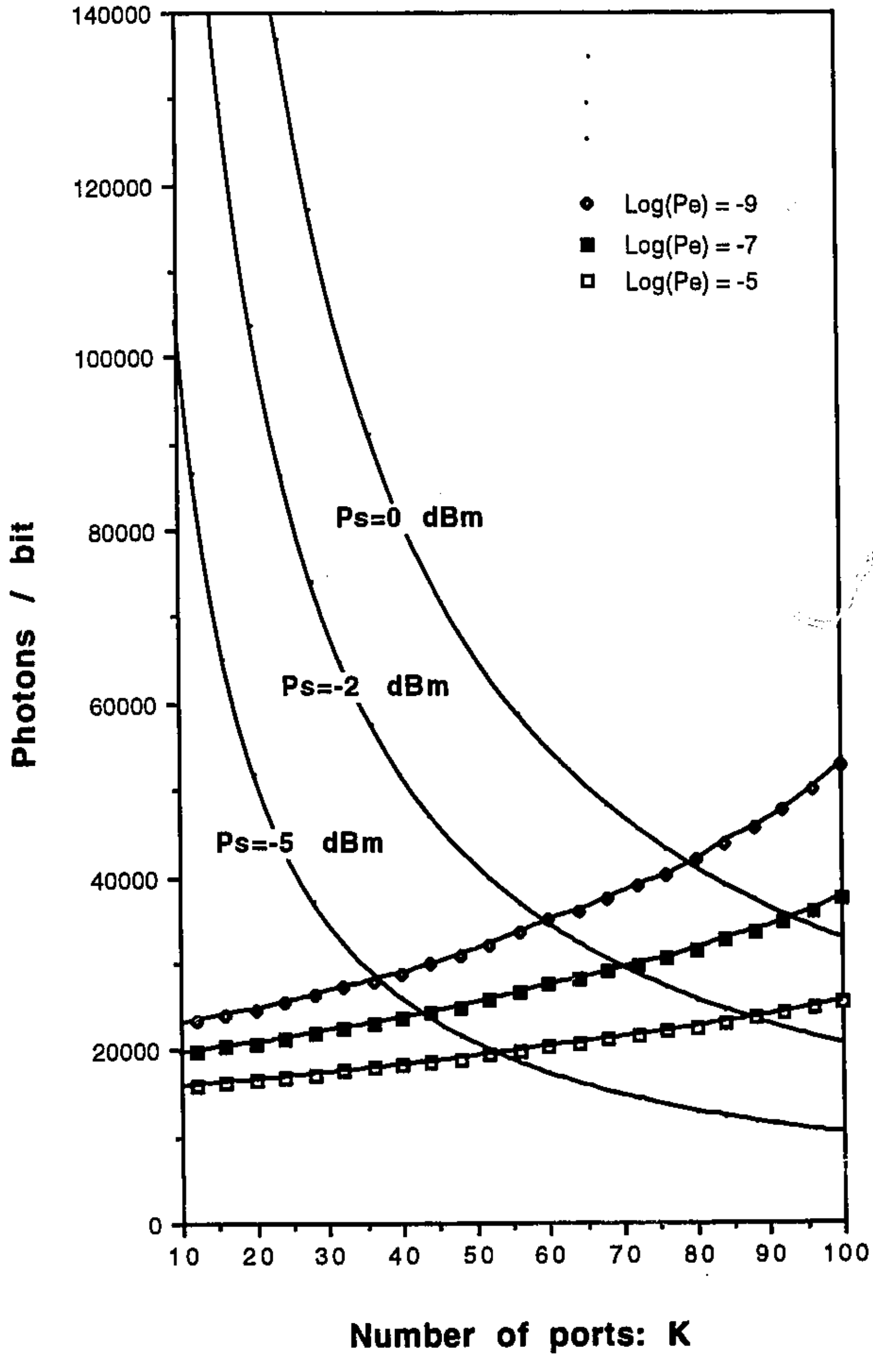

Fig.7.11: Number of photons/bit needed for a fixed Pe, N=127, M-sequences, PIN photodetectors.

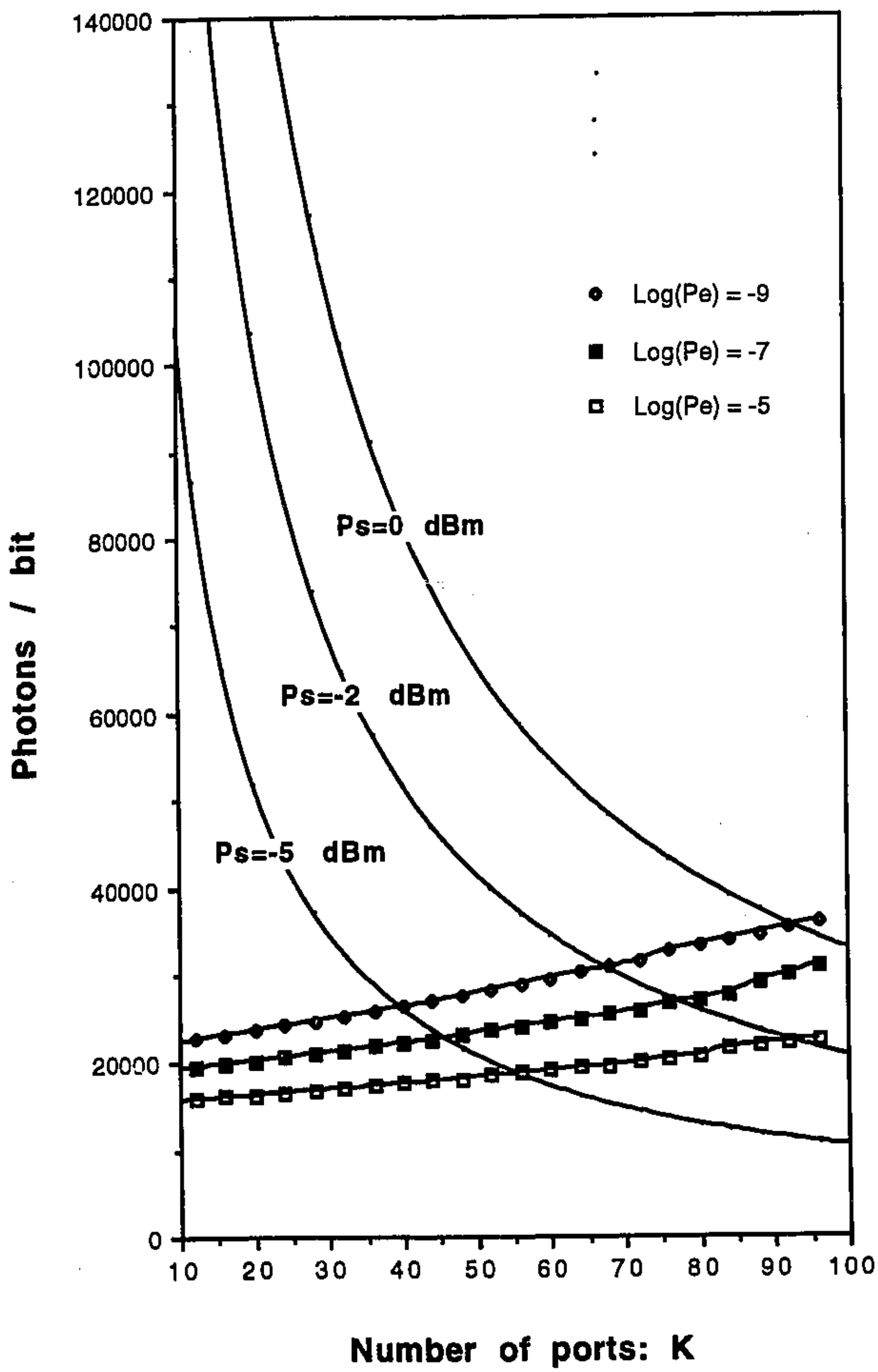

Fig.7.12: Number of photons/bit needed for a fixed Pe, N=128, Hadamard codes, PIN photodetectors.

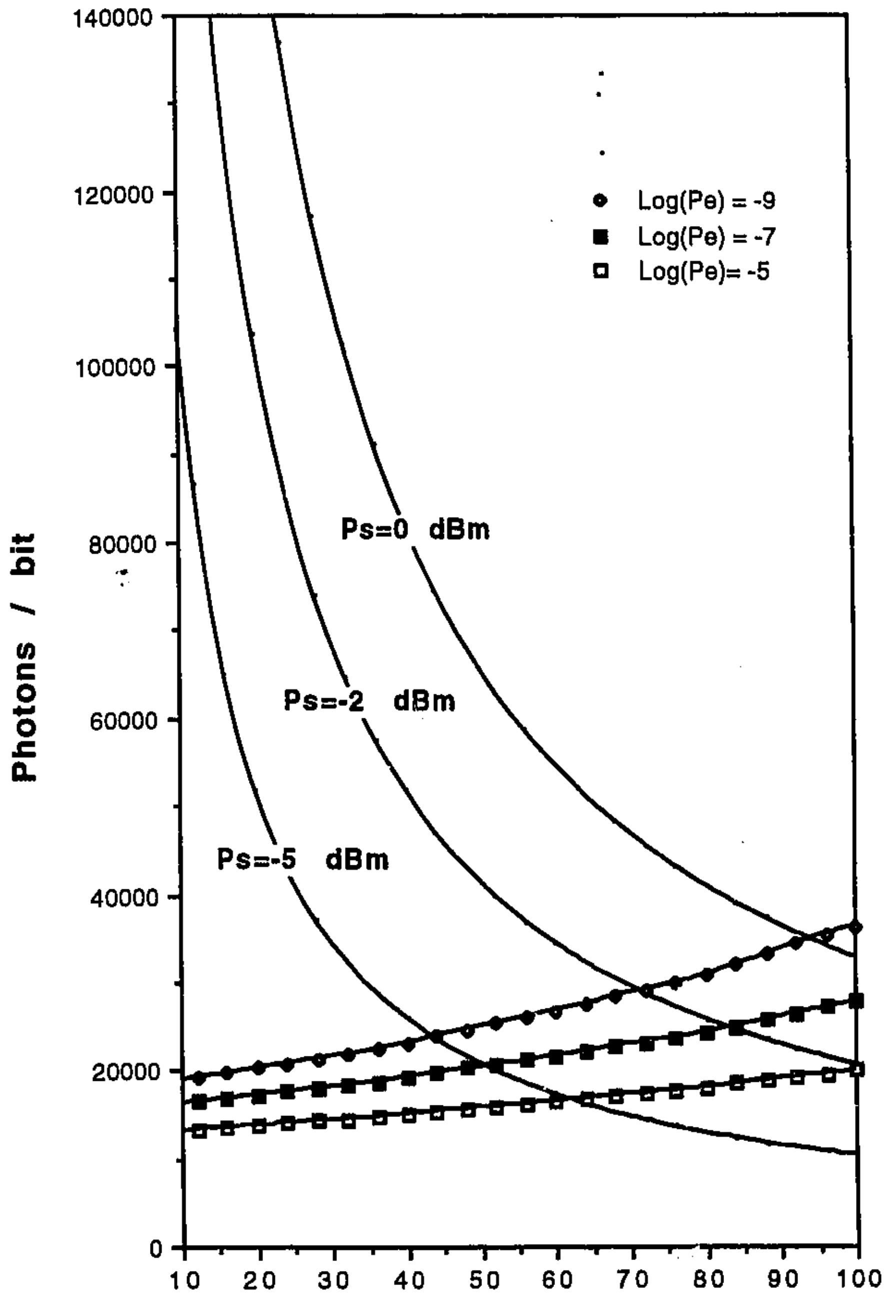

Fig.7.13: Number of photons/bit needed for a fixed Pe, N=511, M-sequences, PIN photodetectors.

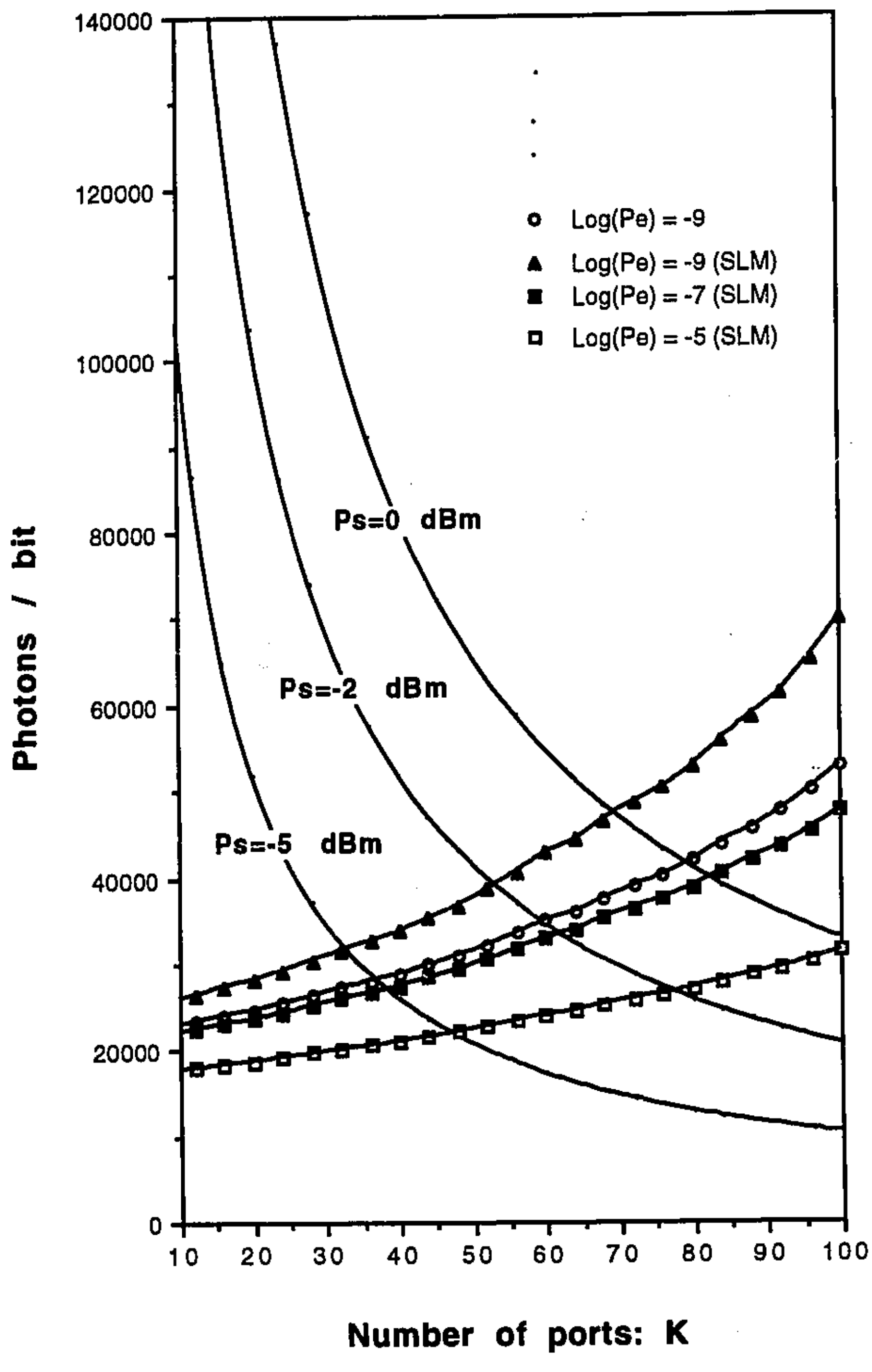

Fig.7.14: Number of photons/bit needed for a fixed Pe, N=127, M-sequences, contrast ratio=10 dB.

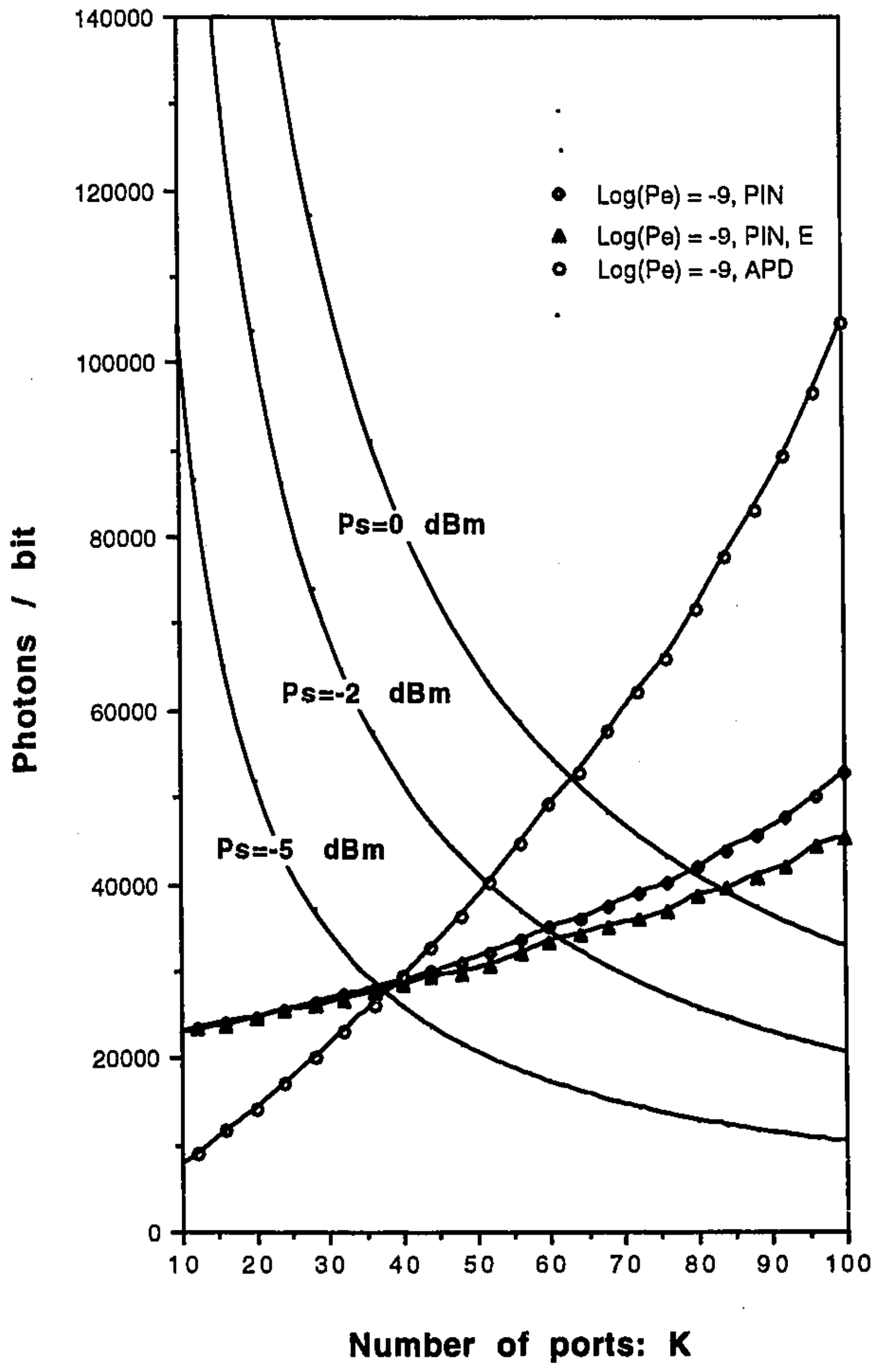

Fig.7.15: Number of photons/bit needed for Log(Pe) = -9, N=127, M-sequences.

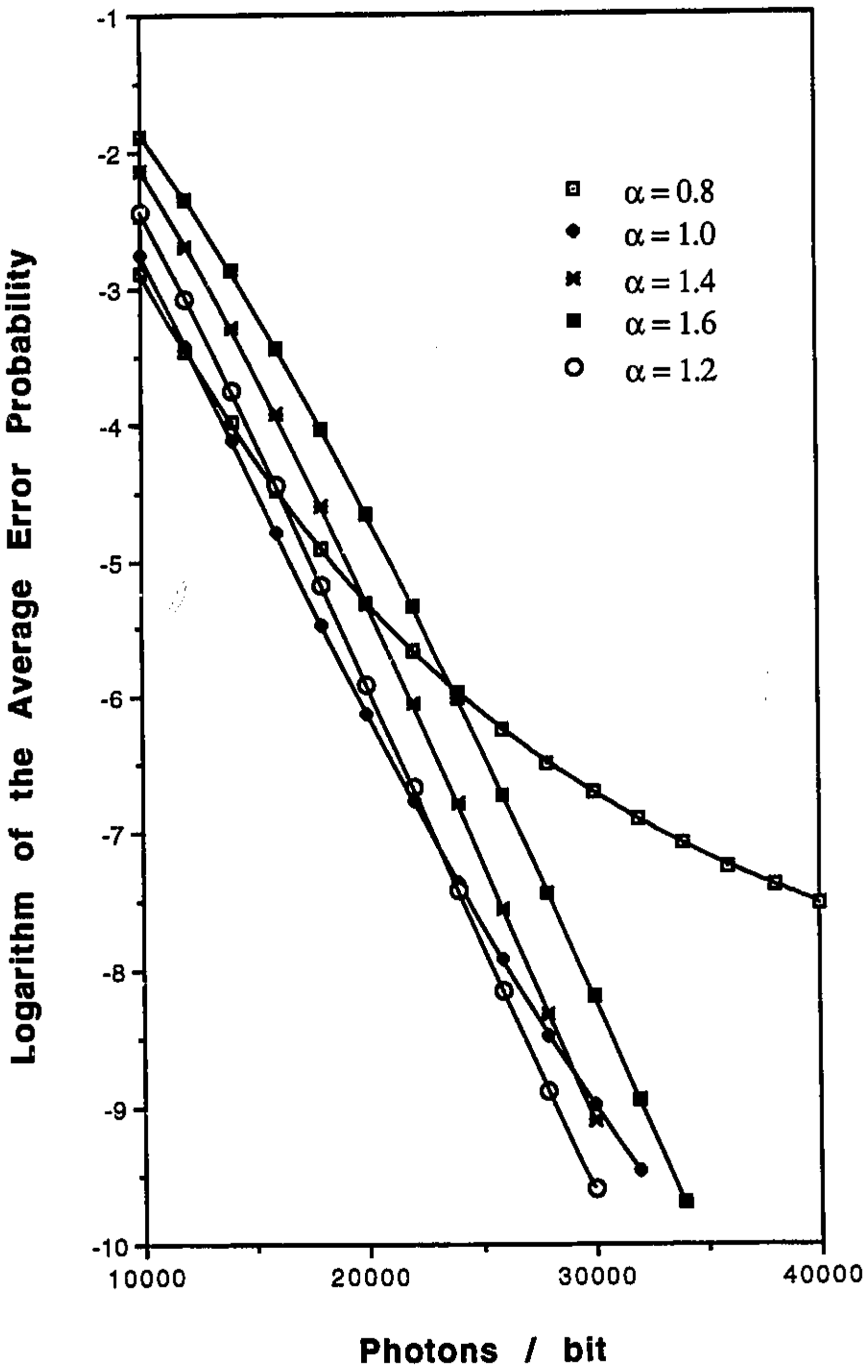

Fig.7.16: Performance as the encoded bandwidth is varied; N=127, M-sequences, K=40.

7.12 Conclusion

In this chapter we have presented a new type of CDMA system based on frequency encoding of optical broadband sources. We first briefly reviewed the system proposed by Salehi and Wiener, and qualitatively discussed the effects of chromatic dispersion on the multiple-access capacity. We then presented in detail a new design based on noncoherent sources. The system proposed has the advantage of using inexpensive optical sources, and simple direct detection receivers with bandwidth requirements equal to the bit rate. The spreadig gain is independent of the bit rate since the spectral shaping of the sources does not affect the signals in time domain. It was shown that a large number (from 70 to 100) interfering users can be supported, for a moderate code length of $N = 127$, and with $P_e = 10^{-9}$. The application of our system as the routing technique for ATM switches was also briefly discussed.

Chapter 8

Summary and Suggestions for Future Work

Two main multiplexing techniques were studied in this thesis. In the first one, the coding is done in the time domain, while for the other one the coding is done in the frequency domain. Generally speaking, the work done in this thesis had, as an objective, to find efficient architectures for using code-division multiplexing in optical systems, and to accurately evaluate the performance obtained, while limiting ourselves to direct-detection receiver. The probability of bit error as a function of the number of active users was the main criterion used to evaluate the performance.

In Chapter 2, we gave a brief overview of the different CDMA systems presented so far in the literature. The systems are categorized in terms of the types of sources they require (coherent or incoherent), on the codes used, on the architectures used for the encoders/decoders, on the correlation principle (field or power addition), and finally on the types of receiver, direct detection or coherent detection. In Chapter 3, we reviewed the properties of some well-known codes, such as M-sequences and Gold codes, and discussed a construction method for perfect ternary sequences. A simple way to encode bipolar codes into unipolar ones was presented.

In Chapter 4, we presented new and efficient architectures that combine electro-optic elements and pure optical processing elements, for both coherent and incoherent optical sources. We also proposed the use of Kronecker sequences in order to obtain very simple encoder/decoder structures where programmability of the delay lines is no longer required.

In Chapter 5, a new analytical technique was developed to accurately evaluate the probability of error for CDMA systems with coherent optical sources and direct detection. Three modulation schemes, ASK, CPFSK and LD-FSK, were studied. The chip-synchronous and chip-asynchronous assumptions were both studied. Performance comparison between ordinary sequences and Kronecker sequences was done, for different choices of the inner sequences. Partial cross-correlation effects, due to an optical filter with a non ideal bandwidth were studied by means of an upper bound on the error probability. In the future, it would be interesting to develop more accurate means to evaluate the effect of an optical filter with a non ideal bandwidth, as well as the effect of frequency drifts of the optical sources. Studying the case of ASK with a finite extinction ratio is also of interest, since it might affect its apparent performance superiority compared to CPFSK.

In Chapter 6, the performance evaluation of incoherent systems using a 2-PPM encoding of bipolar sequences was provided. A simple saddlepoint approximation technique was used to calculate the probability of bit error. The major sources of interference were considered, e.g. the dominating Multiple-Access-Interference (MAI), the shot noise and the thermal noise. Detailed results as a function of the number of active users were given, for many different cases. It was shown that orthogonal coding is much more suitable than ASK. The use of Kronecker sequences seems suitable since they allow a major performance improvement, in terms of number of users the system can support, by adding a few non-programmable delay lines. For incoherent systems to behave as expected, the coherence time of the sources much be smaller than any delay in the encoder/decoder. It would be interesting to study quantitatively how sensitive is the performance of theses systems, when there is a deviation from this requirement, as it would likely occur for very short optical pulses. The effects of fiber dispersion on the correlation properties is also of interest.

In Chapter 7, we studied optical CDMA systems in which the coding is done in the frequency domain. We first reviewed a system based on coherent sources. We then proposed a new type of frequency-encoded system based on simple incoherent sources. A description of the encoder/decoder required was given. Suitable codes were given, and a detailed performance analysis was done. We showed that our system allows more than 100 simultaneous active users, each transmitting with a probability of error less than 10^{-9}. We further showed that our design has a spreading gain independent of the bit rate, and therefore allows multiple types of services to be used on the same network without any performance degradation. Practical considerations were discussed in detail and their effects were quantitatively evaluated. Its application as the routing technique for ATM switches using optical interconnects was also considered. Proving the feasibility of this system experimentally is an interesting challenge. Starting from this design, many research directions can be explored, among them, finding a more practical encoding structure which is based on waveguides, and therefore less unstable mechanically. The effects of fiber dispersion should also be considered if one is to use this technique for other than local area networks. We believe that using orthogonal dimensions for optical CDMA systems is probably the most efficient approach, since the information rate is not penalized by the coding. We have considered the frequency and time dimensions. Another possibility would be to consider the time/space approach, either for unguided systems, or for systems using fibers on short distances [79].

REFERENCES

[1] S.D.Personick, "Towards Global Information Networking," *IEEE Proc.*, Vol.81, pp.1549-1557, Nov. 1993.

[2] D.Zaccarin and M.Kavehrad, "New Architectures and Coding Strategies for Unipolar Codes to Achieve Bipolar Capacity," *OFC'94 Technical Digest*, paper WN1, 1994. Feb. 1994.

[3] D.Zaccarin and M.Kavehrad, "New Architectures for Incoherent Optical CDMA to Achieve Bipolar Capacity," *Electron. Lett.*, Vol.3, pp.258-259, Feb. 1994.

[4] D.Zaccarin and M.Kavehrad, "Performance Evaluation of Optical CDMA Systems using Bipolar Codes and Non-coherent Detection," *IEEE/OSA J.Lightwave Technol.*, Vol.12, pp.96-105, Jan. 1994.

[5] J.A.Salehi, A.M.Weiner and J.P.Heritage, "Coherent Ultrashort Light Pulse Code-Division Multiple Access Communication Systems," *IEEE/OSA J.Lightwave Tech.*, Vol.8, pp.478-491, March 1990.

[6] D.Zaccarin and M.Kavehrad, "An Optical CDMA System based on Spectral Encoding of LED," *IEEE Photonics Technol. Lett.*, Vol.4, pp.479-482, April 1993.

[7] D.Zaccarin and M.Kavehrad, "Ultrafast ATM Switching using Optical CDMA based on Spectral Encoding of LED," *ICC 1994 Proc.*, pp.1369-1373, 1994.

[8] J.A.Salehi and C.A.Brackett, "Code division multiple-user techniques in optical fiber networks-Part I:Fundamental Principles," *IEEE Trans. Commun.*, Vol.37, pp.824-833, Aug. 1989.

[9] J.A.Salehi and C.A.Brackett, "Code division multiple-user techniques in optical fiber networks-Part II:Systems Performance Analysis," *IEEE Trans. Commun.*, Vol.37, pp.834-842, Aug. 1989.

[10] P.R.Prucnal, M.R.Santoro and T.R.Fan, "Spread-Spectrum Fiber-Optic Local Area Network Using Optical Processing," *IEEE/OSA J.Lightwave Tech.*, Vol.4, pp.547-554, May 1986.

[11] F.R.Chung and J.A.Salehi, "Optical Orthogonal Codes: Design, Analysis, and Applications," *IEEE Trans. on Inform. Theory*, Vol.35, pp.595-604, May 1989.

[12] S.V.Maric et al., "A New Family of Optical Code Sequences for Use in Spread-Spectrum Fiber-Optic Local Area Networks," *IEEE Trans. Commun.*, Vol.41, pp.1217-1221, Aug. 1993.

[13] Z.Kostic, E.L.Titlebaum and S.V.Maric, "The Design of New Optical Codes and Time-Hopping Patterns for Synchronous Spread-Spectrum Code-Division Multiple-Access Communication Systems," *ICC 1991 Proc.*, pp.20.2.1-20.2.5, 1991.

[14] K.C.M. Varnum and R.C.Robertson, "'Error Probabilities of Coherent Optical Heterodyne FSK-CDMA Signals in a Noncoherent Detection System Degraded

by Laser Phase Noise," *Journal of Optical Commun.*, Vol.13, pp.85-92, 1992.

[15] S.Benedetto and G.Olmo,"Performance Evaluation of Coherent Optical Code Division Multiple Access," *Electron. Lett.*, Vol.27, pp.2000-2002, Oct.1991.

[16] D.D.Sampson and D.A.Jackson,"Spread-Spectrum Optical Fiber Network Based on Pulsed Coherent Correlation," *Electron. Lett.*, Vol.26, pp.1550-1552, Sept. 1990.

[17] M.E.Marhic and Y.L.Chang,"Pulse coding and coherent decoding in fiber-optic ladder networks," *Electron. Lett.*, Vol25, pp.1535-1536, Oct. 1989.

[18] R.A.Griffin, D.D.Sampson and D.A.Jackson,"Demonstration of Data Transmission Using Coherent Correlation to Reconstruct a Coded Pulse Sequence," *IEEE Photonics Technol. Lett.*, Vol.4, pp.513-515, May 1992.

[19] A.Homes and R.Syms,"All-optical CDMA Using quasi-prime codes," *IEEE/OSA J.Lightwave Tech.*, Vol.10, pp.279-286, Feb. 1992.

[20] D.J.Derickson et al.,"Short Pulse Generation using Multi-Segment Mode-Locked Semiconductor Lasers," *IEEE J. Quantum Electron.*,Vol 28, pp, Oct. 1992.

[21] A.Takada and H.Miyazawa,"30 GHz picosecond pulse generation from actively mode-locked erbium-doped fibre laser," *Electron. Lett.*, Vol.16, pp.182-183, 1990.

[22] T.Suzaki et al.,"Ten-Gbit/s transmitter module using modulator driver IC and semiconductor modulator," *OFC'92 Technical Digest*, paper TuL6, 1992.

[23] K.Runge et al.,"A 27-Gbit/s 1:2 regenerating demultiplexer, 20 Gbit/s decision circuit and an 11 Gbit/s laser driver IC fabricated using AlGaAs/GaAs HBTs," *OFC'92 Technical Digest*, paper Tul4, 1992.

[24] S.Shimada et al.,"Very-high speed optical signal processing," *IEEE Proc.*, Vol.81, pp.1633-1646, Nov. 1993.

[25] K.Uchiyama et al.,"100 Gbit/s all-optical demultiplexing using nonlinear optical loop mirror with gating-width control," *Electron. Lett.*, Vol.29, pp.1870-1871, Oct. 1993.

[26] K.Sasayama et al.,"Frequency-division-multiplexing multichannel selector using a coherent optical transversal filter," *OFC'92 Technical Digest*, paper TuC2, 1992.

[27] N. Takato et al., "Silica-based integrated optical Mach-Zehnder multiplexer, demultiplexer family with channel spacing of 0.01-250 nm," *IEEE J.S.A.C.*, Vol.8, pp.1120-1127, August 1990.

[28] D.V.Sarwate and M.B.Pursley,"Crosscorrelation Properties of Pseudorandom and Related Sequences," *IEEE Proc.*, Vol.68, pp.593-619, May 1980.

[29] W.E.Stark and D.V.Sarwate,'Kronecker Sequences for Spread-Spectrum

Communications," *IEE Proc.*, Vol.128, Pt.F, pp.104-109, April 1981.

[30] J.Wolfmann, "Almost Perfect Autocorrelation Sequences," *IEEE Trans. on Inform. Theory*, Vol.38, pp.1412-1418, July 1992.

[31] T.Hoholdt and J.Justesen, "Ternary Sequences with Perfect Periodic Autocorrelation," *IEEE Trans. on Inform. Theory*, Vol.29, pp.597-600, July 1983.

[32] D.A.Shedd and D.V.Sarwate, "Construction of Sequences with Good Correlation Properties," *IEEE Trans. on Inform. Theory*, Vol.25, pp.94-97, Jan. 1979.

[33] G.Vanucci, "Combining Frequency-Division and Code-Division Multiplexing in a High-Capacity Optical Network," *IEEE Network Mag.*, Vol.3, pp.21-30, March 1989.

[34] G.Vanucci and S.Yang, "Experimental Spreading and Despreading of the Optical Spectrum," *IEEE Trans. Commun.*, Vol.37, pp.777-780, July 1989.

[35] K.Inoue et al., "A four-channel optical waveguide multi/demultiplexer fabricated for 5 GHz spaced optical FDM transmission," *IEEE/OSA J.Lightwave Technol.*, Vol.6, pp.339-345, June 1988.

[36] P.A. Humblet, "Design of optical matched filters," *Globecom 1991 Proc.*, pp.35.1.1-35.1.5, 1991.

[37] S.Kawanishi et al. "100 Gbit/s, 50 km Optical Transmission Employing All-Optical Multi/Demultiplexing and PLL Timing Extraction," *OFC'92, Postdeadline paper PD-2*, 1992.

[38] Y.L.Chang and M.E.Marhic, "Fiber-Optic Ladder Networks for Inverse Decoding Coherent CDMA," *IEEE/OSA J.Lightwave Technol.*, Vol.10, pp.1952-1962, Dec.1992.

[39] M.Jinno, "49.6 Gb/s Electrooptic Demultiplexing Using Cascaded ON/OFF Gates," *IEEE Photonics Technol. Lett.*, Vol.4, pp.641-644, June 1992.

[40] K.Sasayama, "Coherent Optical Transversal Filter using silica-based singlemode waveguides," *Electron. Lett.*, Vol.25, pp.1508-1509, Oct. 1989.

[41] N.Takato et al., "Silica-Based Single-Mode Waveguides on Silicon and their Application to Gided-Wave Optical Interferometers," *IEEE/OSA J.Lightwave Tech.*, Vol.6, pp.1003-1010, June 1988.

[42] P.E.Green et al., "All-optical Packet Switched Metropolitan-Area Network Proposa," *IEEE/OSA J.Lightwave Tech.*, Vol.11, pp.754-763, May/June 1993.

[43] F.J.Scire, "A Probability Density Function Theorem for the Modulo y values of the Sum of Two Statistically Independent Processes," *IEEE Proc.*, Vol.56, pp.204-205, Feb.1968.

[44] A.W.Lam and A.M.Hussain, "Performance Analysis of Direct-Detection Optical CDMA Systems with Avalanche Photodiodes," *IEEE Trans. Commun.*,

Vol.40, pp.810-821, April 1992.

[45] W.R.Bennett, "Distribution of the Sum of Randomly Phased Components," *Quart.Appl.Math.*, Vol.5, pp.385-393, April 1948.

[46] G.H.Golub and J.H.Welsch, "Calculations of Gauss Quadrature Rules," *Math. Comput.*, Vol.26, pp.221-230, April 1969.

[47] S.O.Rice, "Probability Distribution for Noise Plus Several Sine waves- The Problem of Computation", *IEEE Trans. Commun.*, Vol.22, pp.851-857, June 1974.

[48] C.W.Helstrom, "Computing the performance of optical receivers with avalanche diode detectors," *IEEE Trans. Commun.*, Vol.36, pp.61-66, Jan. 1988.

[49] A.M.Wiener et al., "High-Resolution femtosecond pulse shaping," *J.Opt.Soc. Am.B*, Vol.5, pp.1563-1572, Aug. 1988.

[50] M.B.Danailov and I.P.Christov, "Time-Space shaping of light pulses by Fourier optical processing," *J.Mod.Optics*, Vol.36, pp.725-731, 1989.

[51] D.J.Hajela and J.A.Salehi, "Limits to the Encoding and Bounds on the Performance of Coherent Ultrashort Light Pulse Code-Division Multiple-Access Systems," *IEEE Trans. Commun.*, Vol.40, pp.325-336, Feb. 1992.

[52] A.M.Wiener et al., "Programmable Shaping of Femtosecond Optical Pulses by Use of 128-Element Liquid Crystal Phase Modulator," *IEEE J. Quantum Electron.*, Vol.28, pp.908-919, April 1992.

[53] D.Marcuse, "Pulse distortion in single-mode fibers," *Applied Optics*, Vol.19, pp.1653-1660, May 1980.

[54] M.Stern and J.P.Heritage, "Grating Compensation of Third-Order Fiber Dispersion," *IEEE J. Quantum Electron.*, Vol.28, pp.2742-2748, December 1992.

[55] E.B.Treacy, "Optical Pulse Compression with Diffraction Gratings," *IEEE J. Quantum Electron.*, Vol.5, pp.454-458, Sept. 1969.

[56] O.E.Martinez, "3000 Times Grating Compressor with Positive Group Velocity Dispersion: Application to Fiber Compensation in 1.3-1.6 um Region," *IEEE J. Quantum Electron.*, Vol.23, pp.59-64, Jan. 1987.

[57] A.Frenkel, J.P.Heritage and M.Stern, "Compensation of dispersion in optical fibers for the 1.3-1.6 um region with gratings and telescope," *IEEE J. Quantum Electron.*, Vol.25, pp.1981-1984, Sept.1989.

[58] X.S.Yao et al., "Limitations on Peak Pulse Power, Pulse width, and Coding Mask Misalignment in a Fiber-Optic Code-Division Multiple-Access System," *IEEE/OSA J.Lightwave Technol.*, Vol.11, pp.836-846, May/June 1993.

[59] A.M.Wiener et al., "Femtosecond Spectral Holography," *IEEE J. Quantum Electron.*, Vol.28, pp.2251-2261, Oct.1992.

[60] T.E.Chapuran, S.S.Wagner and T.P.Lee, "Wavelength-dependent power pe-

nalites in spectrally sliced WDM networks," *OFC'92 Technical Digest*, paper TuN4, 1992.

[61] G.D.Collins,"Achromatic Fourier Transform holography," *Applied Optics*, Vol.20, pp.3109-3119, Sept. 1981.

[62] P.Andrs, J.Lancis and W.D.Furlan,"White-Light Fourier Transformer with low chromatic aberration," *Applied Optics*, Vol.31, pp.4682-4687, Aug. 1992.

[63] P.Cielo and C.Delisle,"Transmission d'images par modulation du spectre," *Can.J.Phys.*, Vol.54, pp.2332-2339, 1976.

[64] A.Lacourt and P.Boni,"Transmission d'images et d'hologrammes par une nappe de fibres optiques au moyen d'un codage chromatique," *Optics Commun.*, Vol.27, pp.57-60, Oct. 1978.

[65] T.Ohtuka et al.,"Single-Mode Fiber Transmission Using Edge-Emitting LED for Broadband Subscriber Loops," *Elect. Commun. in Japan*, Part 1, Vol.72, May 1989.

[66] Y.Kashima et al.,"Performance and Reliability of InGaAsP Superluminescent Diode," *IEEE/OSA J.Lightwave Tech.*, Vol.11, pp.1644-1649, Nov. 1992.

[67] P.Wysocki et al.,"Spectral Characteristics of High-Power 1.5 μm Broad-Band Superluminescent Fiber Sources," *IEEE Photonics Technol. Lett.*, Vol.2, pp.178-180, March 1990.

[68] S.F.Su et al.,"Gain Equalization in Multiwavelength Lightwave Systems Using Acoustooptic Tunable Filters," *IEEE Photonics. Technol. Lett.*, Vol.4, pp.269-271, March 1992.

[69] H.Ichikawa et al.,"Dynamic space-variant optical interconnections using liquid crystal spatial light modulators," *Optics Commun.*, Vol.93, pp.145-150, Oct. 1992.

[70] T.Matsunaga et al.,"Photonic ATM Switching Technologies", *NTT Review Mag.*, Vol.5, pp.46-54, Jan. 1993.

[71] K.Johnson, D.McKnight and I.Underwood,"Smart Spatial Light Modulators Using Liquid Crystals On Silicon," *IEEE J. Quantum Electron.*, Vol.29, pp.699-714, Feb. 1993.

[72] G.Andersson et al.,"Submicrosecond electro-optic switching in the liquid-crystal smectic A Phase: the soft-mode ferroelectric effect," *Appl. Phys. Lett.*, Vol.51, pp.640-642, 1987.

[73] J.Gourlay, P.McOwan and D.G.Vass, "Time-Multiplexed optical Hadamard image transforms with ferroelectric-liquid-crystal-over-silicon spatial light modulators," *Applied Optics*, Vol.18, pp.1745-1747, Oct. 1993.

[74] A.Cisneros and C.A.Brackett,"A Large ATM Switch Based on Memory Switches and Optical Star Couplers", *IEEE J.S.A.C.*, Vol.9, pp.1348-1360, Oct.

1991.

[75] N.Shimosaka et al.,"Wavelength-addressed optical network using an ATM cell-based access scheme", *OFC'93 Technical Digest*, paper TuJ6, p.49.

[76] A.Jajszcyk and H.T.Mouftah,"Photonic Fast ATM Switching", *IEEE Commun. Mag.*, Vol.31, pp.58-65, Feb. 1993.

[77] K.Y.Eng, M.J.Karol and Y.S.Yeh,"A Growable Packet (ATM) Switch Architecture: Design Principles and Applications," *IEEE Trans. Commun.*, Vol.40, pp.423-430, Feb. 1992.

[78] H.Kuwahara et al.,"A shared buffer memory switch for an ATM exchange," *ICC 1989 Proc.*, pp.4.4.1-4.4.5.

[79] S.Fukushima and T.Kurokawa,"Parallel Interconnection Through an Optical Fiber Using Phase Conjugation Mirror Acceptable for Optical Data Pattern," *IEEE J.Quantum Electron.*, Vol.29, pp.613-618, Feb. 1993.